

The Impact of High-Fat Diet on Skeletal Muscle Stem Cell Recruitment in CD36 Deficient Mice

Sandrine Verpoorten BSc. MSc.

Doctorate of Philosophy (PhD) in Medical Science

The University of Hull and the University of York
Hull York Medical School

December 2019

Abstract

The prevalence of obesity is a major risk factor for cardiovascular and metabolic diseases including impaired skeletal muscle regeneration. Given the importance of skeletal muscle function in the context of obesity, it is paramount to understand the underlying mechanisms of impaired muscle health. Since skeletal muscle regeneration is regulated by muscle stem cells, the so-called satellite cells (SC), this thesis aims to investigate the effects of diet-induced obesity (DIO) on SC function. This study provides evidence that SC function is impaired in obesity, possibly linked to ectopic lipid infiltration via the fatty acid translocase CD36. Ectopic lipid infiltration was further linked to altered gene expression involved in skeletal muscle redox homeostasis and lipid metabolism. The CD36-deficient mouse model (CD36 KO) used for this study provides, for the first time, evidence of improved redox signalling and decreased oxidative stress in skeletal muscle under high-fat diet conditions, potentially linked to an altered mitochondrial bioenergetic profile. CD36 KO mice showed improved skeletal muscle lipid metabolism but interestingly developed signs of hepatic steatosis when exposed to a high-fat diet. Furthermore, the observed impairment of SC function in WT animals on a high-fat diet was attenuated in CD36 deficiency. However, CD36 was also identified as a key regulator of SC terminal differentiation. CD36 KO mice showed impaired regeneration after acute skeletal muscle injury, possibly linked to the decreased SC differentiation capacity. Additionally, this study reports a decrease in macrophage infiltration in CD36 KO mice following skeletal muscle injury, possibly due to inefficient inflammation resolution, subsequently resulting in impaired regeneration.

This demonstrates that CD36 deficiency protects against DIO, intramuscular lipid deposition and oxidative stress but results in impaired SC differentiation, delayed muscle regeneration and hepatic steatosis. CD36 is a key mediator of fatty acid uptake in skeletal muscle, linking obesity with SC function and muscle regeneration.

TABLE OF CONTENTS

List of Figures	1
List of Tables	3
Thesis output	4
External events	4
Internal events	5
Acknowledgements	6
Declaration	7
Abbreviation	8
1 CHAPTER 1- General Introduction	10
1.1 Chapter overview	11
1.2 Skeletal muscle.....	12
1.2.1 Anatomy and morphology	12
1.2.2 Skeletal muscle fibre heterogeneity.....	14
1.2.2.1 Skeletal muscle plasticity and exercise induced changes	16
1.2.2.2 Reactive oxygen species and aging induced muscle changes .	17
1.2.3 Stem cells and skeletal muscle regeneration.....	19
1.2.4 Muscle changes in pathological conditions	20
1.2.4.1 Obesity related changes in skeletal muscle plasticity and mass	20
1.2.4.2 Obesity related fibre type changes	21
1.2.4.3 Impact of obesity on skeletal muscle maintenance and	
regeneration	23
1.2.4.4 Ectopic lipid infiltration and lipotoxicity	23
1.2.4.5 Satellite cell function in obesity	25
1.2.4.6 Mitochondrial dysfunction in obesity	26
1.2.5 Experimental models of skeletal muscle regeneration.....	27
1.2.5.1 Mouse models of obesity and induced muscle regeneration	28
1.2.6 Calcium signalling	30
1.3 Fatty acid transporters and binding proteins.....	31
1.3.1 Tissue specific fatty acid uptake and transport.....	35
1.3.2 Skeletal muscle fatty acid transport	36
1.3.3 Expression and biological function of CD36	37
1.3.3.1 CD36 deficient mouse models.....	38
1.3.3.2 Blood lipid levels in WT and CD36 KO animals	40

1.3.3.3	CD36 deficiency in humans.....	40
1.3.4	Impact of high-fat diet feeding in CD36 deficient animal models	41
1.4	Liver morphology and function.....	46
1.4.1	Liver diseases in obesity	46
1.4.2	Development of NAFLD.....	48
1.4.2.1	Impact of fatty acid transporters and binding proteins in the development of NAFLD	49
1.5	Aims and Objectives	50
2	CHAPTER 2- General Materials and Methods.....	51
2.1	Practical Methods	52
2.1.1	Animals.....	52
2.1.2	Tissue sampling and freezing.....	52
2.1.3	Tissue embedding and cryosectioning.....	53
2.1.4	Cardiotoxin (CTX) induced muscle injury <i>in vivo</i>	53
2.2	Technical Methods.....	54
2.2.1	Histological analysis for lipid accumulation.....	54
2.2.2	Histochemical analysis of relative mitochondrial activity	55
2.2.3	Immunofluorescence	56
2.2.4	Single fibre isolation and culture.....	57
2.2.5	Satellite cell isolation and proliferation	57
2.2.6	Satellite cell differentiation.....	59
2.3	C2C12 cell culture.....	59
2.3.1	C2C12 proliferation.....	59
2.3.2	C2C12 differentiation	60
2.4	Cell culture maintenance	60
2.5	Immunohistochemistry.....	61
2.5.1	EdU cell proliferation assay	61
2.5.2	Immunofluorescence for histological analysis of myofiber composition.....	63
2.5.3	Satellite cell activation pattern in cultured myofibres by immunofluorescence	64
2.6	Immunofluorescence of isolated satellite cells	65
2.7	Digital imaging and analysis.....	66
2.8	Protein extraction and Immunoblotting.....	66
2.8.1	Tissue homogenisation and protein extraction.....	66
2.8.2	SDS Page.....	67
2.8.3	Protein transfer by Wet Blotting	68

2.8.4	Immunoblotting for oxidative protein modification	69
2.8.4.1	Assessment of protein adducts	69
2.9	Thiobarbituric acid reactive substance (TBARS)	70
2.10	Dihydroethidium (DHE) assay for reactive oxygen species	70
2.11	RNA isolation	71
2.11.1	cDNA synthesis	72
2.12	Primer design	74
2.13	Quantitative real time Polymerase Chain Reaction (PCR) assay	74
2.14	Seahorse XFp extracellular flux measurements	77
2.15	Statistical Analysis	78
3	CHAPTER 3- The effect of CD36 deficiency and high-fat diet feeding on weight gain and skeletal muscle morphology	79
3.1	Overview	80
3.2	Aims	81
3.3	Materials and Methods	81
3.3.1	Animals	81
3.3.2	Tissue sampling and freezing	82
3.3.3	Tissue embedding and cryosectioning	82
3.3.4	Histological analysis for lipid accumulation	82
3.3.5	Histochemical analysis of relative mitochondrial activity	83
3.3.6	Immunofluorescence	84
3.3.7	RNA isolation, cDNA synthesis and quantitative RT-PCR	84
3.4	Results	86
3.4.1	Effect of high-fat diet feeding in WT and CD36 deficient mice	86
3.5	Discussion	102
3.5.1	Body and tissue weight	103
3.5.2	Myofibre morphology and composition	103
3.5.3	Lipid accumulation and metabolism	104
3.5.3.1	Skeletal muscle lipid accumulation	104
3.5.3.2	Skeletal muscle lipid metabolism	105
3.5.3.3	Hepatic lipid accumulation	105
3.6	Conclusion	106
4	CHAPTER 4- The effect of CD36 deficiency and high-fat diet on skeletal muscle redox biology and oxidative stress	108
4.1	Overview	109
4.2	Aims	112

4.3	Materials and Methods	112
4.3.1	Thiobarbituric acid reactive substance (TBARS)	112
4.3.2	Protein extraction and Immunoblotting	113
4.3.3	Immunoblotting for posttranslational oxidative protein modification 114	
4.3.4	RNA isolation, cDNA synthesis and quantitative RT-PCR	114
4.3.5	Dihydroethidium (DHE) assay for reactive oxygen species detection 115	
4.4	Results	116
4.5	Discussion	125
4.5.1	Protein modification and adducts	125
4.5.2	ROS production.....	127
4.5.2.1	Skeletal muscle and isolated satellite cells	127
4.5.3	Calcium signalling in oxidative stress	128
4.6	Conclusion	129
5	CHAPTER 5- The effect of CD36 deficiency and high-fat diet on skeletal muscle satellite cell biology	130
5.1	Overview.....	131
5.2	Aims.....	133
5.3	Materials and Methods	133
5.3.1	Satellite cell isolation, proliferation and differentiation.....	133
5.3.2	Immunofluorescence of satellite cell activation pattern in cultured myofibres	134
5.3.3	C2C12 proliferation and differentiation.....	134
5.3.4	EdU cell proliferation assay	135
5.4	RNA isolation, cDNA synthesis and quantitative RT-PCR.....	135
5.5	Immunofluorescent of isolated satellite cells in culture	137
5.5.1	Cardiotoxin (CTX) induced muscle injury <i>in vivo</i>	138
5.5.2	Tissue embedding and cryosectioning.....	138
5.6	Results	138
5.6.1	CD36 exhibits different functions during satellite cell proliferation and differentiation.....	138
5.6.2	Loss of CD36 alters the metabolic profile of satellite cells and leads to impaired myotube formation.....	141
5.6.3	Palmitate treatment as well as loss of CD36 both negatively impact satellite cell differentiation capacity.....	143

5.6.4	Both high fatty acid availability and CD36 deficiency alter satellite cell transcription factor expression <i>in vitro</i> , resulting in impaired late stage differentiation.....	145
5.6.5	CD36-deficiency impairs skeletal muscle regeneration following acute damage with cardiotoxin.....	147
5.7	Discussion.....	150
5.7.1	Single fibre associated satellite cells.....	150
5.7.2	Isolated satellite cells.....	151
5.7.3	Single fibre associated satellite cells treated with palmitate and/or SSO	152
5.7.4	Skeletal muscle injury <i>in vivo</i>	153
5.8	Conclusion.....	154
6	CHAPTER 6- Effect of CD36 inhibitor SSO and high fatty acid availability on mitochondrial bioenergetic profile in myoblasts.....	155
6.1	Overview.....	156
6.1.1	Mitochondrial function in skeletal muscle.....	156
6.2	Aims.....	158
6.3	Materials and Methods.....	158
6.3.1	Seahorse XFp extracellular flux measurements.....	158
6.4	Results.....	159
6.4.1	CD36 deficient satellite cells and WT satellite cells show distinct bioenergetic profiles in the presence of high fatty acid availability.....	159
6.4.2	C2C12 cells display an altered bioenergetic profile in the presence of high fatty acid availability which is distinct from that of satellite cell derived myoblasts.....	165
6.5	Discussion.....	170
6.6	Conclusion.....	173
7	Chapter 7- General Discussion.....	175
7.1	Overview.....	176
7.2	Body weight and skeletal muscle lipid metabolism.....	177
7.3	Oxidative protein modification and DNA damage.....	180
7.4	Myofibre morphology and composition.....	180
7.5	Impact of CD36 deficiency and HF diet conditions on satellite cell function.....	181
7.6	Calcium signalling in oxidative stress.....	184
7.7	Skeletal muscle injury <i>in vivo</i>	188
7.8	Hepatic lipid accumulation.....	189
7.9	Limitations.....	191

7.10	Future Work.....	191
7.11	Concluding remarks.....	192
8	References.....	196
9	Appendix.....	215
9.1	List of materials.....	215
9.2	List of antibodies.....	217
9.3	PCR primer sequences.....	219

List of Figures

	Page
Figure 1.1: Basic skeletal muscle anatomy.	13
Figure 1.2: Satellite cell expression profile during myogenic lineage progression	19
Figure 1.3: FATP expression profile	31
Figure 2.1: Representative standard curve of BSA concentration measurement	61
Figure 3.1: Body weight changes in WT and CD36 KO mice after high-fat diet feeding	79
Figure 3.2: Tissue specific weight changes in wild-type and CD36 deficient mice	80
Figure 3.3: Diet and genotype dependent morphometric changes in EDL muscle	83
Figure 3.4: Diet and genotype dependent morphometric changes in Soleus muscle	86
Figure 3.5: Relative mitochondrial oxidative capacity in EDL muscle	88
Figure 3.6: Effect of CD36 deficiency on high-fat diet-induced lipid accumulation in skeletal muscle	89
Figure 3.7: Effect of CD36 deficiency on high-fat diet-induced lipid accumulation in the liver	92
Figure 4.1: High-fat diet induced protein modification and antioxidant gene expression in skeletal muscle	107
Figure 4.2: High-fat diet induced reactive oxygen species production in skeletal muscle and satellite cells of CD36 deficient mice	110
Figure 4.3: Palmitate alters Ca ²⁺ signalling in satellite cells isolated from WT and CD36 KO animals	113
Figure 5.1: CD36 deficiency attenuates satellite cell proliferation in high-fat diet fed mice	126
Figure 5.2: CD36 is critical for satellite cell maturation and differentiation	128
Figure 5.3: Palmitate impairs satellite cell differentiation in WT and CD36 deficient satellite cells	131
Figure 5.4: Increased fatty acid availability as well as CD36 deficiency impair late stage differentiation	133
Figure 5.5: CD36 deficiency impairs skeletal muscle regeneration after acute injury	135
Figure 6.1: CD36 deficiency effects mitochondrial bioenergetics during proliferation	145

Figure 6.2: CD36 deficiency and increased fatty acid availability effect the mitochondrial bioenergetic profile during differentiation	148
Figure 6.3: Proliferating C2C12 cells show a distinct bioenergetic profile compared to satellite cells	150
Figure 6.4: Differentiating C2C12 cells show a distinct bioenergetic profile compared to satellite cells	152
Figure 7.5: Theoretic scheme of proposed underlying mechanism involved SC differentiation linked to CD36	164

List of Tables

	Page
Table 1.3.1: Tissue specific fatty acid uptake and transport	32
Table 1.3.3.2: Blood lipid levels in WT and CD36 KO animals	37
Table 2.1: Diet composition of standard laboratory chow and high-fat (HF) diet	48
Table 2.2: Primary and secondary antibodies for immunohistochemistry	51
Table 2.3: Satellite cell growth medium and proliferation medium	53
Table 2.4: Satellite cell differentiation medium	54
Table 2.5: Myoblast growth medium	54
Table 2.6: Myoblast differentiation medium	55
Table 2.7: EdU proliferation assay kit	56
Table 2.8: EdU proliferation fluorescent signal detection	57
Table 2.9: Primary and secondary antibodies for myofibre immunofluorescence	58
Table 2.10: Primary and secondary antibodies for satellite cell immunofluorescence	59
Table 2.11: Excitation and Emission of Dyes	60
Table 2.12: Composition of the resolving and stacking gel used for SDS page	62
Table 2.13: Primary and secondary antibodies used for wet blotting	63
Table 2.14: MasterMix with DNase I to eliminate DNA contaminations	66
Table 2.15: MasterMix composition for cDNA synthesis and reverse transcription	66
Table 2.16: MasterMix composition RT-PCR	68
Table 2.17: Incubation time and cycles for RT-PCR analysis	68
Table 3.3.7: Primer sequences	78
Table 4.3.4: Primer sequences	105
Table 5.4: Primer sequences	124
Table 9.1: List of materials	215
Table 9.2: List of antibodies	217
Table 9.3: PCR primer sequences	219

Thesis output

Publications:

Verpoorten S., Sfyri P., Scully D., Mitchell R., Tzimou A., Mougios V., Patel K., Matsakas A. Loss of CD36 protects against diet-induced obesity but results in impaired muscle stem cell function, delayed muscle regeneration and hepatic steatosis. Published research article **Acta Physiol** (Oxf), Oct 2019

Scully D., Sfyri P., Verpoorten S., et al. Platelet releasate promotes skeletal myogenesis by increasing muscle stem cell commitment to differentiation and accelerates muscle regeneration following acute injury. **Acta Physiol** (Oxf), Oct 2018

External events

Verpoorten, S., Sfyri, P., Scully, D., Tzimou, A., Berger, M., Mougios, V., Matsakas, A. CD36 deficiency protects against diet-induced obesity and maintains skeletal muscle health, but leads to hepatic steatosis. Oral presentation at the **H3 symposium Muscle physiology and metabolism**, London, UK, Nov 2017.

Verpoorten, S., Sfyri, P., Scully, D., Berger, M., Mougios, V., Matsakas, A. CD36-Deficiency Protects Against Diet- Induced Obesity and Modulates Skeletal Muscle Satellite Cell Recruitment Pattern. Poster presentation at the **North of England Cell Biology Forum**, 2017 Sep 15; Hull, England

Verpoorten S., Sfyri P., Tzimou A., Scully D., Mougios V., Matsakas A. CD36 deficiency protects against diet-induced obesity, but leads to hepatic steatosis and impaired stem cell differentiation. Poster presentation at the **North of England Cell Biology Forum**; 2018 Aug 29; Huddersfield, England

Verpoorten S., Sfyri P., Tzimou A., Scully D., Mougios V., Matsakas A. Diet-induced obesity impairs muscle stem cell recruitment patterns and induces oxidative stress in skeletal muscle that are mitigated by CD36 deletion. Oral and Poster presented at the **Europhysiology 2018** conference, London 14 Sep 2018.

Verpoorten S., Sfyri P., Scully D., Matsakas A. CD36 deficiency restores impaired satellite cell proliferation in response to high-fat diet. Poster presentation at the **Muscle Wasting Conference**, Ascona, Switzerland 24 Sep 2018.

Verpoorten S., Sfyri P., Tzimou A., Scully D., Mougios V., Matsakas A. Diet-induced obesity impairs muscle stem cell function and redox homeostasis, which is linked to CD36 in mice. Poster presentation at the **Physiology 2019**, Aberdeen 8 July 2019, UK

Internal events

Verpoorten S., Sfyri P., Tzimou A., Scully D., Mougios V., Matsakas A. CD36 Deficiency Attenuates Adiposity and Protects Muscle Health, but Leads to Hepatic Steatosis. Oral talk and poster presentation at the **Allam Lecture 2018**, Hull York Medical School Apr 20, 2018. **(Awarded prized oral presentation)**

Verpoorten, S., Sfyri, P., Berger, M., Matsakas, A. The impact of high fat diet on skeletal muscle metabolism and satellite cell function in CD36 deficient mice. Poster presented at: **Hull York Medical School (HYMS) Postgraduate Student Conference**, York, UK, May 2016

Verpoorten, S., Sfyri, P., Scully, D., Berger, M., Matsakas, A. CD36-deficiency protects against diet-induced obesity and modulates skeletal muscle satellite cell recruitment patterns. Oral presentation at the **HYMS Postgraduate Research Conference**, Hull, UK, May 2017 **(Awarded prized oral presentation)**

Verpoorten S., Sfyri P., Tzimou A., Scully D., Mougios V., Matsakas A. Loss of CD36 protects from diet-induced obesity and improves muscle health; but leads to hepatic steatosis and impaired muscle stem cell differentiation. Oral presentation at the **HYMS Postgraduate Research Conference**, Hull, UK, July 2018

Acknowledgements

I would like to express my gratitude to my supervisor Dr. Antonios Matsakas for giving me the opportunity to pursue this PhD and for his valuable guidance and support throughout. My gratitude extends to the University of Hull and The Hull York Medical School for the financial support and to Dr. Pagona Sfyri for her teaching and guidance. I am especially grateful to Dr. David Scully for his support and remarkable attention to detail. This work would not have been successfully published without him.

Dr. Vassilis Mougios and Anastasia Tzimou processed our samples for the gas chromatography analysis of skeletal muscle lipid content. I would like to place on record my best regards to Prof. Khalid Naseem from the University of Leeds for allowing me to conduct my experiments on their CD36 KO mouse line.

Special thanks to my family who have always supported me along the way.

This thesis is dedicated to my grandparents Wera and Karl-Heinz Verpoorten. Thank you for always believing in me.

Diese Doktorarbeit widme ich meinen Großeltern Wera und Karl-Heinz Verpoorten. Danke, dass ihr immer an mich geglaubt habt.

Declaration

I confirm that this work is original and that if any passage(s) or diagram(s) have been copied from academic papers, books, the internet or any other sources these are clearly identified by the use of quotation marks and the reference(s) is fully cited. I certify that, other than where indicated, this is my own work and does not breach the regulations of HYMS, the University of Hull or the University of York regarding plagiarism or academic conduct in examinations. I have read the HYMS Code of Practice on Academic Misconduct, and state that this piece of work is my own and does not contain any unacknowledged work from any other sources'. If applicable, the declaration should also include; 'I confirm that any patient information obtained to produce this piece of work has been appropriately anonymised

Abbreviation

AICAR	5-Aminoimidazole-4-Carboxamide
AMPK	AMP-activated protein kinase
ANOVA	Analysis of variance
ATP	Adenosine triphosphate
BaCl ₂	Barium chloride
Ca ²⁺	Calcium ion
Cat	Catalase
CCK1	Cholecystokinin 1 receptor
CD36	Cluster of differentiation 36
CD68	Cluster of differentiation 68
cDNA	Copy deoxyribonucleic acid
Cidea	Cell Death Activator CIDE-A
Cpt1a	Carnitine palmitoyltransferase 1a
CSA	Cross sectional area
CTX	Cardiotoxin
Cyp	Cyclophilin
DAG	Diacylglycerol
DAPI	4',6-diamidino-2-phenylindole
DHE	Dihydroethidium
DIO	Diet induced obesity
DNA	Deoxyribonucleic acid
DNase	Deoxyribonuclease I
EDL	Extensor digitorum longus
FA	Fatty acid
FABPpm	Plasma-membrane fatty acid binding protein
FAT	Fatty acid translocase
Fatp1,2,3,4,5,6	Fatty acid transport protein 1,2,3,4,5,6
FDA	U.S. Food and drug administration
FFA	Free fatty acid
FFAR1,2,3,4	Free fatty acid receptor 1,2,3,4
FI	Freeze injury
FSF	Fat signal fraction
Gas	Gastrocnemius
Glut4	Glucose transporter type 4
GPCRs	G-protein coupled receptors
HDL	High density lipoprotein
HF	High fat
HGF	Hepatocyte growth factor
hLPL	Human lipoprotein lipase
Hprt	Hypoxanthine guanine phosphoribosyl transferase
IL 1,6	Interleukin 1,6
kDa	Kilodalton
KO	Knock-out
LCFA	Long chain fatty acid
LDL	Low density lipoprotein
Lep	Leptin
LFABP	Liver type fatty acid binding protein

LKB1	Liver kinase B1
Met	Metformin
MHCI	Myosin heavy chain type I
MHCIIA	Myosin heavy chain type IIA
MHCIIIB	Myosin heavy chain type IIB
MHCIIIX	Myosin heavy chain type IIX
MyoD	Myoblast determination protein 1
MyoG	Myogenin
mRNA	Messenger ribonucleic acid
NADPH	Nicotinamide adenine dinucleotide phosphate
NAFLD	Non-alcoholic fatty liver disease
NBT	Nitrotetrazolium blue chloride
NF- κ B	Nuclear factor kappa beta
NTX	Notexin
Ogg1	Oxoguanosine DNA glycosylase 1
ORO	Oil Red O
oxHDL	Oxidized high density lipoprotein
oxLDL	Oxidized low density lipoprotein
PBS	Phosphate arterial disease
PCR	Polymerase chain reaction
PFA	Paraformaldehyde
Pgc1a	Peroxisome proliferator activated receptor
PI3K	Phosphatidylinositol-3-kinase
PPAR α , γ , δ	Peroxisome-proliferator-activated-receptor α , γ , δ
QD	Quadriceps
qRT-PCR	Quantitative reverse transcription PCR
RNA	Ribonucleic acid
ROS	Reactive oxygen species
SC	Satellite cells
SDH	Succinate dehydrogenase
SDS	Sodium Dodecyl Sulfate
Sol	Soleus
SSO	Sulfo-N-succinimidyl oleate
STAT3	Signal transducer and activator of transcription 3
TA	Tibialis anterior
TBARS	Thiobarbituric acid reactive substance
TEMED	Tetramethylethylenediamine
TG	Triglyceride
TNF α	Tumor necrosis factor alpha
VLDL	Very low density lipoprotein
WHO	World Health Organisation
WT	Wild-type
ZDF	Zucker diabetic rats
3NT	3-nitrotyrosine
4-HNE	4-hydroxy-2-nonenal

1 CHAPTER 1- General Introduction

1.1 Chapter overview

Skeletal muscle stem cells, also called satellite cells, are the major source of newly forming myoblasts and of crucial importance for postnatal muscle growth, maintenance, regeneration and hypertrophy (Mauro, 1961, Montarras et al., 2005, Shea et al., 2010). Satellite cells are located between the basal lamina and the sarcolemma, where they reside in a mitotically quiescent state in the healthy adult skeletal muscle (Mauro, 1961, Zammit et al., 2002, Nagata et al., 2006). Upon stimulation by muscle maintenance pathways or injury, satellite cells exit their quiescent state and enter the cell cycle. The vast majority will then continue to proliferate and differentiate towards the myogenic lineage, forming new myoblasts, whereas a small number of satellite cells return to a quiescent state, replenishing the skeletal muscle stem cell pool (Mauro, 1961, Montarras et al., 2005, Shea et al., 2010, Zammit et al., 2002, Zammit et al., 2004). Satellite cell function is a complex and tightly regulated process with particular relevance for muscle biology and metabolism. For example, impaired satellite cell function has been associated with a variety of muscle diseases such as Duchenne muscular dystrophy and age-related degenerative loss of muscle mass, also known as sarcopenia (Dumont et al., 2015, Wang et al., 2017, Rozo et al., 2016).

Accumulating evidence shows that skeletal muscle function and regeneration is compromised in obesity and type 2 diabetes (D'Souza et al., 2015, Nguyen et al., 2011, Fu et al., 2016). Perturbed muscle metabolic capacity leads to insulin resistance, increased fatty acid uptake and intramuscular triglycerol accumulation in skeletal muscle of obese and diabetic individuals (Kahn and Flier, 2000, Hilton et al., 2008). CD36, as one of the major fatty acid transporters in skeletal muscle (Bonen et al., 1999, Han et al., 2007, Febbraio et al., 2001, Glatz et al., 2013, Luiken et al., 2000), has been shown to be upregulated under high-fat diet conditions (Cameron-Smith et al., 2003, Koonen et al., 2007), further facilitating the transport and ectopic accumulation of lipids. Translocation and elevated expression of CD36 in various tissues such as cardiac tissue (Aguer et al., 2010, Mansor et al., 2017) result in lipid overload and lipotoxicity (Bonen et al., 2004, Glatz et al., 2013), accelerating the development of metabolic disorders, collectively described as the metabolic syndrome. Previous studies have revealed several unfavourable changes in the obese condition, such as increased

susceptibility to muscle damage (Knoblauch et al., 2013, Kim and So, 2018), decline in general muscle health and impaired regenerative capacity (Xu et al., 2018, Fu et al., 2016). However, the underlying cellular and metabolic changes are still poorly understood.

1.2 Skeletal muscle

Skeletal muscle has multiple mechanical and metabolic functions including force generation, locomotion, postural stability as well as heat production, substrate storage, oxygen and fuel consumption during periods of physical activity and energy demand. As an insulin sensitive tissue skeletal muscle further contributes to the maintenance of blood glucose levels (Wolfe, 2006, Jensen et al., 2011). Skeletal muscle accounts for 40% of the total body mass, contains 50- 75% of the body's proteins and accounts for 30- 50% of whole-body protein turnover (Frontera and Ochala, 2015, Wolfe, 2006). The homeostasis of protein synthesis and degradation regulates muscle mass, which is tightly controlled by various factors such as hormones, nutrient availability as well as exercise and disease (Matsakas and Patel, 2009).

1.2.1 Anatomy and morphology

Skeletal muscle is surrounded by the epimysium and attached via tendons to the skeleton. The muscle itself consists of several fibre bundles, which are all individually surrounded by the perimysium with several blood vessels in close proximity. The muscle fibre bundles consist of individual fibres, forming the motor unit of the skeletal muscle (**Figure 1.1**). The individual fibres of the skeletal muscle are giant, multinucleated cells. Their sarcoplasm contains all cytoplasmic organelles with numerous nuclei at the periphery of the muscle fibre (Greising et al., 2012) with each nucleus regulating a specific area of the fibre; called myonuclear domain (Murach et al., 2018). Each muscle fibre has an approximate length of 1000µm and a diameter of 100µm (Fortin et al., 2014). Muscle fibres originate from the fusion of a large number of myoblasts, resulting in a multinucleated cell, contributing to muscle growth and repair, as well as muscle maintenance and regeneration (Frontera and Ochala, 2015).

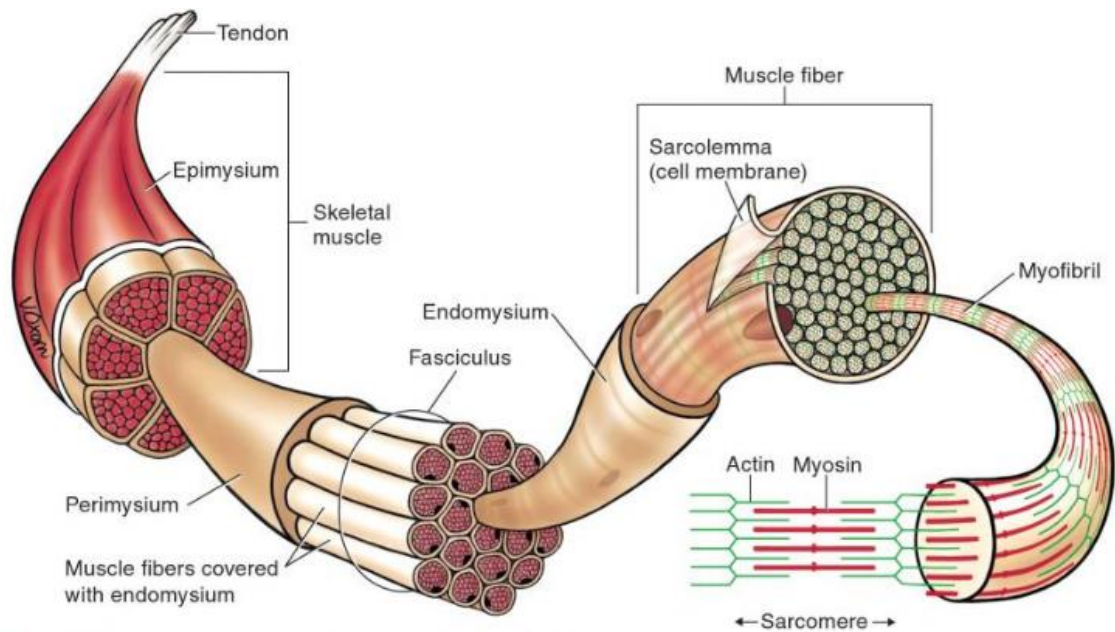


Figure 1.1: Basic skeletal muscle anatomy. The muscle itself is surrounded by the epimysium and consist out of several muscle fibres grouped together, which themselves are surrounded by the perimysium. Individual muscle fibres are surrounded by the endomysium and contain several nuclei underneath the sarcolemma. The next smaller unit of the muscle fibre is the myofibril, which contains thin filaments (actin) and thick filaments (myosin) forming a contractile unit -the sarcomere- running from one Z-line to the next one. Different bands exist due to the actin and myosin overlap during different stages of muscle contraction. Adapted from Kraemer et al. 2014 Exercise Physiology: Integrating Theory and Application (Kraemer and Fleck, 2014).

Myofibrils are the next smaller unit of the myofibres and are aligned along the longitudinal axis of the muscle fibre. Myofibrils are made up by sarcomeres which are the responsible element for muscle contraction. They consist out of two types of filaments which are the thick filaments and the thin filaments. The thin filaments are composed of the protein actin, whereas the thick filaments are composed of a protein called myosin. Together the two filaments form partially overlapping layers, resulting in the appearance of dark and light bands (**Figure 1.1**). The dark bands are called A bands with the H-zone at the centre, whereas the light filaments form the I bands are found between the A bands. The I bands are centred on a region known as Z line, forming the boundary between individual subunits called the sarcomere, which are the basic contractile units of the muscle (Squire, 2016). The skeletal muscle produces force via tens of thousands of these sarcomeres. Based on the sliding-filament and cross-bridge theory the

sarcomere can change in size and produce muscle force due to actin-myosin interaction. The sliding filament theory, which was independently introduced in 1954 by the two researchers Andrew Huxley and Rolf Niedergerke as well as by Hugh Huxley and Jean Hanson, explains the underlying mechanism of muscle contraction based on myosin filaments (thick) sliding past the actin filaments (thin) during muscle contraction (HUXLEY and NIEDERGERKE, 1954, HANSON and HUXLEY, 1953). During muscle contraction, the actin filaments move into the A bands between the myosin filaments while the absolute length of the two groups of filaments remain relatively constant.

It was later postulated by Hugh Huxley that the filament sliding occurs due to cyclic attachment and detachment of myosin and actin filaments, with contraction occurring due to the pulling movement of myosin on the actin filament towards the centre of the A band. On the molecular level, the contracting force is regulated by the actin binding proteins troponin and tropomyosin in a Ca^{2+} dependent process. Once the contraction is initiated, Ca^{2+} is released by the sarcoplasmic reticulum and binds troponin C which then undergoes a conformational change. This motion allows tropomyosin to relax, resulting in the exposure of myosin binding sites on actin. Two myosin heads which extend from the thick myosin filament can now attach to the thin actin filament resulting in muscle force generation. Once Adenosine Triphosphate (ATP) attaches to the myosin head, it detaches from the actin and ATP is hydrolysed by myosin. In order to bind to a different actin molecule, two Ca^{2+} ions have to bind again to troponin C on the actin filament to release the block of the actin binding site by tropomyosin. The periodic detachment from actin and re-attachment to the next actin molecule creates a force; also referred to as stroke which is the underlying mechanism of shortening sarcomeres and muscle contraction known as the cross-bridge cycle (Herzog, 2018, Longyear et al., 2017).

1.2.2 Skeletal muscle fibre heterogeneity

Mammalian fibre types are very heterogeneous with four major fibre types of distinct myosin composition. In general, these fibre types contain four different myosin heavy chain (MHC) isoforms; type I, which is a slow fibre type and type

Ila, Iix and Iib (MHCIIa, MHCIIx and MHCIIb) fibre types, representing fast fibres (Bloemberg and Quadrilatero, 2012). It is noteworthy to mention that, in contrast to mice, human skeletal muscle does not have type Iib fibres (Tellis et al., 2004). Skeletal muscle fibres are either slow-oxidative type I fibres with a large number of mitochondria or fast-glycolytic type II MHCII fibres with fewer mitochondria and larger cross-sectional area (CSA). The distribution of different fibre types not only depends on the species but also on the type of skeletal muscle. Furthermore, it has been shown that fibre type distribution can vary quite significantly between individuals of the same species (Schiaffino and Reggiani, 2011). The underlying heterogeneity allows the muscle to adapt to different tasks such as continuous low-intensity activities on one side and strong, maximum force production on the other side (Schiaffino and Reggiani, 2011).

Histochemical methods are often used to identify different fibre types by enzymatic histochemistry and according to their myosin heavy chain expression (Bloemberg and Quadrilatero, 2012). For enzyme histochemistry, succinate dehydrogenase (SDH) activity has been used as an indicator for the oxidative capacity of skeletal muscle fibres. Due to their high number of mitochondria correlated to increased oxidative capacity, type I fibres are stained SDH-positive whereas SDH-low or negative fibres are less oxidative or nonoxidative fibres (Schiaffino and Reggiani, 2011). Furthermore, immunofluorescence approaches can be used to distinguish between different muscle fibres due to their fibre-specific myosin heavy chain expression (Matsakas et al., 2015). Fibres expressing more than one distinct MHC isoform are called hybrid-fibres and exist as type I/IIA in humans and IIX/IIB in mouse muscle, which translates into their oxidative and glycolytic potential as well as cross-sectional area (Bloemberg and Quadrilatero, 2012).

As a fast-twitch muscle, the extensor digitorum longus (EDL) muscle is mainly comprised of type IIB, IIX and IIA fibres which, due to their glycolytic properties results in strong and fast movements (Matsakas et al., 2015). On the contrary, the soleus muscle -as a slow-twitch muscle- mainly consists of type I, type IIA and type IIX fibres with a higher oxidative potential resulting in a high resistance to fatigue during prolonged muscle activity (Valdez et al., 2012). However, fibre phenotypes and composition can change, for example upon environmental or

hormonal changes as well as neural influence and adaptation to activity. This adaptation of the skeletal muscle is referred to as muscle plasticity and has been subject of intense investigation (Schiaffino and Reggiani, 2011). In fact, skeletal muscle activity has proven to be beneficial in the prevention of many chronic and metabolic diseases. Therefore, the underlying pathways involved in mediating fibre type changes may help to identify new potential therapeutic targets in the field of metabolic disorders (Schiaffino and Reggiani, 2011).

1.2.2.1 Skeletal muscle plasticity and exercise induced changes

It is a long-standing observation, that skeletal muscle structure and metabolism changes significantly upon physical exercise. Depending on the type of exercise that is performed, different molecular pathways are activated, leading to muscle adaptation, possibly resulting in hypertrophy (Lamon et al., 2014). Chronic muscle contraction such as endurance exercise, or also called aerobic exercise, is a type of exercise involving large numbers of muscle bundles for a prolonged time, improving the energetic potential of the skeletal muscle. The physiological and biochemical adaptation of the skeletal muscle include mitochondrial biogenesis, angiogenesis and are linked to endurance exercise-initiated changes which occur in enzymes of the Krebs cycle, enzymes involved in fatty acid activation, as well as those participating in oxygen consumption (Lamon et al., 2014, Yan et al., 2012). Following endurance exercise, skeletal muscle shows an increased efficiency in its contractile properties due to structural adaptation including greater development of the sarcoplasmic reticulum, increased mitochondrial quantity and greater enzyme activity, involved in the Krebs cycle (Seene et al., 2011, Yan et al., 2012). It has been shown that endurance exercise is linked to enhanced protein synthesis, mitochondrial biogenesis as well as interleukin-6 (IL-6) release, linked to the inhibition of the tumour necrosis factor- α (TNF- α), further resulting in the inhibition of skeletal muscle apoptotic pathways. Additionally, it has been suggested that endurance exercise exerts a significant positive impact on a number of diseases, including obesity, diabetes and cardiovascular diseases, possibly due to anti-inflammatory aspects and anti-atrophy effects related to the inhibition of TNF- α (Strasser et al., 2018, Chen et al., 2011, Meng and Yu, 2010, Menshikova et al., 2006).

These adaptive changes are highly associated with the structural plasticity of the muscle contractile apparatus, possibly leading to a change in fibre type composition from a glycolytic to an oxidative phenotype (type IIB/IIX to IIA). It is known that MHC type I and type IIA fibres co-exist in the same skeletal muscle of humans that undergo endurance training and it was found that in professional athletes the number of type I fibres is increased after several years of intense training. However, exercise-induced transformation into type I fibres is still a matter of investigation (Yan et al., 2011).

Mechanisms for exercise-dependent skeletal muscle structural changes can also be found in resistance exercise, which is a type of anaerobic physical activity, driving muscle strength and further induces hypertrophy of the skeletal muscle fibres, based on the positive muscle protein balance and the addition of satellite cells to the muscle fibres (Phillips, 2014). It is due to the increased protein synthesis which exceeds the protein catabolism, that fibres increase in their dimensions and become hypertrophic as a result of resistance exercise (Phillips, 2014, Blaauw and Reggiani, 2014, Nader et al., 2014). Not only has resistance training been shown to induce hypertrophy but also to attenuate both fibre atrophy and pro-apoptotic signalling pathways in addition to increased mitochondria enzyme activity and inhibition of TNF- α , which is further contributing to the decrease in apoptosis (Phillips, 2014, Blaauw and Reggiani, 2014, Melov et al., 2007, de Guia et al., 2019).

Skeletal muscle is highly adaptive in the response to energetic changes and functional demands. Due to its plasticity skeletal muscle can improve in performance upon both endurance and resistance exercise which promotes phenotypical alterations. Exercise elicits a significant impact on a number of metabolic diseases such as obesity and diabetes. The strong negative correlation between physical exercise and mortality further elucidates the importance of muscle performance in combating the metabolic syndrome.

1.2.2.2 Reactive oxygen species and aging induced muscle changes

It is well established that physical exercise can cause increased levels of reactive oxygen species (ROS) resulting in oxidative stress. During intense and prolonged

exercise, skeletal muscle production of ROS often can cause cellular changes resulting in damage to proteins and lipids of the muscle fibre (Powers et al., 2011). At the same time, an adaptive response is stimulated which protects the body against oxidative stress and facilitates the rapid recovery and remodelling of skeletal muscle after acute periods of stress damage (Brioché 2016, Archer 2018). It has been observed that a single period of muscle contraction increases the activity of muscle antioxidant defence mechanisms such as superoxide dismutase and catalase together with the upregulation of heat shock proteins in mice (Jackson and McArdle, 2011, McArdle et al., 2001). However, during the process of aging, the adaptive response to ROS, induced by skeletal muscle contractile activity, is severely attenuated (Jackson and McArdle, 2011). This age-related loss of skeletal muscle ROS homeostasis is thought to be one of the main underlying mechanisms related to oxidative damage in skeletal muscle and subsequent development of functional deficits with aging (Jackson and McArdle, 2011). Not only is aging associated with a decrease in muscle function but also with a decline in muscle mass. This is partly due to both intrinsic age-related metabolic changes as well as environmental influences (Tieland et al., 2018). Although mostly stable during early life, muscle mass starts to decline after the age of 50 years at a rate of 1% each year in men and around 0.5% in women (Siparsky et al., 2014). At the same time, an increasing accumulation of fat mass has been observed (Siparsky et al., 2014). The typical age-related loss in muscle mass is further associated with a decline in contractile protein material which links to the reduction of cross-sectional area of type II fast twitch fibres and, as a result, a decline in muscle strength and force production (Nilwik et al., 2013). In contrast, the size of type I muscle fibres seems to remain constant in aging (Tieland et al., 2018). Further adding to the age-related decline in muscle function is the increased accumulation of fat mass seen in the elderly (Hunter et al., 2019). Underlying mechanisms related to poorer metabolic health in aging and aging-associated diseases such as obesity and diabetes are therefore a matter of intense investigation (Hunter et al., 2019).

1.2.3 Stem cells and skeletal muscle regeneration

The ability of skeletal muscle to undergo growth and regeneration relies on a population of adult muscle stem cells, the so-called satellite cells (SCs). SCs are characterised by their location between the sarcolemma and the basal lamina. First described in 1961, they are named based on their elevated, anatomic position on the surface of a differentiated skeletal muscle fibre (Mauro, 1961). Initially described as myogenic precursor cells, they were later redefined as myogenic stem cells due to their capacity to self-renew and their differentiation capacity. In a healthy adult organism, satellite cells reside in their niche in a quiescent state until they become activated due to muscle maintenance processes or muscle injury (Anderson, 2000, Schultz et al., 1978, Alonso-Martin et al., 2016). Upon activation, SCs retain the ability to proliferate and differentiate, subsequently leading to the formation of new myoblasts. These myoblasts fuse with the muscle fibre, while a subpopulation of SCs exits the cell-cycle and re-enters a quiescent state to maintain a constant stem-cell pool (Zammit et al., 2004). A homeostatic state of differentiating and self-renewing SCs is of major importance to maintain the regenerative capacity of the muscle. Several molecular markers have been described over the years to identify and detect satellite cells, making it easier to study their role in regeneration and to trace their progeny (Alonso-Martin et al., 2016). Quiescent SCs express the paired box transcription factor family member Pax7 (Pax7) and lack the expression of myoblast determination protein1 (MyoD) and Myogenin (MyoG). Upon activation, due to injury or exercise, SCs enter the cell cycle and start to co-express MyoD, thereby initiating the myogenic programme. Most proliferating cells continue to differentiate and give rise to new skeletal muscle cells (**Figure1.2**). Only a small proportion of daughter cells return to a quiescent state which remain Pax7 positive and negative for MyoD and Myogenin retaining their self-renewing potential. The vast majority of proliferating cells progressively downregulate Pax7 while upregulating MyoD. They further lose their capacity to undergo self-renewal, permanently downregulate Pax7 and upregulate MyoG when entering the final stage of differentiation (Nabeshima et al., 1993, Zammit et al., 2004). Differentiating Pax7 negative and MyoD/MyoG positive cells then give rise to newly formed myoblasts with the ability to fuse with the damaged fibre resulting in a multinucleated myotube (Zammit et al., 2006).

This sequential pattern of activation, proliferation and differentiation is essential for effective restoration of muscle structure and function after injury. Impairment of this sensitive sequential regulation can compromise the regenerative capacity of the muscle which may terminate in the development of severe muscle malfunction as well as muscle dystrophies.

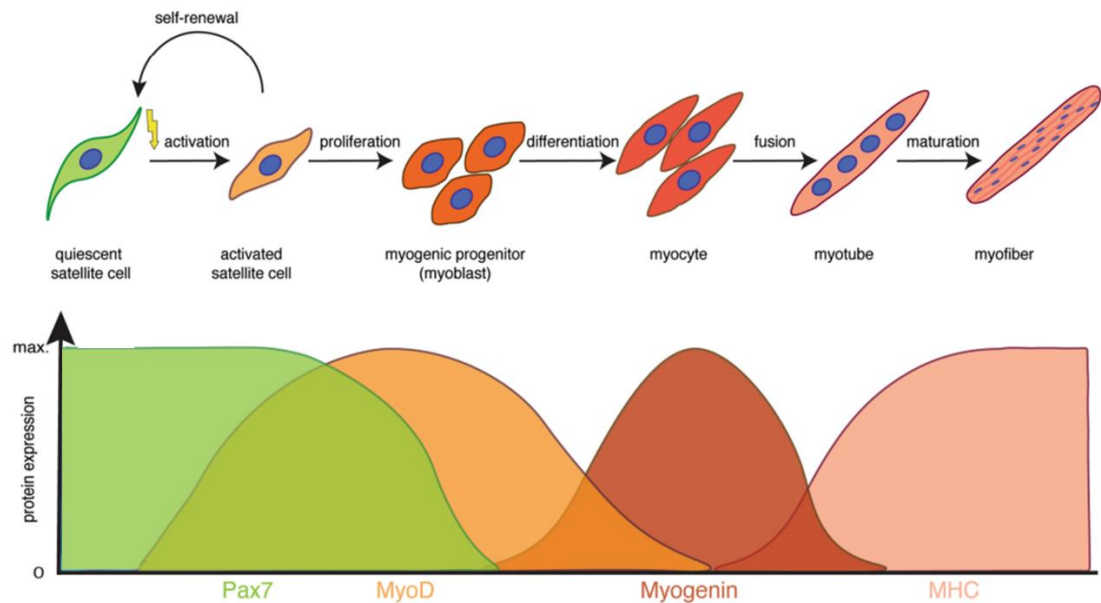


Figure 1.2: Satellite cell expression profile during myogenic lineage progression. Schematic illustration of key myogenic transcription factor expression during quiescence (Pax7), activation, e.g. due to injury and subsequent proliferation of myogenic progenitor cells (MyoD). Following differentiation (Myogenin), the myoblasts start to fuse and form mature myofibres (MHC). Adapted from Schmidt et al. 2019 (Schmidt et al., 2019)

1.2.4 Muscle changes in pathological conditions

1.2.4.1 Obesity related changes in skeletal muscle plasticity and mass

Obesity, which is defined as an excessive accumulation of fat is a major risk factor for several metabolic diseases, including cardiovascular diseases and diabetes (WHO, 2019). According to the World Health Organisation (WHO), obesity is one of the greatest health challenges of the 21st century in European countries. Obesity is responsible for 2-8% of health costs and 10-13% of deaths in different parts of the European Region and the numbers of those regions affected is rising at an alarming rate (WHO euro, 2019). Not only is obesity correlated with insulin

resistance and diabetes but also coincides with the loss of skeletal muscle mass (Meex et al., 2019). Evidence suggests that the increased flux of fatty acids from adipose tissue to the liver and skeletal muscle results in skeletal muscle mitochondrial dysfunction and impaired insulin signalling (Marchesini et al., 2008, de Mello et al., 2018). Recently published data further correlates increased skeletal muscle lipid accumulation with the development of muscle atrophy. It has been recognized that muscle strength is deteriorating in patients with diabetes; a problem that is even accelerated during the aging process with up to five-fold higher muscle loss in diabetic patients compared to the normal population at an age older than 65 years (Park et al., 2006, Meex et al., 2019). Consequently, people with obesity-induced impairments of muscle function suffer from poor physical performance and a decreased quality of life. Importantly, the exact correlation between obesity-induced changes in the skeletal muscle and the resulting loss in muscle mass and strength is still an ongoing matter of investigation. Therefore, it is essential to understand the underlying mechanisms leading to muscle atrophy in the setting of obesity and diabetes. Although much has been discussed regarding the relationship between the loss of muscle mass and the development of type 2 diabetes, it remains unclear whether muscle loss is the cause or the consequence of the development of insulin resistance. It is unlikely that a complex disease such as type 2 diabetes is purely depending on a reduction in skeletal muscle mass, nevertheless, there is accumulating evidence in the literature that skeletal muscle lipid accumulation and expansion of adipose tissue plays a crucial role in muscle atrophy and consequently, in the development of metabolic disorders (Hunter et al., 2019).

1.2.4.2 Obesity related fibre type changes

Due to its plasticity, skeletal muscle is capable of remodelling in response to a sedentary lifestyle or exercise, as well as disease, overuse or dietary changes. A growing body of evidence suggests that obesity and its associated increase of adipose tissue, exert significant effects on muscle fibres and muscle fibre type composition. Several studies have shown that obesity effects the fibre type distribution in human skeletal muscle tissue. Evidence suggests that obesity correlates with a decrease in type I and type IIa fibres, while at the same time an

increase in the proportion of type IIb fibres has been observed, indicating alterations in skeletal muscle metabolism and oxidative capacity (Tanner et al., 2002, Oberbach et al., 2006). Similarly, in rodent models of obesity a decrease in type IIa fibres has been observed, paralleled by a reduction in oxidative-metabolism related gene expression (Adachi et al., 2007).

Interestingly, some evidence suggests underlying mechanistic differences between male and female mice. It has been shown by a study from DeNies and colleagues, that male mice kept on a high-fat diet for one year exhibited a significantly reduced proportion in slow type I fibres. They further showed that an inverted relation of body mass and relative proportion of type I fibres exists in these mice. At the same time, the decrease in type I fibres was paralleled by an increase in type I/IIA fibres in male on a high-fat diet. However, these observations were purely made in male mice, whereas female mice showed no association between body fat gained and muscle fibre type alterations. Results therefore indicate that type I fibres are especially susceptible to high-fat diet associated changes and that these fibre type changes occur in a sex-specific way in rodents (Denies et al., 2014). Furthermore, it has been hypothesised that a type I fibre phenotype exhibits a protective mechanism against the development of obesity and that in turn, the oxidative capacity of the muscle is a marker to predict insulin sensitivity more effectively than intramuscular lipid deposition (Wang et al., 2004, Bruce et al., 2003). Although most studies performed in humans suggest a decrease in type I fibres associated with obesity and further showed that lean people possess a higher percentage of type I fibres when compared with other individuals from the same ethnicity, it is worth mentioning that in humans the muscle fibre type distribution can vary extensively. Simoneau and Bouchard showed that in the North American Caucasian population a range of 13- 98% type I fibres has been reported in the vastus lateralis (Simoneau and Bouchard, 1995). Additionally, it has been reported that, without account to obesity, the African American ethnicity is associated with a reduction of type I fibres when compared to Caucasians (51.8 ± 1.8 vs. $43.7 \pm 2.8\%$). At the same time, skeletal muscle tissue from African American subjects revealed a significant increase in type IIb fibres, which further underlines the significant interaction of

ethnicity and muscle-fibre distribution with possible implications for the development of skeletal muscle insulin resistance.

1.2.4.3 Impact of obesity on skeletal muscle maintenance and regeneration

It has long been hypothesised, that obesity-induced type 2 diabetes negatively impacts muscle health and function. The involvement of obesity in the development of insulin resistance is a well-established fact. Less known, however, is the impact of obesity on skeletal muscle function and especially regeneration.

More specifically, it has been suggested, that the observed ectopic lipid infiltration in the skeletal muscle of obese individuals plays a crucial role in the development of lipotoxicity, with potential impact on skeletal muscle maintenance and regeneration.

1.2.4.4 Ectopic lipid infiltration and lipotoxicity

An increased accumulation of lipid droplets has been observed in muscle biopsies of obese individuals (Akhmedov and Berdeaux, 2013). It has further been suggested that the deposition of those lipids in obese humans has a negative impact on cell signalling pathways and metabolism, collectively described as lipotoxicity which refers to lipotoxic species that are, at least partly, responsible for skeletal muscle insulin resistance (Akhmedov and Berdeaux, 2013). Previously published data shows that incubating cultured muscle cells with an overload of lipids markedly reduced their ability to express myogenic transcription factors and results in increased apoptosis (Akhmedov and Berdeaux, 2013). This suggest a direct link between increased lipid availability and impaired muscle fibre and satellite cell function.

In an elegant study conducted by K. P. Tamilarasan et al. the group showed that lipid overload in skeletal muscle tissue causes lipotoxicity leading to impaired skeletal muscle repair and skeletal muscle damage (Tamilarasan et al., 2012). For their studies they used a mouse model with muscle specific overexpression of human lipoprotein lipase (hLPL) as well as C2C12 murine myoblasts overexpressing LPL. hLPL facilitates the entry of lipids into the muscle tissue by

the catalysed hydrolysis of lipoprotein triglycerides or unesterified free fatty acids (FFA) associated with albumin. Uptake of esterified lipids, which are not hydrolysed in the plasma, is also influenced by LPL, a process which might not involve LPL enzymatic activity (Goldberg et al., 2009). When fed a normal chow, muscle-specific hLPL expression enhanced muscle lipid content in these animals. Analysing the physical endurance of these transgenic mice showed that these animals had a 6-fold decreased physical endurance compared to wild type (WT) mice. This decrease in physical endurance was accompanied by an increase in muscle lipid content in hLPL transgenic mice as well as increased protein degradation and lipoapoptosis. These findings coincide with the decreased regenerative capacity after cardiotoxin injection into skeletal muscles of hLPL transgenic mice. Another model system used in this study is the murine myoblast cell line C2C12, representing a frequently used model organism in the field of myogenic research. Findings show that the hLPL -overexpressing C2C12 cells exhibit a decrease in myoblast fusion as well as the expression of myogenic markers indicating a reduction in the overall differentiation potential. Both model organisms used in this study reveal the important role of free fatty acids (FFA) and skeletal muscle lipid infiltration, linking lipid-associated changes with impaired myogenic potential and muscle function as well as decreased regenerative capacity, eventually resulting in the development of severe myopathies (Tamilarasan et al., 2012). Another study, conducted by D'Souza et al. investigates the impact of diet-induced obesity (DIO) on skeletal muscle regenerative capacity and functionality of the muscle satellite cells. Comparing animals fed a 60% kcal high-fat diet versus animals on a standard chow for 8 weeks they analysed muscles from mice subjected to cardiotoxin (CTX) induced injury. Not only do they report prolonged necrosis in muscles following injury with DIO, but also collagen content is significantly enhanced. Using myosin3 as a marker for myofibre regeneration they further support their findings of delayed myofibre repair by quantifying regenerating fibre size from the two diet-groups. Although no difference in basal SC activation could be observed, external hepatocyte growth factor (HGF) induced activation showed impaired SC responsiveness in muscle fibres isolated from DIO mice. Furthermore, HGF expression following injury was found to be down-regulated in DIO compared to normal chow. MyoD expression patterns revealed a prolonged proliferative phase

in DIO muscles compared to control, supporting the findings of attenuated proliferation and disruption of SC function. This study provides further evidence for the decline of skeletal muscle health and function due to impaired SC function in obesity (D'Souza et al., 2015).

A recently conducted study by Xing Fu et al. subsidises the afore mentioned findings. In order to test the mediatory role of AMP-activated protein kinase (AMPK) inhibition found in obesity on SC function and impaired muscle regeneration an AMPK α 1 knockout model was used. Evidence suggests a pivotal role of AMPK α 1 for SC function and muscle regeneration. Following 3 months of a 60% high fat diet to induce obesity in a mouse model, results show reduced AMPK activity in muscles of obese animals. Additionally, CTX induced injury indicates that AMPK activation in satellite cells is negatively affected in DIO. Further comparison of muscle regeneration between diet groups confirms attenuated muscle repair and poorly restored fibre structure in obese mice compared to control mice after injury. Although isolated SC showed no difference in myogenic differentiation *in vivo* results reveal decreased expression of myogenic markers important for SC proliferation and differentiation, possibly linking diet-induced obesity with altered AMPK activity. AMPK α 1 KO mice were used to mimic AMPK inhibition as it can be observed in obesity. Results show attenuated muscle regeneration and lower basal satellite cell density in AMPK α 1 KO mice pointing towards a combined effect of reduced SC number and decreased myogenic differentiation. Moreover, the activation of AMPK in obese mice seems to partially rescue the phenotype and improved muscle regeneration after CTX induced injury. These recent results emphasise not only the impact of DIO on skeletal muscle function and regeneration but also provide a possible drug target to facilitate muscle regeneration in obesity (Fu et al., 2016).

1.2.4.5 Satellite cell function in obesity

An accumulating body of evidence suggests that obesity is tightly linked to a decreased capacity of skeletal muscle to regenerate, possibly due to altered satellite cell function. Obese mice showed severely impaired skeletal muscle regeneration following injury. Although muscle regeneration has not been studied

in detail for obese and type 2 diabetic humans, evidence exists which points towards the possibility of altered satellite cell function due to intramuscular lipid overload underlying impaired skeletal muscle maintenance and repair (Akhmedov and Berdeaux, 2013). Furthermore, low grade inflammation has been linked to alterations in skeletal muscle maintenance in rodent models of obesity, including leptin-deficient mice and obese Zucker rats, as well as in mice kept on a high-fat diet. It is a long-standing observation that, in obesity, not only do individuals show increased lipid infiltration in adipose tissues but also in non-adipose tissues such as the skeletal muscle. This so-called ectopic lipid deposition is partly a result from increased circulating plasma levels of fatty acids. Within the skeletal muscle, lipids can be localised in extramyocellular compartments between myofibres as well as intra-myocellular; inside the muscle cells (Sinha et al., 2002). In human subjects lipid deposition in the muscle has been associated with insulin resistance, suggesting that muscle weight itself is changed in obesity (Goodpaster et al., 2000, Leon et al., 2013). The effect of lipids on muscle function and performance is still an ongoing matter of investigation. Another important finding is the reduced regeneration and recovery of skeletal muscle mass and function in obese animal models (Hu et al., 2010, Nguyen et al., 2011, Tamilarasan et al., 2012). Considering the importance of satellite cells for effective muscle regeneration, it has been a matter of investigation whether lipid overload in skeletal muscle negatively impacts satellite cell function and hence leads to the observed reduced regenerative capacity after muscle injury.

1.2.4.6 Mitochondrial dysfunction in obesity

It is a long-standing theory that impaired mitochondrial function, due to altered fatty acid oxidation, leads to the development of insulin resistance. Previous studies suggest that obesity-related insulin resistance in skeletal muscle is linked to excessive mitochondrial β -oxidation (Koves et al., 2008). This finding is paralleled by the observation that mitochondria show an impaired switch to carbohydrate metabolism during the transition from fasted to fed in an obese environment (Koves et al., 2008). Results reported by a study from Petersen et al. showed that in the elderly population, a decrease in mitochondrial oxidative

capacity was accompanied by increased levels of triglyceride and insulin resistance in the muscle (Petersen et al., 2003). This mirrors the reported decrease in complex 1-linked respiration and β -oxidation (Bonnard et al., 2008). In line with this, results showed that genes such as PGC-1alpha and NRF1, involved in mitochondrial oxidative phosphorylation, were decreased in muscle tissue of pre-diabetic and diabetic patients (Mootha et al., 2003). Additionally, recent findings identified an increase in ROS production and altered mitochondrial biogenesis in the muscle tissue of high-fat fed mice (Bonnard et al., 2008). It is however still a matter of investigation if insulin resistance is the cause or rather consequence of mitochondrial dysfunction.

1.2.5 Experimental models of skeletal muscle regeneration

Different approaches to test satellite cell function and muscle regeneration have previously been conducted. Experimental approaches include the intra-muscular injection of myotoxic agents such as cardiotoxin (CTX), notexin (NTX) or barium chloride (BaCl_2), to induced muscle injury and subsequent regeneration in animal models (Hardy, 2016). Another commonly used experimental method to induce muscle regeneration is freeze injury (FI) induced muscle damage. It has been shown that out of all methods, the FI induced muscle damage is the most severe, with up to 96% of all satellite cells together with their surrounding being destroyed in the process. Following muscle injury, muscle regeneration takes place in sequential steps. First, inflammatory macrophages infiltrate the injured tissue and stimulate myogenic cell proliferation. Second, a switch from inflammatory M1 to anti-inflammatory M2 macrophages occurs, promoting muscle cell differentiation. At the same time, angiogenesis and connective tissue formation and remodelling occur (Arnold et al., 2007, Hardy et al., 2016). All methods, except FI, show no remaining muscle fibrosis 28-days post-injury. Inflammatory cells return to baseline levels in the CTX and BaCl_2 models, however, inflammatory cells have been shown to remain high even after 1-month post-injury, if the animals were treated with NTX or FI (Hardy et al., 2016).

Due to its reproducibility, animal models with myotoxic agent-induced injuries, are believed to be one of the most effective and accurate ways to study muscle

regeneration, especially in pathological conditions such as myopathies. Another approach to study muscle regeneration in regards to satellite cell function, includes the isolation of individual muscle fibres and the development of satellite cell purification methods from skeletal muscle with subsequent *in vitro* cell culture. Isolation and culturing of individual fibres and their satellite cells is especially powerful in assessing the capacity of satellite cells to undergo activation, proliferation and differentiation (Motohashi et al., 2014, Neal et al., 2012) while at the same time, this approach can be used to analyse the expression profiles of specific transcription factors linked to the process of myogenesis (Alonso-Martin et al., 2016). A third approach to assess skeletal muscle regeneration includes the use of myogenic cell lines such as L6 or C2C12 myoblasts (Tamilarasan et al., 2012, Turpin et al., 2006). C2C12 cells, which are an immortalised cell line derived from a murine myoblast cell line, are used to study myoblast precursor proliferation and fusion, and are a useful myoblast cell model to understand the process and multiple molecular steps of myoblast lineage progression (Yaffe and Saxel, 1977, Sapoznik et al., 2018). Most commonly, differentiation in myoblast precursor cells can be assessed visually, due to the drastic change in morphology from individual fibres to mature myotubes. Furthermore, differentiation can be assessed using immunohistochemical or genomic approaches. Immunohistochemistry also allows for the calculation of the fusion index, which is defined as the ratio of nuclei number in myocytes with two or more nuclei versus the total number of nuclei per unit area (Bajaj et al., 2011, Sapoznik et al., 2018). However, although C2C12 cells are useful to gain mechanistic insight into muscle regeneration, they are distinct from primary human myoblasts which needs to be taken into account (Cheng et al., 2014).

1.2.5.1 Mouse models of obesity and induced muscle regeneration

Obesity is a world-wide increasing risk factor for the development of the metabolic syndrome, cardiovascular disorders, and type 2 diabetes mellitus, which is often accompanied by lipid deposition in adipose and non-adipose tissues such as the liver, pancreas, heart and skeletal muscle (Consitt et al., 2009, Saltiel and Olefsky, 2017).

Recently, accumulating evidence suggests that obesity impairs myogenesis, which is at least partially due to ectopic skeletal muscle lipid accumulation, altered satellite cell function and signalling (Akhmedov and Berdeaux, 2013, D'Souza et al., 2015). The world-wide rising incidence of obesity and the complexity of its related comorbidities are making animal models of obesity pivotal to develop new targets for novel preventions and treatments (Lutz and Woods, 2012). Animal models for obesity can be divided into two groups, one being based on underlying mutations and those animal models that show increased weight gain due to an obesogenic environment such as a high-fat diet maintenance. Various animal models exist to investigate diet-induced obesity in the presence of hyperphagia, altered energy metabolism and energy expenditure. Monogenic mutations in the leptin pathway have been targeted to model obesity in mouse and rat models such as the ob/ob mouse or db/db mouse which are leptin deficient. The s/s mouse as well as the Zucker and ZDF rat exhibit disrupted Signal Transducer and Activator of Transcription (STAT3) dependent signal of the leptin receptor and mutated leptin receptors, respectively. Furthermore, obesity models with a defective downstream signalling of the brain leptin receptor and monogenic models, such as the cholecystokinin 1 (CCK1) receptor knockout rat model, have been extensively studied, especially in the context of strong phenotypes including hyperphagia, decreased energy expenditure, hyperglycaemia and insulin resistance. Additionally, diet-induced polygenic models add to the body of obesity-models, including high-fat diets, overfeeding as well as age-related obese mice. The choice of animal model is dependent on the experimental setup, however, it is believed that the diet-induced obesity model is best to mimic the state of common obesity in humans, whereas genetically modified animals best serve the purpose of testing potential therapeutics (Lutz and Woods, 2012).

It has been demonstrated previously, that diet induced obesity in rodents is followed by a decline in muscle health and increased muscle insulin resistance (Shortreed et al., 2009), which might relate to impaired muscle satellite cell activation and muscle repair through alterations in hepatocyte growth factor signalling (D'Souza et al., 2015). The impact of obesity on muscle health and maintenance has been addressed in several animal models, including the leptin-

deficient $Lep^{ob/ob}$ mice and obese Zucker rats as well as diet-induced obesity rodent models (Nguyen et al., 2011, Peterson et al., 2008).

1.2.6 Calcium signalling

Calcium signalling is a key regulator of various pathways, including cell migration, bone formation as well as wound healing (Shannon et al., 2017, Blair et al., 2007, Tsai et al., 2015). In the muscle tissue Ca^{2+} acts to regulate contraction and relaxation, involving the troponin-tropomyosin complex system, the myosin light chain kinase mechanism and the directly initiated muscle contraction via binding of calcium ions to myosin. The calcium dependent excitation-contraction coupled process involves the binding of acetylcholine to its receptor, subsequently leading to the opening of voltage-gated sodium channels. The following depolarisation initiates a conformational change in the L-type calcium channels, which allows the release of Ca^{2+} from the sarcoplasmic reticulum. Intracellular Ca^{2+} can then bind to troponin C, which in turn forms a cross-bridge between actin and myosin filaments (Wakabayashi, 2015). The subsequent shortening of the sarcomeres is the fundamental basic principle leading to muscle contraction. Conversely, muscle relaxation is associated with a rapid decrease of intracellular Ca^{2+} levels. This is regulated via sarcoplasmic reticulum calcium-ATPase pumps by which calcium is transported back into the sarcoplasm (Agrawal et al., 2018). Dysregulation of the calcium homeostasis has been linked with serious diseases, including aging and heart failure (Berridge, 2003, Chandran et al., 2019, Weisleder et al., 2006). It is a well-known fact, that calcium signalling is very important for muscle contraction and relaxation, however its involvement in skeletal muscle differentiation and repair is still a matter of ongoing investigation.

Satellite cells play a crucial role in skeletal muscle development and regeneration. Therefore, it is of crucial importance to understand underlying signalling mechanisms that are activated upon injury and subsequent satellite cell recruitment to the injured muscle tissue. Calcium signalling has been extensively studied in the context of skeletal muscle development, homeostasis and regeneration (Tu et al., 2016). The importance of Ca^{2+} signalling is reflected by the broad spectrum of species where there is clear evidence for molecular

mechanisms with underlying Ca^{2+} participation in muscle development. This has been shown for example by inhibiting Ca^{2+} transients, which interferes severely with muscle development in *Xenopus laevis* embryos, leading to disrupted myofibril organisation and sarcomere assembly (Ferrari et al., 1996). Further studies investigating regulatory pathways of muscle differentiation reported the response of several calcium related genes to growth performance and differentiation (Park et al., 2018). Importantly, *in vitro* human myoblast differentiation is regulated by a rise in intracellular Ca^{2+} , induced by a change in the membrane potential (Konig et al., 2006). Konig and colleagues showed that human myoblasts differentiation, derived from single satellite cells, is characterised by the generation of an intracellular Ca^{2+} signal. This signal is further linked to the transcription factor Myogenin, which is a key regulator involved in myoblast fusion and differentiation (Konig et al., 2006).

1.3 Fatty acid transporters and binding proteins

CD36 is a fatty acid transporter and enhances cellular fatty acid uptake. CD36 expression has been supposed as a central link to obesity and obesity-related diabetes. CD36 can translocate to the mitochondria during muscle contraction, thereby increasing fatty acid oxidation. CD36 is an important regulator of fatty acid transport into the skeletal. However, in the absence of CD36, it has been shown that other fatty acid transporters, such as fatty acid transport proteins (FATPs) can be upregulated, suggesting a collaborative network in the maintenance of fatty acid metabolism. In line with this, previous studies reported an upregulation of FATP1 and FATP4 in mice lacking CD36 mediated fatty acid transport into the skeletal muscle (Sebastián et al., 2009). FATPs are a family of six related proteins important for fatty acid uptake and activation (Gimeno, 2007). They are highly conserved and can be found in all vertebrate and invertebrate species and have been reported to increase fatty acid uptake upon overexpression. FATPs can be found in basically all tissues with different expression patterns and tissue distribution (**Figure 1.3 and Table 1.3.1**). Their expression levels can be influenced by a variety of mediators involved in insulin signalling, exercise as well as inflammatory regulators such as $\text{TNF}\alpha$ and IL-1. FATP1 expression is especially high in white and brown adipose tissue, as well

as in skeletal muscle, heart and to a lesser extent in the lung, kidney and brain (Kazantzis and Stahl, 2012, Hirsch et al., 1998, Chabowski et al., 2008, Anderson and Stahl, 2013, Moullé et al., 2012). Although FATP2 has been shown to be expressed at high levels in the liver and kidney, the deletion of FATP2 in mice showed no obvious phenotype and no pathological alterations of the liver or kidney anatomy (Hirsch et al., 1998, Gimeno, 2007). Little is known about the function of FATP3, which is widely expressed in various tissues including lung, testes, liver, brain and endothelium (Anderson and Stahl, 2013). Recent evidence suggests a role for FATP3 in endothelial cell fatty acid metabolism but due to the lack of animal models targeting FATP3 its function *in vivo* has yet to be determined (Anderson and Stahl, 2013). Interestingly, FATP4 has been confirmed to be involved in the development of skin and hair. Given its high expression in the intestine, it has further been hypothesised to play a role in fatty acid uptake and absorption. However, mice overexpressing FATP4 displayed no difference in weight, intestinal lipid absorption nor faecal fat losses when fed a high fat diet. It has been suggested that FATP4 plays a role in early embryonic fat absorption with possible implications in adult dietary lipid uptake (Anderson and Stahl, 2013). FATP5, which is solely expressed in the liver, has been associated with hepatic triglyceride and fatty acid content and fatty acid synthase expression. FATP5 KO mice displayed reduced long-chain fatty acid (LCFA) uptake and redistribution of lipids from the liver to other tissues. More recently, FATP5 has gained a lot of interest in the context of Non-alcoholic fatty liver disease (NAFLD). Findings from studies in both mice and humans suggest a pivotal role of FATP5 in fatty acid uptake in the liver, suggesting FATP5 as a possible novel target for the treatment of NAFLD (Anderson and Stahl, 2013). FATP6 can be found primarily in the heart where it colocalises with CD36. FATP6 functions as a LCFA transporter and increases lipid uptake by the heart. Recent findings suggest an important role of FATP6 in the development of lipid-related cardiac disorders. The precise role of FATP6 is however still a matter of investigation as animal models targeting FATP6 have not been generated yet (Anderson and Stahl, 2013).

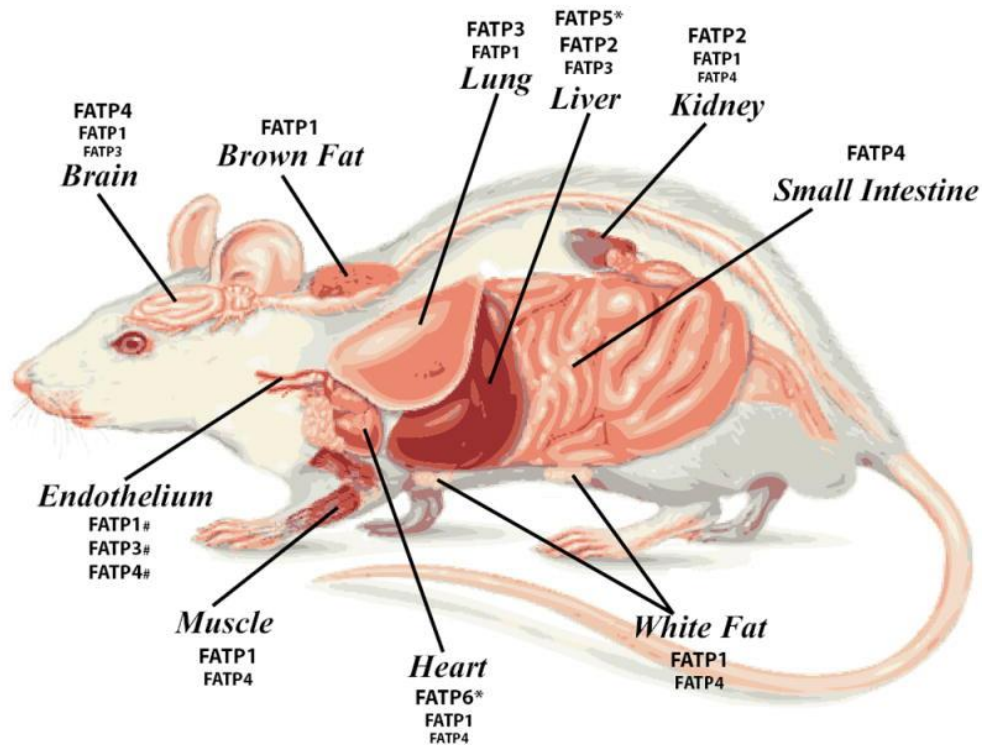


Figure 1.3: FATP expression profile. SLC27 family proteins, known as FATPs and their expression in different tissues in rodents. Schematic model of FATP1, 2, 3, 4, 5 and 6 tissue distribution. FATP5 is expressed only in the liver. Adapted from Courtney Anderson et al. 2013 (Anderson and Stahl, 2013).

Liver type fatty acid binding protein (L-FABP) is the only mammalian FABP that can transport lipids to membranes via aqueous diffusion. Previous studies revealed a partial translocation of LFABP to the nucleus and a potential interaction with PPAR α , further suggesting the regulation of certain genes involved in fatty acid metabolism. Moreover, L-FABP KO mice have been shown to be protected from hepatic steatosis on a high-fat diet or following fasting (Storch and McDermott, 2009). In addition, several G protein-coupled receptors (GPCRs) were identified as free fatty acid receptors (FFARs) with FFAR1 protein levels in the pancreatic islets associated to insulin secretion with potential therapeutic value for the treatment of type 2 diabetes (Ichimura et al., 2014). FFAR2 and FFAR3 are both receptors for gut microbiota-derived short-chain fatty acids (SCFAs) which have been suggested as potential therapeutic targets for metabolic disorders such as obesity (Ang et al., 2018). FFAR2 expression has be

reported in the intestinal tract and adipose tissue (Ichimura et al., 2014), whereas FFAR3 was found in the intestinal tract and to some extent in the sympathetic nerve involved in noradrenalin secretion (Ichimura et al., 2014). Current literature shows that FFAR4 is expressed widely in several tissues such as the intestinal tissue, adipose tissue, macrophages and pancreas suggesting multiple functions and has further been linked to the metabolic syndrome due to the development of obesity in FFAR4 KO mice (Ichimura et al., 2014). Amongst other fatty acid transporters, the peroxisome-proliferator-activated receptors (PPARs) are of fundamental importance in regulating lipid metabolism and energy homeostasis. The PPAR family of nuclear receptors consist of three members, PPAR α , PPAR γ and PPAR δ . Interestingly, out of the three PPAR members, PPAR γ has been identified as the master regulator of adipogenesis with hepatic PPAR γ expression shown to be markedly increased in several obese or diabetic mouse models. Further research suggests a tight link between PPAR γ expression in the liver and the development of liver steatosis (Wang, 2010). CD36 is a fatty acid transporter and enhances cellular fatty acid uptake. CD36 expression has been supposed as a central link to obesity and obesity-related diabetes. Not only does CD36 facilitate fatty acid uptake, it further enhances intracellular metabolism, i.e., esterification, suggesting a central role in fatty acid metabolism (Xu et al., 2013). In mice that lack CD36, fatty acid uptake is significantly impaired by heart, skeletal muscle and adipose tissue. CD36 mutations in rodent models were further linked to improved insulin sensitivity and protection from diet-induced obesity. Several stimuli such as muscle contraction or insulin signalling can recruit CD36 from intracellular stores to the plasma membrane and fatty acid uptake is enhanced. CD36 is expressed on taste bud cells of the tongue as well as in the digestive tract where it plays a key role in the formation of chylomicrons. CD36 deficiency is relatively common in the Asian and African population (2- 7%) with similar phenotypes as in rodents, including decreased fatty acid uptake in skeletal muscle and heart tissue but no relevant effect on fatty acid uptake in the liver (Goldberg et al., 2009, Hirano et al., 2003). CD36 mediated fatty acid uptake is involved in physiological and pathological pathways. How these pathways overlap and their regulation is still lacking in detail.

1.3.1 Tissue specific fatty acid uptake and transport

Gene	Tissue	Publication
FATP1	Muscle, Adipose tissue	(Hirsch et al., 1998, Anderson and Stahl, 2013)
	Heart	(Chabowski et al., 2008, Anderson and Stahl, 2013)
	Brain	(Moullé et al., 2012, Anderson and Stahl, 2013)
	Brown Adipose Tissue Kidney, Lung, Endothelium	(Anderson and Stahl, 2013)
FATP2	Liver	(Hirsch et al., 1998, Anderson and Stahl, 2013) (<i>Associated with nonalcoholic fatty liver disease</i>)
	Kidney	
FATP3	Liver, Testes	(Hirsch et al., 1998)
	Lung	(Anderson and Stahl, 2013)
	Brain, Endothelium	(Anderson and Stahl, 2013)
FATP4	Brain, Small Intestine, Endothelium, Muscle, Kidney, Adipose tissue	(Anderson and Stahl, 2013)
FATP5	Liver	(Hirsch et al., 1998, Anderson and Stahl, 2013)
FATP6	Heart	(Hirsch et al., 1998, Chabowski et al., 2008, Anderson and Stahl, 2013)
LFABP	Liver	(Storch and Thumser, 2010)
FFAR1	Pancreas (β -cells)	(Ichimura et al., 2014)
FFAR2	Intestine, Adipose tissue	(Ichimura et al., 2014)
FFAR3	Intestine	(Ichimura et al., 2014)
FFAR4	Intestine	(Ichimura et al., 2014)
	Adipose tissue Macrophages Pancreas	
PPAR γ	Adipose tissue, Brown adipose tissue, Liver	(Wang, 2010) (<i>Associated with liver steatosis</i>)
CD36	Heart, Skeletal muscle Adipose tissue, Taste buds on tongue Stomach Small intestine	(Goldberg et al., 2009)

1.3.2 Skeletal muscle fatty acid transport

Long-chain fatty acids (LCFA) are a major energy source for several tissues, including the skeletal muscle. First thought to be freely diffusible, it is now known that LCFA are being transported into many tissues by various fatty acid transport proteins. In the past, a number of different fatty acid transport proteins has been identified, including the plasma membrane fatty acid binding protein (FABPpm, 43 kDa), fatty acid translocase (FAT/CD36, 88 kDa) and selected fatty acid transport proteins (FATP1 and -4) which can all be found in the skeletal muscle tissue (Bonen et al., 1998). Recently, it has been shown that CD36 plays a key role in muscle fuel selection and muscle fatty acid oxidation due to its metabolically flexible expression, as it can be induced to translocate from the cytoplasm to the sarcolemma by stimuli such as insulin-stimulated activation of phosphatidylinositol-3-kinase (PI3K) as well as muscle contraction and the activation of muscle AMPK (Jain et al., 2015). More specifically it has been observed that acute physical stimuli induce CD36 translocation to the plasma membrane, whereas chronic stimuli, such as exercise training, pharmaceutical activation of PPAR δ and peroxisome proliferator-activated receptor gamma coactivator 1-alpha (PGC-1 α) overexpression lead to an increased expression of CD36 alongside with increased activity of mitochondrial fatty-acid oxidation (Jain et al., 2015).

Additionally, it has been shown that genetically induced alterations in CD36, influence the rate of fatty acid transport and oxidation in skeletal muscle. Interestingly, the observed CD36-dependent, facilitated fatty acid transport occurs independently of mitochondrial density and of the expression of fatty acid oxidation-related genes (McFarlan et al., 2012). It has therefore been suggested, that CD36 plays a crucial role in the regulation of skeletal muscle fuel selection during exercise, as well as during the adaptation of fatty acid oxidation in chronic metabolic stimulation such as endurance exercise. CD36 thereby allows for different regulation of substrate metabolism at rest and during exercise revealing its fundamental role in skeletal muscle metabolic processes.

1.3.3 Expression and biological function of CD36

CD36 -a class B scavenger receptor- is a heavily glycosylated 88 kilo Dalton (kD) integral membrane protein involved in the high-affinity uptake of long chain fatty acids into a diversity of different tissues and therefore contributes to fat metabolism and storage. For example, it has been shown that long-chain fatty acid uptake is facilitated by CD36 in muscle as well as in adipose tissue of mice and humans. Additionally, accumulating evidence correlates CD36 expression with several aspects related to fat metabolism, including oral fat perception, intestinal fat absorption and chylomicron production as well as fat intake and absorption and fatty acid utilisation by the muscle and adipose tissue. Not only does CD36 bind to fatty acids, it can also recognise numerous other lipid ligands such as oxidized phospholipids, diacylglycerol and cholesterol and further binds to naïve (high, low and very low-density lipoproteins; HDL, LDL, VLDL) and oxidized lipoproteins (oxLDL and oxHDL). Interaction with those lipid ligands has been shown to modulate CD36-dependent signalling pathways linked to angiogenesis, inflammation and metabolic regulation of fatty acid handling. More recent findings implicate CD36 in the regulation of cytosolic Ca^{2+} signalling, which can be both independent of or dependent on direct fatty acid interaction (Kuda et al., 2011, Sundaresan et al., 2013). Binding of CD36 to lipid ligands leads to increased free cytoplasmic Ca^{2+} which can further lead to the release of Ca^{2+} from intracellular stores coupled with calcium influx across the plasma membrane. The function of CD36 in regulating calcium signalling has been further implicated in its role in fat perception, chylomicron production and release of intestinal peptides during fat absorption.

Furthermore, due to multiple ligands -and signal transduction capabilities, CD36 plays numerous roles related to the immune response, inflammation, angiogenesis, atherogenesis and thrombosis. It has been shown that CD36 can bind to thrombospondin 1 and collagen and belongs to a group of highly conserved cellular adhesion receptors found –among other cell types- on platelets, immune cells, endothelial cells, adipocytes and myocytes (Pepino et al., 2014). CD36 has two intracellular domains, two transmembrane segments and one large extracellular domain, responsible for the binding of lipid ligands. One of the intracellular termini, the C-terminus, can associate to the Src tyrosine

kinase which is involved in many CD36-dependent downstream signalling pathways. Both the N- and C- termini are involved in the localisation of CD36 to membrane lipid rafts due to their palmitoylation sites. The three disulphide bridges of the extracellular domain located in the carboxyl-terminal half have been found to be important in the translocation of CD36 to the plasma membrane. Furthermore, posttranslational changes such as ubiquitination, phosphorylation and palmitoylation can modulate CD36 trafficking between the plasma membranes and intracellular compartments and therefore influences its ligand uptake or signalling function (Pepino et al., 2014). The abundant expression of CD36 has been shown in the proximal segment for the small intestine of mice and humans alike and reduced expression has been reported for the ileum and colon where it is likely to have a signalling function linked to chylomicron formation. Additionally, CD36 might facilitate the absorption of cholesterol in the intestine; important for optimal chylomicron formation (Pepino et al., 2014). To further study the involvement of CD36 in fatty acid uptake and its related signal transduction, many studies used sulfo-N-succinimidyl oleate (SSO), which irreversibly binds to CD36, inhibiting its function in various different cell types (Kuda et al., 2013).

Several studies identified the role of CD36 in high affinity fatty acid uptake and utilisation. Emerging evidence suggests an important role for CD36 for cellular fatty acid uptake and metabolism, which is correlated to the findings in CD36 deficient rodents and humans, revealing alterations in plasma lipid levels and susceptibility to the metabolic syndrome (Pepino et al., 2014).

1.3.3.1 CD36 deficient mouse models

Rodent models of obesity suggest that indeed, absence of CD36 protects mice from diet-induced adiposity and adipose tissue inflammation. Likewise, CD36 KO mice expressed decreased markers of adipose tissue inflammation, as well as macrophage and T-cell accumulation (Cai et al., 2012). This is paralleled by a study conducted by Koonen et al. in 2007, which associates the development of dyslipidemia with diet-induced obesity linked increased hepatic CD36 expression (Koonen et al., 2007). Similarly, middle-aged CD36 KO mice fed a high-fat diet

displayed decreased skeletal muscle fatty acid transport and lipid accumulation when compared to age-matched wild-type animals, suggesting a relevant role in delaying age-associated insulin resistance and metabolic disorders (Koonen et al., 2010). These findings are further supported by a study conducted by Gharib et al, suggesting a link between CD36 and oxidative stress in the heart in the context of obesity (Gharib et al., 2016). Leptin-CD36 double null mice used in this study showed markedly reduced cardiac steatosis, improved insulin sensitivity and glucose utilization, while displaying reduced fatty-acid uptake and oxidation. Furthermore, CD36 was shown to be an important regulator of Nicotinamide adenine dinucleotide phosphate (NADPH) oxidase-dependent reactive-oxygen species (ROS) production (Gharib et al., 2016). In line with this, studies in rodents suggest an important implication of CD36 in metabolic disorders, including obesity and its comorbidities (Cai et al., 2012). CD36 has been found to be expressed on a variety of different cell types, including platelets, macrophages, gastro-intestinal cells, muscle cells, hepatocytes, macrophages and adipocytes. Evidence supports its key role in fatty acid translocation and intracellular signal transduction in response to dietary fatty acid uptake, which is further linked to inflammation and lipid storage in an excess fat environment (Kennedy and Kashyap, 2011). Among many others, CD36 is involved in signaling pathways that have been linked to insulin resistance, atherosclerosis and thrombosis. Although several studies proposed a connection between CD36 deficiency and impaired cardiac fatty acid uptake, and altered lipid plasma levels, there is contradicting evidence showing that the lack of CD36 might be beneficial with an atheroprotective mechanism (Love-Gregory et al., 2011). Further evidence has been published which is in line with this finding, showing that increased CD36 expression in the liver is associated with NAFLD and elevated CD36 levels on monocytes have been linked to the development of insulin resistance (Love-Gregory et al., 2011).

It has further been recognised, that CD36 plays an important role in the development of the metabolic syndrome and associated cardiac diseases. Irreversible blocking of CD36 using small molecular weight chemicals or generalised CD36 KO showed that inhibition resulted in reduced arterial lipid deposition, decreased plasma triglyceride and glucose concentrations (**Table**

1.3.3.2), while at the same time, insulin resistance was improved. These results suggest that CD36 is inversely correlated with insulin sensitivity and plays a key role in the development of the metabolic syndrome due to its pathophysiological activity, making it a potential therapeutic target (Geloen et al., 2012). Additionally, there is evidence from the literature, increasingly implicating CD36 in the development of cardiac lipotoxic diseases due to redistribution from intracellular stores to the plasma membrane. Translocation of CD36 to the plasma membrane results in abnormal myocardial fatty acid uptake which is one of the earliest changes occurring in the development of obesity and type 2 diabetes (Glatz et al., 2013).

1.3.3.2 Blood lipid levels in WT and CD36 KO animals

	CD36 KO ND vs. WT ND	CD36 KO HF vs. WT HF
Total Cholesterol	↑0- 1.3fold (Febbraio et al., 1999, Goudriaan et al., 2003, Brundert et al., 2011)	No difference (Berger et al., 2019)
VLDL/IDL	↑1.4 fold (Masuda et al., 2009)	↑3fold (Masuda et al., 2009)
LDL	No difference (Masuda et al., 2009)	↑2-fold (Masuda et al., 2009)
TGs	↑1.3fold- 2.4fold (Goudriaan et al., 2005, Febbraio et al., 1999, Coburn et al., 2000, Masuda et al., 2009, Goudriaan et al., 2003, Hajri et al., 2002)	↑1.3fold (Goudriaan et al., 2005, Hajri et al., 2002)
FFA	↑1.4- 1.9 fold (Febbraio et al., 1999, Masuda et al., 2009, Goudriaan et al., 2005, Goudriaan et al., 2003, Hajri et al., 2002)	↑1.4-2fold (Masuda et al., 2009, Koonen et al., 2010, Hajri et al., 2002)
Glucose	↓0.5- 0.7fold (Goudriaan et al., 2003, Hajri et al., 2002)	↓1.8- 1.9 fold (Koonen et al., 2010, Hajri et al., 2002)

1.3.3.3 CD36 deficiency in humans

The CD36 gene is located on chromosome 7q11.2 and encoded by 15 exons of which exons 3 and 14 encode the N-terminal and C-terminal domains of the protein, respectively (Rać et al., 2007). CD36 genetic deficiency in humans was

first described in 1989, identified in a patient with refractoriness to multiple platelet transfusions (Tomiyama et al., 1990). Originally identified on platelets, CD36 absence has been found to be relatively common in Asian and African populations (Hirano et al., 2003). In humans, CD36 deficiency has been classified into two different types, namely type I CD36 deficiency, which lack CD36 expression on both monocytes and platelets, as well as type II CD36 deficiency, which is classified by positive CD36 expression in monocytes but no CD36 expression on platelets (Imai et al., 2002). Type I CD36 deficiency was found to be associated with defective fatty acid uptake into the heart (Furuhashi et al., 2004). Taking into account that fatty acids are the main source of energy for the heart, it has been suggested that CD36 may be related to the development of cardiomyopathies (Hirano et al., 2003). Human patients with type II CD36 deficiency had significantly higher plasma triglyceride levels, lower high-density lipoprotein cholesterol levels and higher plasma glucose levels than individuals with a normal CD36 expression (Hirano et al., 2003). Furthermore, type II CD36 deficiency was linked to insulin resistance in human patients. The CD36 type II deficient state was further correlated with increased fatty acid uptake into the liver, whilst being reduced in muscle, heart and adipose tissue (Hirano et al., 2003, Hames et al., 2014). CD36 deficient individuals also showed a postprandial diminished clearance of plasma lipids as well as an altered chylomicron formation (Love-Gregory and Abumrad, 2011). Interestingly, it was further observed that CD36 type I deficient patients show an increased risk for acute coronary syndromes and cardiovascular events, linked to the development of the metabolic syndrome and vasospastic angina (Love-Gregory and Abumrad, 2011, Kamiya et al., 2006).

1.3.4 Impact of high-fat diet feeding in CD36 deficient animal models

As a result of the epidemic progression of obesity worldwide, the prevalence of type 2 diabetes mellitus increased dramatically, coinciding with a variety of associated metabolic complications. Skeletal muscle insulin resistance plays a major role in the progression from obesity to the development of type 2 diabetes. Previous studies shed light on some of the underlying mechanisms leading to the pathogenesis of skeletal muscle insulin resistance. The scavenger receptor

CD36 has been first identified on platelets and was linked to metabolism in 1993 when its function as macrophage receptor for oxidized LDL and as an adipocyte receptor/ transporter for long-chain fatty acids (FAs) was discovered.

CD36 deficiency has been shown to inhibit FA utilisation in a diversity of tissues, including the heart, skeletal muscle, and adipose tissue. The ablation of CD36 in mice resulted in increased fasting plasma triglycerides (TG) and FA levels and a decrease in FA uptake, enhancing tissue insulin sensitivity as well as protecting against diet-induced obesity.

In muscle, contractions as well as insulin trigger the upregulation of CD36 levels. CD36 function is regulated by its subcellular distribution which varies between intracellular vesicles, the mitochondria membrane or the plasma membrane to which it translocates from intracellular stores to enhance FA uptake (Goldberg et al., 2009).

Given that lipid infiltration and accumulation in skeletal muscle tissue has been linked to skeletal-muscle insulin resistance, mechanisms involved in this lipid transport represent a great target for preventing high fat diet associated complications in obesity. In humans and in rodents it has been shown previously that high-fat diet induced skeletal-muscle insulin resistance is associated with an increased efficiency of fatty acid uptake into skeletal muscle. This facilitated fatty acid transport is at least partly regulated by the elevated protein expression of CD36, also involved in free fatty acid (FFA) uptake into skeletal muscle, heart and adipose tissue.

One of the first studies on the relationship between CD36 and insulin sensitivity was conducted by Goudriaan et al. in 2003 (Goudriaan et al., 2003). Examining the insulin-stimulated whole-body and tissue specific glucose uptake in CD36 deficient mice, they showed that whole-body and muscle-specific insulin-mediated glucose uptake is increased in CD36 KO mice when compared to WT littermates. Interestingly insulin failed to suppress endogenous glucose production in CD36 deficient mice compared to a 40% reduction in WT animals. They thereby showed that insulin sensitivity is impaired at the hepatic level, which is accompanied by increased liver TG content and decreased hepatic activation of protein kinase B when stimulated with insulin. They thereby not only link CD36

to the insulin-resistant syndrome but also describe the dissociation between increased muscle and decreased liver insulin sensitivity in CD36 KO mice.

Furthermore, Bonen and colleagues studied the involvement of the fatty acid translocase CD36 in regulating the uptake of long-chain fatty acids into muscle tissue (Bonen et al., 2007). Using a WT vs. a CD36 KO mouse model, they analysed the contribution of CD36 to fatty acid metabolism. Muscles of the CD36 KO mice showed normal insulin and 5-Aminoimidazole-4-Carboxamide Ribonucleoside (AICAR) sensitivity when compared to WT mice. Additionally, fatty acid oxidation key enzymes proved to be unaltered in CD36 deficient mice. However, when challenged, using an insulin perfusion of the hindlimbs, the net increase of fatty acid esterification increased three-fold compared to WT mice under the same conditions. Moreover, Bonen et al. showed that CD36 plays a critical role in regulating fatty acid oxidation when stimulated with AICAR. These results further highlight the necessity to examine the impact of CD36 on fatty acid metabolism during metabolic challenges. Furthermore, metabolic challenges proved to impair fatty acid metabolism and translocation of CD36 but not FABPpm (Han et al., 2007). Han and colleagues examined basal and stimulated fatty acid transporter translocation, fatty acid uptake and metabolism in lean and obese Zucker rats. In lean rats, translocation of CD36 and the plasma-membrane associated binding protein FABPpm from cytosol storage-vesicles to the plasma membrane has been observed due to stimulation with insulin or muscle contraction. These results are in line with facilitated fatty acid uptake into skeletal muscle as well as increased muscle palmitate esterification and oxidation. However, in obese Zucker rats, the basal levels of sarcolemmal CD36 (+33%) and FABPpm (+14%) are increased, along with fatty acid uptake (+30%) and esterification (32%). In contrast, fatty acid oxidation is reduced which highlights the disparity between fatty acid storage and utilisation. Insulin perfused muscles of obese Zucker rats not only fail to reduce fatty acid oxidation but also show impaired fatty acid uptake and esterification. Muscle contraction in obese Zucker rats, however, led to a normal increase in fatty acid uptake, esterification and FABPpm translocation. In contrast, CD36 translocation was impaired and fatty acid oxidation blunted, pointing towards impaired fatty acid metabolism at several levels. Han et al. thereby showed that obese Zucker rats are insulin resistant with

respect to CD36 translocation, fatty-acid uptake, esterification and oxidation and resistant to contraction-stimulated fatty acid oxidation as well as CD36 translocation. Interestingly, obese muscles are neither insulin nor contraction resistant at the level of FABPpm. It can be concluded that insulin and contraction-signalling pathways involved in CD36 plasmalemmal translocation are impaired in muscles of obese Zucker rats (Han et al., 2007).

Previously, sarcolemmal CD36 signalling has been linked to co-ordinated FA uptake and oxidation through AMPK. As increase in muscle energy needs activation of AMPK and CD36 translocation, a resulting rise in FA uptake and oxidation has been observed. Using different cell types, including myocytes, Samovski et al. explored the impact of membrane CD36 signalling on AMPK activation. For the first time, they describe CD36 as a key regulator in a protein complex composed of the liver kinase B1 (LKB1), AMPK, and the src kinase Fyn. Evidence suggests that CD36 acts as a negative regulator of AMPK, keeping it quiescent, while it mediates AMPK activation in the presence of fatty acids. In the absence of fatty acids, CD36 inhibits AMPK due to the Fyn dependent phosphorylation of LKB1 and its nuclear sequestration. When fatty acids interact with CD36, Fyn is dissociated from the protein complex, thereby allowing LKB1 to remain cytosolic and activate AMPK. Depletion of CD36 via transfection of short-interfering RNA (anti-mouse CD36) reveals increased expression of pAMPK and no further increase in activation after palmitate treatment since basal pAMPK levels are already high. CD36 deficient mice have been shown to exhibit increased AMPK activation in skeletal muscle and heart tissue, indicating that CD36 depletion activates muscle AMPK *in vivo*. These mice showed enhanced FA oxidation and decreased myocardial TG content. CD36 therefore plays an important role in controlling LKB1 dependent AMPK activation and thereby regulates FA homeostasis (Samovski et al., 2015).

A study performed by Smith et al. in 2007 further investigates potential lipid-related mechanisms of metformin (Met) and/or exercise in blunting the progression of insulin-resistant associated complications in a diabetic rat model (Smith et al., 2007). Lean and diabetic Zucker rats were analysed for impaired muscle insulin-stimulated glucose transport, increase in the fatty acid transporter CD36 and associated accumulation of muscle lipids such as ceramides and

diacylglycerol (DAG) when fed a high fat diet alone, or with Metformin, with treadmill exercise, or with both Metformin and exercise interventions. Results show the development of hyperglycaemia was significantly attenuated with all interventions, as was skeletal muscle CD36 abundance, and lipid content. Interestingly, improvements in insulin-stimulated glucose transport and Glut4 transporter expression could only be observed in interventions including treadmill exercise. All diabetic Zucker rats showed decreased FA oxidation and increased TG synthesis which remained unaltered by all interventions. However, modest increase was observed in the expression of proliferator-activated receptor gamma coactivator 1 alpha, citrate synthase, and beta-hydroxyl-CoA dehydrogenase activity in exercised Zucker diabetic rats. Their findings further emphasise skeletal muscle CD36 signalling as an important mechanism involved in preventing diet-induced progression of insulin resistance in skeletal muscle (Smith et al., 2007).

Taking into account the physiological changes that occur during the onset of middle age and the possible effects this might have on the development of insulin resistance, a study by Koonen et al. investigates whole-body glucose utilisation, fatty acid handling and triglyceride accumulation within skeletal muscle as well as diet-induced insulin resistance in a middle-aged mouse model. Showing that middle-aged mice have a lower metabolic rate compared to young mice, they suggest that their findings indicate an increased susceptibility to weight gain, obesity and metabolic diseases. They further investigate energy sensing pathways by analysing phosphorylated AMPK levels and downstream targets involved in mitochondrial β -oxidation. Both show a reduced phosphorylation status emphasising altered energy sensing pathways in middle-aged mice. Given that according to Koonen et al. whole-body glucose tolerance as well as fasted-insulin levels were not different in middle-aged mice compared to young mice they conclude that age-induced alterations in fatty-acid handling and energy expenditure might precede the development of skeletal muscle insulin resistance and metabolic diseases. However, when challenged with a high fat diet, middle-aged mice showed a significant increase in body weight and dramatically elevated insulin levels compared to young mice fed a high fat diet. Additionally, impaired whole-body glucose tolerance in middle-aged mice further supports

their increased susceptibility to develop insulin resistance (Koonen et al., 2010). Given that increased CD36-mediated fatty acid transport may lead to lipid accumulation and impaired insulin sensitivity in skeletal muscle of mice fed a high fat diet, it has been suggested that ablation of CD36 might represent a protective mechanism and target therapy.

Interestingly, CD36 ablation protects mice against diet-induced weight gain when fed a high-fat diet, which might be partly explained by their increased overall activity and heat production (Koonen et al., 2010). Although CD36 KO mice fed a high fat diet showed elevated serum free fatty acid levels, CD36 ablation resulted in a significant reduction in intramuscular lipid accumulation in a middle-aged mouse model. Moreover, reduced triglyceride content in CD36 KO mice was associated with improved whole-body glucose tolerance, lower fasting blood glucose levels, reduced fasting insulin levels and improved insulin-induced glucose clearance when fed a high fat diet compared to high fat fed wild-type (WT) mice. These results hint towards restored insulin sensitivity in the presence of a high fat diet by preventing skeletal muscle lipid accumulation via the ablation of CD36 (Koonen et al., 2010).

1.4 Liver morphology and function

1.4.1 Liver diseases in obesity

Although several tissues are involved in fatty acid metabolism, there are three that are quantitatively the most important. Amongst the adipose tissue and skeletal muscle, the liver resembles one of those tissues. In adipose tissue lipids can be stored and released into the blood stream, whilst skeletal muscle uses lipids as an energy source during oxidation (Frayn, Arner and Yki-Järvinen, 2006). As a key metabolic and insulin sensitive organ, the liver is both capable of storing and releasing fatty acids and interacts with adipose tissue as well as muscle tissue. In line with this, results by Doege et al. showed that for example FATP1 is strongly involved in the redistribution of fatty acids from adipose tissue and skeletal muscle to the liver in high fat diet conditions (Doege et al., 2006). Due to the well-established cooperation amongst the tissues, it is of crucial

importance to take changes in liver lipid-metabolism into account when studying skeletal muscle metabolic changes in a high fat diet setting.

The liver is a key player in lipid metabolism (Nguyen et al., 2008). Lipid metabolism in the liver involves both the synthesis of fatty acids as well as the release of lipids into the circulation. The liver is also capable of storing lipids, which eventually, can lead to accumulation of lipid droplets into the hepatocytes, resulting in hepatic steatosis. Lipid storage and content of hepatocytes is regulated by several cellular molecules involved in the facilitated fatty acid uptake, synthesis and esterification. The fatty acids can bind to receptors implicated in the regulation of genes involved in lipid metabolism (Nguyen et al., 2008). Non-esterified fatty acids uptake into the liver can occur via different mechanisms. Among those mechanisms are those via plasma-membrane associated proteins, including fatty acid transport proteins (FATP), fatty acid binding proteins (FABPpm) or fatty acid translocase (FAT)/CD36 regulated ways, as well as passive diffusion (Nguyen et al., 2008). Importantly, *de novo* lipogenesis, which is controlled by the lipogenic flux, and tightly regulated by hormonal and nutritional conditions, is of key importance to fat deposition. Adipose tissue as well as the liver are capable of *de novo* lipogenesis. In humans, the liver represents the main site of newly formed lipids; in rodents however, both the liver and adipose tissue play a key role in the process of lipogenesis (Patel et al., 1975, Pullen et al., 1990). After being emulsified by bile acids within the gastrointestinal system, dietary lipid molecules are resynthesised into triglycerides by enterocytes and packaged into chylomicrons. These chylomicrons enter the plasma and are taken up by various tissues such as adipose tissue and muscle tissue. Those triglycerides remaining in the chylomicrons are then further transported to the liver (Lowe, 2002). Under normal circumstances, lipids are passed on to the lymphatic system where they are transported via the thoracic duct inside chylomicrons and enter the blood stream via the left subclavian vein, thereby bypassing the portal vein into the liver (Alves-Bezerra and Cohen, 2017). Interestingly, the expression of CD36 has been associated with the formation of chylomicrons, revealing that lipids in CD36 KO mice accumulate in the small intestine showing a decreased transport of lipids to the lymphatic system (Drover et al., 2005). This might suggest a redirection of

absorbed lipids by the small intestine to the portal vein into the liver in CD36 deficient mice.

In the setting of increased dietary lipids, excess fatty acids are stored in the form of triglycerides, leading to hepatic lipid accumulation and very-light density lipoprotein (VLDL) overproduction, which are then secreted into the bloodstream (Kawano and Cohen, 2013).

1.4.2 Development of NAFLD

Non-alcoholic fatty liver disease (NAFLD) is one of the most common liver diseases, associated with obesity and type 2 diabetes (Sarwar et al., 2018). The healthy liver should contain little or no fat, with a mean fat-signal fraction (FSF) of 3.9 for women and 4.69 for men with normal BMI. However, in obesity liver tissue can accumulate large amounts of lipids which is frequently linked to the development of NAFLD. Paralleled by the incline in obesity is the prevalence of nonalcoholic liver disease which increases by a factor of 4.6 in those individuals with a body-mass index of at least 30 (Angulo, 2002). The fact that NAFLD leads to an increased morbidity and mortality makes interventional approaches and treatments key in the complex pathophysiology. Possible strategies include life-style changes as well as investigational drug development with a focus on pathways involved in lipid metabolism, inflammation as well as reducing fibrosis. Current treatment options include life-style and diet-changes with proven beneficial effects of exercise and a Mediterranean diet (Vilar-Gomez et al., 2015, Sofi et al., 2013). Currently no FDA-approved drugs exist to treat NAFLD, however the use of metformin and statins has shown to improve insulin resistance and cardiovascular events in NAFLD patients (Li et al., 2013, Athyros et al., 2010, Sarwar et al., 2018). However, it remains fact, that currently, no effective treatments for NAFLD exist, except changes in lifestyle with paralleled dietary interventions and weight loss (Alves-Bezerra and Cohen, 2017).

1.4.2.1 Impact of fatty acid transporters and binding proteins in the development of NAFLD

So far, although well established for heart and skeletal muscle, the role of CD36 in the development of NAFLD remains unresolved. CD36 overexpression has been associated with liver triglyceride content, however underlying pathological processes are still subject of investigation. Interestingly, liver specific deletion of CD36 has been shown to reduce hepatic lipid content and accumulation in a high-fat diet mouse model (Wilson et al., 2016, Coburn et al., 2000). Furthermore, recently published data suggests that in a whole-body knock-out of CD36 fatty acid uptake by the heart, skeletal muscle and adipose tissue is reduced, whereas liver fatty acid uptake remains unaltered (Coburn et al., 2000). Moreover, it has been shown that CD36 is a transcriptional target of peroxisome proliferator activated receptor (PPAR) gamma, which further emphasises the role of CD36 in the development of NAFLD (Tontonoz et al., 1998). It is however worth mentioning, that under normal circumstances, CD36 does not play a major role in fatty acid uptake into the liver. Fatty acid transport into the liver is mostly regulated via fatty acid transport proteins such as FATP2 and FATP5 (Hirano et al., 2003, Doege et al., 2006). FATP2 is highly expressed in liver and kidney, whereas FATP5 is almost exclusively expressed in the liver (Falcon et al., 2010, Doege et al., 2006).

Only second to the adipose tissue, the liver has the greatest capacity to store triglycerides in the form of lipid droplets (Walther and Farese, 2012). CIDE proteins such as Cidea have been shown to be localised to hepatocytes containing large lipid droplets and act in the process of lipid droplet formation and fusion (Wu et al., 2014). The upregulation of hepatic Cidea has been associated with diabetes in mice as well as obesity in humans. Furthermore, mice with PPAR gamma induced hepatic steatosis showed a robust increase of the expression of Cidea. This, once more, emphasises the complexity of hepatic lipid droplet formation linked to upregulation of Cidea. Although the association of Cidea to hepatic lipid accumulation is robust, the involvement of CD36 in this context is still lacking details regarding the development of NAFLD.

1.5 Aims and Objectives

Given the fact that the impact of obesity on satellite cell function and skeletal muscle regeneration is still poorly understood, the aim of this thesis was to characterise for the first time key aspects of skeletal muscle biology and regeneration in the context of obesity. Furthermore, this thesis sought to explore the role of the fatty acid transporter CD36 in the development of obesity related skeletal muscle regenerative impairment, altered satellite cell function as well as liver biology, focusing on the role of diet and oxidative stress.

It was hypothesised that:

- i. High-fat diet-induced obesity would have a negative impact on the metabolic and physiological homeostasis of skeletal muscle and liver tissue
- ii. CD36-deficiency attenuates the effect of a high-fat diet on skeletal muscle homeostasis, oxidative stress and stem cell function
- iii. Loss of CD36 protects from ectopic skeletal muscle lipid accumulation with a positive impact on skeletal muscle regeneration

These hypotheses were tested by addressing the following objectives:

- To characterise liver and skeletal muscle physiology and homeostasis (i.e. myofiber composition, lipid accumulation and redox homeostasis) in obese mice
- To establish whether CD36 plays a key role in diet-induced changes of skeletal muscle biology, CD36 deficient mice and WT mice were exposed to a high-fat diet with focus on genotype-specific alterations of skeletal muscle phenotype and metabolism in order to verify any protective effects indicative of improved skeletal muscle satellite cell function
- To examine if CD36 presents a possible therapeutic target for obesity-related impaired skeletal muscle regeneration

2 CHAPTER 2- General Materials and Methods

2.1 Practical Methods

2.1.1 Animals

CD36 deficient mice were generated by targeted homologous recombination in a C57Bl/6 background (Febbraio et al., 1999). Exon3, which contains the first 40 amino acids of CD36, was deleted entirely. Mice were kindly supplied by Prof. Khalid Naseem and bred in house. The mice used in this study were males to avoid hormonal variations associated with the female menstrual cycle. Additionally, previous results by DeNies et al. suggest that diet induced obesity alters skeletal muscle fibre types of male but not female mice (Denies et al., 2014). For these reasons and to ensure better comparability due to a larger body of data on male mice, this study used male mice to assess dietary induced changes in the skeletal muscle. The animals were housed in a temperature-controlled facility under standard conditions with 12 hours light/ dark cycle. At the age of 16-20 weeks, mice were randomly separated into two groups; receiving either a standard laboratory chow (EURodent Diet, 5LF 22%, LabDiet, St.Louis, US) or a high fat diet (SDS 824053 High-Fat diet, 45%, SDS Diets Grangemouth, Falkirk, UK) for 12 weeks to induce obesity adjusted from Elashry, et al. (Elashry et al., 2019) Mice were given ad libitum access to water and food. Initial body weight measurements were taken one week before the experiment and body weight changes were sequentially analysed on a weekly basis for the duration of the study. All experiments were in accordance with UK Animals (Scientific Procedures) Act 1986.

Table 2.1: Diet composition of standard laboratory chow and high-fat (HF) diet.

Component	EURodent Diet, 5LF5 22% (%gg ⁻¹)	SDS 824053 High-Fat diet, SDS Diets
Proteins, %	22.0	20.0
Fat (ether extract),%	3.5	45.0
Carbohydrate	55.0	35.0

2.1.2 Tissue sampling and freezing

After 13 weeks of dietary treatment, final body weight measurements were recorded. Mice were then sacrificed using a CO₂ overdose. Subcutaneous adipose tissue, heart, liver, kidney, Extensor Digitorum Longus (EDL), Tibialis Anterior (TA), Gastrocnemius (Gas), Quadriceps (Quad) and Soleus (Sol) muscle

were precisely dissected, weighed and immediately snap frozen in isopentane (2-methylbutane) which was immersed in liquid nitrogen to avoid freezing artefacts. Samples were stored at -80°C until further use.

2.1.3 Tissue embedding and cryosectioning

Skeletal muscle, heart and liver tissue samples were embedded in optimal compound temperature tissue mounting medium (Tissue OCT, VWR International S.A.S, France), immersed in 100% ethanol on dry ice to prevent samples from thawing. Samples were then either stored at -80°C or used for cryosectioning. OCT blocks containing embedded tissues were equilibrated to -21°C for 10- 15 minutes prior to cryo-sectioning and transverse sections of 10µm thickness were obtained and mounted on microscopy glass slides coated with Poly-L-lysine. Subsequently, the mounted sections were dried on the microscopy glass slides for 30 minutes at room temperature (RT) and stored at -80°C for further analysis. Skeletal muscle tissues were analysed for morphology and potential pathophysiological features as well as reactive oxygen species (ROS) production and assessed using histochemical or immunohistochemical staining procedures. Additionally, liver sections were prepared to analyse histological and potential pathophysiological features and were examined regarding lipid accumulation.

2.1.4 Cardiotoxin (CTX) induced muscle injury *in vivo*.

Tibialis anterior (TA) muscle injury was induced as previously described (Scully et al., 2019). Briefly, mice were injected with a total of 30µL, 50 µmol/L *Naja pallida* CTX (Latoxan, Valence France) into the TA muscle. Mice were humanely euthanized 5- and 10-days post-injury and the TA muscles were collected for subsequent immunohistochemistry. Immunohistochemistry was used to identify necrotic tissue and damaged fibres (H&E, IgG), as well as newly formed fibres (embryonic myosin heavy chain; eMHC; 1:200, SantaCruz, UK). Macrophage infiltration was further assessed by CD68 (1:200; SantaCruz, UK) immunofluorescent staining.

2.2 Technical Methods

For material details please refer to Section 9. Appendix

2.2.1 Histological analysis for lipid accumulation

Oil Red O (ORO, 1-[4-(Xzylazo)xylyl]-2-naphtol, 1-[2,5-dimethylphenylazo]phenylazo]-2-naphthol) staining was performed to examine lipid accumulation in liver tissue after 13 weeks of HF diet or standard laboratory chow. As previously described (Sfyri et al., 2018) ORO (Fisher Scientific, UK) working solution (75% ORO stock solution and 25% deionised water) was prepared fresh from the stock solution (250mg ORO powder in 50mL of 60% triethyl-phosphate) and filtered through a 45µm filter in order to remove precipitates. Mounted tissue sections on microscopy glass slides were equilibrated to RT dried and rehydrated using deionised water. Sections were fixed with 4% paraformaldehyde (PFA, Sigma-Aldrich, UK) and washed with deionised water. Fixed sections were then stained with Harris' haematoxylin (1:15 in PBS) for 5 minutes and subsequently rinsed with tap water. Following haematoxylin, eosin was added for 5 minutes and the slides were rinsed with tap water. The haematoxylin-eosin (H&E) solution was used to visualize cell membranes and nuclei (Sigma-Aldrich, UK). Subsequently, sections were incubated with the ORO working solution for 10 minutes and washed with running tap water to remove excess staining solution. Slides were mounted using Hydromount (National Diagnostics, UK) and immediately processed for image acquisition and analysis.

BODIPY® (4,4-Difluoro-1,3,5,7,8-Pentamethyl-4-Bora-3a,4a-Diaza-s-Indacne) is a fluorescent dye with a long-wavelength absorption that can be used to visualise and quantify neutral lipids. Upon binding with neutral lipids, BODIPY (493/503; D3922, ThermoFisher, UK) emits a green fluorescence signal (excitation wavelength 480nm, emission maximum 515nm). As previously described (Sfyri et al. 2018) mounted tissue sections on microscopy glass slides were equilibrated to RT dried and rehydrated with phosphate buffer (PBS), and incubated with 20µg/mL BODIPY for 30 mins and subsequently washed three times with PBS for 10 mins. All samples were mounted with fluorescent mounting medium (Dako, Denmark), supplemented with 2.5µg/ml 4,6-diamidino-2-phenylindole (DAPI,

Sigma-Aldrich, UK) and digital images were obtained using a Zeiss Axio Imager.A1, HBO 100 fluorescent microscope.

2.2.2 Histochemical analysis of relative mitochondrial activity

Succinate Dehydrogenase (SDH), also known as Complex II, is a mitochondrial enzyme complex, used as a marker of muscle fibre oxidative capacity and to study mitochondrial respiratory activity. It plays a part in both the citric acid cycle as well as the respiratory electron transfer chain (Zogby et al., 2017). Part of the citric acid cycle is the oxidation of succinate to fumarate which is catalysed by SDH. SDH can therefore be used as an indicator for the mitochondrial oxidative potential. Nitro blue tetrazolium (NBT) is used as an artificial electron acceptor, which upon reduction changes colour and can be monitored spectrophotometrically.

SDH staining was performed in EDL and Sol muscles. The SDH staining method was adapted from Matsakas et al. (Matsakas et al., 2010). In brief tissue sections on microscope glass slides were equilibrating to room temperature, dried and rehydrated with miliQ H₂O for two minutes. Samples were then incubated for 15 mins (Soleus) or 35 minutes (EDL) with a mix of NBT/PBS (12.23mM NBT, 0.99M KCN and 6.33M EDTA in 0.2M PBS, Fisher Scientific, UK) and Succinate buffer (500mM Sodium Succinate in 0.2M phosphate buffer) at a ratio of 1:3 in a 38°C incubator. During the electron transfer from Succinate to NBT which is catalysed by SDH, a change in colour occurs, representing SDH activity. Subsequently, the samples were fixed with 4% PFA for 15 minutes and washed with miliQ H₂O before mounting with Hydromount (National Diagnostics, UK) and immediately processed for further imaging. Digital images were obtained with a Zeiss Axioimager A.1 microscope (Zeiss, Germany) and an AxioCam MRm monochrome digital camera (Zeiss, Germany) and quantified manually using the Zen imaging software (Germany, Oberkochen). Calculated was the relative number of stained (positive) and unstained (negative) fibres for each muscle section.

2.2.3 Immunofluorescence

Immunofluorescence describes a technique via which tissues or cells can be stained using specific ligands or antibodies, that are either conjugated or indirectly labelled with a fluorescent dye, to visualise the distribution of an antigen of choice in physiological and pathophysiological conditions. Directly-conjugated antibodies allow for minimal manipulation of the cells or tissue and offer a time efficient method for routine staining procedures in the laboratory. Indirect staining, which uses specific antibodies that are not conjugated, requires an additional step, detecting the primary antibodies with a second, fluorochrome-conjugated antibody. Once the antibodies of a specific target are exposed to the sample of choice, they can be detected in a second incubation step using a secondary antibody specific for the primary antibody. This method provides both visibility as well as amplification of the signal from the primary antibody. Fluorescent imaging was performed using the Zen Axioimager A.1 microscope (Zeiss, Germany) together with the ZEN imaging software (Germany, Oberkochen). Filters used for the captured images were Alexa 488, Alexa 594, Alexa 633 and Alexa 355, depending on the excitation and emission of the particular secondary antibody.

Immunofluorescence and immunohistochemistry were performed using the following primary and secondary antibodies in table 2.2. (Donaldson, 2001, Duraiyan et al., 2012).

Table 2.2: Primary and secondary antibodies for immunohistochemistry

Antigen	Species	Dilution	Supplier, Cat Number
CD68	Mouse	1:200	Santa Cruz, sc-20060
Mhcl	Mouse	undiluted	DSHB A4.84
MhcIIA	Mouse	undiluted	DSHB A4.74
MhcIIB	Mouse	undiluted	DSHB BF.F3
Pax7	Mouse	1:200	Santa Cruz, sc-81648
MyoD	Rabbit	1:200	Santa Cruz, sc-760
Myogenin	Rabbit	1:200	Santa Cruz, sc-570
Alexa fluor 488 anti-mouse	Goat	1:200	Life Technologies A11029
Alexa fluor 488 anti-rat	Goat	1:200	Life Technologies A11006
Alexa fluor 488 anti-rabbit	Goat	1:200	Life Technologies A11034
Alexa fluor 594 anti-rabbit	Goat	1:200	Life Technologies A11037
Alexa fluor 633 anti-mouse	Goat	1:200	Life Technologies A20146

2.2.4 Single fibre isolation and culture

Satellite cells (SC's) are the stem cells of the skeletal muscle. They are located between the basal lamina and the sarcolemma of the muscle fibres and normally in a quiescent state, where they express -amongst others- the transcription factor Pax7. Upon activation the satellite cells start to upregulate another transcription factor, called MyoD. The expression of MyoD marks the re-entry of the satellite cells into the cell cycle and can be used to analyse proliferation. Following from proliferation, the satellite cells can undergo diverging fates. Upregulation of the transcription factor Myogenin marks them for differentiation and they become mature myoblasts, on the other hand they can upregulate Pax7, exit the cell cycle and go back to quiescence, thereby replenishing the stem cell pool of the fibre (Zammit et al., 2006).

The satellite cell expression profile was analysed in isolated muscle fibres, extracted from EDL and BB muscle as it has been previously described by Scully et al. (Scully et al. 2018). The EDL muscle was precisely dissected from tendon to tendon and immediately submerged in digestion medium (2mg/ml Collagenase type I; Sigma Aldrich, UK). After 3-5 hours of incubation of the muscle tissue in the digestion medium at 37°C and 5% CO₂, the muscle was transferred in a horse serum coated petri dish with DMEM medium (Dulbecco's Modified Eagles Medium, high glucose, Pyruvate supplemented, Thermo Scientific, UK) and the fibres were carefully separated by trituration using a wide-bore fire-polished glass pipette. After removing all debris and dead fibres the healthy fibres were either fixed in 4% PFA or transferred to horse serum coated dishes and cultured at 37°C and 5% CO₂ in growth medium (10% horse serum, 0.5% chicken embryo extract and 1% penicillin/streptomycin) for further analysis at 24, 48 and 72 (T24, T48 and T72) hours after the initial isolation.

2.2.5 Satellite cell isolation and proliferation

Satellite cells are the stem cells of the muscle. They are considered to be the major source of newly formed myofibres and of crucial importance during muscle growth and repair.

To isolate primary satellite cells from individual muscle fibres the EDL muscle was precisely dissected from tendon to tendon and immediately submerged in digestion medium (2mg/ml Collagenase type I; Sigma Aldrich, UK). Satellite cell isolation was adopted from a previous published protocol from Syverud et al. (Syverud et al., 2014). After 3-5 hours of incubation of the muscle tissue in the digestion medium at 37°C and 5% CO₂, the muscle was transferred in a horse serum coated petri dish with DMEM medium (Dulbecco's Modified Eagles Medium, high glucose, Pyruvate supplemented, Thermo Scientific, UK) and the fibres were carefully separated by trituration using a wide-bore fire-polished glass pipette. Subsequently, the fibres were incubated in 1mL 0.125% Trypsin-EDTA (in PBS) for 5 minutes at 37°C and 5% CO₂. Following the addition of 1mL Satellite cell Growth Medium (30% fetal bovine serum, 1.5% chicken embryo extract; FischerScientific, UK), the cell suspension was transferred into 50mL tubes and centrifuged at 16,000 xg for 5 minutes. The supernatant was discarded and the remaining cell pellet re-suspended in 3mL satellite cell growth medium. The cell suspension was then transferred into Matrigel-coated cell culture dishes (Matrigel; Corning, Bedford, UK, 354234; final concentration 1mg/mL), followed by three-day incubation at 37°C and 5% CO₂ in satellite cell growth medium. After three days the medium was changed to fresh satellite cell proliferation medium (10% fetal bovine serum, 0.5% chicken embryo extract; FischerScientific, UK) and subsequently changed every two days until the cells reached 80% confluency.

Table 2.3: Satellite cell growth medium and proliferation medium

Satellite cell Growth Medium (GM)	In DMEM with Pyruvate
L-Glutamine (4mM)	1%
Fetal bovine serum (FBS)	30%
Penicillin/Streptomycin (PenStrep, 100 U/ml penicillin and 100µg/mL streptomycin)	1%
Chicken embryo extract (CEE)	1.5%

Satellite cell Proliferation Medium (PM)	In DMEM with Pyruvate
L-Glutamine (4mM)	1%
Fetal bovine serum (FBS)	10%
Penicillin/Streptomycin (PenStrep, 100 U/ml penicillin and 100µg/mL streptomycin)	1%
Chicken embryo extract (CEE)	0.5%

2.2.6 Satellite cell differentiation

Cells that reached 80% confluency were further processed and differentiated towards myotubes using satellite cell differentiation medium (5% horse serum; FischerScientific, UK). Medium was changed every two days. Satellite cells were cultured for 4-6 days in differentiation medium until cell fusion and myotube formation was visually confirmed.

Table 2.4: Satellite cell differentiation medium

Satellite cell Differentiation Medium (DM) in DMEM with Pyruvate	
L-Glutamine (4mM)	1%
Horse Serum	5%
Penicillin/Streptomycin (PenStrep, 100 U/ml penicillin and 100µg/mL streptomycin)	1%

2.3 C2C12 cell culture

C2C12 cells are an established, mouse-derived myoblast cell line. They have been widely investigated as a model to study myogenesis, regarding myoblast cellular behaviour, such as proliferation, differentiation and migration, especially in the context of muscular dystrophies (Bajaj et al., 2011).

2.3.1 C2C12 proliferation

According to previously published methods by Scully et al. (Scully et al. 2018) C2C12 myoblasts were seeded at a density of 25,000cells per T25 flasks and cultured in growth medium (GM: Dulbecco's modified Eagle medium; supplemented with 1% L-Glutamine, 20% fetal bovine serum (FBS), 1% PenStrep; Thermo Scientific, UK) in standard conditions (37°C, 5% CO₂). Media

was changed every 48 hours until the cells reached around 80% confluency, for seeding into experimental conditions.

Table 2.5: Myoblast growth medium

Myoblast Growth Medium (GM) in DMEM without Pyruvate	
L-Glutamine (4mM)	1%
FBS	20%
Penicillin/Streptomycin (PenStrep, 100 U/ml penicillin and 100µg/mL streptomycin)	1%

2.3.2 C2C12 differentiation

When serum-deprived, C2C12 cells exit the cell-cycle and start to initiate cell fusion and differentiation, resulting in the formation of multi-nucleated myotubes (Bajaj et al., 2011). Once the proliferating C2C12 cells reached around 80% confluency, the growth medium was changed to myoblast differentiation medium (DM; Dulbecco's modified Eagle medium; supplemented with 1% L-Glutamine, 2% horse serum (HS), 1% PenStrep; Thermo Scientific, UK). The media was changed every 48 hours for approximately 4-6 days until cell fusion and myotube formation could be visually confirmed.

Table 2.6: Myoblast differentiation medium

Myoblast Differentiation Medium (DM) in DMEM without Pyruvate	
Horse Serum (HS; heat-inactivated)	2%
Penicillin/Streptomycin (PenStrep, 100 U/ml penicillin and 100µg/mL streptomycin)	1%

2.4 Cell culture maintenance

When the cells reach sufficient confluency (for C2C12 and satellite cells ~ 80% confluency) the GM is removed and 2.5mL of PBS was added to the T25 cell culture flask, in order to remove medium left overs. To detach the cells, 3ml of 0.25% Trypsin/EDTA (Thermo Scientific, UK) is added to the cells, which are subsequently incubated for 5 minutes at 37°C, 5% CO₂. Trypsin/EDTA as an enzyme of the pancreatic duct was first discovered by the German physiologist Wilhelm Kühne (Perutka and Šebela, 2018). It is now used as a cell dissociation reagent, to detach adherent cell-cultures. Trypsin catalyses a hydrolytic reaction,

breaking down peptide bonds. Following the trypsinisation step, the flasks are gently tapped against an open hand to help detaching the cells. Growth medium is added at a ratio of 1:1 to the trypsin/cell solution to stop the enzymatic reaction. The cell solution is then transferred into 50mL tubes and centrifuged at 16,000 xg for 5 minutes to pellet the cells. After removing the supernatant, the cell pellet is resuspended in 1mL fresh growth medium. The respective cell number can be calculated by using the haemocytometer (Neubauerkammer), a cell counting chamber with a defined volume capacity. The cell suspension is diluted by sequentially transferring 50µL cell suspension into 50µL PBS and transferring 50µL of the resulting solution into 50µL TrypanBlue, resulting in a final 1:4 dilution. The number of the cells is calculated using the following formula:

$$\frac{\text{Total number of cells} \times 10^4 \times 4(\text{dilution factor})}{4(\text{squares measured})} = \text{Total cell number per mL}$$

The appropriate cell number can now be calculated depending on the desired density. For 25,000 cells/T25 cell culture flask the appropriate volume was calculated accordingly.

$$\frac{25,000 \text{ cells}}{(\text{Total number of cells in } 1000\mu\text{L})} = \text{Volume (cell suspension)}$$

2.5 Immunohistochemistry

2.5.1 EdU cell proliferation assay

The cell proliferation rate of the satellite cells (SC) was analysed using the EdU (5-ethynyl-29-deoxyuridine) incorporation assay. Briefly, the cells were isolated and cultured for three days in SC growth medium. Cell proliferation is an important indicator for cell-cycle functionality and general cell health. Cell proliferation can be determined by adding EdU, which is a nucleoside analogue to thymidine and is incorporated into DNA during active DNA synthesis. The EdU Click Assay Kit can be used to stain cells during the replication phase. By

intercalating with the DNA, EdU emits a fluorescent signal which can then be detected using a fluorescent microscope. The proliferation rate was determined as described previously by Scully et al. (Scully et al. 2018) in isolated satellite cells from EDL muscle tissue. After the initial isolation the satellite cells were cultured until they reached approximately 80% confluency. Subsequently the cells were split at a density of 10,000 cells/well in a 24 well plate. EdU was used 24 hours later at 10 μ M for three hours; diluted in culture media (DMEM and Penicillin/Streptomycin). The fluorescent signal detection was performed by immunostaining with Dye Azide (BCK-EdU488, Baseclick GmbH Neuried, Germany).

Table 2.7: EdU proliferation assay kit

Product number	Dye	Excitation (nm)	Emission (nm)	Filter
BCK-EdU488*	6-FAM Azide	496	516	Green

* EdU Cell Proliferation Kit (BCK-EdU488, Baseclick GmbH Neuried, Germany)

Following a three-hour incubation with EdU the cells were fixed with 4% PFA, washed in PBS and permeabilized with Perm Buffer for 20 minutes. Washing was performed with wash buffer twice and a reaction cocktail was applied according to the manufacturer's instruction. The reaction cocktail contains the secondary antibody 6-FAM Azide to visualise the EdU signal. The cells were incubated for 30 minutes in the reaction cocktail, subsequently washed and mounted with DAPI (Sigma-Aldrich, UK) supplemented mounting medium and imaged using the Zen Axioimager A.1 microscope (Zeiss, Germany) and manually quantified using the ZEN imaging software (Germany, Oberkochen).

Table 2.8: EdU proliferation fluorescent signal detection

Material	Volume (μ L); (700 μ L total)
Deionized water	530.6
Reaction buffer (10X)	70
Catalyst solution	28
Dye Azide (10mM)	1.4
Buffer additive (10x)	70

2.5.2 Immunofluorescence for histological analysis of myofiber composition

Histological analysis of muscle specific fibre type distribution was performed using Myosin Heavy Chain (MHC) specific antibodies as previously published (Matsakas et al., 2013). Simultaneous staining of two different myofibre types was used to examine type IIA, type I and type IIB fibres and to subsequently identify type IIX fibres. Mounted EDL and Soleus muscle tissue sections on microscopy glass slides were equilibrated to room temperature, dried and rehydrated using PBS. Sections were then incubated with permeabilisation buffer (Triton X-100 in PBS; Sigma Aldrich) and further incubated with wash buffer (5% fetal bovine serum, 0.05% Triton X-100, 0.1% Sodium Azide; Sigma Aldrich) to increase cell permeability and reduce unspecific binding of the antibodies. Primary antibodies MHCII:A4.74 IgG (DSHB, 1:2), type IA MHC I:A4.84 IgM (DSHB, 1:1) and type IIB MHC IIB:BF.F3 IgM (DSHB, 1:1) were individually added on the tissue (undiluted) and incubated over night at 4°C. Firstly, primary antibody against type IIA fibres was used on the sections. After an overnight incubation the sections were washed with wash buffer and incubated for one hour at RT with the Alexa Fluor 488 antiMouse IgG (A11029; 488nm) secondary antibody to visualise type IIA fibres. Secondly, wash buffer incubation for 10 minutes was used before applying the second primary antibody against type IIB or type I. After another over-night incubation Alexa 633 antiMouse IgM (A21046; 633nm) was added for one hour at RT and used to identify type IIB or type I fibres. Slides were mounted using DAPI-supplemented mounting medium (Sigma-Aldrich, UK) and then proceeded to image capturing.

Pictures were taken and analysed using the Zen Axioimager A.1 microscope (Zeiss, Germany). Quantification of the fibre type composition was performed manually using the ZEN imaging software (Germany, Oberkochen). Unstained muscle fibres negative for either type IIB, type IIA or type I MHC were considered type IIX fibres and calculated via subtraction of positively stained fibres from the absolute amount of fibres.

Table 2.9: Primary and secondary antibodies for myofibre immunofluorescence

Primary Antibody			
Code	Fibre Type		Antibody
A4.74	IIA		IgG
A4.84	I		IgM
BF.F3	IIB		IgM

Secondary Antibody (Alexa Fluor)				
Code	Antibody		Emission	Dilution
A11029 (type IIA)	Goat	AntiMouse IgG	488nm	1:200
A21046 (type I and IIB)	Goat	AntiMouse IgM	633nm	1:200

2.5.3 Satellite cell activation pattern in cultured myofibres by immunofluorescence

Myofibre fixation was performed using 4% PFA (in PBS) in which the fibres were incubated for 15 mins at RT. After the removal of the excess PFA, the fibres were subsequently washed with PBS and stored at 4°C until further use. For the following immunofluorescent staining the excess PBS was removed and fibres permeabilised with permeabilisation buffer (Perm buffer; Triton X-100 in PBS; Sigma Aldrich) for 15 mins prior to the primary antibody incubation. Primary antibodies for Pax7 (Santa Cruz), MyoD (Santa Cruz) and Myogenin (Santa Cruz) were diluted (1:200) and the fibres were incubated overnight at 4°C. On the following day the primary antibody was removed and after several wash steps with wash buffer (Triton X-100, 4% PFA, Sodium Azide Solution; Sigma Aldrich) the appropriate secondary antibody Alexa Fluor was added and incubated for one hour at RT in the dark. Secondary antibodies were added individually and fibres were washed in between with wash buffer to avoid unspecific binding. Followed by a final wash step in wash buffer the fibres were transferred to glass microscopy slides and mounted with DAPI (Sigma-Aldrich, UK) supplemented mounting medium. Digital images were obtained with a Fluorescent imaging was performed using the Zen Axioimager A.1 microscope (Zeiss, Germany) and manually quantified using the ZEN imaging software (Germany, Oberkochen).

Table 2.10: Primary and secondary antibodies for satellite cell immunofluorescence

Primary Antibody		
Code	Timepoint after the isolation (T0-T72)	
Pax7 sc-81648	T0	Pax7 mouse monoclonal IgG
Pax7 sc-81648; MyoD sc-760	T24 and T48	Pax7 mouse monoclonal IgG MyoD rabbit polyclonal IgG
Pax7 sc-81648; Myogenin sc-576	T72	Pax7 mouse monoclonal IgG Myogenin rabbit polyclonal IgG

Secondary Antibody (Alexa Fluor)			
Code	Antibody	Emission	Dilution
A11029 (Pax7)	Goat AntiMouse IgG	488nm	1:200
A21046 (MyoD and Myogenin)	Goat AntiMouse IgM	633nm	1:200

2.6 Immunofluorescence of isolated satellite cells

Satellite cells were isolated, proliferated and differentiated according to the Method section 2.2.5 and 2.2.6. Following cell fixation for 15 minutes using 4% PFA (in PBS), excess PFA was removed and the cells were washed in PBS 2 x 5 minutes. For the following immunofluorescent staining the excess PBS was removed and the cells permeabilised with permeabilisation buffer (Perm buffer; Triton X-100 in PBS; Sigma Aldrich) for 15 mins prior to the primary antibody incubation. Primary antibodies for differentiated myotubes was Myogenin (Santa Cruz), diluted (1:200) and incubated overnight at 4°C. On the following day the primary antibody was removed and after several wash steps with wash buffer (Triton X-100, 4% PFA, Sodium Azide Solution; Sigma Aldrich) the appropriate secondary antibody Alexa Fluor was added and incubated for one hour at RT in the dark. Followed by a final wash step in wash buffer the cells were co-stained with DAPI (Sigma-Aldrich, UK) supplemented mounting medium. Digital images were obtained with a Fluorescent imaging was performed using the Zen Axioimager A.1 microscope (Zeiss, Germany) and manually quantified using the ZEN imaging software (Germany, Oberkochen).

2.7 Digital imaging and analysis

Images were taken using a Zeiss Axioimager A.1 microscope (Zeiss, Germany) and the AxioCam MRm camera (60N-C 1" 1,0 x 426114, Zeiss, Germany) to perform fluorescent and bright field (BF) imaging. Different objective lenses with x5, x10, x20 and x40 magnification were used to obtain images. For the fluorescent images the four different filter sets used were 1.DAPI, 2.GFP (Alexa488), 3.Cy3 (Alexa594), 4.Cy5 (Alexa633). For phase contrast pictures channel 5.DIC and for bright field images channel 6.BF were used. Quantification and analysis were performed using the ZEN imaging software (Germany, Oberkochen). For image acquisition, processing and analysis the ZEN 2 (blue edition) was used. The ZEN software was further used to improve the contrast, brightness and colour adjustment as well as for noise suppression and enhancing sharpness. Interactive measurements can be performed to acquire multi-channel images using the ZEN 2 software.

Table 2.11: Excitation and Emission of Dyes

Antigen	Excitation	Emission
DAPI	340	488
Alexa Fluor 488	496	519
Alexa Fluor 594	590	617
Alexa Fluor 633	632	647

2.8 Protein extraction and Immunoblotting

2.8.1 Tissue homogenisation and protein extraction

Protein extraction was performed by homogenisation of the tissue submerged in RIPA lysis buffer containing 1% v/v Nonidet P 40 substitute (NP-40, Sigma Aldrich, UK), 0.1% w/v SDS (Fisher Scientific, UK) and 0.5% w/v sodium (in PBS). Pre-cooled RIPA buffer (1mL) was added to the frozen tissue (approximately 50mg) and homogenised with an IKA Ultra-Turrax T-25 (Sigma Aldrich, UK) for 30 to 40 seconds at 18,000 x rpm. Once completely homogenised, the samples were centrifuged at 4°C for 15 minutes at 14,000 x g. The supernatant was then diluted 1:5 in RipA buffer and protein quantification is performed using the Pierce BCA protein assay (ThermoFisher Scientific, USA) and a BSA standard. For the BSA standard a serial dilution is performed from a 2mg/mL BSA stock solution in order to quantify the protein concentration from the tissue samples. Sample and

standard are pipetted into a 96 well plate and the working solution is added. Due to an alkaline environment Cu^{2+} is reduced to Cu^{1+} , resulting in a colorimetric detection due to bicinchoninic acid (BCA).

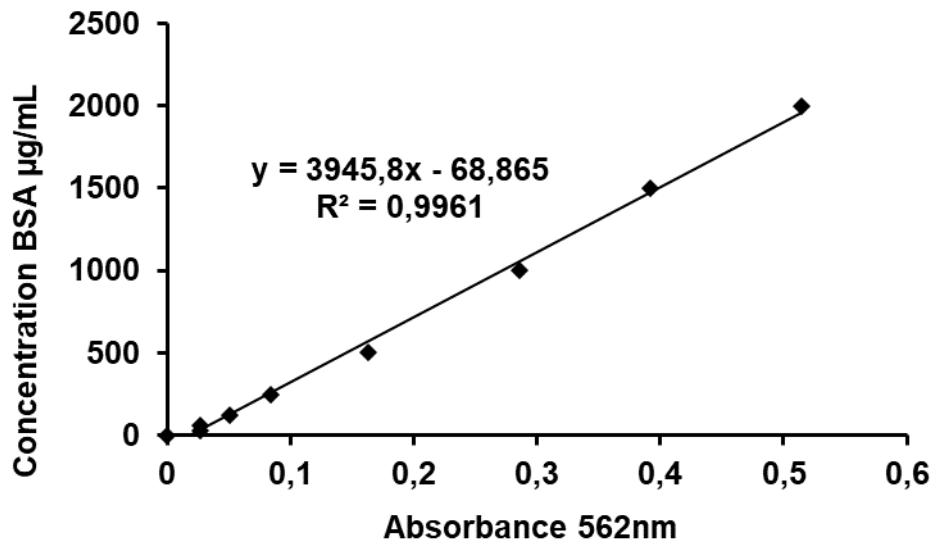


Figure 2.1 Representative standard curve of BSA concentration measurement (range 20- 20,000µg/mL)

The purple reaction product can then be measured using the almost linear absorbance for a protein concentration between 20-2,000µg/mL. Protein extracts were diluted 1:5 in RIPA buffer and assayed along with the BSA standards. After an incubation of 30 minutes at 37°C the absorbance can be measured at 562nm in the TECAN M200 plate reader (Tecan Trading AG).

2.8.2 SDS Page

Protein extracts (30µg) were diluted 1:1 with Laemlli's buffer (0.025M Tris-HCl, 20% glycerol, 0.002% bromophenol blue, 4% w/v SDS and 10% 2-mercaptoethanol; Fisher Scientific, UK) and boiled at 95°C for 10 minutes to break apart disulphide bonds and denature proteins for separation by their molecular weight. In order to separate the proteins, a resolving gel with 0.1% SDS is used. The gel is left to solidify for one hour, and a stacking gel is prepared to be poured on top of the resolving gel. After 20 minutes the gel is completely solidified and can be used to load the samples.

Table 2.12: Composition of the resolving and stacking gel used for SDS page

Resolving gel (10%)	
Compound	Amount for 2 gels
dH ₂ O	6.48mL
1.5M Tris 8.8 (Buffer 1)	4mL
30% Acrylamide	5.3mL
APS (10%) 0.1g in 1mL dH ₂ O	100 μ L
TEMED	10 μ L

Stacking gel (3%)	
Compound	Amount for 2 gels
dH ₂ O	4.87mL
0.5M Tris 8.8 (Buffer 1)	1.87mL
30% Acrylamide	750 μ L
APS (10%) 0.1g in 1mL dH ₂ O	100 μ L
TEMED	10 μ L

The gel was secured in a casting stand and subsequently placed into the electrophoresis module assembly (Mini Protean Tetra Cell Tank; Biorad, UK) and submerged in running buffer (25mM Tris Base, 192mM Glycine, 0.1% SDS). Together with a molecular weight marker (10- 250 kDa, Fisher Scientific, UK) the samples were loaded into the pockets of the gel. The samples were separated using electrophoresis at 100 Volt for 120 minutes. Once complete, the gel is removed from the glass plates and the protein can be transferred via wet blotting.

2.8.3 Protein transfer by Wet Blotting

The gel is placed in-between foam pads and blot paper, which are both soaked in Transfer buffer (25mM Tris base, 192mM glycine and 20% methanol). A polyvinylidene membrane (Amersham Hybond 0.45 μ m PVDF) was activated by the addition of methanol and subsequently submerged with Transfer buffer for 5 minutes. Inside a holder cassette, the methanol-activated PVDF membrane was placed onto the gel and between the blot papers and foam pads. The holder cassette was placed into a Mini Trans-Blot Module (Biorad, UK) and an electric current of 100 Volt for 80 minutes is used to transfer the proteins from the gel onto the PVDF membrane. After the transfer of the proteins onto the PVDF membrane, an incubation for 45 minutes in 5% non-fat milk (in TBS-Tween buffer;

150mM NaCl, 20mM Tris Base, 0.1% Tween 20 and pH 7.6; Sigma Aldrich and Fisher Scientific, UK) was used to block unspecific binding sites. Subsequently, the membrane is incubated at 4°C overnight with the primary antibodies for 3NT or 4HNE (in 2% milk or 2% BSA in TBS). Following the incubation with the primary antibodies, the membrane is washed with TBS/0.1% Tween for 4x5 minutes and incubated with polyclonal anti-mouse IgG secondary antibody for one hour (1:10,000, in TBS/0.2% Tween and 0.01% SDS). Following a wash step in TBS/0.1% Tween for 4x 5 minutes and 5 minutes in TBS alone, the bands were visualised using Licor or an X-ray film (chemiluminescence) by adding ECL1 (10% Tris Base pH 8.8, 0.25mM Luminol and 0.45mM P-Coumaric acid in 88.6mL deionised water) and ECL2 (10% Tris Base pH 8.8, 0.064mL 30% H₂O₂ in 90mL deionised water) in a 1:1 ratio to the membrane. The densitometric analysis was performed using ImageJ software (NIH, USA). The levels of protein were expressed relative to the signal of β tubulin.

2.8.4 Immunoblotting for oxidative protein modification

2.8.4.1 Assessment of protein adducts

Reactive oxygen species can cause specific structural modifications in proteins, leading to alterations in their properties and function. Tyrosin nitration (TYR) to 3-Nitrotyrosine (3NT) is catalysed by Peroxynitrite (PN) and the resulting posttranslational nitration of proteins has been used as a marker for reactive oxygen species (ROS) and oxidative stress. Increased posttranslational protein modification due to the addition of nitro-groups has been associated with aging as well as mechanisms regarding neuropathological diseases such as Alzheimer's disease (Swomley et al., 2014). The nitration of protein tyrosine residues to 3NT is a useful biomarker to assess ROS production and indirectly measure oxidative stress. Protein nitration (3NT; Cayman, USA) was analysed by using specific antibodies, determined by immunofluorescence. Furthermore, 4HNE (4HNE, R&D, UK), which is one of the most common and reactive carbonyl-adducts generated during the process of polyunsaturated fatty acid oxidation, was used as a marker of protein modification. 4HNE protein adducts are linked to dysregulation of the redox homeostasis and cellular stress signalling. Protein was extracted from gastrocnemius muscle and protein content was

assessed using the BCA assay according to protocols on section 2.7.1. For the immunoblotting the following antibodies were used:

Table 2.13: Primary and secondary antibodies used for wet blotting

Primary and secondary antibodies			
3NT	Mouse	1:500	Santa Cruz 32757
4HNE	Mouse	1:1,000	R&D Systems MAB3249
β tubulin	Mouse	1:1,000	EMD Millipore, 05-661
HRP Conjugated anti-mouse	Goat	1:1,0000	Sigma Aldrich, A9044

2.9 Thiobarbituric acid reactive substance (TBARS)

Thiobarbituric acid-reactive substance (TBARS) levels have been associated with oxidative damage and represent a useful tool to assess oxidative stress and the overall impact on the redox homeostasis (Dawn-Linsley et al., 2005). Due to its stable form the TBARS assay is a frequently used assay to measure malondialdehyde (MDA); a by-product of oxidative deterioration of lipids (Almroth et al., 2005). TBARS expression as an indicator for oxidative protein modification and oxidative stress in skeletal muscle tissue. Briefly, protein extracts from gastrocnemius muscle were diluted 1:5 in RIPA buffer and a serial dilution (1:10) of MDA in RIPA lysis buffer was prepared. After adding equal volumes of protein sample (20 μ L) and SDS to all samples, 500 μ L of TBA Buffer was added in each tube and the samples incubated at 95°C for an hour. Samples were cooled down and centrifuged at 3,000 x rpm for 15 minutes at RT. Subsequently, 100 μ L of supernatant were transferred into a 96 well plate. The fluorescence signal in a TECAN M200 (Excitation 530nm, emission 570nm) plate reader was used to calculate the MDA concentration.

2.10 Dihydroethidium (DHE) assay for reactive oxygen species

Due to their highly reactive character, free radicals are difficult to measure directly. Dihydroethidium (DHE) can form a fluorescent product as a result of

redox reactions, detecting superoxide ($O_2^{\cdot-}$) products (Dikalov and Harrison, 2014). Upon the reaction of DHE with superoxides the two-electron oxidation product ethidium (E^+) is formed, which intercalates with the DNA, yielding a red fluorescent signal (excitation 518nm; emission 605nm). DHE can therefore be used as a qualitative staining method to evaluate superoxide production in cells and tissues. DHE staining was performed as previously published (Paolini et al., 2018). Briefly, the frozen tissue sections on glass slides were equilibrated to RT and rehydrated using PBS. For DHE staining in living cells, the cell cultures on glass cover slips were washed with PBS. Subsequently, the sections or cells were incubated with 10 μ M DHE (in PBS; ThermoFisher Scientific, USA) for 30 minutes at 37°C. The sections or cells were washed with PBS and mounted with DAPI containing mounting medium. Sections were imaged using a Zeiss Axioimager A1 microscope and an AxioCam MRm monochrome camera. Alexa 594 filters were used to visualize the DHE staining.

2.11 RNA isolation

Muscle, liver and cell RNA was extracted as previously described by Sfyri et al. (Sfyri et al. 2018), using the E.Z.N.A. total RNA kit I (Omega Bio-Tek, USA) according to the manufacturer instruction. Briefly, 50-100mg frozen gastrocnemius muscle or liver tissue were homogenised at 18,000x rpm with an IKA Ultra-Turrax T-25 (Sigma-Aldrich, UK) in 1mL of prechilled TRIzol (Fisher Scientific, UK). TRIzol is a monophasic solution of phenol and guanidinium isothiocyanate used to solubilize biomaterial and simultaneously denature proteins. The homogenised muscle was transferred to a fresh collection tube and 200 μ L of 100% chloroform was added, followed by vigorously shaking the samples. After a short incubation for two minutes at RT the samples were centrifuged for 15 minutes at 4°C, 12,000x g to cause phase separation, with protein being extract in the organic phase, DNA at the interphase and RNA remaining in the aqueous phase (Rio et al., 2010). The RNA containing aqueous phase was transferred into a fresh collection tube and 500 μ L/mL of 100% isopropyl alcohol was added for the precipitation of nucleic acids whilst samples were stored for 10 minutes at RT. The resulting mixture was then loaded onto a HiBind RNA Column with subsequent centrifugation of the samples for one

minute at 10,000x g. The flow-through was discarded and 500µL RNA Wash Buffer I added to the HiBind RNA Column and centrifuged at 4°C for one minute at 10,000x g. The flow-through was discarded and 500µL RNA Wash Buffer II was added to the HiBind RNA Column, followed by centrifugation at 4°C for one minute at 10,000x g. The flow-through was discarded and the procedure repeated once more. In order to dry the HiBind RNA Column before the RNA elution, a final centrifugation step at 4°C for two minutes at 13,000x g was performed. RNA was eluted by adding 20µL of ultrapure water to the HiBind RNA Column. The centrifugation was performed following an incubation at RT for one minute. Subsequently, the samples were centrifugation at 4°C for two minutes at 12,000x g. The concentration (ng/µL) and purity (A_{260}/A_{280}) of isolated RNA was determined by performing a NanoDrop spectrometric analysis (ThermoFisher Scientific, USA). The samples were stored at -80°C until use or further processed for DNase I treatment. In order to eliminate DNA contaminations of the samples a total amount of 10µg RNA of each sample was treated with 0.5U/µL DNase I, 10x DNase I buffer and ultrapure water reaching a final volume of 20µL.

Table 2.14: MasterMix with DNase I to eliminate DNA contaminations

Total RNA	10µg (X µL)
DNase I	5 µL (5U/ µL)
10x DNase I Buffer	2 µL
Ultrapure Water	to 20 µL

The mixture of RNA, DNase I, DNase I buffer and ultrapure water were transferred into a reaction tube and incubated for 30 minutes at 37°C in the ThermoCycler (ThermoFisher Scientific, USA). After 30 minutes, 2µL of 50mM Ethylenediaminetetraacetic acid (EDTA) were added in each tube followed by incubation in the ThermoCycler at 65°C for 10 minutes. RNA samples were kept on ice for the following cDNA synthesis.

2.11.1 cDNA synthesis

For the conversion of RNA to complementary DNA (cDNA) by reverse transcription the RevertAid H Minus First Strand cDNA Synthesis Kit

(ThermoFisher scientific, USA) was used as previously reported by Sfyri et al. (Sfyri et al. 2018) and according to the manufacturer's protocol. For each RNA sample a master mix was prepared, including 1 μ L of 100 μ M Oligo(dT)₁₈ Primer, 3 μ L of ultrapure water to which a volume of 8 μ L from each RNA sample was added.

Table 2.15: MasterMix composition for cDNA synthesis and reverse transcription

MasterMix for cDNA	8μL
DEPC H ₂ O	3 μ L
Oligo dTs	1 μ L
RNA template	8 μ L
Total	20 μ L

Additionally, the following master mix for the reverse transcription was used:

MasterMix for cDNA	1x
5x Reaction Buffer	4 μ L
RiboLock Rnase	1 μ L
10mM dNTP Mix	2 μ L
Ultrapure Water	to20 μ L
Revertaid H minus,	1 μ L (200 U/ μ L)
Reverse Transcriptase	

From the Reverse Transcription MasterMix 8 μ L were added to the RNA template containing mix, giving a final volume of 20 μ L. Followed by a short pulse spin, the reverse transcription was initiated using a Veriti thermal cycler (Applied Biosystems, USA), using the following cycle times and temperatures:

42°C	60 minutes
70°C	10 minutes

The individual reaction tubes containing the MasterMix for cDNA and the DNase treated RNA samples are then incubated in the Thermocycler for 60 minutes at 42°C and 10 minutes at 70°C. Upon completion of the cDNA synthesis the concentration ($\mu\text{g}/\mu\text{L}$) and purity (A_{260}/A_{280}) of the samples were quantified on a NanoDrop spectrometer (ThermoFisher Scientific, USA). After diluting the cDNA 1:18 in ultrapure water, the samples were stored at -20°C until further use.

2.12 Primer design

Target-specific primers were designed using the NCBI/Primer-Blast software. Primer-Blast is a tool to examine the potential targets by identifying the primers flanking regions of interest which are then searched against an appropriate nucleotide sequence database in order to design target-specific primers. The software supports placing primers based on exon/intron locations excluding single nucleotide polymorphism (SNP) sites in primers (Ye et al., 2012). In this thesis, primers were retrieved from commercial sources and listed in the Appendix.

Primers used in the present study had been verified previously for their efficiency using standard curves. In brief, CT values of different standard dilutions were plotted against the logarithm of input amount of pooled cDNA. A standard curve was generated using a dilution series of 6 different concentrations of the pooled cDNA with the slope of the standard curves indicating the efficiency of the real-time PCR. Ideally, the PCR product should double during each cycle, resulting in a 100% efficacy resulting in exponential amplification of the product (Kubista et al., 2006). Primer efficiency was calculated by the following formula:

$$\text{Efficiency (\%)} = (10^{\frac{-1}{\text{slope}}}-1) \times 100$$

The efficiency score was calculated as percentage. For this study, primers with a efficiency between 95%-110% were used.

2.13 Quantitative real time Polymerase Chain Reaction (PCR) assay

As a method to amplify a small number of cDNA copies with real-time analysis options we used the quantitative Real-Time (RT) Polymerase Chain Reaction (PCR), short RT-qPCR (RT-PCR). This technique makes use of the fluorescent

properties of the SYBR Green compound (Thermo Scientific, UK). Introduced in the early 1990's, SYBR Green has become one of the most popular approaches to detect and quantify gene expression levels in a variety of samples (Zipper et al., 2004). As a non-sequence specific, double-stranded DNA intercalating dye, SYBR Green can be used to reliably detect, at every cycle of the PCR, the amount of the newly formed PCR product (amplicon). The principle is, that upon intercalating with double stranded DNA, SYBR Green can be detected due to its green light emission ($\lambda_{\text{max}} = 520 \text{ nm}$). The amount of dye incorporated is proportional to the amount of amplified target gene (Ponchel et al., 2003, Fernández et al., 2006). The light intensity can therefore be used to measure the total amount of DNA that has been produced during repetitive RT-qPCR cycles to reach conclusions about different gene expression levels in the analysed sample size.

The MasterMix for the qPCR was prepared using SYBR Green (7.5 μL), Forward Primer (0.15 μL ; dilution 1:10), Reverse Primer (0.15 μL ; dilution 1:10), ultrapure water (3.2 μL) for each reaction well. Reactions were performed in a 96 PCR well plate (ThermoFisher Scientific, UK).

Table 2.16: MasterMix composition RT-PCR

PCR MasterMix	Each reaction well
SYBR Green	7.5 μL
Forward Primer (10 μM)	0.15 μL
Reverse Primer (10 μM)	0.15 μL
Ultrapure water	3.2 μL
cDNA template (derived from 3.68 μg RNA)	4 μL

For each sample two technical replicates were performed with an added volume of 4 μL of RNA template to each reaction well. Incubation time and cycles were adjusted appropriately.

Table 2.17: Incubation time and cycles for RT-PCR analysis

Holding Stage	50°C for 2min
	95°C for 10min
Cycling Stage	95°C for 15sec Denaturation
	61°C for 1min Annealing/Extension
Melt Curve Stage	95°C for 15sec
	60°C for 15sec
	95°C for 15sec

A single cycle was used for the holding stage, followed by 40 cycles for the cycling stage and another single cycle for the melt curve stage.

RT-PCR analysis and interpretation by the comparative CT method ($2^{-\Delta\Delta CT}$ method)

The $2^{-\Delta\Delta CT}$ method is a relative quantification strategy for quantitative real-time polymerase chain reaction (RT-PCR) data analysis. This method is extensively used for relative quantification of gene expression levels between samples using threshold cycles (CT) generated by the RT-PCR system. The threshold cycle is the cycle at which the fluorescent signal first reaches a certain amount (threshold) which is detected by the system and can be compared in between samples to draw conclusions about the relative gene amount in each well.

Detection of relative gene expression amongst groups was conducted by using baseline CT values from the relative amplification rate using the StepOne software V2.0 (Livak and Schmittgen, 2001). To correct for differences in between sample DNA/RNA amount, reference genes, so called housekeeping genes, were used as internal control. Popular housekeeping genes are genes such as glyceraldehyde 3-phosphate dehydrogenase (*GAPDH*), cyclophilin 1 (*Cyp1*), β -actin or *Hprt* which are equally and stable expressed in most tissues independent of treatment (Livak and Schmittgen, 2001). In this study the reference genes *Cyp* and *Hprt* (Appendix) were used to normalise the gene expression in all groups. Initially the difference between the reference gene and the target gene is used to calculate the ΔCT value according to the following publication (Livak and Schmittgen, 2001). Briefly, the CT value of the target gene (CT_{target}) is normalised

to the mean CT of the reference gene ($C_{t_{\text{reference}}}$) and the the calibrator sample ($C_{t_{\text{cal}}}$), according to following equation:

$$\Delta C_{t_{\text{sample}}} = C_{t_{\text{target}}} - C_{t_{\text{reference}}}$$

$$\Delta C_{t_{\text{cal}}} = C_{t_{\text{target, cal}}} - C_{t_{\text{reference, cal}}}$$

The $\Delta\Delta CT$ value is derived from the following equation:

$$\Delta\Delta CT = \Delta C_{t_{\text{sample}}} - \Delta C_{t_{\text{cal}}}$$

The basic assumption for the $2^{-\Delta\Delta CT}$ method is a PCR amplification efficiency of 100% across all samples. The relative gene expression of the reference gene is usually set to one, for the $\Delta\Delta CT$ is equal to 0 ($2^0 = 1$) and therefore the final result of the method is represented as fold change of target gene expression.

2.14 Seahorse XFp extracellular flux measurements

C2C12 myoblasts and isolated satellite cells were seeded at a density of 10,000 cells per well in 8-well XF plates. Cells were pre-incubated in DMEM medium supplemented with 10% horse serum, 0.5% chicken embryo extract and 1% Penicillin/Streptomycin for 24 hours. Prior to the experiment, sensor cartridges were hydrated with XF calibrate solution (pH 7.4), as recommended by the manufacturer's instructions and incubated at 37 °C in a non-CO₂ environment for 24 hours. The cell culture medium was replaced with assay medium containing 1mM sodium pyruvate and incubated for one hour in a non-CO₂ incubator. Oligomycin (1 μM final concentration), carbonyl cyanide 4-(trifluoromethoxy)phenylhydrazone (FCCP; 5 μM final concentration) and Antimycin (2.5 μM final concentration) were diluted in the assay medium and

loaded into ports A, B and C, respectively. The Seahorse XFp Analyzer (Seahorse Biosciences) was then used to measure the oxygen consumption rate (OCR) and extracellular acidification rate (ECAR) in real time. Baseline measurements of OCR and ECAR were taken before sequential injection of Oligomycin, FCCP and antimycin. After three basal assay cycles, Oligomycin was injected to inhibit the ATP synthase. Following three more cycles, FCCP was injected to measure maximal mitochondrial respiration by uncoupling ATP synthesis from electron transport. After another four more cycles, Antimycin was injected to measure the non-mitochondrial respiratory rate. Immediately after the measurement, the assay medium was aspirated and the protein concentration was measured by bicinchoninic acid assay (BCA; Pierce Biotechnology). The seahorse data was normalised to total protein (μg) and analysed using the Wave software from Agilent Technologies.

2.15 Statistical Analysis

Differences between two groups were detected by Student's *t*-test or non-parametric procedures in case that data were not normally distributed. Statistical significance in experiments comparing more than 2 groups was determined by two-way ANOVA (genotype x diet), followed by Tukey post hoc test. For the detection of differences in lipid size analysis as well as CSA, the Chi square (χ^2) test was performed. All significant differences ($p < 0.05$) are given in the figures and/or figure legends. Statistical analysis was carried out using Graph Pad Prism (GraphPad Software, CA, USA) or IBM SPSS software (IBM SPSS Statistics version 24). Significant differences were considered for $p < 0.05$.

3 CHAPTER 3- The effect of CD36 deficiency and high-fat diet feeding on weight gain and skeletal muscle morphology

3.1 Overview

Obesity and being overweight are major risk factors for several chronic diseases, including diabetes, non-alcoholic fatty liver disease (NAFLD), as well as cardiovascular and metabolic diseases (Kahn and Flier, 2000). In obese individuals, the ectopic lipid infiltration in non-adipose tissue like skeletal muscle is one of many complications seen in obesity, leading to impaired muscle function with possible negative implications for skeletal muscle regeneration (Hu et al., 2010, Brown et al., 2015). Evidence suggests impaired muscle stem cell function in obese conditions, revealing the importance of understanding the loss of muscle health in diet-induced obesity (DIO) (D'Souza et al., 2015, Mebarek et al., 2007). CD36, a fatty acid translocase, has been associated with increased lipid accumulation and cell death in DIO (Cai et al., 2012). The scavenger receptor CD36 is involved in high affinity long chain fatty acid uptake and is widely expressed in several tissues; including platelets, immune cells, adipocytes, and myocytes. The broad expression mirrors its various roles related to the immune response, inflammation as well as lipotoxicity (Pepino et al., 2014, Glatz et al., 2013). Recently, CD36 has gained a lot of attention as a potential therapeutic target for obesity related comorbidities, such as cardiac lipotoxicity and insulin resistance (Glatz et al., 2013). Interestingly, CD36 deficient mice are protected against obesity and insulin resistance when fed a high-fat (HF) diet (Yang et al., 2018); yet the underlying protective mechanism remains elusive. This study investigates the impact of high-fat diet feeding on weight gain and skeletal muscle lipid accumulation in WT and CD36KO mice with regards to tissue specific changes, including the skeletal muscle and the liver, representing two-metabolically linked- insulin sensitive tissues. In particular, the satellite cell function in both WT and CD36KO mice was assessed under normal and high-fat feeding conditions. Furthermore, the skeletal muscle redox homeostasis was analysed to provide mechanistic insights into the underlying protective mechanism seen in CD36-deficiency.

3.2 Aims

The overall aim of this chapter was to investigate the impact of CD36-deficiency alone or in combination with a high-fat (HF) diet on overall body weight gain after 13 weeks as well as skeletal muscle morphology, lipid accumulation and homeostasis. It was hypothesised that HF diet feeding would lead to increased weight gain and negatively affect lipid homeostasis and metabolic properties in skeletal muscle tissue of WT animals. It was furthermore hypothesised that CD36-deficient mice would show decreased fatty acid uptake into skeletal muscle tissue, ameliorating the effects seen of HF diet feeding in WT animals. To test this hypothesis, the following objectives were addressed:

- i. To study the effect of genotype and/or diet on body weight gain in a 13-week period
- ii. To evaluate tissue specific weight gain and lipid accumulation in a genotype and/or diet dependent manner
- iii. To examine the effect of genotype and/or diet on muscle fibre composition and morphology
- iv. To determine mitochondrial bioenergetics and metabolic properties in skeletal muscle tissue

3.3 Materials and Methods

3.3.1 Animals

CD36 deficient mice were generated by targeted homologous recombination in a C57Bl/6 background and accessed via a collaboration with Prof. Khalid Naseem. The mice used in this study were males to avoid hormonal variations associated with the female menstrual cycle. The animals were housed in a temperature-controlled facility under standard conditions with 12 hours light/ dark cycle. At the age of 16-20 weeks, mice were randomly separated into two groups; receiving either a standard laboratory chow (22%), or a high fat diet (45%) for 12 weeks to induce obesity adjusted from Elashry, et al. (Elashry et al., 2019). Mice were given ad libitum access to water and food. Initial body weight measurements were taken one week before the experiment and body weight changes were sequentially analysed on a weekly basis for the duration of the study. All experiments were in accordance with UK Animals Act 1986.

3.3.2 Tissue sampling and freezing

After 13 weeks of treatment, final body weight measurements were taken. Mice were then sacrificed using a CO₂ overdose. Subcutaneous adipose tissue, heart, liver, kidney, EDL, TA, Gas, Quad and Sol muscle were precisely dissected, weighed and immediately snap frozen in isopentane which was immersed in liquid nitrogen to avoid freezing artefacts. Samples were stored at -80°C until further use.

3.3.3 Tissue embedding and cryosectioning

Skeletal muscle, heart and liver tissue samples were embedded in optimal compound temperature tissue mounting medium, immersed in 100% ethanol on dry ice to prevent samples from thawing. Samples were then either stored at -80°C or used for cryo-sectioning. OCT blocks containing embedded tissues were equilibrated to -21°C for 10- 15 minutes prior to cryo-sectioning and transverse sections of 10µm thickness were obtained and mounted on microscopy glass slides coated with Poly-L-lysine. Subsequently, the mounted sections were dried on the microscopy glass slides for 30 minutes at RT and stored at -80°C for further analysis. Skeletal muscle tissues were analysed for morphology and potential pathophysiological features as well as ROS production and assessed using histochemical or immunohistochemical staining procedures. Additionally, liver sections were prepared to analyse histological and potential pathophysiological features and were examined for lipid accumulation.

3.3.4 Histological analysis for lipid accumulation

Oil Red O (ORO) staining was performed to examine lipid accumulation in liver tissue after 13 weeks of HF diet or standard laboratory chow. As previously described (Sfyri et al., 2018), ORO working solution was prepared fresh from the stock solution and filtered through a 45µm filter in order to remove precipitates. Mounted tissue sections on microscopy glass slides were equilibrated to RT dried and rehydrated using deionised water. Sections were fixed with 4% PFA and washed with deionised water. Fixed sections were then stained with Harris' H&E solution to visualize cell membranes and nuclei. Sections were incubated with the

ORO working solution for 10 minutes and subsequently washed with running tap water to remove excess staining solution. Slides were mounted using Hydromount and immediately processed for image acquisition and analysis.

BODIPY® is a fluorescent dye with a long-wavelength absorption that can be used to visualise and quantify neutral lipids. Upon binding with neutral lipids, BODIPY emits a green fluorescence signal. As previously described (Sfyri et al., 2018) mounted tissue sections on microscopy glass slides were equilibrated to RT, dried and rehydrated with PBS, and incubated with 20µg/mL BODIPY for 30 mins and subsequently washed three times with PBS for 10 mins. All samples were mounted with fluorescent mounting medium, supplemented with DAPI, and digital images were obtained using a Zeiss Axio Imager.A1, HBO 100 fluorescent microscope.

3.3.5 Histochemical analysis of relative mitochondrial activity

SDH, also known as Complex II, is a mitochondrial enzyme complex, used as a marker of muscle fibre oxidative capacity and to study mitochondrial respiratory activity. It plays a part in both the citric acid cycle as well as the respiratory electron transfer chain. Part of the citric acid cycle is the oxidation of succinate to fumarate which is catalysed by SDH. SDH can therefore be used as an indicator for the mitochondrial oxidative potential. NBT is used as an artificial electron acceptor, which upon reduction changes colour and can be monitored spectrophotometrically.

SDH staining was performed in EDL and Sol muscles. The SDH staining method was adapted from Matsakas et al. (Matsakas et al., 2010). In brief tissue sections on microscope glass slides were equilibrating to room temperature, dried and rehydrated with milliQ H₂O for two minutes. Samples were then incubated for 15 mins (Soleus) or 35 minutes (EDL) with a mix of NBT/PBS and Succinate buffer at a ratio of 1:3 in a 38°C incubator. During the electron transfer from Succinate to NBT which is catalysed by SDH, a change in colour occurs, representing SDH activity. Subsequently, the samples were fixed with 4% PFA for 15 minutes and washed with milliQ H₂O before mounting with Hydromount and immediately processed for further imaging. Digital images were obtained with a Zeiss

Axioimager A.1 microscope and an AxioCam MRm monochrome digital camera and quantified manually using the Zen imaging software. Calculated was the relative number of positive-stained fibres and unstained, negative fibres for each muscle section.

3.3.6 Immunofluorescence

Histological analysis of muscle specific fibre type distribution was performed using Myosin Heavy Chain (MHC) specific antibodies as previously published (Matsakas et al., 2013). Simultaneous staining of two different myofibre types was used to examine type IIA, type I and type IIB fibres and to subsequently identify type IIX fibres. Mounted EDL and Soleus muscle tissue sections on microscopy glass slides were equilibrated to RT, dried and rehydrated using PBS. Sections were then incubated with permeabilisation buffer and further incubated with wash buffer to increase cell permeability and reduce unspecific binding of the antibodies. Primary antibodies for type IIA, type I and type IIB fibres were individually added on the tissue and incubated over night at 4°C. Firstly, primary antibody against type IIA fibres was used on the sections. After an overnight incubation the sections were washed with wash buffer and incubated for one hour at RT with the Alexa Fluor 488 anti-Mouse IgG secondary antibody to visualise type IIA fibres. Secondly, wash buffer incubation for 10 minutes was used before applying the second primary antibody against type IIB or type I. After another over-night incubation Alexa 633 anti-Mouse IgM was added for one hour at RT and used to identify type IIB or type I fibres. Slides were mounted using DAPI-supplemented mounting medium and then proceeded to image capturing.

Pictures were taken and analysed using the Zen Axioimager A.1 microscope. Quantification of the fibre type composition was performed manually using the ZEN imaging software. Unstained muscle fibres negative for either type IIB, type IIA or type I MHC were considered type IIX fibres and calculated via subtraction of positively stained fibres from the absolute amount of fibres.

3.3.7 RNA isolation, cDNA synthesis and quantitative RT-PCR

Muscle, liver and cell RNA was extracted as previously described by Sfyri et al. (Sfyri et al., 2018) using the E.Z.N.A. total RNA kit I according to the manufacturer

instruction.. Briefly, 50-100mg frozen gastrocnemius muscle or liver tissue were homogenised in 1mL of prechilled TRIzol. The homogenised muscle was transferred to a fresh collection tube and 200µL of 100% chloroform was added, followed by vigorously shaking the samples. After a short incubation for two minutes at RT the samples were centrifuged for 15 minutes at 4°C, 12,000x g to cause phase separation. The RNA containing aqueous phase was transferred into a fresh collection tube and 500µL/mL of 100% isopropyl alcohol was added for the precipitation of nucleic acids whilst samples were stored for 10 minutes at RT. The resulting mixture was then loaded onto a HiBind RNA Column with subsequent centrifugation of the samples for one minute at 10,000x g. The flow-through was discarded and 500µL RNA Wash Buffer I added to the HiBind RNA Column and centrifuged at 4°C for one minute at 10,000x g. The flow-through was discarded and 500µL RNA Wash Buffer II was added to the HiBind RNA Column, followed by centrifugation at 4°C for one minute at 10,000x g. The flow-through was discarded and the procedure repeated once more. In order to dry the HiBind RNA Column before the RNA elution, a final centrifugation step at 4°C for two minutes at 13,000x g was performed. RNA was eluted by adding 20µL of ultrapure water to the HiBind RNA Column. The centrifugation was performed following an incubation at RT for one minute. Subsequently, the samples were centrifugation at 4°C for two minutes at 12,000x g. The concentration (ng/µL) and purity (A_{260}/A_{280}) of isolated RNA was determined by performing a NanoDrop spectrometric analysis. The samples were stored at -80°C until use or further processed for DNase I treatment. In order to eliminate DNA contaminations. cDNA synthesis was performed by reverse transcription the RevertAid H Minus First Strand cDNA Synthesis Kit was used according to the manufacturer's protocol. A MasterMix containing the Oligo(dT) Primer was added to initiate the reverse transcription using a Veriti thermal cycler. Quantitative real time PCR was used to detect and quantify gene expression levels in a variety of samples by the addition of the non-sequence specific, double-stranded DNA intercalating dye, SYBR Green to reliably detect, at every cycle of the PCR, the amount of the newly formed PCR product. In this study the reference genes *Cyp* and *Hprt* (Appendix) were used to normalise the gene expression in all groups.

Table 3.3.7: Primer sequences

<i>Cidea</i>	Forward	CATGGTTTGAAACTCGAAAAGGG
	Reverse	TGACATTCATGGGATTGCAGAC
<i>Cpt1</i>	Forward	CACCAACGGGCTCATCTTCTA
	Reverse	CAAAATGACCTAGCCTTCTATCGAA
<i>Fabp3</i>	Forward	ACCTGGAAGCTAGTGGACAG
	Reverse	TGATGGTAGTAGGCTTGGTCAT
<i>Fatp1</i>	Forward	AGGTCAATGAGGACAACGATGGAG
	Reverse	CTGGTACATTGAGTTAGGGTCCAA
<i>Fndc5</i>	Forward	TTGCCATCTCTCAGCAGAAGA
	Reverse	GGCCTGCACATGGACGATA
<i>IL-15</i>	Forward	CATCCATCTCGTGCTACTTGTG
	Reverse	GCCTCTGTTTTAGGGAGACCT
<i>Fatp3</i>	Forward	ACAGTGCCAGGGATTCTACCA
	Reverse	GAACTTGGGTTTCAGCACCAC
<i>Fatp5</i>	Forward	TCTATGGCCTAAAGTTCAGGCG
	Reverse	CTTGCCGCTCTAAAGCATCC
<i>Fatp2</i>	Forward	GATGCCGTGTCCGTCTTTTAC
	Reverse	GACTTCAGACCTCCACGACTC

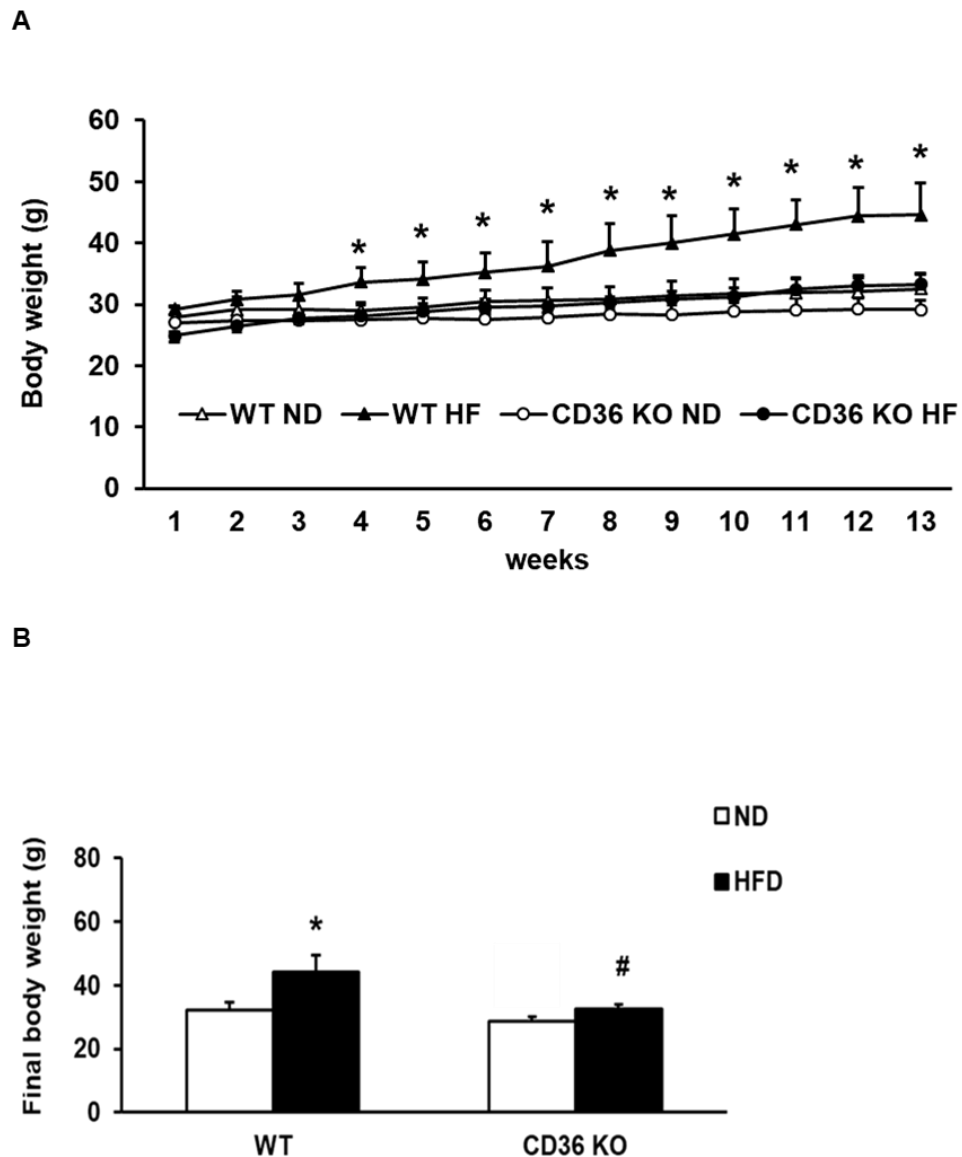
3.4 Results

3.4.1 Effect of high-fat diet feeding in WT and CD36 deficient mice

To determine, whether loss of CD36 effects weight gain in mice, WT and CD36 KO mice were subjected to either a standard chow (ND) or HF diet for 13 weeks. Body weight was recorded weekly, with a final measurement at week 13 before the animals were sacrificed. WT mice and CD36 KO mice showed similar body weights when fed a ND. However, from week 4 onward the HF diet gradually increased the body weight in WT mice, which further continued to increase over the time duration of the experiment. The difference between bodyweights was most pronounced at week 13 (**Figure 3.1A**). WT mice displayed an increased bodyweight by 37% ($44.2 \text{ g} \pm 5.1$ vs. $32.3 \text{ g} \pm 2.5$) after 13 weeks of HF diet (**Figure 3.1B**) feeding and accelerated weight gain compared to the WT littermates maintained on a standard laboratory chow. Conversely, CD36 KO

mice fed a HF diet showed decreased body weight gain compared to the WT HF group ($32.6 \text{ g} \pm 1.3$ vs. $44.2 \text{ g} \pm 5.1$, but no significant difference when compared to WT ND (1%) nor CD36 KO ND (14%) mice (**Figure 3.1B**).

Figure 3.1. Body weight in WT and CD36 KO mice after high-fat diet feeding
(A) Body weight changes in WT and CD36 KO mice fed a standard laboratory chow (ND) or a high-fat (HFD) diet for 13 weeks was assessed at the age of 2 months. **(B)** Final body weight (i.e. week 13) of mice fed a ND or HF diet. Data are mean \pm SD (N=5 per group). Statistical analysis was performed by two-way



ANOVA with repeated measurements, * $p < 0.05$ vs. WT ND, # $p < 0.05$ vs. WT HF. Furthermore, tissue specific weight changes were analysed in WT and CD36 deficient mice when exposed to either ND or HF diet. The absolute weight of skeletal muscle tissue; soleus (Sol), *biceps brachii* (BB), *extensor digitorum*

longus (EDL), *tibialis anterior* (TA) as well as heart and white adipose tissue (WAT) was altered in a diet and genotype dependent way. WT mice fed a HF diet showed increased muscle weight for Sol (**Figure 3.2A**) and BB (**Figure 3.2B**) whereas (11.27 mg \pm 0.6 vs 9.6 mg \pm 1.2 in Sol and 20.6 mg \pm 1.02 vs. 18.6 mg \pm 1.9) CD36KO mice display similar muscle weights independent of diet. No significant weight change was observed in the EDL (**Figure 3.2C**) and TA (**Figure 3.2D**) muscle, neither between WT ND and HF diet nor between CD36KO ND and HF diet animals. CD36 is one of the major fatty acid transporters in the heart (Glatz et al., 2013). To determine the effects of its absence in ND and HF diet conditions the weight of isolated heart tissue from all groups was assessed. There was a weight increase in the heart tissue from WT mice fed a HF diet (216.7 mg \pm 19 vs 187.3 mg \pm 15.5), which was not detected in the CD36KO mice on a HF diet when compared to either control animals or the CD36KO ND group. CD36KO mice on a HF diet showed a reduction in heart weight when compared to WT HF diet animals and no detectable weight difference compared to CD36KO ND littermates (**Figure 3.2E**). WT mice fed a HF diet showed a significant increase in the WAT weight (x4.6 fold; 1303.9 mg \pm 302 vs. 282 mg \pm 137.5), when compared to control WT ND animals. Although CD36KO HF diet animals show increased WAT weight compared to their littermates on a ND (x2.9 fold; 632.4 mg \pm 62 vs. 211.5 mg \pm 49.4), the absolute increase is significantly reduced compared to the WT HF animals (**Figure 3.2F**).

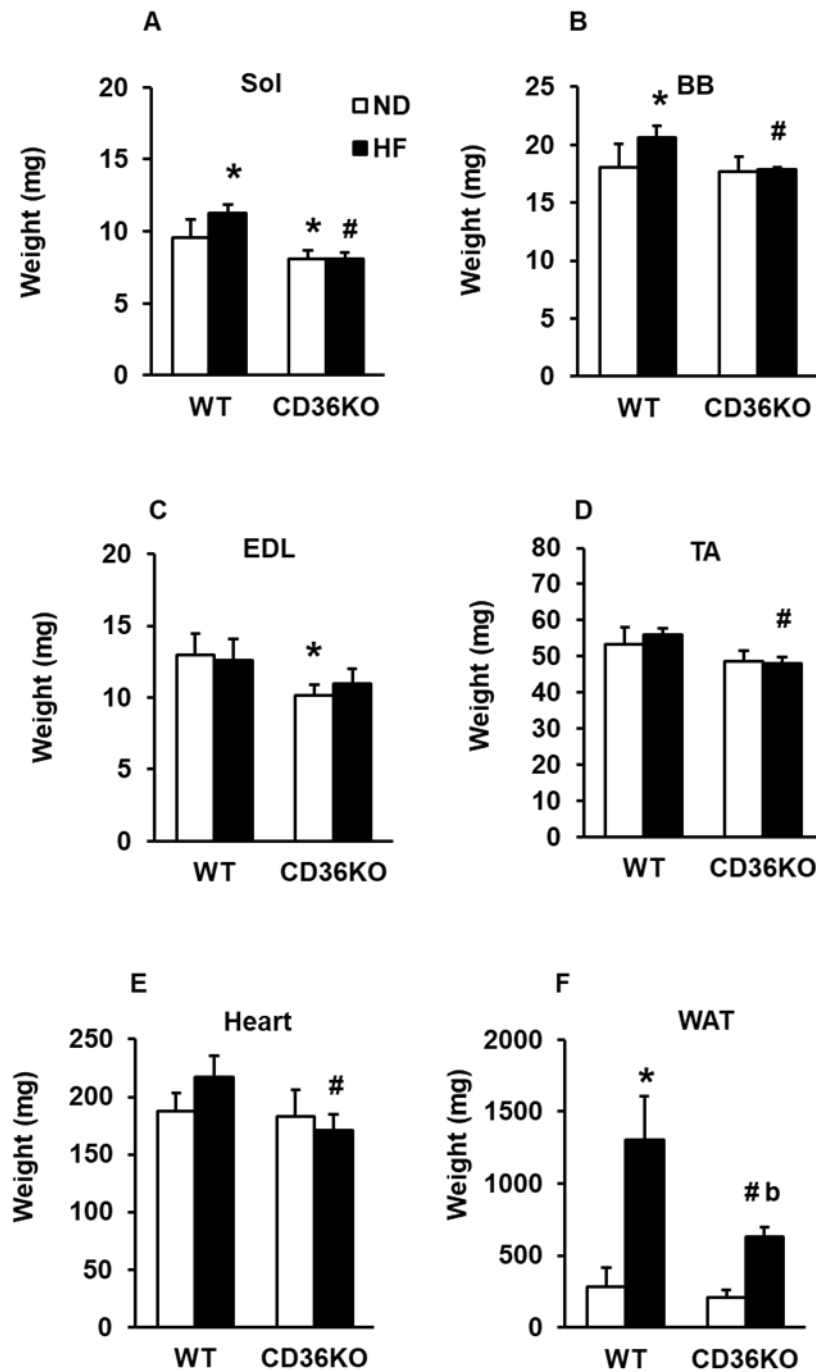
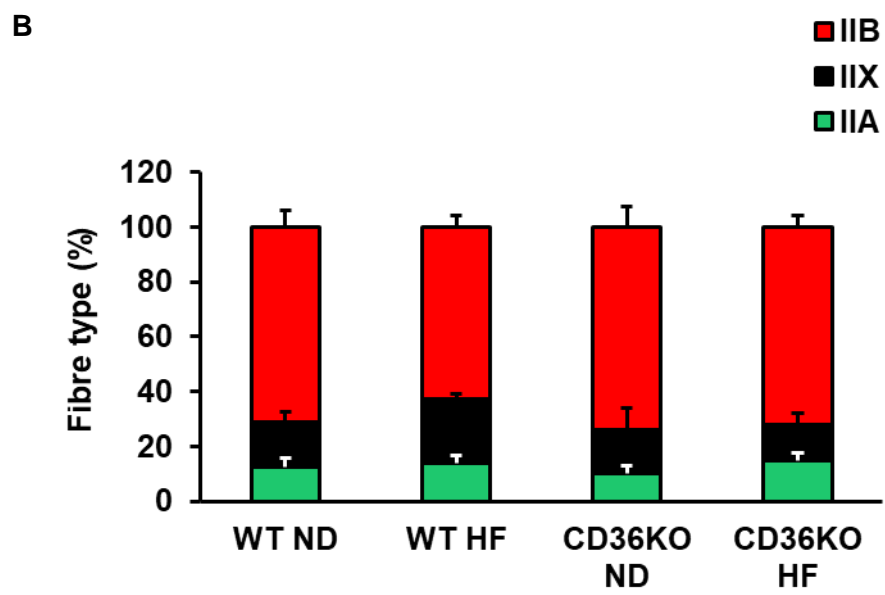
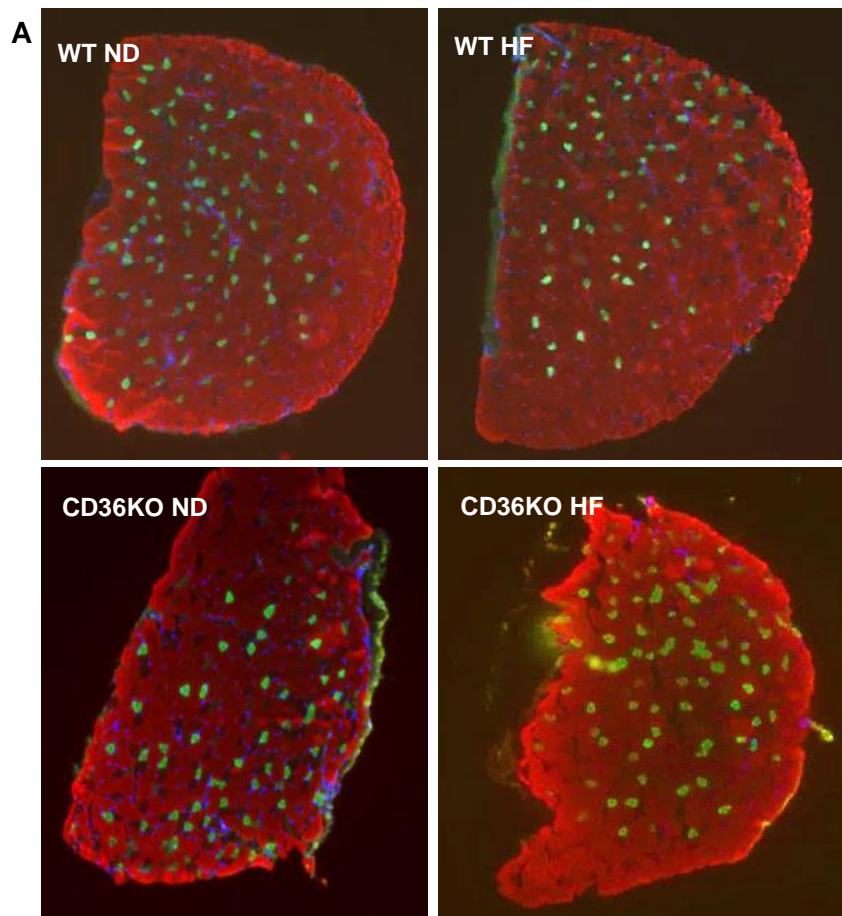


Figure 3.2. Tissue specific weight changes in wild-type and CD36 deficient mice. Tissue weight of Soleus (Sol; **A**), Biceps Bracii (BB; **B**), Extensor digitorum longus (EDL; **C**), Tibialis Anterior (TA; **D**), heart I and White-Adipose-Tissue (WAT; **F**) from WT and CD36 KO mice fed a ND or a HF diet. Data are represented as mean \pm SD (N=5 per group). Statistical analysis was performed using two-way ANOVA, *p<0.05 vs WT ND, #p <0.05 vs WT HF, b p<0.05 vs CD36 KO ND.

Given that obesity and metabolic disorders are often associated with morphological changes of the skeletal muscle, muscle specific changes of the fibre type distribution were assessed. To determine whether HF diet feeding impacts the fibre type composition, EDL muscle - a representative fast-twitch muscle - was immunostained for the myosin heavy chain (MHC) isoforms MHCIIIB and MHCIIA, with unstained fibres identified as MHCIIIX (**Figure 3.3A**). Immunohistochemistry revealed that the HF diet had no significant impact on the EDL fibre type distribution independent of genotype (**Figure 3.3B**). To determine whether the reduction in gained body weight seen in CD36 KO mice on a HF diet paralleled changes of the muscle morphology, the cross-sectional area (CSA) of myofibres was analysed to assess muscle-specific fibre type alteration (**Figure 3.3C,D**). EDL muscle CSA of MHCIIA^{+ve} stained fibres remained unchanged in WT HF animals when compared to control animals. Moreover, no change was observed in the CSA of MHCIIA^{+ve} stained fibres between CD36 KO ND and HF fed animals (**Figure 3.3C,D**). Analysis of MHCIIIB^{+ve} fibres revealed reduced CSA in the WT HF diet group ($1051.6 \mu\text{m}^2 \pm 154$ vs WT ND $1552.7 \mu\text{m}^2 \pm 142$) but no detectable change in CD36 KO HF diet animals (**Figure 3.3C**). This was paralleled by the analysis of the CSA distribution (**Figure 3.3D**) showing a general shift towards smaller fibres in WT HF animals. At the same time, CD36 KO animals showed an opposite trend towards larger CSA of fast twitch fibres (IIB, IIX), possibly linked to the incapability to use the available excess of fatty acids. No changes in the average CSA of MHCIIIX fibres was observed between the experimental groups.



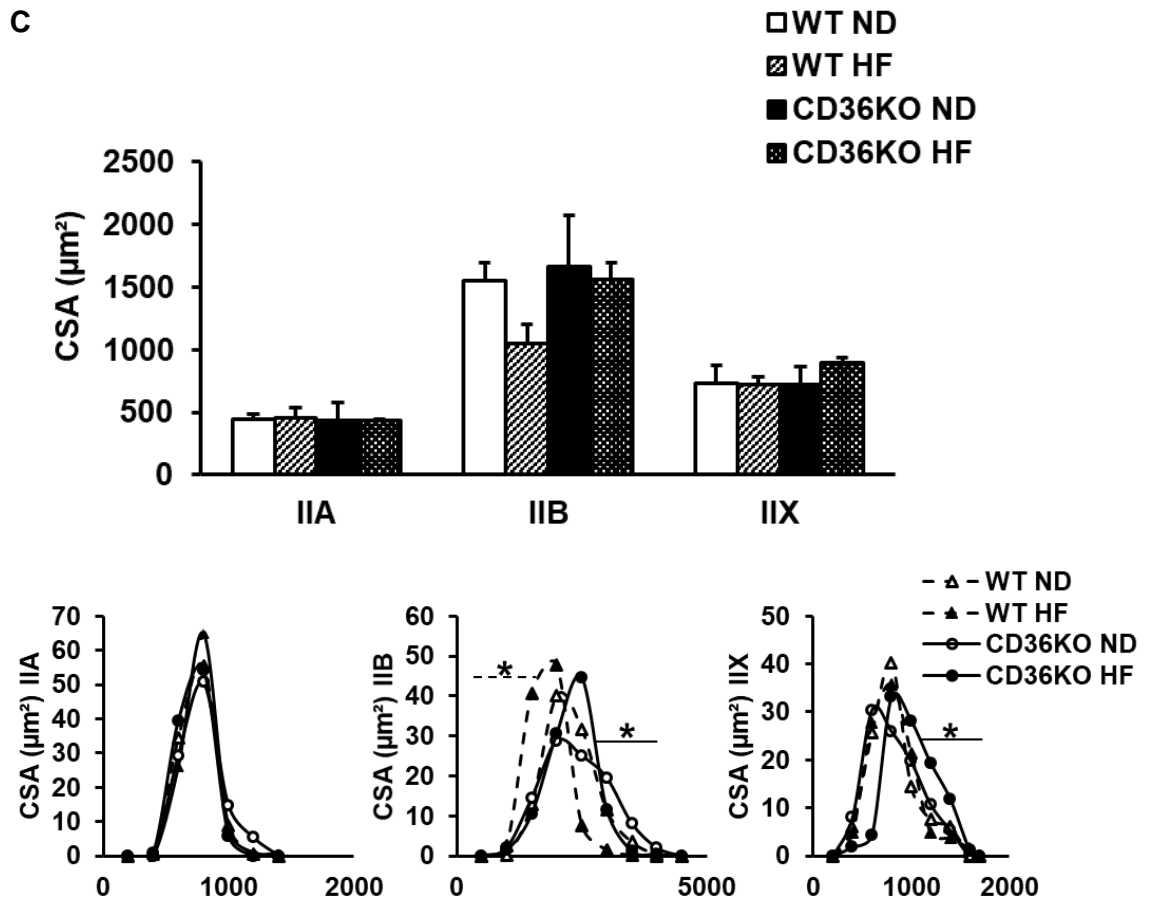
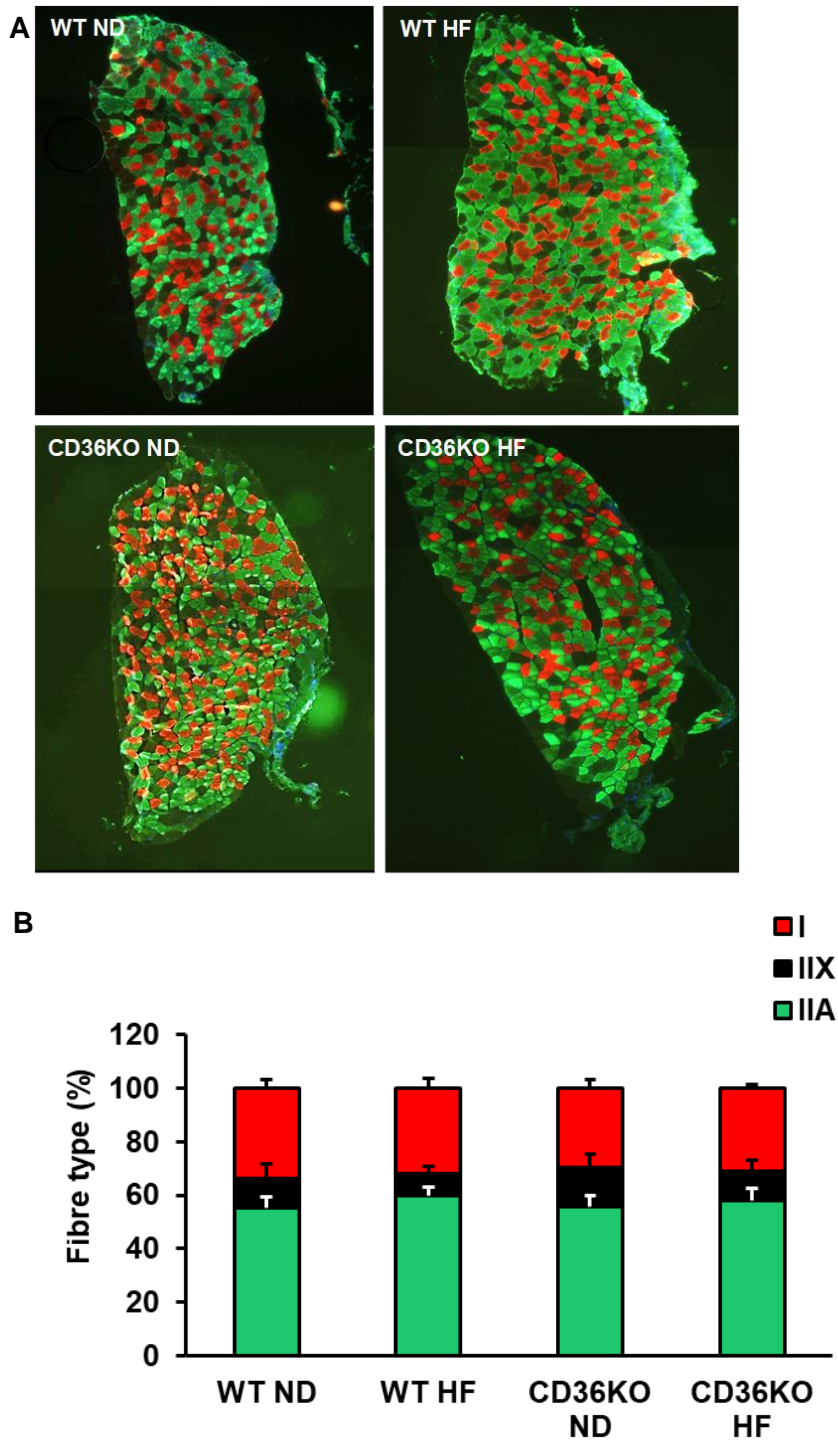


Figure 3.3 Diet and genotype dependent morphometric changes in EDL muscle. (A) Representative images of cross-sections from WT and CD36 KO mice fed a ND or HF diet from EDL skeletal muscle stained for myosin heavy chain (Mhc) isoforms. EDL muscle was examined for fibre type composition (A,B). The fibre type expression profile (IIA IIB IIX) is shown in percentage [%] (B) and the cross-sectional area (CSA) in μm^2 (C,D). Data are represented as mean \pm SD (N=3-4 per group). Statistical analysis was performed using two-way ANOVA, * p <0.05 vs WT ND for B-C and a Chi square (χ^2) test was performed for D, * p <0.05 vs WT ND.

To determine muscle-specific effects of HF diet feeding and the CD36 deficient genotype, fibre type distribution in the Soleus muscle - as a representative slow-twitch muscle - was assessed (Figure 3.4A). MHC immunostaining for type I, type IIX and type IIA fibres revealed no difference in fibre type distribution between the groups (Figure 3.4A,B). Moreover, analysis of the CSA of MHCIIA^{+ve} stained fibres showed no difference between HF diet and ND fed groups, independent of genotype (Figure 3.4C,D). WT mice and CD36 KO mice showed no diet induced change in CSA of MHCI^{+ve} stained fibres. In contrast, the CD36

KO HF diet group displayed a reduced average CSA of MHCIIIX fibres when compared to ND fed littermates ($1452.4 \mu\text{m}^2 \pm 431$ vs. $1967.7 \mu\text{m}^2 \pm 420$) (**Figure 3.4C**) but no change was observed in the overall size distribution (**Figure 3.4D**).



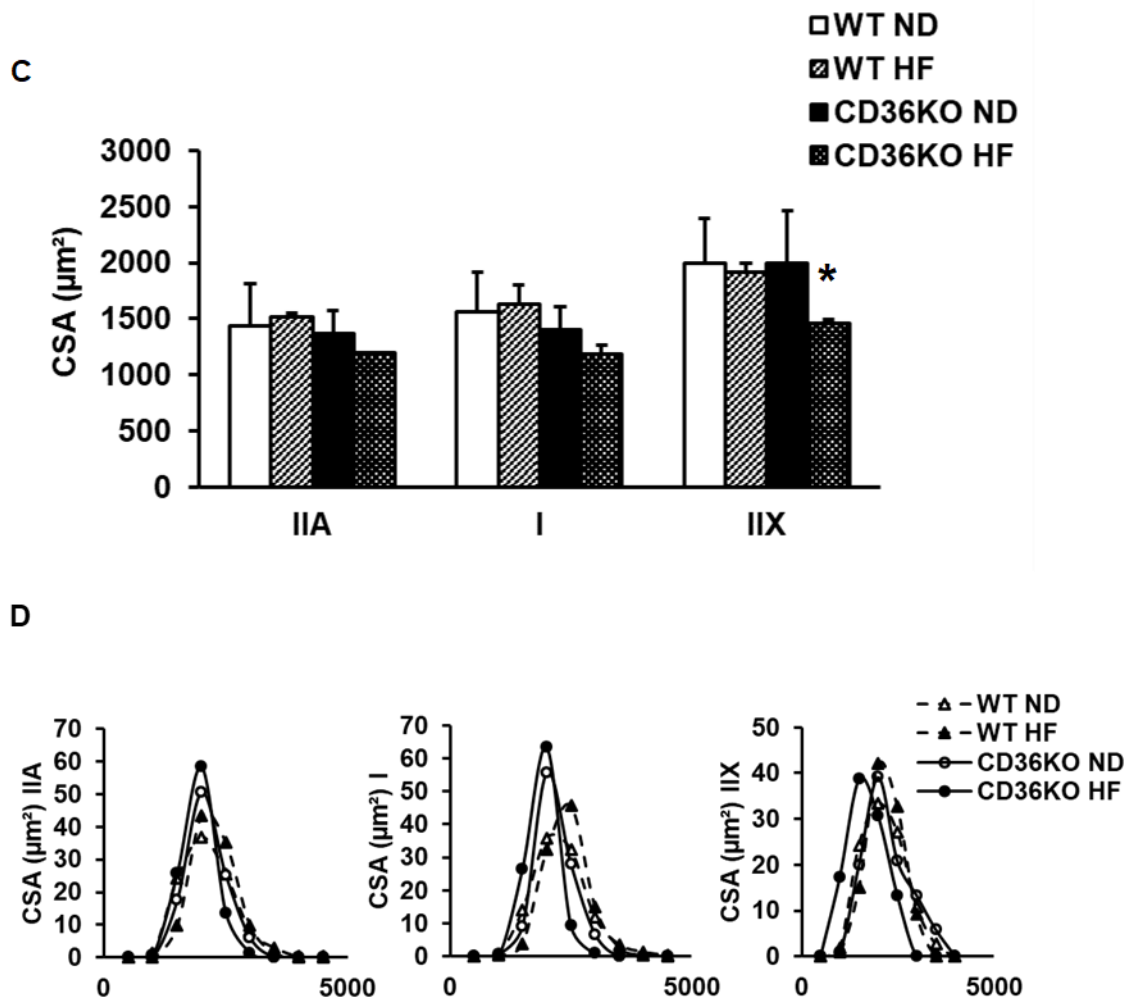


Figure 3.4 Diet and genotype dependent morphometric changes in Soleus muscle. (A) Representative images of cross-sections from WT and CD36 KO mice fed a ND or HF diet from Soleus skeletal muscle stained for myosin heavy chain (Mhc) isoforms. Soleus muscle was examined for fibre type composition (A,B), showing the Soleus fibre type expression profile (IIA I IIX) in percentage [%] (C) and the cross-sectional area (CSA) in μm^2 (D). Data are represented as mean \pm SD (N=3-4 per group). Statistical analysis was performed using two-way ANOVA, * $p < 0.05$ vs WT ND for B-C and a Chi square (χ^2) test was performed for D, * $p < 0.05$ vs WT ND.

To analyse a possible transition towards a more oxidative fibre type due to increased fatty acid availability, relative mitochondrial activity was assessed using SDH staining. Oxidative, slow-twitch fibres, have a high mitochondrial content, slow contraction rate, are resistant to fatigue and show increased reliance on oxidative phosphorylation (Mishra et al., 2015). To assess the impact of high fat diet feeding and increased fatty acid availability on fibre type changes

towards a more oxidative phenotype in WT mice, SDH staining was performed to visualize the oxidative capacity and relative mitochondrial activity of individual fibres in the EDL. SDH staining remained unaltered independent of diet in WT and CD36 KO mice (**Figure 3.5A,B**).

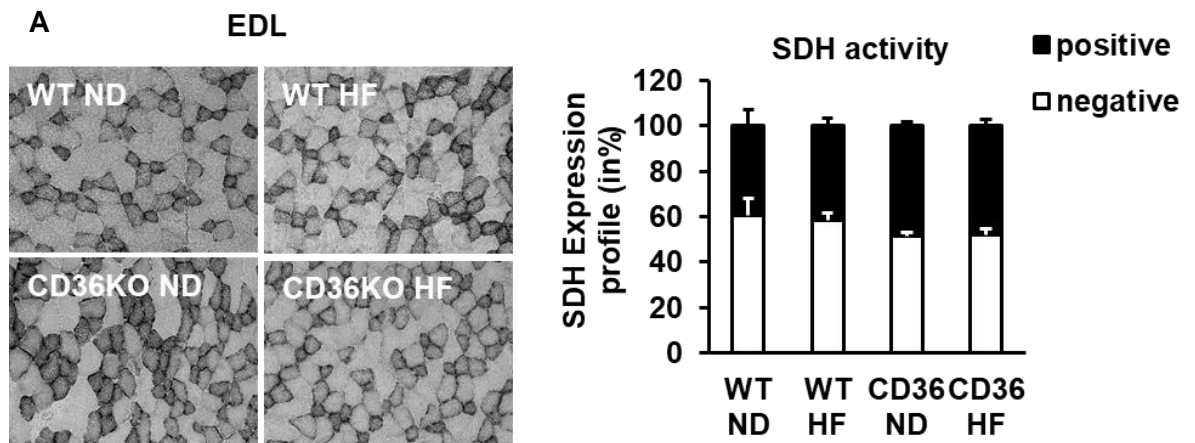
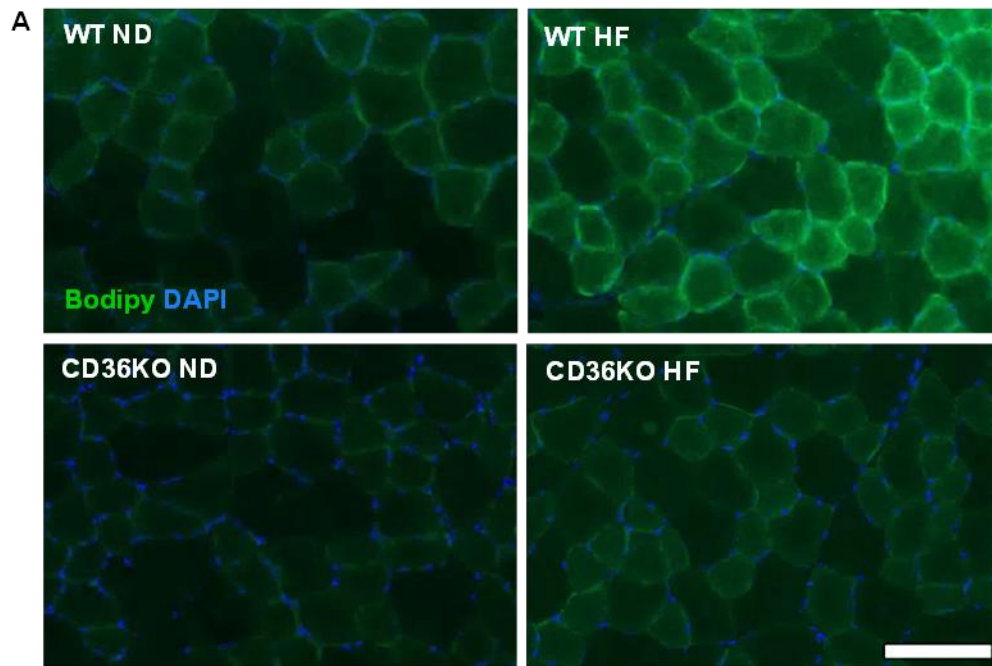


Figure 3.5 Relative mitochondrial oxidative capacity in EDL muscle. Individual fibre oxidative capacity in EDL skeletal muscle was analysed in WT and CD36 KO mice fed either a ND or HF diet for 13 weeks. **(A)** Representative images of SDH staining in EDL cross-sections. **(B)** Quantification of SDH staining in EDL muscle with expression profile of ^{+ve} and ^{-ve} SDH stained fibres in [%]. Data are represented as mean±SD (N=4 per group). Statistical analysis was performed using two-way ANOVA.

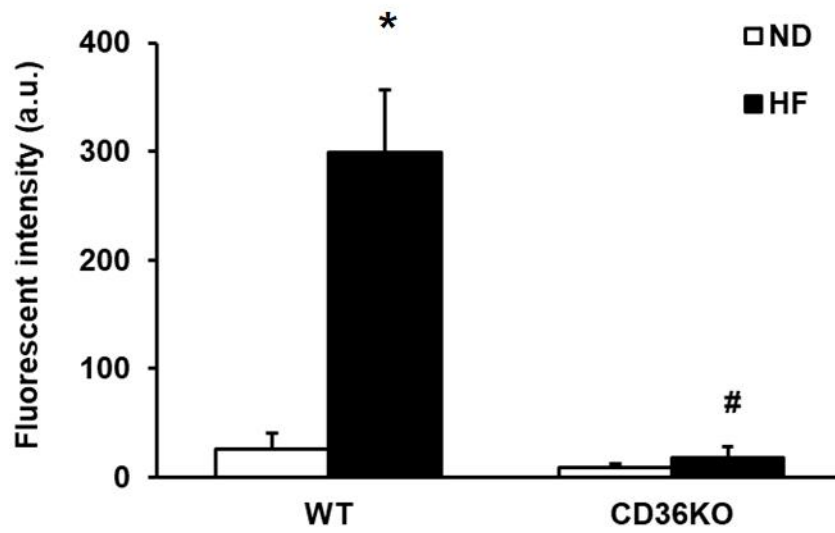
Obesity has been associated with ectopic lipid infiltration and accumulation in non-adipose tissues, including the skeletal muscle and liver (Bonen et al., 2004, Eguchi et al., 2006). To further investigate HF diet-induced fatty acid accumulation in the skeletal muscle, cross-sections from the Tibialis Anterior (TA) muscle were immunostained to test the effect of CD36 deficiency on lipid deposition.

Immunohistochemical staining of neutral lipids was performed by BODIPY staining. HF diet feeding induced significantly higher lipid accumulation in the TA muscle of WT mice compared to control littermates on a ND (298.8 a.u. ± 57.5 vs. 25.8 a.u. ± 15.4, P<0.001; **Figure 3.6A, B**). Conversely, CD36 KO mice on a HF diet showed minimal levels of BODIPY staining (9.1 a.u. ± 3.3 CD36 KO ND vs 18.4 a.u. ± 10.5), suggesting reduced lipid infiltration of the skeletal muscle.

These findings were further confirmed by the quantification of triglycerides (TG) in the gastrocnemius muscle, by gas chromatography. WT HF animals showed an increase in TG content in the muscle ($177.4 \mu\text{mol/g} \pm 28.2$ in WT HF vs. $98.1 \mu\text{mol/g} \pm 36$ in WT ND) whilst no significant changes were observed in CD36 KO HF diet animals when compared to CD36 KO ND. The gas chromatography results were performed by collaborators from the Laboratory of Evaluation of Human Biological Performance, Aristotle University of Thessaloniki (**Figure 3.6C**). In order to assess the expression profile of genes involved in FA uptake and utilisation as well as cross-talk between adipose tissue and skeletal muscle, quantitative RT-PCR to analyse relative mRNA expression was performed. Relative mRNA expression was significantly increased in CD36 KO HF versus WT ND conditions for Fibronectin type III domain-containing protein 5 (*Fndc5*; $1.57 \text{ fold} \pm 0.3$) and Interleukin 15 (*IL-15*; $2.3 \text{ fold} \pm 0.5$), which have been identified as important myokines. Furthermore, levels of Fatty acid binding protein 3 (*Fabp3*; $3.64 \text{ fold} \pm 1.2$) and Carnitine palmitoyltransferase I (*Cpt1*; $2.28 \text{ fold} \pm 0.4$); important players of the fatty acid metabolism; were significantly increased in CD36 KO mice (*Cpt1*) or both in WT and CD36 KO mice on a HF diet (*Fabp3*) when compared to control littermates (**Figure 3.6D**).



B



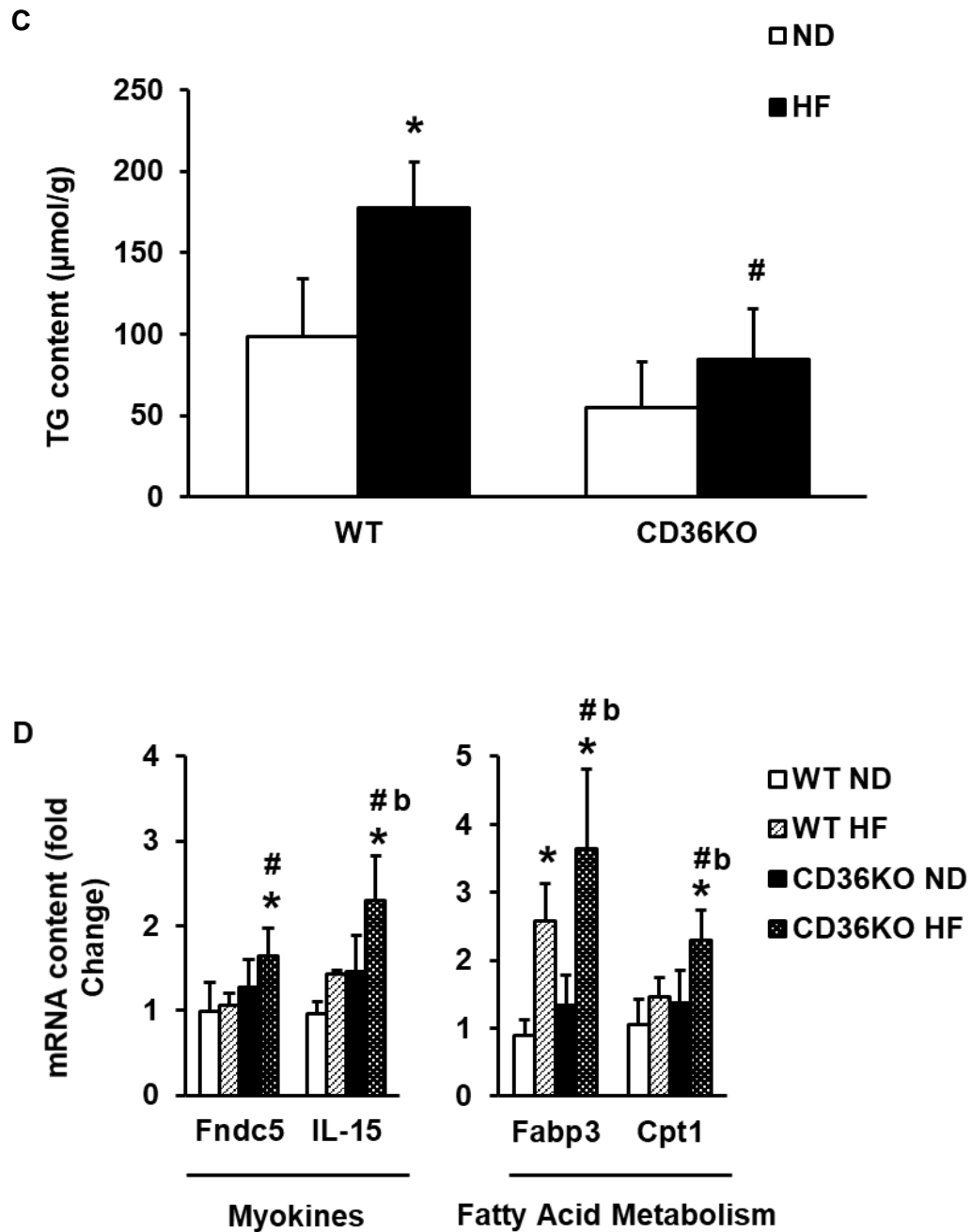
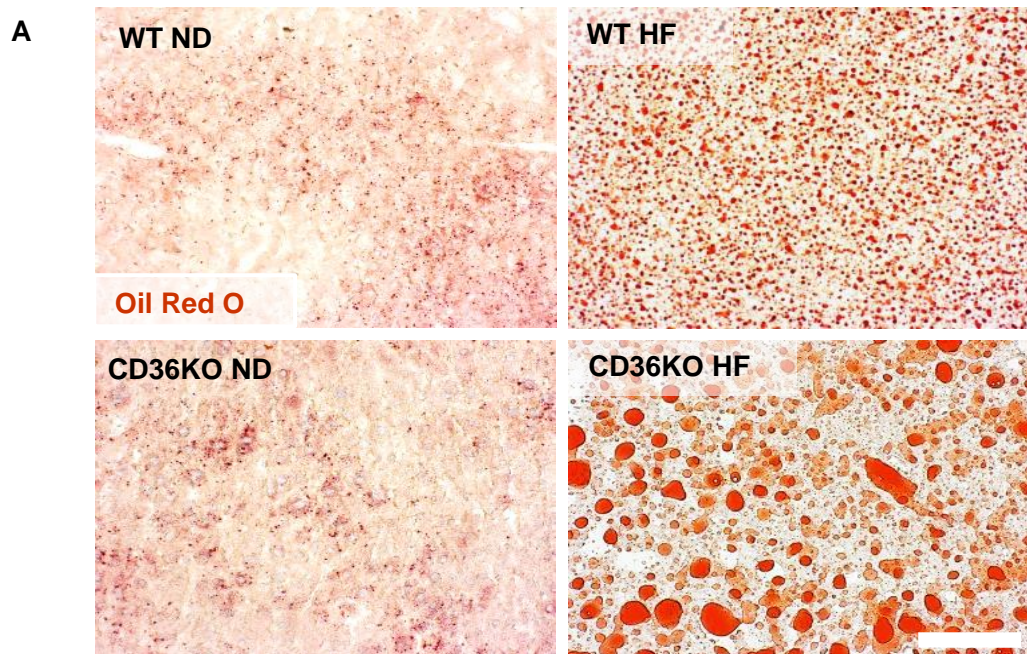


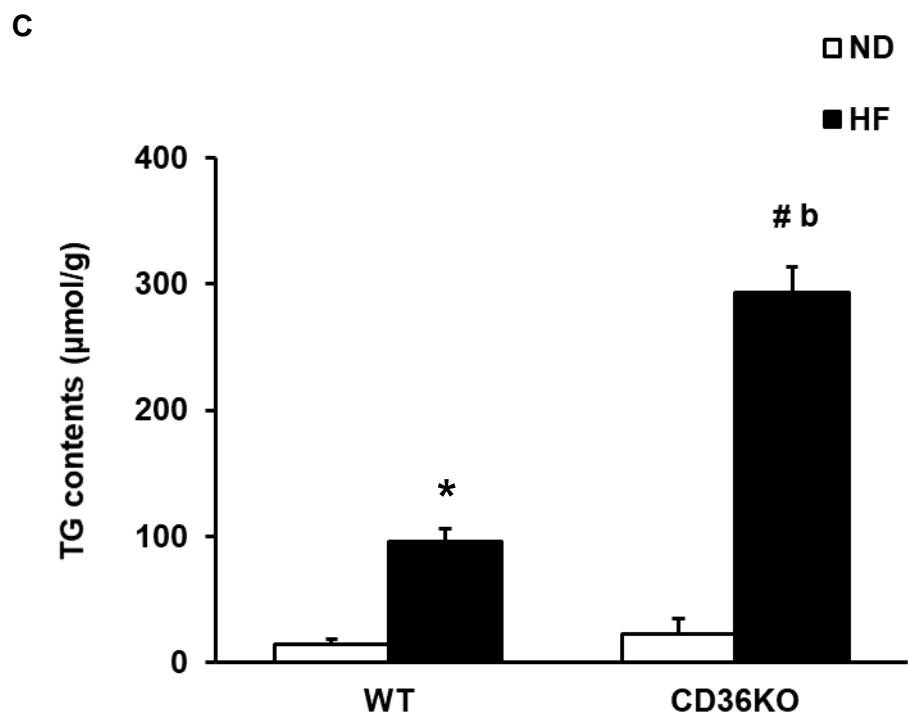
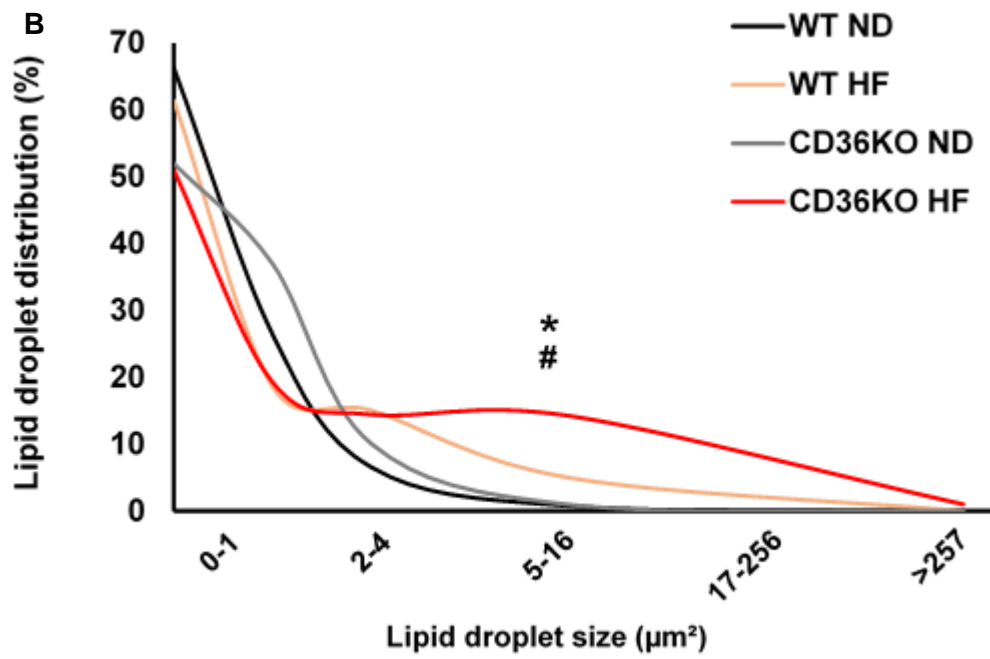
Figure 3.6. Effect of CD36 deficiency on high-fat diet-induced lipid accumulation in skeletal muscle. (A) Skeletal muscle lipid accumulation in WT and CD36 KO mice on either ND or HF diet was detected by BODIPY staining (20x, scale bar=100µm). (B) Quantification of fluorescence intensity shown in arbitrary units (a.u.) of pixel intensity. (C) Gas chromatography was performed in skeletal muscle, quantifying the triglyceride (TG) content (µmol/g). (D) Relative gene expression in skeletal muscle was analysed by RT-PCR. Values were normalised to Cyclophilin 1 (Cyp1) and hypoxanthine guanine phosphoribosyltransferase (Hprt). Data are mean±SD (N=5) per group. Statistical analysis was performed by two-way ANOVA, *p<0.05 vs. WT ND, #p<0.05 vs. WT HF b p<0.05 vs. CD36KO ND.

Non-alcoholic fatty liver (NAFLD) has been associated with visceral fat accumulation and the development of insulin resistance and obesity. To evaluate the general phenotype of the CD36 deficient mouse and the relationship between HF diet feeding as well as the visceral fat accumulation and fatty liver development, cross-sections of the liver were assessed using Oil Red O to visualise fat infiltration. As expected, WT mice on a HF diet showed a significant increase in lipid accumulation in the liver tissue as shown by Oil Red O staining compared to WT and CD36 KO mice on a standard chow. Remarkably, CD36 KO mice on a high-fat diet showed a significant increase of lipid accumulation in the liver compared to all other groups, which is evident in the larger lipid number as well as lipid size (**Figure 3.7A,B**). These findings were again confirmed by collaborators, who performed gas chromatography to quantify hepatic TG accumulation. Whilst WT and CD36 KO on a ND showed only small amount of TG accumulation there was a significant increase in WT on a HF diet ($96.28 \mu\text{mol/g} \pm 9.5$ vs WT $14.8 \mu\text{mol/g} \pm 3.9$) and CD36 KO on a HF diet ($293 \mu\text{mol/g} \pm 20.9$ vs WT $14.8 \mu\text{mol/g} \pm 3.9$) revealing a striking phenotype in the CD36 KO condition (**Figure 3.7C**).

Fatty acid transport in the liver is predominantly regulated by fatty acid transport proteins (FATP), fatty acid binding proteins (FABP), cluster of differentiation CD36, as well as passive diffusion. Recently published data has shown that the FATP isoforms FATP2 and FATP5 are mainly expressed in the liver. Knock-down of FATP2 in a mouse model of obesity, reduced fatty acid uptake and ameliorated signs of hepatic steatosis (Falcon et al., 2010). Likewise, evidence has been published that FATP5 mediates fatty acid uptake into the liver (Doege et al., 2008) and facilitating the development of hepatic steatosis. Moreover, the fatty acid transport protein 1 (FATP1) has been identified as an insulin-sensitive fatty acid transporter involved in diet induced obesity. Like CD36, FATP1 has been shown to translocate from an intracellular compartment to the plasma membrane in response to insulin signalling (Wu et al., 2006). FATP1-null mice are protected against diet-induced obesity and insulin desensitization. It has been suggested that FATP1 plays a crucial role in the redistribution of fatty acids from adipose and skeletal muscle tissue to the liver (Wu et al., 2006).

To investigate alternative fatty acid transport mechanisms and altered expression profiles of genes involved in fatty acid transport and metabolism, RT-PCR analysis was performed in the liver tissue of WT and CD36 KO mice, that had been fed a ND or a HF diet. Levels of relative mRNA expression of Fatty acid transporter proteins 1,2,3 and 5 (*Fatp1,2,3,5*) as well as the death-inducing DNA fragmentation factor α -like effector A (*Cidea*) were quantified. Both *Fatp2* and *Fatp1* were significantly increased, 1.5-fold (1.9 ± 0.4 vs. 1.27 ± 0.2) and 2.3-fold (3.9 ± 1 vs. 1.7 ± 0.2) respectively, in livers from CD36 KO HF diet animals when compared to control WT mice on a HF diet. Most strikingly, the expression of *Cidea*, which has been shown to regulate lipolysis (Puri et al., 2008, Viswakarma et al., 2007), showed a 22-fold increase (43.8 ± 16.3 vs. 2 ± 1.5) in CD36 KO HF diet mice compared to WT HF diet mice (**Figure 3.7D**).





D

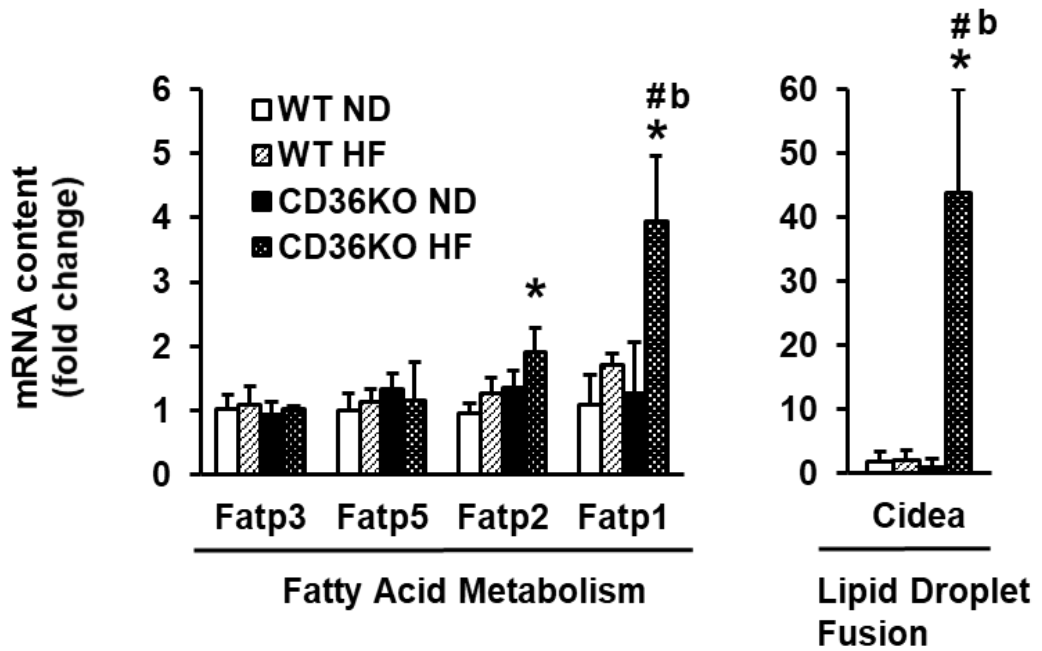


Figure 3.7. Effect of CD36 deficiency on high-fat diet-induced lipid accumulation in the liver (A) Representative pictures of liver lipid accumulation, detected by Oil Red O staining in cross-sections. **(B)** Quantification of lipid size and distribution. **(C)** Gas chromatography was performed in liver tissue, quantifying TG content ($\mu\text{mol/g}$). **(D)** Relative gene expression in liver was analysed by RT-PCR. Values were normalised to Cyclophilin 1 (*Cyp1*) and hypoxanthine guanine phosphoribosyltransferase (*Hprt*). Data are mean \pm SD (N=5) per group. Statistical analysis was performed by two-way ANOVA for **C** and **D**, * $p < 0.05$ vs. WT ND, # $p < 0.05$ vs. WT HF b $p < 0.05$ vs. CD36KO ND and a Chi square (χ^2) test was performed for **B**, * $p < 0.05$ vs. WT ND, # $p < 0.05$ vs. WT HF.

3.5 Discussion

The novelty of this data is that it evaluates the link of CD36 to lipid accumulation as well as lipid homeostasis in insulin sensitive tissues such as the skeletal muscle and the liver with and without HF diet challenge. In order to achieve this, consecutive measurements were taken of the body weight gain during a 13-week experimental set up with subsequent evaluations of the skeletal muscle morphology and molecular features including lipid accumulation and markers of lipid metabolism.

3.5.1 Body and tissue weight

WT and CD36 KO mice at the age of 2-3 months showed no initial difference regarding their body weight when fed a standard laboratory chow (ND). Interestingly, CD36 KO mice on a HF diet displayed decreased weight gain compared to the WT animals fed a HF diet already depicted after 4 weeks following HF diet feeding. This difference was even more pronounced at later time-points, demonstrating that CD36 deficient mice are protected from HF diet-induced obesity, which is in line with previous findings (Cai et al., 2012). Furthermore, tissue specific weight changes were observed, including increased weight for the slow twitch Soleus muscle (**Figure 3.2A**) as well as the fast twitch *Biceps brachii* (**Figure 3.2B**) in WT mice on a HF diet. Furthermore, WT mice fed a HF diet showed a significant weight increase in the WAT when compared to control WT animals on a standard chow. These findings are in line with other recent studies, showing that the visceral fat deposition is decreased in CD36 deficient mice (Koonen et al., 2010). This data further suggest that the reduction in body weight is mainly due to a decreased WAT accumulation observed in CD36-deficient mice on a HF diet (**Figure 3.1A,B**). Moreover, these results indicate that CD36 plays a tissue specific role in fatty acid uptake and accumulation.

3.5.2 Myofibre morphology and composition

Myofibre composition was assessed in the extensor digitorum longus (EDL) muscle, representing a fast twitch muscle, as well as in the Soleus muscle as a representative for a slow twitch muscle. As a fast twitch muscle, the EDL is mainly composed out of type IIB (approximately 60%; glycolytic) fibres and to a lesser degree out of IIA, IIX and type I fibres (Soukup et al., 2002). The Soleus muscle as a slow-twitch muscle is mainly composed of type I (oxidative) and type IIA (approximately 40%) fibres (Carroll et al., 2011). Several studies have indicated a possible relationship between muscle fibre type and obesity (Tanner et al., 2002). Previously published data suggests that obese individuals possess fewer oxidative type I and more glycolytic type IIB fibres. Furthermore, a positive correlation was established between the percentage of excess weight loss and the percentage of type I fibres in obese women (Tanner et al., 2002). As a highly

plastic tissue, the skeletal muscle can adapt to several conditions such as exercise and diet. Transformation of fibres in the muscle tissue as a response to physical and dietary parameters indicates functional adaptation of the tissue to its environment. Interestingly, although approximately 40% of the muscle fibre composition in humans is genetically predetermined, around 45% are determined by other factors such as diet, exercise or aging (Denies et al., 2014). This study aimed to investigate the fibre type composition under high-fat diet feeding in WT and CD36-deficient mice.

Immunohistochemistry revealed that the HF-diet had no major impact on the skeletal muscle fibre type distribution independent of genotype. These findings are paralleled by the observation that oxidative capacity -indicated by SDH staining- and relative mitochondrial activity remained unaltered independent of diet in WT and CD36 KO mice. This is in accordance with published data of diet-induced obesity in mice reporting minimal or no changes in fibre type composition (Turpin et al., 2009). Although gene expression related to mitochondrial biogenesis (*Pgc1a*) was similar in all experimental groups, the gene expression of the mitochondrial integral membrane protein Cpt1 was significantly increased in CD36-deficient mice, suggesting increased mitochondrial β -oxidation.

3.5.3 Lipid accumulation and metabolism

3.5.3.1 Skeletal muscle lipid accumulation

There has been a growing body of evidence supporting the notion that increased ectopic lipid infiltration and lipid accumulation in skeletal muscle is linked to obesity and insulin resistance, leading to the development of type 2 diabetes (Goodpaster and Wolf, 2004). To investigate the impact of high-fat diet feeding and CD36-deficiency on skeletal muscle lipid infiltration, BODIPY staining was performed. WT animals showed a significantly increased BODIPY signal following HF diet feeding, when compared to WT animals on a normal chow (ND). These findings suggest increased ectopic lipid infiltration in WT HF diet animals. However, HF diet feeding induced significantly lower lipid accumulation in the skeletal muscle of CD36 KO mice compared to WT HF diet animals. This is in line with the gas chromatography results; possibly indicating improved skeletal

muscle lipid homeostasis and supported by evidence that CD36 is involved in the development of obesity (Hegarty et al., 2002). Furthermore, these findings suggest an important link between CD36 and diet-induced skeletal muscle lipid infiltration and accumulation with possible implications for skeletal muscle insulin resistance.

3.5.3.2 Skeletal muscle lipid metabolism

FNDC5 has been shown to be increased in rodent models (Dun et al., 2013) as well as humans (Huh et al., 2012) following exercise. This is in line with *IL-15* overexpression to be correlated to enhanced oxidative energy metabolism and improved endurance in male mice (Quinn et al., 2013). Myokines have been shown to be highly involved in muscle lipid metabolism and overall muscle function (Lee and Jun, 2019). The improved skeletal muscle lipid homeostasis in CD36 KO animals observed in this study might be linked to increased myokine mRNA expression levels for *Fndc5* and *IL-15*. Furthermore, elevated levels of Fatty acid binding protein 3 (*Fabp3*) and Carnitine palmitoyltransferase I (*Cpt1*) indicate altered fatty acid metabolism in CD36 deficient mice on a HF diet which further supports the notion of improved skeletal muscle lipid homeostasis.

3.5.3.3 Hepatic lipid accumulation

Several studies have reported an association of the development of the non-alcoholic fatty liver disease (NAFLD) with visceral fat accumulation and insulin resistance (Eguchi et al., 2006). Liver sections stained for neutral lipids using Oil Red O revealed that WT mice on a HF diet had a significant increase in lipid accumulation when compared to WT ND animals. These findings are in agreement with recent evidence suggesting increased CD36 mRNA and protein expression in mice fed a high-fat diet (Koonen et al., 2007). Interestingly, CD36 KO mice fed a HF diet showed a significant increase of lipid accumulation in the liver, when compared to WT HF diet, CD36 KO ND and WT ND animals. This was evident by the increased lipid number as well as larger lipid size. Expression of mRNA levels from both *Fatp2* and *Fatp1* were significantly increased in livers from CD36 KO HF diet animals, compared to control WT mice. Previously

published data demonstrated that knock-down of FATP2 in a mouse model of obesity showed reduced fatty acid uptake and ameliorated signs of hepatic steatosis (Falcon et al., 2010). Moreover, FATP1 has been identified as an insulin-sensitive fatty acid transporter involved in diet induced obesity. Like CD36, FATP1 has been shown to translocate from an intracellular compartment to the plasma membrane in response to insulin signalling (Wu et al., 2006). FATP1-null mice are protected against diet-induced obesity and insulin desensitisation. Under normal circumstances, FATP1 is not detectable or only expressed at low levels in the human liver (Martin et al., 2000). It has been suggested that FATP1 plays a crucial role in the redistribution of fatty acids from adipose and skeletal muscle tissue to the liver (Wu et al., 2006) and is functionally coupled to fatty-acid Co-enzyme A (FA-CoA) synthesis (Clugston et al., 2011). This is in line with the findings from this study, revealing increased expression of *Fatp2* and *Fatp1* in CD36 KO mice on a HF diet, suggesting the development of hepatic steatosis. Furthermore, the expression of *Cidea*, an important regulator of lipolysis and lipid fusion (Puri et al., 2008, Viswakarma et al., 2007), was 22-fold increased in CD36 KO HF diet mice compared to control mice. This data indicates a key role of CD36 in the development of lipid accumulation and hepatic steatosis. Collectively, these findings suggest opposing effects of CD36 deficiency with a protective role in the skeletal muscle due to reduced lipid accumulation, but at the same time leading to an overload of lipid deposition in the liver tissue, possibly indicating a compensatory mechanism.

3.6 Conclusion

This study investigated several parameters of skeletal muscle morphology, linking fatty acid metabolism to CD36 during increased fatty acid availability. CD36 deficient mice exhibited decreased body weight gain when exposed to high-fat diet feeding, indicating protection from diet-induced obesity. Moreover, CD36 is likely to play a tissue specific role, indicated by tissue specific weight changes including skeletal muscle, heart and white adipose tissue (WAT). However, no major significant changes in the skeletal muscle fibre type distribution nor fibre size (CSA) was observed in slow-oxidative and fast-glycolytic muscles, represented by Soleus and EDL muscle, respectively. Although no diet

nor genotype specific fibre type distribution or remodelling were observed, gene expression related to mitochondrial β -oxidation was increased in CD36-deficient mice on a high-fat diet suggesting alterations in mitochondrial activity and bioenergetics.

Moreover, fatty acid uptake and accumulation in skeletal muscle and liver tissue was increased in WT mice fed a high-fat diet. However, the absence of CD36 exerts opposing effects in skeletal muscle and liver tissue, which is evident by the decreased lipid accumulation in skeletal muscle of CD36 KO mice on a HF diet on one side, but on the other side the increased lipid infiltration seen in CD36 KO mice liver sections under HF diet feeding conditions. This further suggests a compensatory effect of the liver in regards to the decreased lipid uptake in the skeletal muscle, which is in agreement with the observed mRNA upregulation of alternative fatty acid transporters such as *Fatp2* and *Fatp1* in the liver of CD36 KO HF diet mice, associated with increased lipid fusion via upregulation of *Cidea*. It should be pointed out that, in human studies of CD36 deficiency, similar observations have been made, revealing impaired fatty acid uptake in the heart and skeletal muscle tissue but unaffected fatty acid uptake in the liver.

The development of non-alcoholic fatty liver disease (NAFLD) is one of the many complications associated with obesity and the development of diabetes. This data suggests an important link between CD36 and *Cidea* with potential implications in the management of NAFLD.

4 CHAPTER 4- The effect of CD36 deficiency and high-fat diet on skeletal muscle redox biology and oxidative stress

4.1 Overview

Obesity and ROS

Reactive oxygen species (ROS) are a naturally occurring by-products of oxygen metabolism. Previously, it has been shown that low levels of ROS play a crucial role in cellular signalling and cell fate (Zhang et al., 2016). ROS can arise from intracellular or extracellular processes. Mitochondrial oxidative metabolism as well as cellular response mechanisms to cytokines and bacteria have been reported as an important origin for ROS production (Zhang et al., 2016). However, if cellular levels increase, ROS can lead to severe toxic effects, resulting in oxidative stress. Increased levels of ROS have been implicated in the pathogenesis of cancer, obesity, the development of insulin resistance and other metabolic disorders as well as immune dysfunction (Di Meo et al., 2017).

Adipokines produce ROS in physiological conditions. In pathophysiological conditions, such as obesity, where adipokines are increased and thus, the ROS production is elevated, this results in oxidative stress and pro-inflammatory processes (Fernández-Sánchez et al., 2011).

Over-production of ROS in combination with reduced efficacy of anti-oxidant mechanisms, lead to increased oxidative stress and cellular damages, further deteriorating the obese and diabetic conditions. It has been postulated that skeletal muscle lipid accumulation along with reduced mitochondrial activity in obesity is one of the major underlying mechanisms leading to the development of lipotoxicity and skeletal muscle insulin resistance. Furthermore, recent reports suggest that increased ROS production interfere with mitochondrial function, possibly promoting mitochondrial alterations and dysfunction (Di Meo et al., 2017). Interestingly, ROS generation due to muscle activity, is elevated in obese individuals, possibly linking the increased rate of cellular respiration and oxygen consumption to the observed high values of post-exercise lipid hydroperoxide in obesity (Vincent et al., 2004). Hence it has been hypothesised that ROS production and pre-inflammatory conditions play a crucial role in the obese conditions and obesity-related co-morbidities (Marseglia et al., 2014). In oxidative stress, free radicals can lead to alteration and post-translational modification of proteins, resulting in loss or gain of function. One possible way of post-

translational modification due to ROS, is the addition of reactive carbonyl functional groups on the proteins. This process, termed protein carbonylation, is referring to a carbonyl protein adduct. One of the most common and reactive carbonyl-adducts generated, is 4-Hydroxy-Nonenal (4HNE), formed during the process of polyunsaturated fatty acid oxidation. 4HNE protein adducts are linked to dysregulation of the redox homeostasis and cellular stress signalling. 4-HNE induced inhibition of the proteasome machinery, which is highly involved in eradicating misfolded proteins, leads to a further increase of malfunctional proteins in oxidative stress conditions (Grimsrud et al., 2008). In addition, obesity has been correlated to elevated levels of nitrogen species, representing an end product of oxidative damage to proteins and amino acids. 3-nitortyrosine (3NT) has been widely used as a marker to assess oxidative damage to evaluate the redox state in obese conditions (Isabella Savini et al. 2013). Thiobarbituric acid-reactive substance (TBARS) levels are linked to end-point oxidative damage and represent another useful tool to assess oxidative stress and the overall impact on the redox homeostasis (Dawn-Linsley et al., 2005). Due to their highly reactive character, free radicals are difficult to measure directly. Dihydroethidium (DHE) can form a fluorescent product as a result of redox reactions, detecting $O_2^{\cdot-}$ specific products (Dikalov and Harrison, 2014).

Evidence reports that oxidative stress plays a critical role in impaired wound healing. This can be observed in aging, several pathological conditions, in individuals treated with immunosuppressive drugs, as well as in the diabetic condition. It has been shown that optimal wound healing is linked to a tightly regulated redox homeostasis, further elucidating the importance of oxidative stress in the context of obesity-related complications (Schäfer and Werner, 2008).

Patients with type 2 diabetes show significantly higher free-fatty acid (FFA) plasma levels, with palmitate, stearate and oleate amongst the most abundant FFAs. It has been shown that palmitate-induced ROS production leads to the accumulation of misfolded or unfolded proteins, resulting from impaired endoplasmic reticulum (ER) activity. The accumulation of unfolded or misfolded proteins initiate the palmitate-induced ER stress response which is associated with sustained reduction of the ER Ca^{2+} pool. Ca^{2+} is a key player in mitochondrial

Krebs cycle activity mitochondrial transport and general metabolism. The observed disruption of intracellular Ca^{2+} homeostasis may initiate pathogenic processes involved in mitochondrial dysfunction observed in obesity (Ly et al., 2017).

4.2 Aims

The aim of this chapter was to identify the impact of high fat diet feeding on oxidative stress development and skeletal muscle redox homeostasis in the presence or absence of CD36. The hypothesis was, that high-fat diet feeding increased lipid uptake mediated via CD36 would ultimately lead to lipid accumulation and the development of oxidative stress in the skeletal muscle of WT mice. Furthermore, it was hypothesised, that in the absence of CD36, diet-induced oxidative stress would be ameliorated, resulting in improved skeletal muscle redox homeostasis. To test this hypothesis the following objectives were identified:

- i. To evaluate skeletal muscle protein modification in obesity
- ii. To study the effect of genotype and/or diet on the levels of reactive oxygen species in skeletal muscle
- iii. To examine the expression of antioxidant enzymes in skeletal muscle
- iv. To determine the effect of genotype and/or treatment on the levels of reactive oxygen species in isolated satellite cells
- v. To evaluate the impact of CD36 in cellular stress development, linked to intracellular calcium signalling

4.3 Materials and Methods

4.3.1 Thiobarbituric acid reactive substance (TBARS)

TBARS levels have been associated with oxidative damage and represent a useful tool to assess oxidative stress. Briefly, protein extracts from gastrocnemius muscle were diluted 1:5 in RIPA buffer and a serial dilution (1:10) of MDA in RIPA lysis buffer was prepared. After adding equal volumes of protein sample and SDS to all samples, 500 μ L of TBA Buffer was added in each tube and the samples incubated at 95°C for an hour. Samples were cooled down and centrifuged at 3,000 x rpm for 15 minutes at RT. Subsequently, 100 μ L of supernatant were transferred into a 96 well plate. The fluorescence signal was used to calculate the MDA concentration.

4.3.2 Protein extraction and Immunoblotting

Protein extraction was performed by homogenisation of the tissue submerged in RIPA lysis buffer containing 1% v/v Nonidet P 40 substitute, 0.1% w/v SDS and 0.5% w/v sodium. Pre-cooled RIPA buffer (1mL) was added to the frozen tissue and homogenised for 30 to 40 seconds at 18,000 x rpm. Once completely homogenised, the samples were centrifuged at 4°C for 15 minutes at 14,000 x g. The supernatant was then diluted 1:5 in RIPA buffer and protein quantification is performed using the Pierce BCA protein assay and a BSA standard. After an incubation of 30 minutes at 37°C the absorbance can be measured at 562nm in the TECAN M200 plate reader. Protein extracts (30µg) were diluted 1:1 with Laemlli's buffer and boiled at 95°C for 10. In order to separate the proteins, a resolving gel with 0.1% SDS is used. The gel is left to solidify for one hour, and a stacking gel is prepared to be poured on top of the resolving gel. After 20 minutes the gel is completely solidified and can be used to load the samples. The gel was secured in a casting stand and subsequently placed into the electrophoresis module assembly and submerged in running buffer. Together with a molecular weight marker the samples were loaded into the pockets of the gel. The samples were separated using electrophoresis at 100 Volt for 120 minutes. Once complete, the gel is removed from the glass plates and the protein can be transferred via wet blotting. The gel is placed in-between foam pads and blot paper, which are both soaked in Transfer buffer. A polyvinylidene membrane was activated by the addition of methanol and subsequently submerged with Transfer buffer for 5 minutes. Inside a holder cassette, the methanol-activated PVDF membrane was placed onto the gel and between the blot papers and foam pads. The holder cassette was placed into a Mini Trans-Blot Module and an electric current of 100 Volt for 80 minutes is used to transfer the proteins from the gel onto the PVDF membrane. After the transfer of the proteins onto the PVDF membrane, an incubation for 45 minutes in 5% non-fat milk was used to block unspecific binding sites. Subsequently, the membrane is incubated at 4°C overnight with the primary antibodies for 3NT or 4HNE. Following the incubation with the primary antibodies, the membrane is washed with TBS/0.1% Tween for 4x5 minutes and incubated with polyclonal anti-mouse IgG secondary antibody for one hour. Following a wash step in TBS/ 0.1%Tween for 4x 5 minutes and 5 minutes in TBS alone, the bands were visualised using Licor or an X-ray film by

adding ECL1 and ECL2 in a 1:1 ratio to the membrane. The densitometric analysis was performed using ImageJ software. The levels of protein were expressed relative to the signal of β tubulin.

4.3.3 Immunoblotting for posttranslational oxidative protein modification

Protein nitration was analysed by using specific antibodies, determined by immunofluorescence. Furthermore, 4HNE was used as a marker of protein modification. Protein was extracted from gastrocnemius muscle and protein content was assessed using the BCA assay according to protocols on section 2.7.1.

4.3.4 RNA isolation, cDNA synthesis and quantitative RT-PCR

As previously published by Sfyri et al. (Sfyri et al., 2018), muscle RNA was extracted using the E.Z.N.A. Total RNA kit I according to the manufacturer instruction.. Briefly, 50-100mg frozen gastrocnemius muscle was homogenised in 1mL of prechilled TRIzol. The homogenised muscle was transferred to a fresh collection tube and 200 μ L of 100% chloroform was added, followed by vigorously shaking the samples. After a short incubation for two minutes at RT the samples were centrifuged for 15 minutes at 4°C, 12,000x g to cause phase separation. The RNA containing aqueous phase was transferred into a fresh collection tube and 500 μ L/mL of 100% isopropyl alcohol was added for the precipitation of nucleic acids whilst samples were stored for 10 minutes at RT. The resulting mixture was then loaded onto a HiBind RNA Column with subsequent centrifugation of the samples for one minute at 10,000x g. The flow-through was discarded and 500 μ L RNA Wash Buffer I added to the HiBind RNA Column and centrifuged at 4°C for one minute at 10,000x g. The flow-through was discarded and 500 μ L RNA Wash Buffer II was added to the HiBind RNA Column, followed by centrifugation at 4°C for one minute at 10,000x g. The flow-through was discarded and the procedure repeated once more. In order to dry the HiBind RNA Column before the RNA elution, a final centrifugation step at 4°C for two minutes at 13,000x g was performed. RNA was eluted by adding 20 μ L of ultrapure water to the HiBind RNA Column. The centrifugation was performed following an incubation at RT for one minute. Subsequently, the samples were centrifugation

at 4°C for two minutes at 12,000x g. The concentration (ng/μL) and purity (A_{260}/A_{280}) of isolated RNA was determined by performing a NanoDrop spectrometric analysis. The samples were stored at -80°C until use or further processed for DNase I treatment, in order to eliminate DNA contaminations. cDNA synthesis was performed by reverse transcription using the RevertAid H Minus First Strand cDNA Synthesis Kit as previously reported by Sfyri et al. (Sfyri et al., 2018) and according to the manufacturer's protocol. A MasterMix containing the Oligo(dT) Primer was added to initiate the reverse transcription using a Veriti thermal cycler. Quantitative real time PCR was used to detect and quantify gene expression levels in a variety of samples by the addition of the non-sequence specific, double-stranded DNA intercalating dye, SYBR Green to reliably detect, at every cycle of the PCR, the amount of the newly formed PCR product. In this study the reference genes *Cyp* and *Hprt* (Appendix) were used to normalise the gene expression in all groups.

Table 4.3.4: Primer sequences

<i>Ogg1</i>	Forward	CAACAACATTGCTCGCATTACTG
	Reverse	TCAAGCTGAATGAGTCGAGGT
<i>Nox2</i>	Forward	TGAATGCCAGAGTCGGGATT
	Reverse	CGAGTCACGGCCACATACA
<i>Cat</i>	Forward	GGATTATGGCCTCCGAGATCTT
	Reverse	TAAAACGTCCAGGACGGGTAA
<i>Prdx1</i>	Forward	CTGGCATGGATTAACACACCC
	Reverse	GGTGCCTTGGGATCTGAT
<i>Mgst1</i>	Forward	CCTCCTATGCAACGATCATTCTT
	Reverse	ACCTTGTTGGTTATCCCTCTGG
<i>Sod1</i>	Forward	TATGGGGACAATACACAAGGC
	Reverse	CGGGCCACCATGTTTCTTAGA

4.3.5 Dihydroethidium (DHE) assay for reactive oxygen species detection

DHE staining was performed as previously published (Paolini et al., 2018). The frozen muscle tissue sections on glass slides were equilibrated to RT and rehydrated using PBS. For DHE staining in living cells, satellite cells were isolated and proliferated (Methods 2.2.5) on glass cover slips and subsequently differentiated (Methods 2.2.6). The cell cultures on glass cover slips were washed

with PBS and incubated with 10 μ M DHE for 30 minutes at 37°C. The sections or cells were washed with PBS and mounted with DAPI containing mounting medium. Images were obtained using a Zeiss Axioimager A1 microscope and an AxioCam MRm monochrome camera. Alexa 594 filters were used to visualize the DHE staining.

4.4 Results

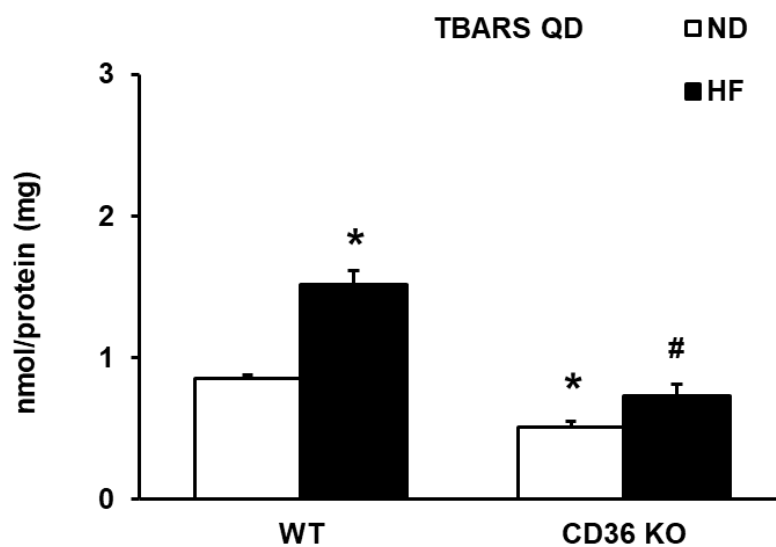
Skeletal muscle from CD36 KO mice is protected from HF diet-induced oxidative stress. Recent evidence indicates a direct link between the production of diet-induced reactive oxygen species (ROS) and levels of oxidative protein modifications such as 4-hydroxynonenal (4-HNE) and 3-nitrotyrosine (3NT) adducts, that are involved in the development of insulin resistance (Pillon et al., 2012, Ingram et al., 2012, Soulage et al., 2018). Loss of CD36 is known to attenuate ROS production, alleviating oxidative stress (Gharib et al., 2016, Okamura et al., 2009). Therefore, to determine the impact of CD36 deficiency and HF diet on the redox homeostasis of the skeletal muscle, lipid peroxidation (Thiobarbituric Acid Reactive Substance; TBARS), protein oxidative modifications (3NT, 4-HNE), DNA damage (Ogg1 relative mRNA expression) and ROS production (Dihydroethidium; DHE staining) were assessed.

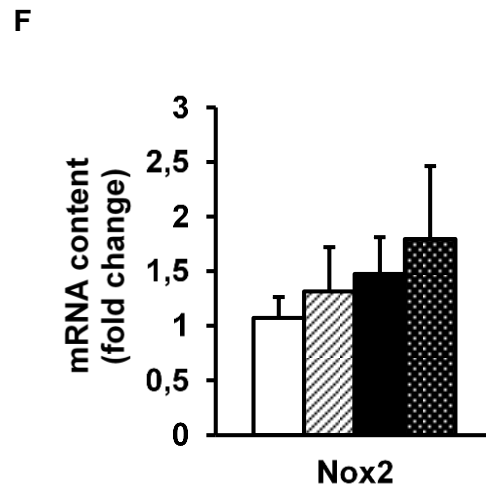
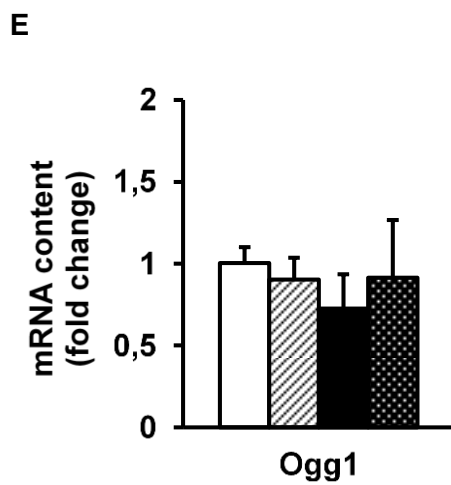
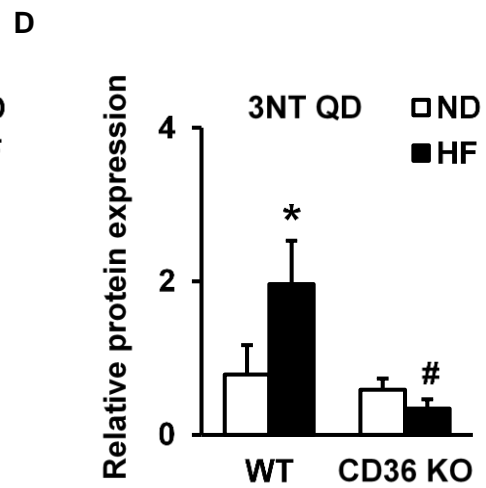
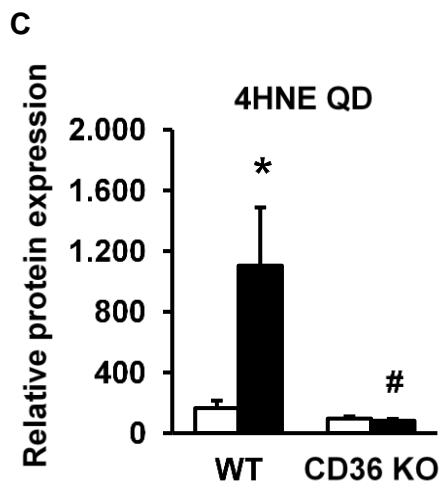
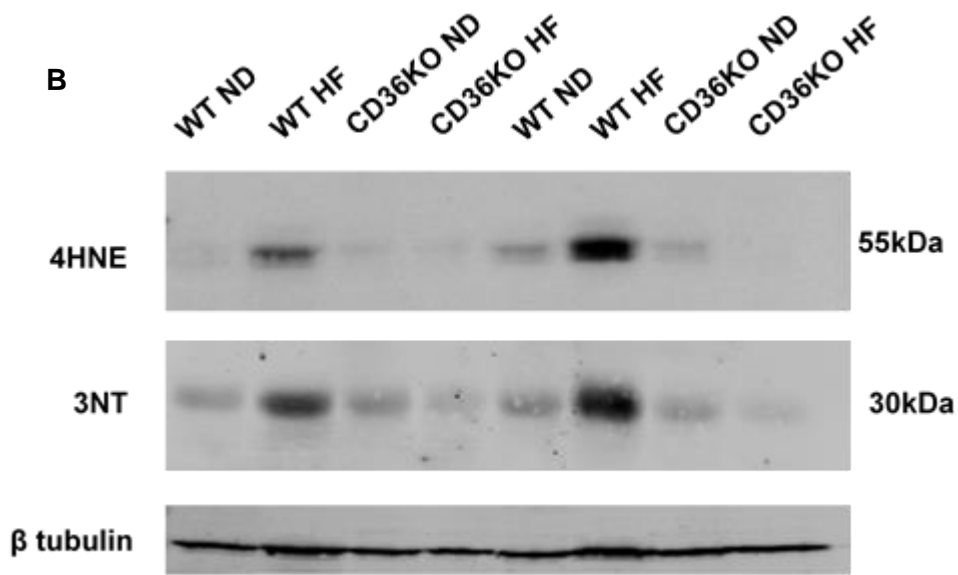
TBARS levels were used as a marker to measure lipid peroxidation, indicating oxidative injury. Skeletal muscle TBARS levels were significantly increased in the WT HF diet group compared to the WT ND group (1.51 nmol/mg \pm 0.1 vs. 0.85 nmol/mg \pm 0.02 which is in accordance with previously published data (Furukawa et al., 2004). In contrast, HF diet fed CD36 KO mice showed TBARS levels comparable to the CD36 KO ND and WT ND control group (**Figure 4.1A**).

Compared with the WT ND group, WT animals fed a HF diet showed significantly increased (WT ND 165.6 \pm 47.8 vs. WT HF 1103.7 \pm 384.8) levels of 4-HNE protein adducts (**Figure 4.1B,C**). CD36 KO mice fed a HF diet showed no elevated 4-HNE levels when compared to their CD36 KO ND littermates as well as to WT ND mice. Similarly, WT HF diet mice displayed an increase in 3NT (WT ND 0.8 \pm 0.4 vs. WT HF 2 \pm 0.6) levels (**Figure 4.1B,D**), which is an indirect marker of increased mitochondrial ROS levels, leading to increased protein

modification. However, CD36 KO mice on a HF diet displayed significantly reduced 3NT levels compared to WT HF diet animals and similar 3NT levels to those seen in the CD36 KO ND animals and the WT ND control group. To explore the mechanism of altered markers for oxidative stress levels, the relative mRNA expression levels of 8-Oxoguanine glycosylase (*Ogg1*; DNA repair enzyme), Nicotinamide adenine dinucleotide phosphate oxidase 2 (*Nox2*; oxidative stress marker), *Catalase*, Peroxiredoxin-1 and microsomal Glutathione S-Transferase 1 (*Cat*, *Prdx1*, *Mgst1*, *Sod1*; antioxidant genes) were determined by RT-PCR. There were no significant changes in the relative mRNA expression level of DNA-repair gene *Ogg1*, nor in the expression of the oxidative-stress marker gene *Nox2* (**Figure 4.1E,F**). However, the expression of the anti-oxidant enzyme *Catalase* was significantly upregulated in WT HF (2-fold; 1.87 ± 0.3), CD36 KO ND (1.4-fold; 1.35 ± 0.2) and CD36 KO HF (2,2 fold; 2.10 ± 0.30) diet animals when compared to control (0.94 ± 0.2) littermates (**Figure 4.1G**). Furthermore, the expression level of the antioxidant gene *Prdx1* was significantly increased in CD36KO HF diet animals (1.66 ± 0.4) when compared to CD36 ND (0.82 ± 0.2), WT HF (1.02 ± 0.1) and WT ND ($1.01 \pm 0,1$) animals. Additionally, *Mgst1* and *Sod1* were increased in CD36 deficient mice on a HF diet (1.21 ± 0.2 , 1.18 ± 0.2) when compared to the CD36 KO ND (0.81 ± 0.23 , 0.93 ± 0.14) and WT HF (0.83 ± 0.2 , 0.9 ± 0.1) diet groups (**Figure 4.1G**).

A





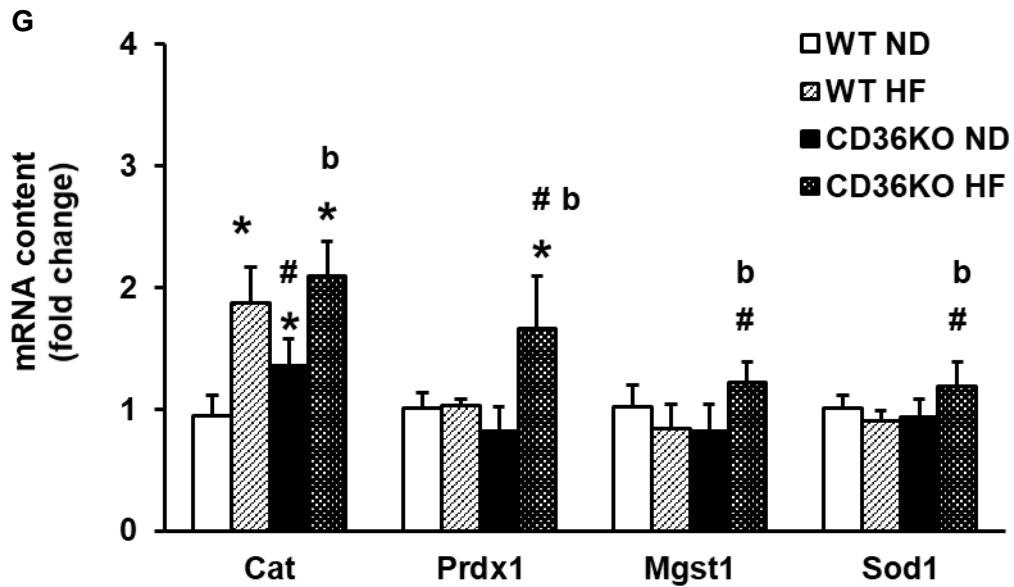


Figure 4.1. High-fat diet induced protein modification and antioxidant gene expression in skeletal muscle. WT and CD36 KO mice on either ND or HF diet were investigated for markers of lipid peroxidation, oxidative stress and general lipid metabolism. **(A)** Skeletal muscle lipid peroxidation was analysed using TBARS. **(B,C,D)** Skeletal muscle protein modification was assessed by Western Blot **(B)** analysis in quadriceps muscle using 4-HNE **(C)** and 3NT **(D)** as reporter for oxidative protein adducts with representative images of protein adduct blot **(B)**. **(E,F,G)** RNA was isolated from skeletal muscle and RT-PCR was performed. Values were normalised to *Cyp1* and *Hprt*. Data are represented as mean±SD (N=3-4) per group. Statistical analysis was performed using two-way ANOVA, *p<0.05 vs. WT ND, #p<0.05 vs. WT HF, b p<0.05 vs. CD36 KO ND.

To further investigate the impact of increased fatty acid availability on oxidative stress levels, skeletal muscle cross-sections as well as isolated satellite cells were assessed for their ROS content, using Dihydroethidium (DHE) as indicator for superoxide production. DHE has been used extensively in the past to detect intracellular ROS and to monitor superoxide production, due to its ability to freely permeate cell membranes (Wang and Zou, 2018). Upon the reaction of DHE with superoxide anions, the resulting fluorescent product (ethidium) intercalates with the DNA, resulting in a fluorescent signal that can be detected by fluorescent microscopy.

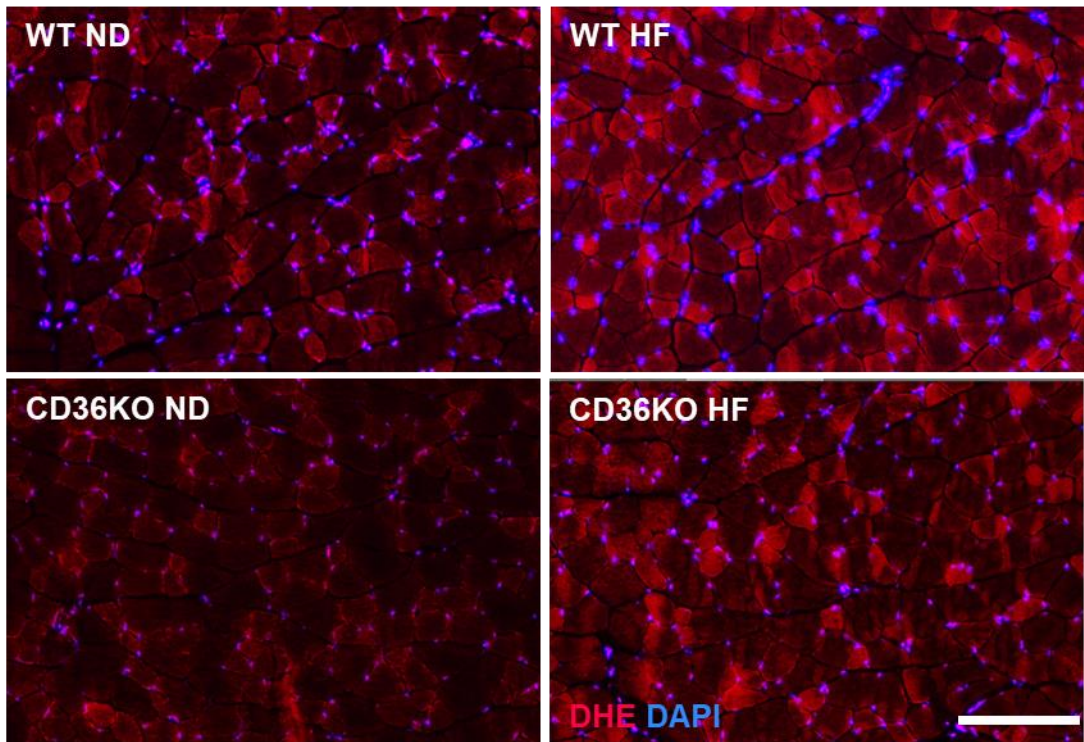
DHE staining of EDL cross-sections revealed that WT mice fed a HF diet show a trend towards an increased DHE signal but no significance was detected. Interestingly, the CD36 KO mice on a ND revealed significantly lower baseline

(112k Gray \pm 84k) DHE levels when compared to CD36 KO HF (407k Gray \pm 124k) diet animals (**Figure 4.2A, B**).

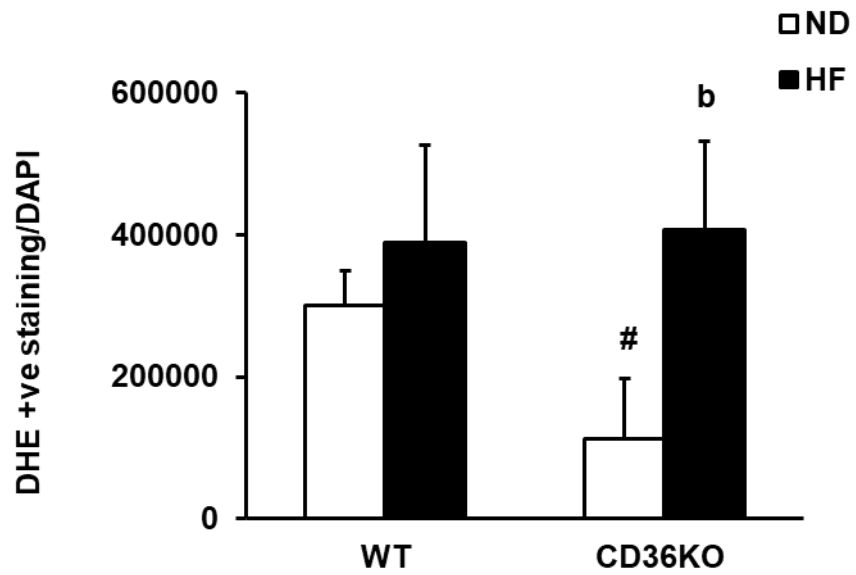
Inflammation and oxidative stress have been shown to critically affect satellite cell function (Alway et al., 2014, Beccafico et al., 2007), which is crucial for skeletal muscle physiology and regeneration. To assess the effect of increased fatty acid availability on ROS production in satellite cells, isolated satellite cells from WT and CD36 deficient animals were differentiated and stained for DHE in the presence or absence of palmitate.

After 5 days of culture in differentiation medium (DM), satellite cells from WT and CD36 KO animals were treated with Palmitate (PA) and histochemically-stained with DHE as indicator for ROS production (**Figure 4.2C**). After a 24-hour treatment with PA the total number of DHE ^{+ve} stained nuclei/total DAPI was significantly increased in WT cell culture conditions (14.6 ± 1.7), compared to CD36 KO cells (7.7 ± 2.6). Similarly, WT satellite cell cultures treated with PA had significantly increased numbers of DHE ^{+ve} nuclei/Myotube/total DAPI (5.1 ± 0.6) when compared to CD36 KO +PA (2.4 ± 1.3) culture conditions (**Figure 4.2D**). Moreover, the nuclear size in cultured satellite cells from WT animals was significantly decreased after the 24-hour treatment with PA. In contrast, PA treatment did not induce alterations in nuclear size in satellite cells derived from CD36 KO mice (**Figure 4.2E**).

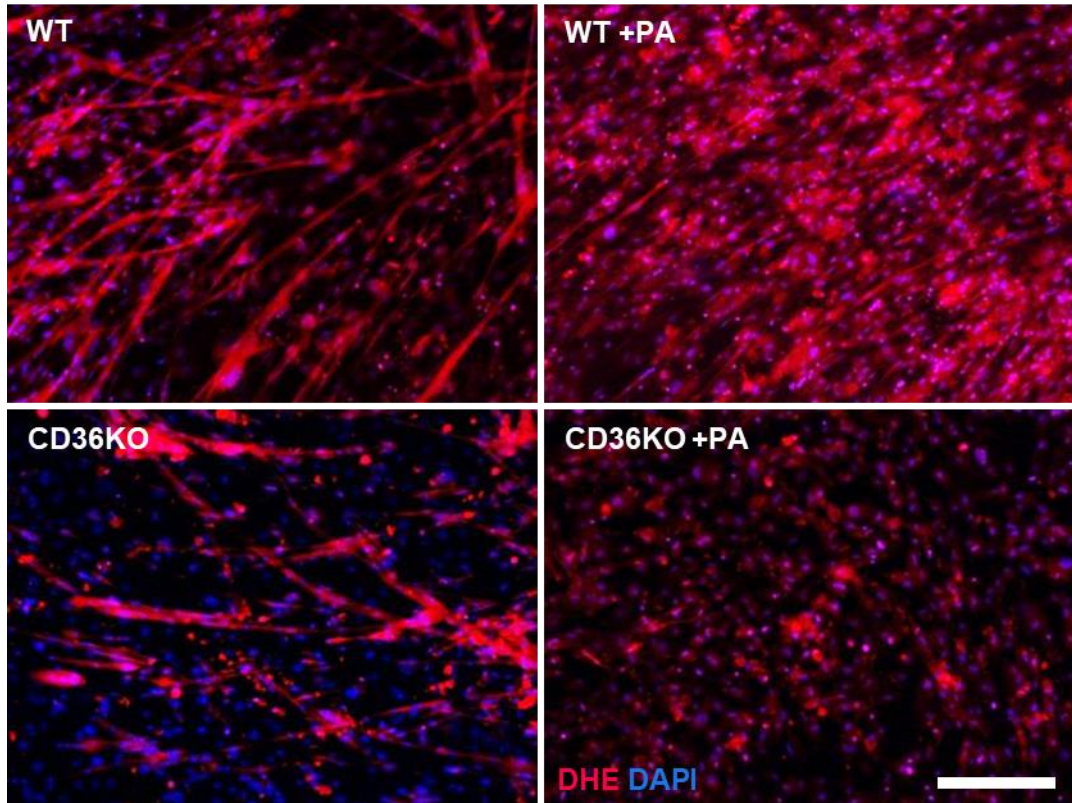
A



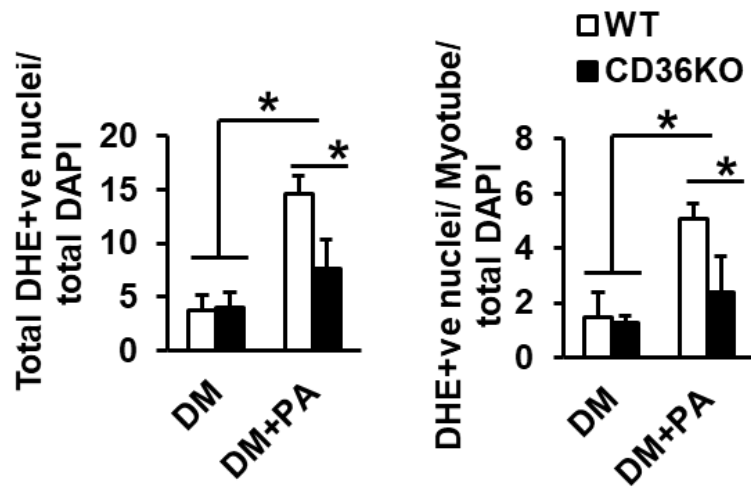
B



C



D



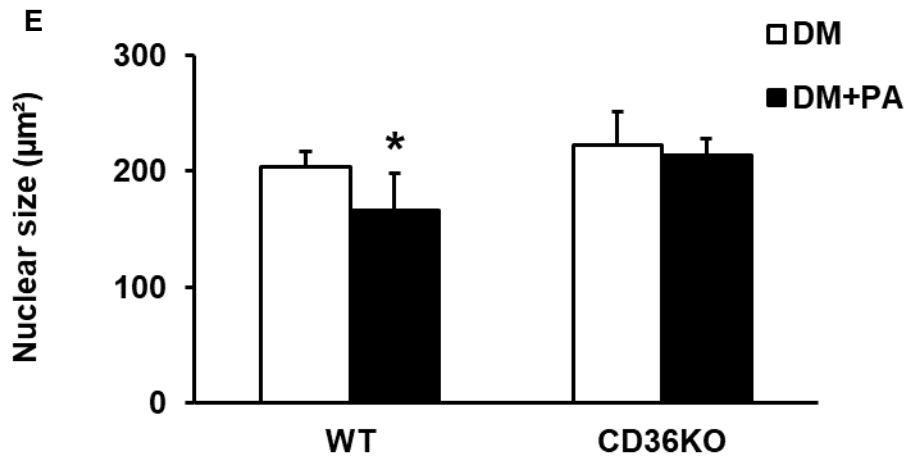


Figure 4.2. High-fat diet induced reactive oxygen species production in skeletal muscle and satellite cells of CD36 deficient mice. WT and CD36 KO mice on either ND or HF diet were investigated for markers of oxidative stress. **(A)** Representative images of skeletal muscle ROS levels in EDL cross-sections (x10 scale bar 200µm) with analysis **(B)**. **(C)** Representative images of isolated satellite cells (x20 scale bar 100µm) using DHE ^{+ve} fluorescent staining as a readout for superoxide species production and DAPI as co-staining of the nuclei. **(D)** Quantification of DHE ^{+ve} staining in differentiated satellite cells from WT and CD36 KO mice in cell culture, treated with palmitate and stained with DHE (Total DHE ^{+ve} nuclei/DAPI and DHE +nuclei/Myotube/total DAPI) with quantification. **(E)** Nuclear size quantification from differentiated satellite cells. Data are represented as mean±SD (N=3-4) per group. Statistical analysis was performed using two-way ANOVA, *p<0.05 vs. WT ND, #p<0.05 vs. WT HF, b p<0.05 vs. CD36 KO ND.

One of the underlying mechanisms leading to inflammation in metabolic diseases is the disturbed cellular homeostasis and impaired function of the endoplasmic reticulum (ER), leading to the activation of several cellular stress pathways. CD36 has been associated with increased ER-stress due to its function as a fatty acid transporter, facilitating fatty acid transport and intracellular lipid accumulation (Seimon et al., 2010). Previous data suggests that CD36 furthermore participates in the transduction of intracellular signals, involved in the stress kinase response implicated in insulin signalling (Kennedy et al., 2011).

Several major signalling pathways controlling mechanisms for muscle adaptation can be affected by altered ROS production. Previously, it has been shown that high levels of ROS not only cause functional oxidative damage to proteins, lipids,

nucleic acids and cell components but also induce a significant rise in intracellular Ca^{2+} levels, initiating signalling cascades for apoptosis or autophagy (Barbieri and Sestili, 2012, Di Filippo et al., 2016). Emerging evidence connects CD36 to $[\text{Ca}^{2+}]$ signalling and the regulation of $[\text{Ca}^{2+}]$ dynamics. Recently published results showed that CD36-dependent signalling is involved in the cellular stress response in cardiac tissue (Pietka et al., 2012).

Due to the known implication of ROS in $[\text{Ca}^{2+}]$ signalling pathways in skeletal muscle cells and the implication in impaired satellite cell function, $[\text{Ca}^{2+}]$ flux was measured in isolated satellite cells from WT and CD36 KO animals, with or without palmitate (PA) treatment. To test for the impact of palmitate on $[\text{Ca}^{2+}]$ flux, satellite cells were isolated from WT and CD36 KO animals and proliferated for 24-hours prior to the calcium signalling analysis. The calcium signal was detected by the FlexStation system, in the absence of extracellular Ca^{2+} . Baseline $[\text{Ca}^{2+}]$ flux was reduced in palmitate treated satellite cells derived from WT and CD36 KO animals compared to palmitate-free conditions. Following the treatment with thapsigargin (TG), satellite cells treated with palmitate exhibited a diminished Fura-2 response signal and a decrease in the Fura₃₄₀/Fura₃₈₀ ratio in the presence of extracellular calcium (2mM) (**Figure 4.3A**). These results might indicate that palmitate alters satellite cell calcium homeostasis independent of genotype. However, further experiments will be needed to validate this finding.

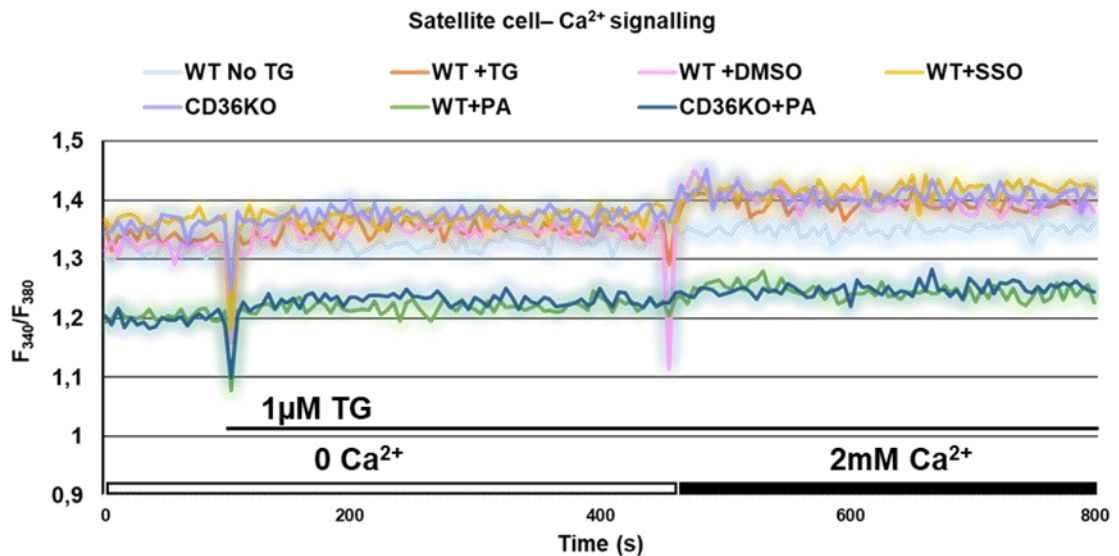
A

Figure 4.3. Palmitate alters Ca²⁺ signalling in satellite cells isolated from WT and CD36 KO animals. Satellite cells from WT and CD36 KO mice were isolated and treated with palmitate (200μM) to investigate their [Ca²⁺] flux in the absence or presence of thapsigargin (TG) and extracellular Ca²⁺ (N= 1). **(A)** [Ca²⁺] flux in isolated satellite cells was assessed by the Fura₃₄₀/Fura₃₈₀ ratio.

4.5 Discussion

4.5.1 Protein modification and adducts

Reactive oxygen species -short ROS- are highly reactive by-products of aerobic metabolism. Under physiological conditions they function as signalling molecules, initiating several important biological pathways such as NFκB, MAPKs and Ca²⁺ signalling (Zhang et al., 2016). However, elevated levels of ROS have been associated with oxidative stress, suggesting an essential role in the development of pathological conditions linked to protein modifications and DNA damage (Schieber and Chandel, 2014). Increased levels of ROS have been correlated to hyper-activation of the inflammatory responses and tissue damage (Dandona et al., 2004). Additionally, dysregulation of ROS has been linked to pathological complications seen in diabetes (Green et al., 2004). Evidence suggests a direct link between the production of diet-induced ROS levels and oxidative protein modifications. During oxidative stress, elevated levels of ROS lead to a variety of metabolic outcomes including oxidatively modified proteins and lipids (Grimsrud et al., 2008).

Thiobarbituric acid reactive substances (TBARS) assay measures malondialdehyde (MDA) in a sample, which is a by-product of lipid peroxidation (Dawn-Linsley et al., 2005).

Lipid peroxidation, which is an indicator of oxidative stress, was significantly increased in the WT HF diet group compared to the WT ND group (TBARS), which is in accordance with previously published data (Furukawa et al., 2004), suggesting increased oxidative stress in high-fat feeding conditions. Interestingly, CD36 KO mice on a high-fat diet showed similar TBARS level when compared to CD36 ND and WT ND control group. This data suggests, that CD36 KO mice show attenuated lipid peroxidation under high-fat diet conditions possibly mitigating oxidative stress. Another indicator of lipid peroxidation is the generation of reactive lipid mediators such as 4HNE and the nitration of tyrosine residues which occur during oxidative damage to proteins from the reaction of nitric oxide with superoxide radicals (Zhong and Yin, 2015) or through nitrite-dependent peroxidase activity (Danielson and Andersen, 2008). Both 4HNE and 3NT have been associated with pathological conditions in humans such as Duchenne muscular dystrophy (DMD) and (Moraes et al., 2015) obesity (Alfaradhi et al., 2014).

In this study, WT mice fed a high-fat diet showed increased levels of 4-HNE and 3NT protein adducts, suggesting elevated protein modification and oxidative damage to proteins. However, the CD36-deficient mice on a high-fat diet showed similar 4-HNE and 3NT levels than littermates on a ND as well as WT ND animals. This further suggests that absence of CD36 attenuates oxidative protein modification and improves the oxidative stress response in high-fat diet conditions. This chapter shows significantly decreased levels of protein modification in CD36 KO HF diet fed mice, indicating a causal role of CD36-mediated fatty acid uptake in skeletal muscle ROS production and oxidative stress which is in line with previously published data (Gharib et al., 2016, Okamura et al., 2009)

Antioxidant and DNA-repair gene expression

Not only has obesity been linked to the oxidative modification of proteins, but has been shown to play a significant role in DNA damage and DNA repair inhibition,

resulting from disturbed cell metabolism in oxidative stress (Zaki et al., 2018). 8-Oxoguanine glycosylase (*Ogg1*) has been described as base excision repair gene, involved in oxidative-stress induced cell death (Wang et al., 2018). Expression of *Ogg1* mRNA in skeletal muscle tissue revealed similar levels in all experimental groups. However, mRNA gene-expression of the anti-oxidant enzyme *Catalase* was significantly upregulated in WT mice on a high-fat diet and even further upregulated in CD36 KO mice independent of diet. The most pronounced increase was observed for *Catalase* in CD36 KO mice on a high-fat diet, indicating a protective mechanism against oxidative stress. Furthermore, the anti-oxidant gene *Prdx1* was significantly increased in CD36 KO animals on a HF diet. *Prdx1* has been shown to preserve telomeric DNA and to safeguard telomeres from oxygen radicals (Aeby et al., 2016), making it an important indicator for improved ROS homeostasis in CD36 deficient mice

4.5.2 ROS production

4.5.2.1 Skeletal muscle and isolated satellite cells

Obesity and associated pathologies such as insulin resistance and diabetes have been linked to alterations in ROS homeostasis (Bailey-Downs et al., 2013). DHE is a potent indicator for superoxide production and has been used extensively in the literature to study intracellular superoxide production in obesity (Bailey-Downs et al., 2013, Tucsek et al., 2014). In the present study, DHE fluorescence in nuclei from skeletal muscle cross-sections showed a significant increase in DHE levels in WT and CD36 KO animals on a high-fat diet. Interestingly, CD36 KO animals on a ND revealed a significantly lower baseline DHE content when compared to WT ND animals.

Inflammation and oxidative stress have been shown to critically affect satellite cell function (Alway et al., 2014, Beccafico et al., 2007). Isolated WT satellite cells showed similar baseline DHE levels when compared to CD36 KO derived satellite cells. Interestingly, WT satellite cells had significantly increased DHE levels following palmitate (PA) treatment when compared to CD36 KO derived satellite cells. Satellite cells are detrimental for skeletal muscle regeneration (Relaix and

Zammit, 2012). These findings support the notion of an improved oxidative stress response with possible implications for skeletal muscle regeneration.

Moreover, the nuclear size of isolated satellite cells was significantly lower in WT cells following PA treatment. However, CD36 KO derived satellite cells showed no alteration in nuclear size after PA treatment when compared to WT ND conditions. Shrinking nuclear size has been previously correlated with hypoxia-induced cell death (Shinzawa and Tsujimoto, 2003). Together, our data suggest that CD36 KO mice have an altered oxidative stress signalling response, partly due to increased antioxidant enzyme activity. These results indicate that ectopic fat accumulation in skeletal muscle tissue via CD36 is primarily involved in increased oxidative stress pathways.

4.5.3 Calcium signalling in oxidative stress

Intracellular calcium signalling plays an important role in several physiological conditions such as muscle cell contraction as well as cell signal transduction and neurotransmitter release (Tanabe et al., 1988, Clapham, 2007). Accumulating data indicates that intracellular $[Ca^{2+}]$ modulates ROS generation as well as ROS clearance. This cross talk between ROS and $[Ca^{2+}]$ further modulates the antioxidant defence system (Zhang et al., 2016). An increasing body of evidence connects CD36 to $[Ca^{2+}]_i$ signalling and the regulation of $[Ca^{2+}]$ dynamics (Xu et al., 2015). Recently published results showed that CD36-dependent signalling is involved in the cellular stress response in cardiac tissue (Pietka et al., 2012). Changes in $[Ca^{2+}]_i$ by extracellular Ca^{2+} addition were compared between WT and CD36 KO derived satellite cells. Additionally, WT derived satellite cells were treated with the potent CD36 inhibitor SSO. The calcium rise was almost completely prevented when the satellite cells were treated with palmitate which was independent of CD36 inhibition. These results might indicate that palmitate alters the Ca^{2+} flux in proliferating satellite cells, which could possibly impact several physiological signalling pathways involved in the oxidative stress response. Further research will however be necessary to confirm this finding.

4.6 Conclusion

This chapter aimed to investigate the redox homeostasis and markers of oxidative stress in skeletal muscle and isolated satellite cells from WT and CD36 KO mice. Furthermore, the impact of HF diet feeding or high availability of fatty acids in form of palmitate treatment on ROS production was examined.

ROS are highly reactive by-products and important second messengers in several physiological conditions including cellular signalling pathways and general cellular function (Zhang et al., 2016). However, alterations in the ROS homeostasis have been linked to severe pathological conditions such as inflammation, protein modification (Schieber and Chandel, 2014) and insulin resistance resulting in metabolic disorders such as obesity and diabetes (Dandona et al., 2004). Several indicators of protein modification and oxidative stress were significantly increased in WT animals on a HF diet when compared to the CD36 KO animals on a HF diet. These findings suggest that fatty-acid uptake and accumulation leads to a disturbed ROS homeostasis and altered calcium signalling, which is partly regulated through CD36. Furthermore, antioxidant gene expression was shown to be significantly upregulated in CD36 KO HF mice, suggesting improved redox signalling and decreased oxidative stress in the skeletal muscle as well as in satellite cells in the presence of high fatty-acid availability. CD36 expression has been shown to be associated with tissue inflammation (Febbraio et al., 2001) and increased oxidative stress (Gharib et al., 2016). This thesis shows that markers of oxidative stress are reduced, paralleled by increased antioxidant enzyme gene expression in CD36-deficient mice under HF diet conditions, suggesting improved redox homeostasis. These findings are in line with recently published data showing decreased obesity-associated oxidative stress in the hearts of CD36 deficient mice (Gharib et al., 2016).

5 CHAPTER 5- The effect of CD36 deficiency and high-fat diet on skeletal muscle satellite cell biology

5.1 Overview

Skeletal muscle stem cells, also called satellite cells, are crucial for skeletal muscle maintenance and repair after injury. Originally discovered in 1961 (Mauro, 1961), it was demonstrated, that satellite cells initially provide myoblasts to support muscle growth in the developing muscle tissue, until they become mitotically quiescent as the muscle matures. Under normal conditions, satellite cells remain in their niche in a quiescent state until they are activated due to routine muscle fibre homeostasis or upon muscle injury. In a quiescent state, satellite cells reside in a niche on the surface of the muscle fibre, expressing the transcription factor Pax7. Upon activation, satellite cells start to co-express the transcription factor myogenic differentiation 1 (MyoD), which marks the proliferation state of these newly formed myoblasts (Zammit et al., 2002). Following the proliferation phase, most Pax7/MyoD-expressing myoblasts transition to differentiation, which is marked by the upregulation of the transcription factor Myogenin, whilst downregulating the expression of Pax7. Only a small percentage of cells maintain Pax7^{+ve} and downregulate MyoD, reverting to a quiescent state to maintain a steady stem cell pool (Nagata et al., 2006). Satellite cell function is crucial for skeletal muscle repair. Genetic ablation of satellite cells (Lepper and Fan, 2012) as well as the satellite-cell specific absence of Pax7 have been linked to deleterious defects in muscle growth and repair (Seale et al., 2000). Furthermore, several severe muscle diseases with impaired regenerative capacity have been linked to the malfunction of the satellite cells. One of the most severe skeletal muscle diseases is the Duchenne muscular dystrophy (DMD). It has been hypothesised, that DMD is linked to the exhausted potential of satellite cells due to recurrent cycles of muscle injury and regeneration (Kottlors and Kirschner, 2010). DMD is characterised by progressive skeletal muscle weakening and degeneration, which is connected to a mutation in the dystrophin gene resulting in either complete loss or the expression of non-functional dystrophin protein. The absence of functional dystrophin has been shown to interfere with satellite cell polarity, which in turn leads to intrinsic satellite cell dysfunction and impaired regeneration (Koenig et al., 1987). Additionally, impaired satellite cell function has been linked to skeletal muscle wasting in aging, also called sarcopenia (Alway et al., 2014).

Sparse findings indicate that in obesity, skeletal muscle ectopic lipid infiltration impairs satellite cell activation leading to a decrease of skeletal muscle regeneration potential (Xu et al., 2018, D'Souza et al., 2015). It has been suggested, that HF-diet induced impairment of satellite cell function in HF conditions might be linked to impaired myogenesis and skeletal muscle healing as well as the observed decreased muscle mass and muscle function seen in obese humans (Hilton et al., 2008). This notion is further supported by previously published evidence showing that palmitate treatment in C2C12 cells inhibits differentiation in cell culture conditions.

As a way to measure skeletal muscle regeneration, several injury models have been used in the past. One of the most frequently used injury models to study the underlying physiological processes of skeletal muscle regeneration uses cardiotoxin (CTX), performed as a single or several injections into the muscle of the mouse. The dynamics of skeletal muscle regeneration can be assessed over several days following the initial injury. Important post-injury timepoints to assess the process of muscle healing are five days and ten days following the injection (Krause et al., 2011). Five days after injury, the structure of the skeletal muscle is severely damaged, which can be visualised by several immunohistochemical methods. One of the main features of regenerating fibres includes the presence of basophilic fibres, which can be identified by their dark-purple stained cytoplasm and centrally located nuclei in H&E stained sections showing injured fibres. Furthermore, the unspecific binding of IgG secondary antibodies is a valuable marker to identify dying or dead fibres in the muscle tissue. At this stage, regenerating myofibres express embryonic Myosin Heavy Chain (eMHC), which is useful to follow up the regeneration process (Janssen and Henson, 2012). Later stages of skeletal muscle regeneration are marked by macrophage infiltration and inflammation, which is a necessary process to remove cellular debris as a process of cellular regulation of the inflammatory response in order to restore healthy tissue (Janssen and Henson, 2012). Additionally, as the regeneration process proceeds, the muscle fibre size and CSA increases, forming a new, tightly organised fibre network which starts to form at approximately 10 days after the initial injury.

5.2 Aims

The aim of this study was to further investigate the effect of genotype and/or diet on skeletal muscle satellite cell function. Furthermore, this chapter addresses the impact of CD36 deficiency during satellite cell activation, proliferation and differentiation. It was hypothesised that high-fat diet feeding would impair satellite cell function mediated, at least partly, through CD36 in the skeletal muscle. Moreover, the absence of CD36 would improve high-fat diet induced alterations in satellite cell function. To investigate the above-mentioned hypothesis, the following objectives were set;

- i. To investigate the impact of diet and genotype on satellite cell number during activation, proliferation and differentiation
- ii. To examine the impact of diet and genotype on the satellite cell expression profile during myogenesis
- iii. To study the expression of genes regulating satellite cell differentiation
- iv. To investigate the impact of CD36 during acute injury *in vivo*

5.3 Materials and Methods

5.3.1 Satellite cell isolation, proliferation and differentiation

To isolate primary satellite cells from individual muscle fibres the EDL muscle was precisely dissected from tendon to tendon and immediately submerged in digestion medium. Satellite cell isolation was adopted from a previous published protocol from Syverud et al. (Syverud et al., 2014). After 3-5 hours of incubation of the muscle tissue in the digestion medium at 37°C and 5% CO₂, the muscle was transferred in a horse serum coated petri dish with DMEM medium and the fibres were carefully separated by trituration using a wide-bore fire-polished glass pipette. Subsequently, the fibres were incubated in 1mL 0.125% Trypsin-EDTA (in PBS) for 5 minutes at 37°C and 5% CO₂. Following the addition of 1mL Satellite cell Growth Medium (30% fetal bovine serum, 1.5% chicken embryo extract) the cell suspension was transferred into 50mL tubes and centrifuged at 16,000 x g for 5 minutes. The supernatant was discarded and the remaining cell pellet re-suspended in 3mL satellite cell growth medium. The cell suspension was then transferred into Matrigel-coated cell culture dishes, followed by a three-day

incubation at 37°C and 5% CO₂ in satellite cell growth medium. After three days the medium was changed to fresh satellite cell proliferation medium (10% fetal bovine serum, 0.5% chicken embryo extract) and subsequently changed every two days until the cells reached 80% confluency. Cells that reached 80% confluency were further processed and differentiated towards myotubes using satellite cell differentiation medium (5% horse serum). Medium was changed every two days. Satellite cells were cultured for 4-6 days in differentiation medium until cell fusion and myotube formation was visually confirmed.

5.3.2 Immunofluorescence of satellite cell activation pattern in cultured myofibres

Myofibre fixation was performed using 4% PFA (in PBS) in which the fibres were incubated for 15 mins at RT. After the removal of the excess PFA, the fibres were subsequently washed with PBS and stored at 4°C until further use. For the following immunofluorescent staining the excess PBS was removed and fibres permeabilised with permeabilisation buffer for 15 minutes prior to the primary antibody incubation. Primary antibodies for Pax7, MyoD and Myogenin were diluted (1:200) and the fibres were incubated overnight at 4°C. On the following day the primary antibody was removed and after several wash steps with wash buffer the appropriate secondary antibody Alexa Fluor was added and incubated for one hour at RT in the dark. Secondary antibodies were added individually and fibres were washed in between with wash buffer to avoid unspecific binding. Followed by a final wash step in wash buffer the fibres were transferred to glass microscopy slides and mounted with DAPI supplemented mounting medium. Digital images were obtained with a Fluorescent imaging was performed using the Zen Axioimager A.1 microscope and manually quantified using the ZEN imaging software.

5.3.3 C2C12 proliferation and differentiation

C2C12 proliferation and differentiation methods were adopted from Scully et al. (Scully et al. 2018) In brief, C2C12 myoblasts were seeded at a density of 25,000 cells per T25 flasks and cultured in growth medium (Dulbecco's modified Eagle medium; supplemented with 1% L-Glutamine, 20% FBS, 1% PenStrep) in standard conditions (37°C, 5% CO₂). Media was changed every 48 hours until

the cells reached around 80% confluency, for seeding into experimental conditions. Once the proliferating C2C12 cells reached around 80% confluency, the growth medium was changed to myoblast differentiation medium (DM Dulbecco's modified Eagle medium; supplemented with 1% L-Glutamine, 2% HS, 1% PenStrep). The media was changed every 48 hours for approximately 4-6 days until cell fusion and myotube formation could be visually confirmed.

5.3.4 EdU cell proliferation assay

The cell proliferation rate of the SC was analysed using the EdU incorporation assay as described previously by Scully et al. (Scully et al. 2018) Briefly, the cells were isolated and cultured for three days in SC growth medium. The proliferation rate was determined in isolated satellite cells from EDL muscle tissue. After the initial isolation the satellite cells were cultured until they reached approximately 80% confluency. Subsequently the cells were split at a density of 10,000 cells/well in a 24 well plate. EdU was used 24 hours later at 10 μ M for three hours; diluted in culture media (DMEM and Penicillin/Streptomycin). The fluorescent signal detection was performed by immunostaining with Dye Azide.

5.4 RNA isolation, cDNA synthesis and quantitative RT-PCR

As previously published by Sfyri et al. (Sfyri et al., 2018), muscle RNA was extracted using the E.Z.N.A. Total RNA kit I according to the manufacturer instruction. Briefly, 50-100mg frozen gastrocnemius muscle was homogenised in 1mL of prechilled TRIzol. The homogenised muscle was transferred to a fresh collection tube and 200 μ L of 100% chloroform was added, followed by vigorously shaking the samples. After a short incubation for two minutes at RT the samples were centrifuged for 15 minutes at 4°C, 12,000x g to cause phase separation. The RNA containing aqueous phase was transferred into a fresh collection tube and 500 μ L/mL of 100% isopropyl alcohol was added for the precipitation of nucleic acids whilst samples were stored for 10 minutes at RT. The resulting mixture was then loaded onto a HiBind RNA Column with subsequent centrifugation of the samples for one minute at 10,000x g. The flow-through was discarded and 500 μ L RNA Wash Buffer I added to the HiBind RNA Column and

centrifuged at 4°C for one minute at 10,000x g. The flow-through was discarded and 500µL RNA Wash Buffer II was added to the HiBind RNA Column, followed by centrifugation at 4°C for one minute at 10,000x g. The flow-through was discarded and the procedure repeated once more. In order to dry the HiBind RNA Column before the RNA elution, a final centrifugation step at 4°C for two minutes at 13,000x g was performed. RNA was eluted by adding 20µL of ultrapure water to the HiBind RNA Column. The centrifugation was performed following an incubation at RT for one minute. Subsequently, the samples were centrifugation at 4°C for two minutes at 12,000x g. The concentration (ng/µL) and purity (A_{260}/A_{280}) of isolated RNA was determined by performing a NanoDrop spectrometric analysis. The samples were stored at -80°C until use or further processed for DNase I treatment. In order to eliminate DNA contaminations. cDNA synthesis was performed by reverse transcription the RevertAid H Minus First Strand cDNA Synthesis Kit was used according to the manufacturer's protocol. A MasterMix containing the Oligo(dT) Primer was added to initiate the reverse transcription using a Veriti thermal cycler. Quantitative real time PCR was used to detect and quantify gene expression levels in a variety of samples by the addition of the non-sequence specific, double-stranded DNA intercalating dye, SYBR Green to reliably detect, at every cycle of the PCR, the amount of the newly formed PCR product. In this study the reference genes *Cyp* and *Hprt* (Appendix) were used to normalise the gene expression in all groups.

Table 5.4: Primer sequences

<i>Myogenin</i>	Forward	GAGACATCCCCCTATTTCTACCA
	Reverse	GCTCAGTCCGCTCATAGCC
<i>Tmem8c</i>	Forward	GTGATGGGCCTGGTTTGTCT
	Reverse	GCATTGTGAAGGTCGATCTCTG
<i>Acta1</i>	Forward	CCCAAAGCTAACCGGGAGAAG
	Reverse	GACAGCACCGCCTGGATAG
<i>Mhc1</i>	Forward	AGTCCCAGGTCAACAAGCTG
	Reverse	TTCCACCTAAAGGGCTGTTG
<i>Srf</i>	Forward	CTGCCTCAACTCGCCAGAC
	Reverse	TCAGATTCCGACACCTGGTAG
<i>Bex1</i>	Forward	ATGGAGTCCAAAGATCAAGGCG
	Reverse	CTGGCTCCCTTCTGATGGTA

5.5 Immunofluorescent of isolated satellite cells in culture

Satellite cells were isolated, proliferated and differentiated according to the Method section 2.2.5 and 2.2.6. Following cell fixation for 15 minutes using 4% PFA (in PBS), excess PFA was removed and the cells were washed in PBS 2 x 5 minutes. For the following immunofluorescent staining the excess PBS was removed and the cells permeabilised with permeabilisation buffer for 15 minutes prior to the primary antibody incubation. Primary antibody for differentiated myotubes was Myogenin, diluted (1:200) and incubated overnight at 4°C. On the following day the primary antibody was removed and after several wash steps with wash buffer the appropriate secondary antibody Alexa Fluor was added and incubated for one hour at RT in the dark. Followed by a final wash step in wash buffer the cells were co-stained with DAPI supplemented mounting medium. Digital images were obtained with a Fluorescent imaging was performed using the Zen Axioimager A.1 microscope and manually quantified using the ZEN imaging software.

5.5.1 Cardiotoxin (CTX) induced muscle injury *in vivo*

Tibialis anterior (TA) muscle injury was induced as previously described (Scully et al. 2019). Briefly, mice were injected with a total of 30µL, 50 µmol/L cardiotoxin (*Naja pallida* CTX) into the TA muscle. Mice were humanely euthanized 5- and 10-days post-injury and the TA muscles were collected for subsequent immunohistochemistry. Immunohistochemistry was used to identify necrotic tissue and damaged fibres (H&E, IgG), as well as newly formed fibres (embryonic myosin heavy chain; eMHC; 1:200). Macrophage infiltration was further assessed by CD68 (1:200) immunofluorescent staining.

5.5.2 Tissue embedding and cryosectioning

Skeletal muscle tissue samples were embedded in optimal compound temperature tissue mounting medium, immersed in 100% ethanol on dry ice to prevent samples from thawing. Samples were then either stored at -80°C or used for cryo-sectioning. OCT blocks containing embedded tissues were equilibrated to -21°C for 10- 15 minutes prior to cryo-sectioning and transverse sections of 10µm thickness were obtained and mounted on microscopy glass slides coated with Poly-L-lysine. Subsequently, the mounted sections were dried on the microscopy glass slides for 30 minutes at RT and stored at -80°C for further analysis. Skeletal muscle tissues were analysed for morphological features following CTX-induced injury after 5 and 10 days.

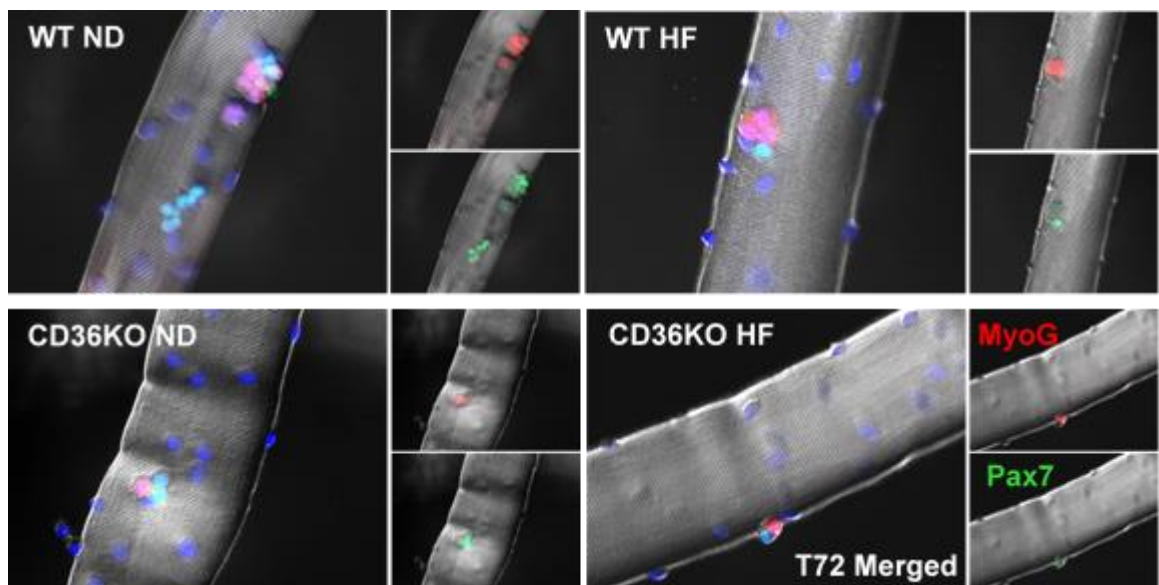
5.6 Results

5.6.1 CD36 exhibits different functions during satellite cell proliferation and differentiation.

Given that lipid accumulation in the skeletal muscle is primarily involved in increased oxidative stress levels, the next aim was to further examine the impact of HF diet on the satellite cell function. The satellite cell number was unchanged at baseline levels between the groups independent of diet and genotype. However, after 24 hours of culture, the number of satellite cells (Pax7^{+ve}/MyoD^{-ve}, Pax7^{+ve}/MyoD^{+ve}, Pax7^{-ve}/MyoD^{+ve}) was significantly reduced in the WT HF diet group (4.7 ± 0.35 vs. WT ND 7.17 ± 0.4) compared to WT ND, CD36 KO ND

and CD36 KO HF diet animals. Following 48 hours in cell culture, the number of activated and proliferating satellite cells remained significantly lower in the WT HF diet (6 ± 0.5 vs. WT ND 8.7 ± 0.7) animals compared to the other groups (**Figure 5.1A-B**). Both CD36 KO ND and CD36 KO HF diet groups showed no sign of decreased total satellite cell number up to 48 hours of cell culture. However, after 72 hours in cell culture, there was a significant decrease in satellite cell number (Pax7⁺/Myogenin⁻, Pax7⁺/Myogenin⁺, Pax7⁻/Myogenin⁺) in all groups (WT HF 8.2 ± 0.7 , CD36 KO ND 8.8 ± 0.7 , CD36 KO HF 7.7 ± 0.5 vs. WT ND 12.8 ± 0.8) compared to the control group (**Figure 5.1B**). Quantification of the satellite cell myogenic marker expression after 24, 48 and 72 hours in cell culture conditions revealed a similar expression pattern in all experimental groups following 24, 48 and 72-hours of cell culture (**Figure 5.1C**). These results suggest that long-term HF diet feeding has a negative impact on satellite cell function and commitment towards proliferation and differentiation, which is linked to fatty acid uptake via CD36. Furthermore, CD36 appears to play a key role during myocyte terminal differentiation, indicated by the diet-independent decrease in satellite cell number at 72 hours in the CD36 KO animals.

A



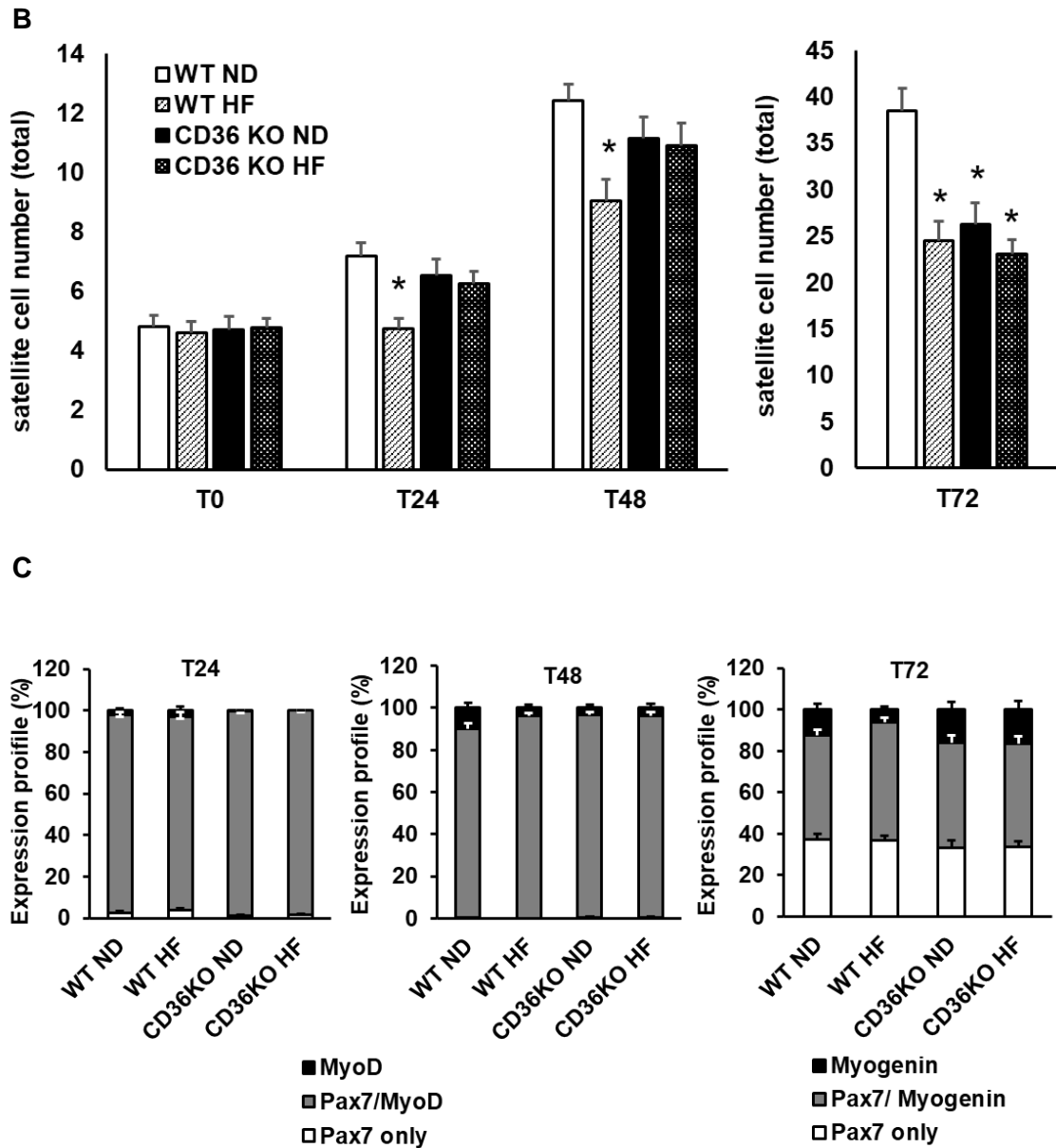
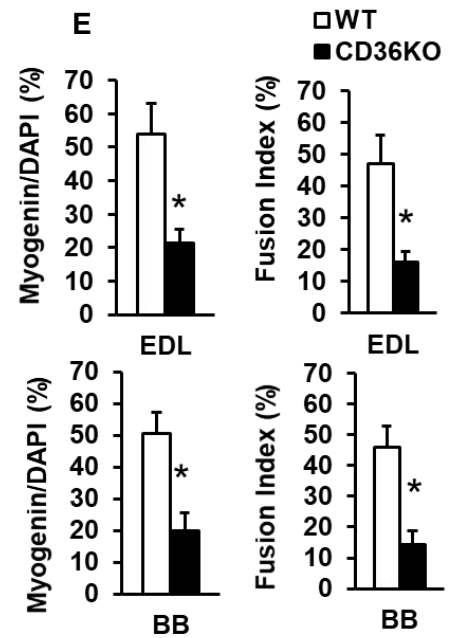
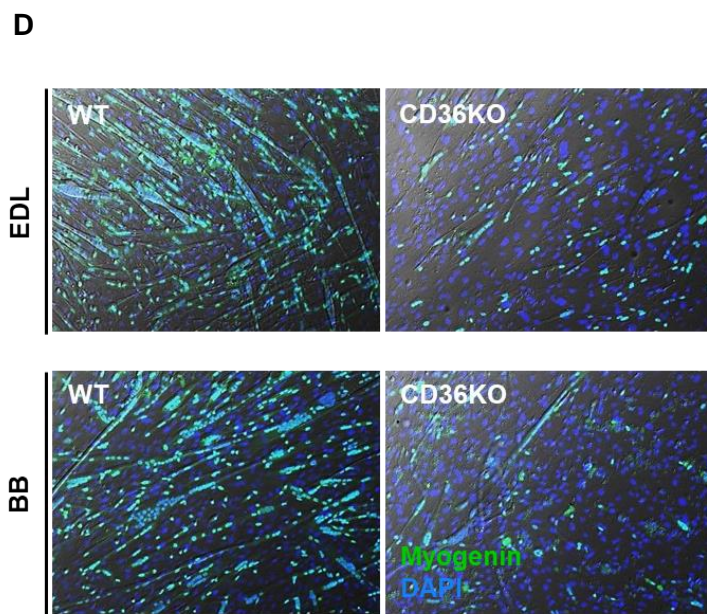
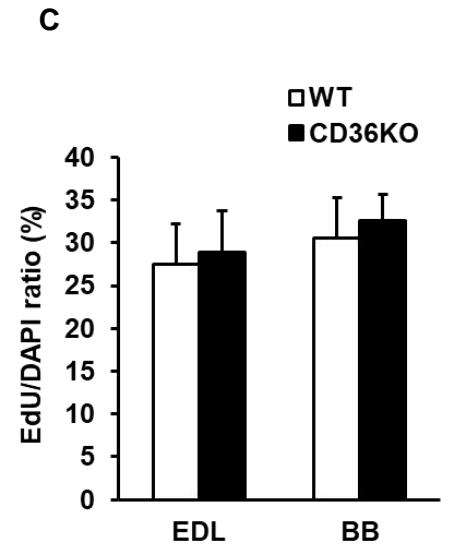
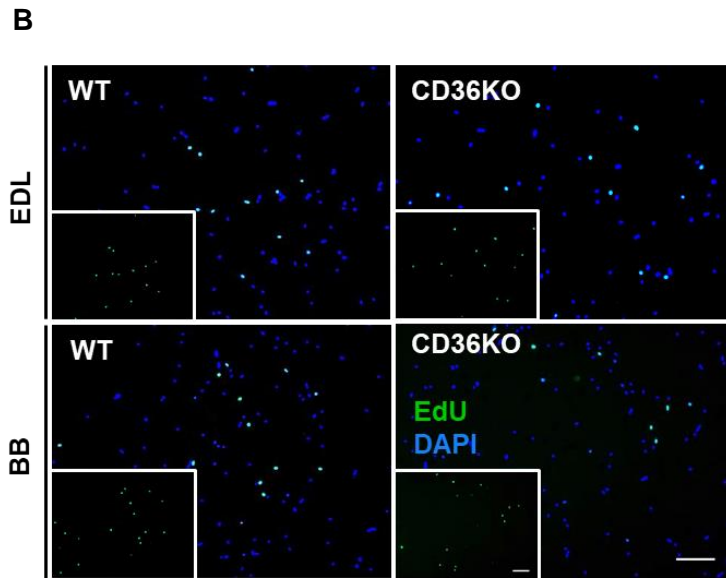
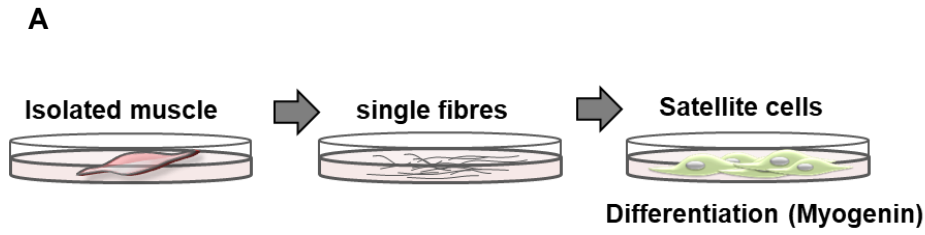


Figure 5.1. CD36 deficiency attenuates satellite cell proliferation in high-fat diet fed mice. Isolated EDL myofibres with their associated satellite cells were either immediately fixed with 4% PFA or further cultured in fibre medium (FM) for T24, T48 and T72 hours. **(A)** Representative pictures of T72 show immunostaining for Pax7, Myogenin with Myonuclei and satellite cell nuclei counterstained using DAPI. **(B)** Quiescent satellite cells were identified (T0 hours) and quantified using immunostaining for Pax7. Satellite cell commitment towards activation and proliferation (T24 and T48 hours) was quantified by Pax7 and MyoD, and Differentiation (T72 hours) by Pax7 and Myogenin immunostaining. **(C)** Expression profiles of the fibre-associated satellite cells was analysed after T24, T48 and T72 hours. Data are represented as mean \pm SEM (N=5 mice per condition; more than 50 individual myofibres were counted). Statistical analysis was performed using two-way ANOVA, *p<0.05 vs. WT ND.

5.6.2 Loss of CD36 alters the metabolic profile of satellite cells and leads to impaired myotube formation.

Previous findings indicate that CD36 plays opposing roles during satellite cell proliferation and differentiation. To further evaluate the function of CD36 during the process of myogenesis, satellite cells derived from WT and CD36 KO mice were isolated from the EDL and *biceps brachii* (further referred to as BB) muscle to further test their myogenic potential *in vitro* (**Figure 5.2A**). In order to assess the proliferative capacity of isolated satellite cells in culture conditions, 5-ethynyl-2'-deoxyuridine (EdU) was used as a readout to quantify proliferation. Proliferation potential of isolated satellite cells derived from either the EDL or BB muscle was comparable between WT and CD36 KO mice 24-hours after the first cell passage (**Figure 5.2B,C**). In contrast, after 5 days culture in differentiation medium, using Myogenin as a marker for satellite cell differentiation, satellite cell differentiation and myotube formation was severely impaired in satellite cells derived from CD36 deficient animals. This was indicated by a significantly lower Myogenin/DAPI (%) ratio (EDL CD36 KO 22 ± 4 vs. WT 54.0 ± 9.2 and BB CD36 KO 19.8 ± 5.7 vs. WT 50.5 ± 6.6) as well as a significantly lower fusion index (FI) in CD36 KO animals (EDL 16.1 ± 3.2 and BB 14.2 ± 4.5) than in WT (EDL 47.1 ± 9 and BB 46.1 ± 6.9) control (**Figure 5.2D,E**). These findings were independent of satellite cell origin from EDL or BB muscle. To examine the expression profile of genes involved in the maturation and fusion of satellite cells, early (1 day in differentiation medium) and late differentiation (5 days in differentiation medium), relative mRNA expression of Myogenin, myoblast fusion factor/myomaker (*Tmem8c*), α -actins (skeletal muscle; *Acta1*), myosin-heavy chain 1 (*Mhc1*), serum response factor (*Srf*) and brain expressed x-linked gene 1 (*Bex1*) were quantified by RT-PCR. Relative expression of *Srf* during the late differentiation phase (5d post differentiation; 0.58 ± 0.09 vs. 1 ± 0.02) and significantly reduced expression of *Bex1* during early (1d post differentiation; 0.69 ± 0.07 vs. WT 1 ± 0.03) and late (5d post differentiation; 0.86 ± 0.06 vs. WT 1 ± 0.03) differentiation was observed in satellite cells isolated from CD36-deficient mice (**Figure 5.2F**). These results suggest that CD36 plays a crucial role during satellite cell terminal differentiation and maturation with possible implications for skeletal muscle regeneration.



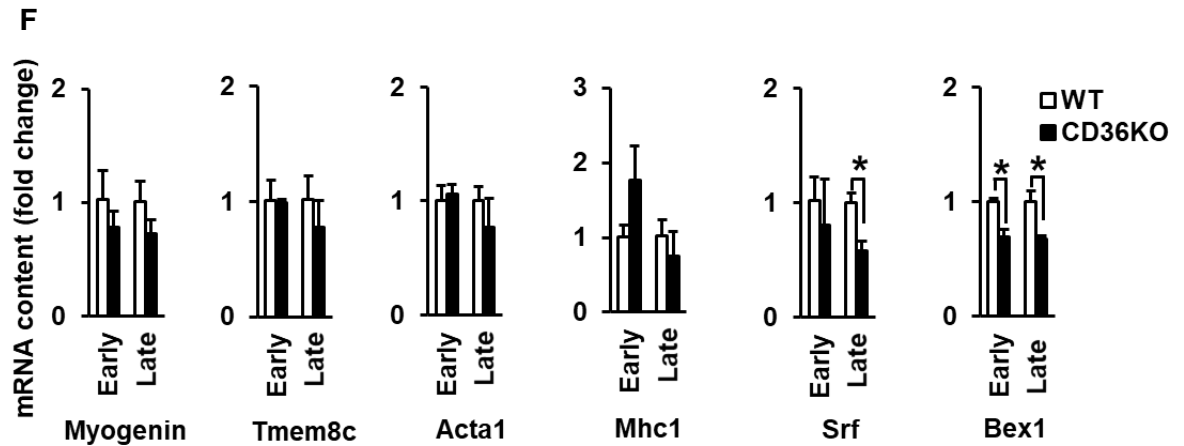


Figure 5.2. CD36 is critical for satellite cell maturation and differentiation.

Immunohistochemistry was performed on isolated, plated satellite cells in proliferation medium (PM) and cultured in growth medium (GM). **(A)** Scheme of satellite cell isolation-protocol from muscle tissue. **(B)** EdU and DAPI co-staining after 24-hour proliferation. **(C)** Proliferation was quantified after 24 hours in GM. Proliferation data was determined as EdU/DAPI ratio. **(D)** Isolated satellite cells were proliferated and differentiation quantified after changing the GM to differentiation medium (DM) for 5 subsequent days. Satellite cells were immunostained for Myogenin and nuclei counterstained using DAPI. Differentiation was determined as Myogenin/DAPI (%) and the Fusion Index (FI) as Myogenin^{+ve} stained nuclei inside myotubes divided by total DAPI. **(F)** RNA was isolated from satellite cells during early (1d) and late (5d) differentiation and RT-PCR was performed. Values were normalised to *Cyp1* and *Hprt*. Data are represented as mean \pm SD (N=3-4) per group. Statistical analysis was performed using two-way ANOVA, *p<0.05 vs WT ND.

5.6.3 Palmitate treatment as well as loss of CD36 both negatively impact satellite cell differentiation capacity.

To further study the effects of CD36 and/or increased fatty-acid availability on muscle stem cell differentiation, isolated satellite cells from WT animals were treated with the potent and irreversible CD36 inhibitor SSO. Once confluent, the cells were further treated with Palmitate (PA) to mimic the HF diet condition in a cell culture setting. Co-immunostaining of Myogenin and DAPI was used to identify differentiated satellite cells (**Figure 5.3A**). After 5 days of culture in differentiation medium, no significant difference was detected in total cell number, calculated by total DAPI staining (**Figure 5.3B**). In contrast, a significant reduced Myogenin/DAPI ratio in satellite cells from WT +PA (9.9 ± 3.8) and CD36 KO +PA groups (10.1 ± 1.2) with a lesser reduction in CD36 KO conditions was observed when compared to the WT (18.5 ± 4.6) untreated condition (**Figure 5.3C**).

However, the calculated fusion index using the Myogenin⁺ve stained nuclei inside myotubes/ DAPI ratio revealed a significant decrease in myoblast fusion in all experimental conditions (WT +PA 4.5 ± 2.4, CD36 KO 8.5 ± 2.3, CD36 KO +PA 6.2 ± 1.5, WT +SSO 5 ± 1.9 vs. WT 17.3 ± 4.3) compared to WT untreated (**Figure 5.3D**). These data further support the previous findings, suggesting that both absence of CD36 and increased fatty acid availability negatively impact satellite cell differentiation.

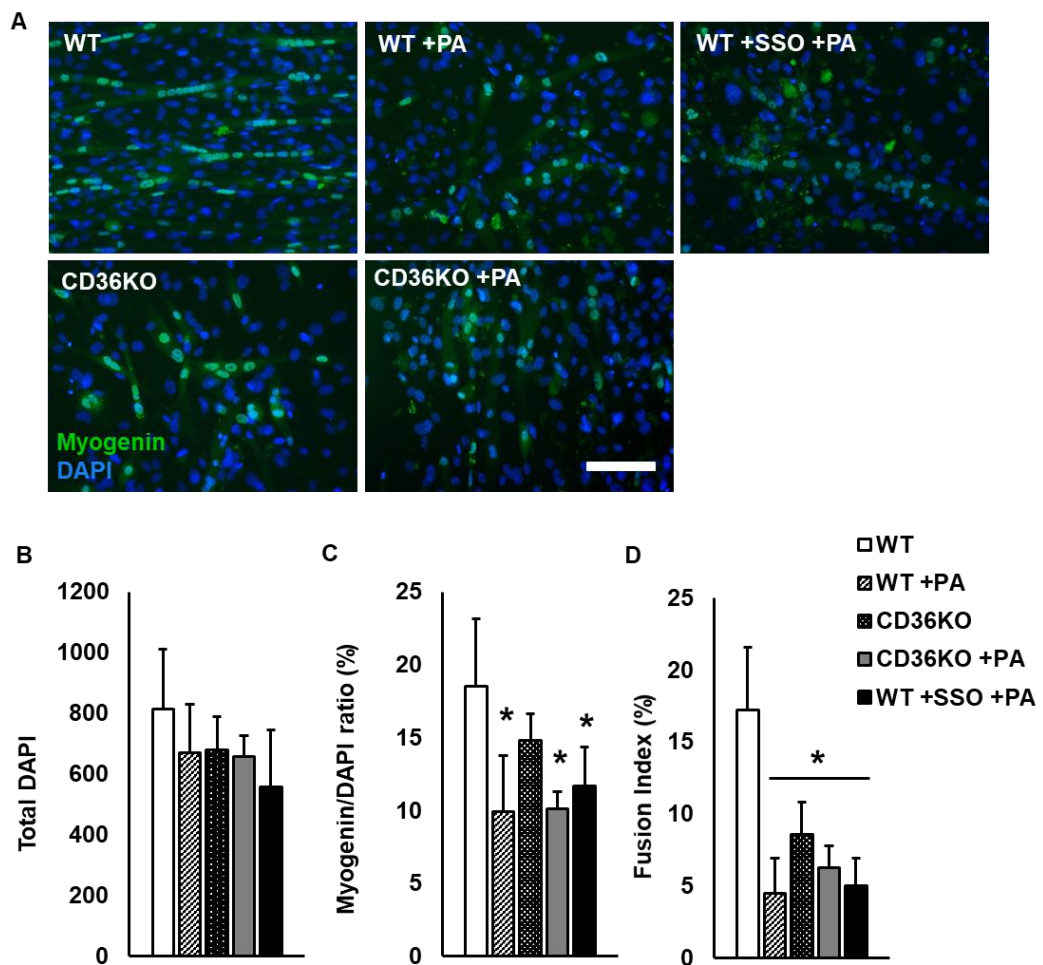
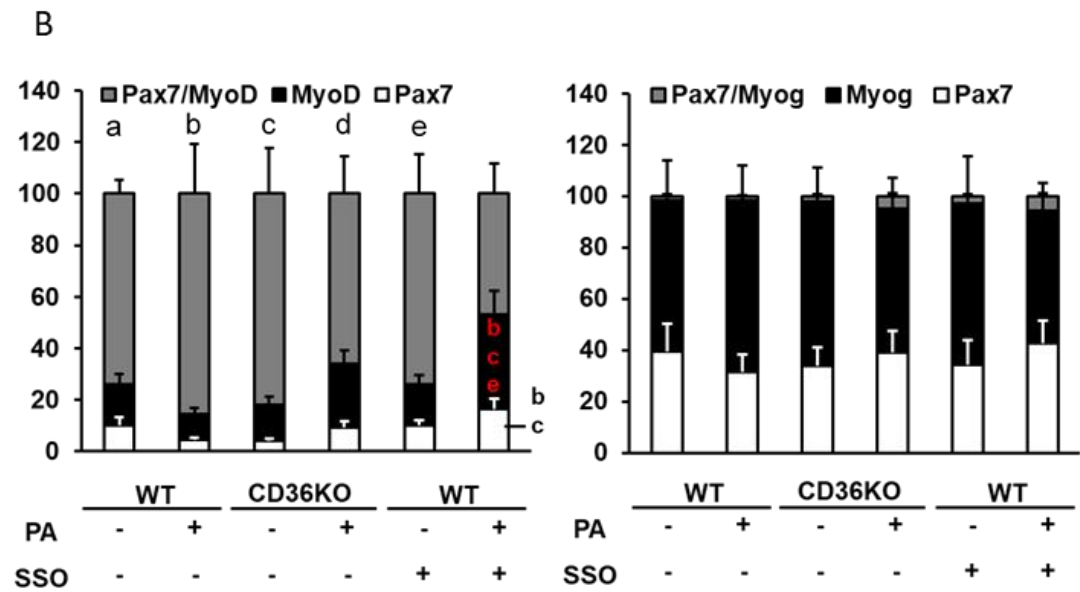
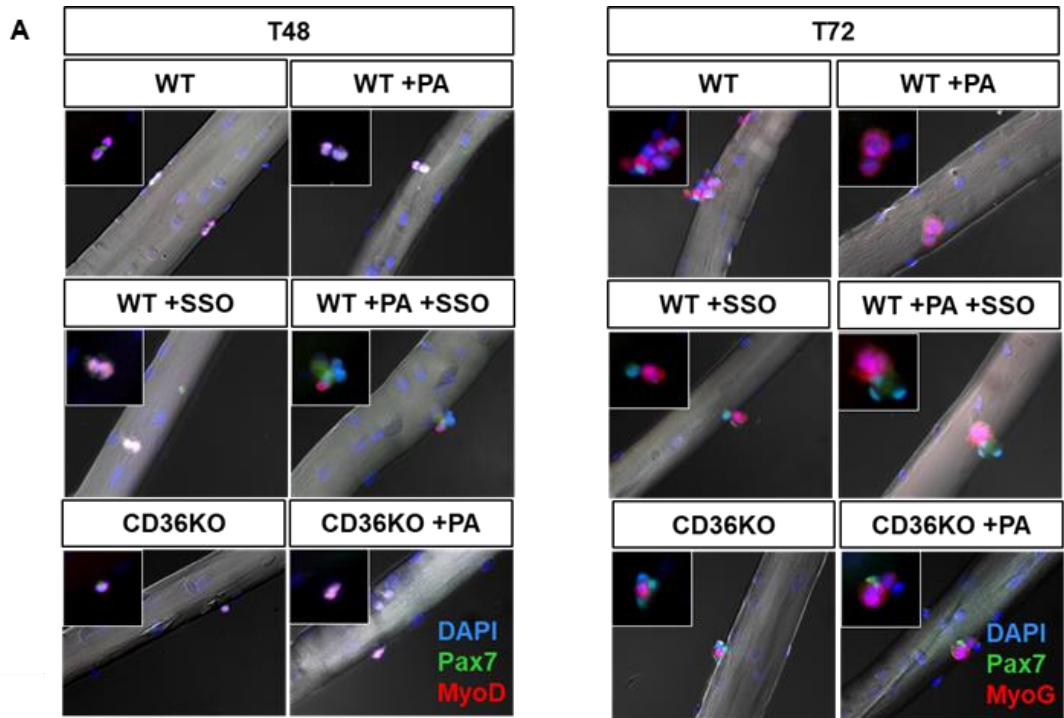


Figure 5.3. Palmitate impairs satellite cell differentiation in WT and CD36 deficient satellite cells. Immunohistochemistry was performed on isolated satellite cells that had been transferred from GM to DM to induce differentiation. Differentiation was quantified after 5 days in DM, following expansion in GM. **(A)** Satellite cells were immunostained for Myogenin and nuclei counterstained using DAPI. **(B)** Total DAPI was used to quantify absolute cell numbers. **(C)** Differentiation was assessed by calculating the Myogenin/DAPI ratio in (%). **(D)** Myogenic Fusion was calculated by Myogenin positive nuclei inside myotubes/DAPI ratio in (%). Data are represented as mean±SD (N=3-4) per group. Statistical analysis was performed using one-way ANOVA, *p<0.05 vs WT.

5.6.4 Both high fatty acid availability and CD36 deficiency alter satellite cell transcription factor expression *in vitro*, resulting in impaired late stage differentiation

Previous results suggest impaired satellite cell differentiation in the presence of high free fatty acid availability. To investigate the effect of palmitate treatment on satellite cells in single fibre culture, individual single fibres were isolated from WT and CD36 KO mice on a ND. Fibres in culture were then either treated with SSO (CD36 inhibitor), palmitate or both, to investigate the influence on satellite cell proliferation and differentiation as well as the effect on satellite cell activation pattern after 48 and 72 hours (**Figure 5.4A**). Although there was no significant difference between WT and CD36 KO derived satellite cell activation patterns when treated with palmitate, the isolated satellite cells from WT fibres treated with PA +SSO showed a significant increase in MyoD compared to WT +PA, CD36 KO and WT +SSO. Furthermore, there was a significant increase in Pax7 expression in WT satellite cells when treated with PA +SSO compared to WT +PA and CD36 KO conditions after 48 hours (**Figure 5.4B**). 72 hours after the initial isolation of the fibres, satellite cells from WT fibres treated with palmitate and SSO showed an increased expression of Pax7/Myogenin when compared to WT untreated, WT +PA and CD36 KO conditions (**Figure 5.4B**). Additionally, the absolute number of satellite cells per fibre were quantified after 48 and 72 hours. Satellite cell numbers after 48 hours in cell culture were independent of genotype and treatment, revealing no significant difference between the groups. However, after 72 hours the satellite cell numbers were significantly reduced in WT+PA, CD36 KO, CD36 KO+PA, WT+SSO and WT+PA +SSO fibres when compared to WT control (10.4 ± 2.2 , 11.5 ± 2.4 , 11.3 ± 2.3 , 8.9 ± 1.8 , 7.5 ± 1.6 vs. 19.6 ± 4.1), further confirming our results that both the absence of CD36 and increased availability of free fatty acids interferes with satellite cell terminal differentiation (**Figure 5.4C**). Analysis of satellite cells/cluster revealed no difference after 48 and 72 hours in culture, independent of genotype and treatment (**Figure 5.4C**).

Overall, data indicated that both palmitate, CD36 deficiency as well as CD36 inhibition lead to altered activation and differentiation in satellite cells, possibly impairing terminal differentiation.



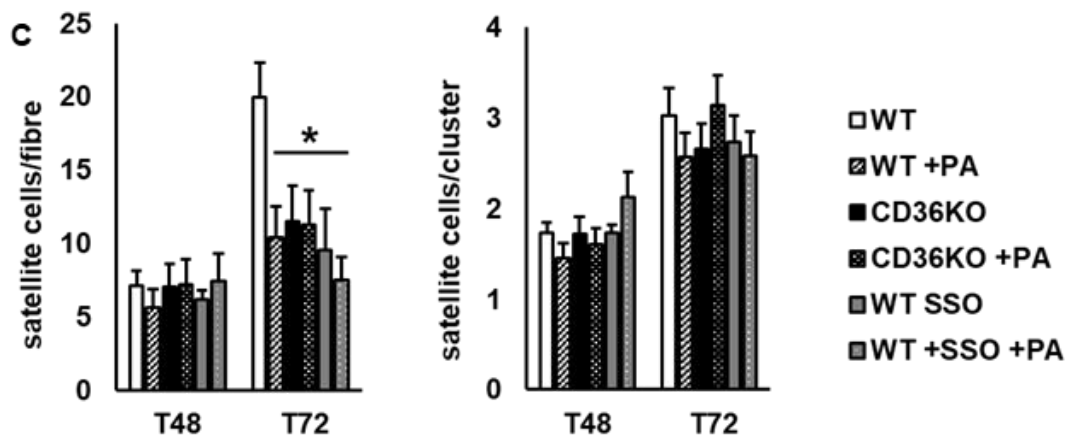


Figure 5.4. Increased fatty acid availability as well as CD36 deficiency impair late stage differentiation. Isolated WT EDL myofibres with their associated satellite cells were cultured in fibre medium (FM) for 48 and 72 hours. Post isolation, fibres remained untreated or were treated with the CD36 inhibitor SSO and/or palmitate. **(A)** Representative muscle fibre pictures show immunostaining for Pax7, MyoD or Myogenin with Myonuclei and satellite cell nuclei counterstained using DAPI, 48 and 72 hours after isolation. **(B)** Expression profiles of the fibre-associated satellite cells were analysed after 48 and 72 hours. Satellite cell commitment towards proliferation (48 hours) was quantified by Pax7 and MyoD, and differentiation (72 hours) by Pax7 and Myogenin immunostaining. **(C)** Total satellite cell number and satellite cells/cluster were calculated at 48 and 72 hours. Data are represented as mean±SEM (N=2 mice per condition; more than 20 individual myofibres were counted). Statistical analysis was performed using two-way ANOVA, a $p < 0.05$ vs. WT, b $p < 0.05$ vs. WT +PA, c $p < 0.05$ vs. CD36 KO, e $p < 0.05$ vs. WT +SSO.

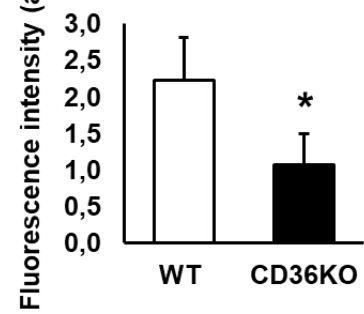
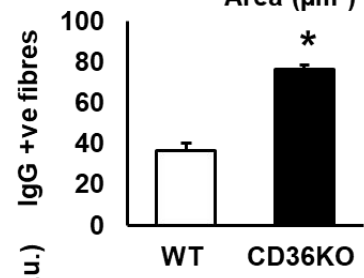
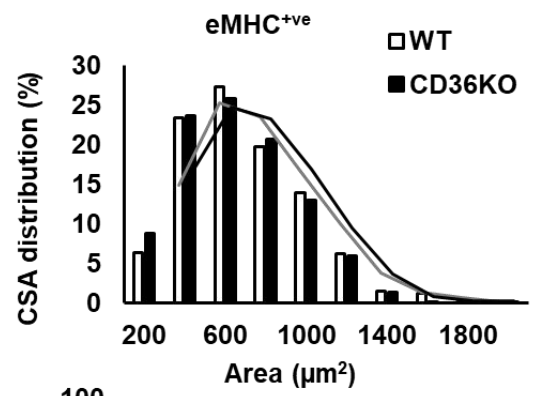
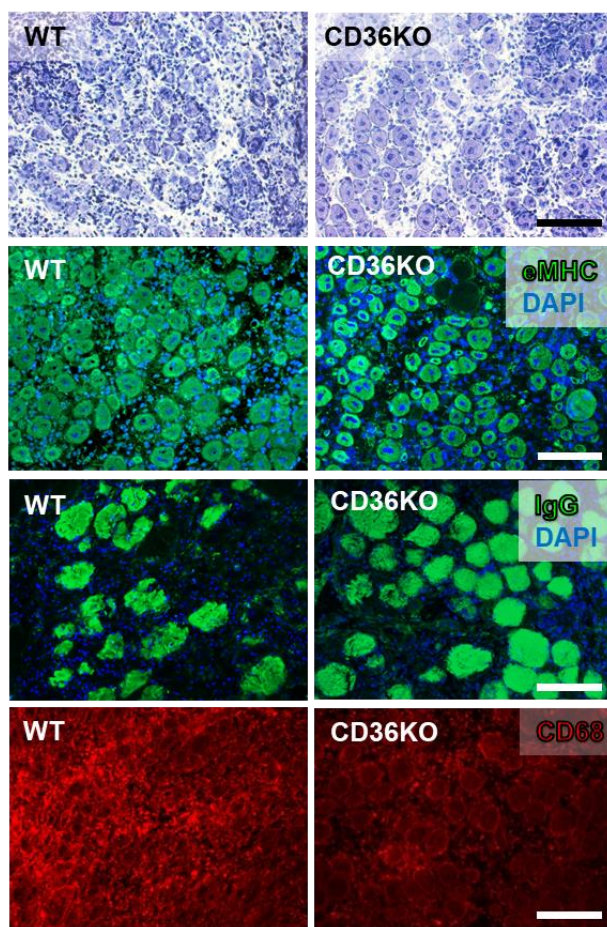
5.6.5 CD36-deficiency impairs skeletal muscle regeneration following acute damage with cardiotoxin.

Having shown that CD36 KO derived satellite cells exhibit reduced commitment towards differentiation, subsequent experiments aimed to examine the impact of CD36 on the regeneration of adult skeletal muscle *in vivo*. Regeneration of skeletal muscle is mainly driven by a highly orchestrated process involving the activation, proliferation, differentiation and fusion of satellite cells. The impact of CD36-deficiency in the context of regeneration was assessed in the *tibialis anterior* muscle that had been injured using cardiotoxin (CTX) injections to induce muscle necrosis. Following injury, necrotic tissue and damaged fibres are replaced by newly formed fibres, originating from the satellite cell progeny. These newly formed, regenerating fibres were identified by the expression of embryonic

myosin heavy chain (eMHC). The CSA of regenerating fibres expressing eMHC was comparable in WT and CD36-deficient (CSA distribution (%)) mice 5 days after injury (**Figure 5.5A**). Next steps aimed to quantify the occurrence of dying and dead fibres, which were identified by the infiltration of IgG into the fibre (IgG^{+ve} fibres). The clearance of dead and dying fibres was significantly impaired in CD36 KO mice when compared to WT animals (CD36 KO 76.3 ± 2.1 vs. WT 36.7 ± 3.7) at 5 days after the CTX injury (**Figure 5.5A**). Along with this, results showed a significant decrease in macrophage infiltration (CD68 fluorescent intensity; a.u.) in CD36 KO ($1.07 \text{ Gray} \pm 0.4$ vs. WT $2.24 \text{ Gray} \pm 0.6$) mice 5 days after CTX injury (**Figure 5.5A**). Furthermore, regeneration was assessed 10 days post injury (**Figure 5.5B**). It was found that the CSA was significantly reduced in regenerating fibres in CD36 KO mice (CSA distribution (%) H&E staining), following 10 days recovery after CTX injection (**Figure 5.5B**). In line with this, results showed that 10 days after CTX injury, regenerating fibres marked by eMHC expression (eMHC^{+ve} fibres) are mostly absent in WT mice (7.7 ± 2.8) but still present in CD36 KO mice (48.8 ± 0.77), suggesting delayed regeneration still present 10 days after muscle injury (**Figure 5.5B**). In summary, this data suggests delayed skeletal muscle regeneration in the absence of CD36, indicated by higher frequency of dead fibres, reduced CSA and decreased macrophage infiltration emphasising a reparative role of CD36 during skeletal muscle regeneration.

A

D5



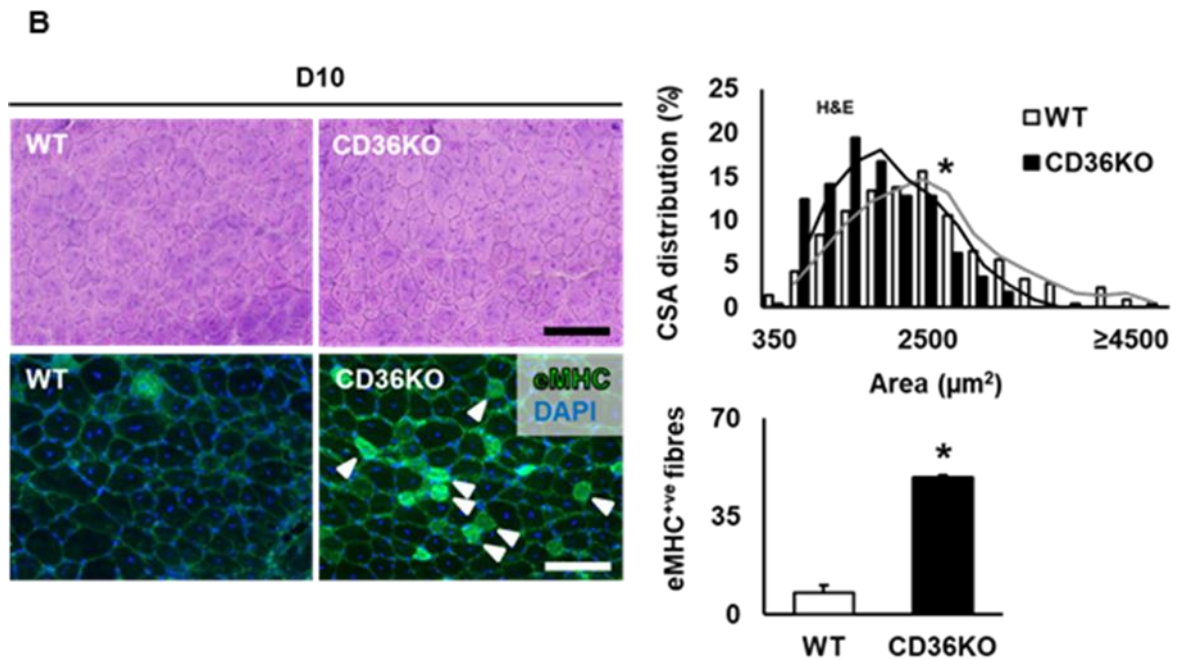


Figure 5.5. CD36 deficiency impairs skeletal muscle regeneration after acute injury. CD36-deficiency impairs skeletal muscle regeneration after cardiotoxin induced injury of tibialis anterior *in vivo*. **(A)** Representative images and quantification of regenerating fibres (Hematoxyline & Eosine/H&E staining, eMHC expression), damaged and dying fibres (Hematoxyline & Eosine/H&E, IgG expression) and macrophage infiltration (CD68 staining) in muscle sections on day 5 post CTX injury. **(B)** Representative images and quantification of CSA from regenerating fibres (Hematoxyline & Eosine/H&E) and evaluation of regenerating, newly formed muscle fibres expressing eMHC 10 days post CTX injury. Data are represented as mean \pm SD (N=3-5 per group). Statistical analysis was performed by Student's *t*-test with * $p < 0.05$ vs. WT injured group.

5.7 Discussion

5.7.1 Single fibre associated satellite cells

Sparse findings suggest that skeletal muscle ectopic lipid infiltration impairs satellite cell activation leading to a decrease of skeletal muscle regeneration potential (Xu et al., 2018, D'Souza et al., 2015). A significant reduction in satellite cell numbers in WT HF-diet mice was observed as early as 24-hours after activation. Moreover, satellite cell numbers in WT animals on a HF diet remained low after 48- and 72-hours following activation. These data suggest that long-term HF diet feeding has a negative impact on satellite cell function as well as commitment towards proliferation and differentiation. Furthermore, HF-diet induced impairment of satellite cell function in HF conditions might be linked to impaired myogenesis and skeletal muscle healing as well as the observed

decreased muscle mass and muscle function seen in obese humans (Hilton et al., 2008). Satellite cells isolated from CD36 deficient mice showed similar satellite cell numbers at baseline as well as during activation and proliferation, when compared to WT ND conditions, independent of diet. The fact that satellite cell numbers were unaffected in CD36 deficient mice on a HF diet further supports our hypothesis that obesity impairs satellite cell function via CD36-dependent pathways. Interestingly, a significantly lower satellite cell number was observed in CD36-deficient mice during differentiation independent of diet. This indicates an important role of CD36 during skeletal myogenesis (Park et al., 2012) with possible implications for skeletal muscle regenerations. Notably, neither CD36 deficiency nor diet altered the relative expression profiles of Pax7, MyoD and Myogenin.

5.7.2 Isolated satellite cells

In line with previous findings from fibre-associated satellite cells, showing unaltered satellite cell activation and proliferation but decreased differentiation capacity, are the following observations from isolated satellite cells in cell culture. Isolated CD36 KO derived satellite cells show similar proliferation potential when compared to WT satellite cells, confirmed by the evaluated EdU/DAPI ratio. However, there was a significant deficit in differentiation and myotube formation seen in isolated satellite cells from CD36-deficient mice, analysed by the total Myogenin/DAPI ratio as well as the calculated Fusion index which only takes into account the Myogenin positive nuclei inside mature myotubes *in vitro*.

To further consolidate the assumption of impaired differentiation in the absence of CD36, myogenic markers gene expression was quantified. *Bex1* (1 and 5 days post differentiation) and *Srf* (5days post differentiation) were found to be significantly reduced in differentiated satellite cells from CD36 deficient mice. Interestingly, *Bex1*-deficiency has been associated with prolonged proliferation and delayed differentiation following recovery after myotrauma (Koo et al., 2007). One possible explanation for the involvement of CD36 in skeletal myogenesis is its interaction with AMPK. CD36 has been shown to inhibit AMPK activation and in the absence of CD36, AMPK has been shown to be constitutively active in

muscle (Samovski et al., 2015). This could possibly lead to the activation and proliferation of satellite cells via non-canonical Sonic Hedgehog (Shh) signalling which induces Warburg-like glycolysis in satellite cells, required for their activation and proliferation during muscle regeneration (Fu et al., 2015). At the same time, AMPK also inhibits myoblast differentiation through PGC-1alpha-dependent pathways (Williamson et al., 2009). Moreover, AMPK has been shown to inhibit mTOR signalling (Thomson, 2018), via the AMPK-Nampt-Sirt1 pathway (Fulco et al., 2008), resulting in the inhibition of differentiation. This offers a plausible explanation for the adverse effect of CD36 on satellite cell proliferation and differentiation.

This is in line with the observation that isolated satellite cells from WT and CD36KO mice after 5 days of culture in differentiation medium, showed no difference in absolute number (total DAPI). However, a significantly reduced Myogenin/DAPI ratio in satellite cells from palmitate (PA) treated groups was observed. Furthermore, the fusion index was significantly lower in all experimental conditions. These data further support previous findings, suggesting that both CD36 deficiency and increased fatty acid availability, negatively impact satellite cell differentiation. This is in line with previously published evidence showing that palmitate inhibits differentiation in C2C12 cells through a decrease in cyclin A and cyclin D1 levels. However, palmitate improved myogenic formation and differentiation in C2C12 cells (Grabiec et al., 2015). Overall data indicated that both palmitate, CD36 deficiency as well as CD36 inhibition lead to altered activation and differentiation in satellite cells, possibly impairing terminal differentiation of satellite cells.

5.7.3 Single fibre associated satellite cells treated with palmitate and/or SSO

In order to consolidate previous findings from isolated satellite cells, fibre-associated satellite cells from WT and CD36KO mice were treated with the CD36 inhibitor SSO in the presence or absence of palmitate. 72 hours after the initial isolation, a significant reduction in fibre associated satellite cell number was observed in all experimental conditions when compared to the WT untreated

group. It is noteworthy to mention, that reduction in satellite cell number during differentiation was not due to reduced cluster formation. This is in line with previous findings, identifying CD36 as potential regulator of satellite cell differentiation (Park et al., 2012).

5.7.4 Skeletal muscle injury *in vivo*

To further elucidate the impact of CD36-deficiency on satellite cell differentiation and ultimately skeletal muscle regeneration, the TA muscle from WT and CD36 KO mice was assessed following acute CTX injury. Haematoxylin/Eosin staining confirmed regeneration after injury, evident by centrally located nuclei. Quantification of eMHC at day 5 after CTX injury showed similar CSA distribution of regenerating fibres in WT and CD36-deficient mice. However, the number of IgG⁺ fibres was significantly higher in TA cross-sections from CD36 KO mice, suggesting an increase in dead fibres. Furthermore, macrophage infiltration was significantly reduced in CD36-deficient cross-sections, indicating an altered inflammatory response post CTX injury.

This thesis shows that CD36-deficiency impairs muscle regeneration following CTX injury, evidenced by an increased occurrence of dying and dead fibres and reduced CSA in the injured muscle of CD36 KO mice. Additionally, these results show a significant decrease in macrophage infiltration in CD36 KO mice 5 days after CTX injury. This is in line with previous data showing impaired macrophage phagocytic capacity due to CD36 inhibition (Lindsey et al., 2019).

This notion is further supported by the attenuated phagocytosis seen in pharmacological inhibition of CD36 which plays an important role during tissue repair and inflammation resolution (Woo et al., 2016). CD36 has been found to be crucial for M2 macrophage polarisation, involved in the transition from the M1 (pro-inflammatory) to the anti-inflammatory response marked by M2 macrophages, identifying CD36-mediated uptake of triglycerol to be crucial for M2 activation (Huang et al., 2014). Furthermore, the CSA in CD36 KO mice was significantly reduced 10 days following CTX injection. This is followed by increased expression of eMHC in CD36 KO compared to WT mice, suggesting delayed regeneration 10 days after muscle injury.

It can be postulated that the impaired regeneration seen *in vivo* is at least in part brought about by the reduced stem cell commitment to differentiation seen in isolated satellite cells. Collectively, these data show that CD36 plays a crucial role in the regenerative process after acute skeletal muscle injury. This outcome is in line with the *in vitro* data in this study, showing impaired differentiation capacity in satellite cells isolated from CD36 KO mice.

5.8 Conclusion

High-fat diet feeding induced a significant reduction in the satellite cell number of WT mice, whereas CD36 deficient mice were protected from the influence of diet on activated and proliferating satellite cells. CD36 functions as a fatty acid transporter and interacts with AMPK. Therefore, CD36 is highly involved in the cellular energy demand. During proliferation and differentiation, cells show switches in their source of energy, changing from glycolytic to oxidative metabolism (Folmes et al., 2011). Recently reported data shows that C2C12 cells rely highly on glucose as a source of energy during proliferation which changes during differentiation, where cells become most dependent on fatty-acid oxidation (Sin et al., 2016). CD36, as a regulator of fatty acid transport (Pohl et al., 2005), is therefore likely to play a significant role in the cellular energy homeostasis (Le Foll et al., 2015), specifically during differentiation when fatty acids have been shown to promote cell cycle exit, myogenic differentiation and myotube growth (Grabiec et al., 2015). This study shows, that CD36 is a key regulator of satellite cell differentiation with possible implications for skeletal muscle regeneration, revealing impaired skeletal muscle regeneration in CD36-deficient mice. Further research will be necessary to clarify the underlying mechanism of impaired skeletal muscle regeneration in the absence of CD36 to provide a basis to better understand the link between CD36 mediated skeletal muscle lipid metabolism in the context of regeneration in obesity.

6 CHAPTER 6- Effect of CD36 inhibitor SSO and high fatty acid availability on mitochondrial bioenergetic profile in myoblasts

6.1 Overview

6.1.1 Mitochondrial function in skeletal muscle

Mature myoblasts are highly metabolically active and heavily rely on energy produced by fatty acid oxidation (OXPHOS). The myoblast precursor cells however rely primarily on glycolysis as a fuel for their metabolic activity and are characterised by a sparse mitochondrial population. During differentiation, the mitochondrial network undergoes an extensive process of network remodelling which has been shown to be of crucial importance for the metabolic switch from glycolysis to oxidative phosphorylation of fatty acids (Sin et al., 2016). Furthermore, it has been shown that mitochondrial biogenesis and activity are increased, leading to an elevated ATP production during the transition from proliferation to differentiation, which supports the notion that they play an important role in the maturation process.

The transport of fatty-acids into mitochondria is a rate-limiting step for ATP production during oxidative-phosphorylation. In rodents (Campbell et al., 2004) as well as in human studies (Bezair et al., 2006) evidence suggests, that CD36 plays an important role in long-chain fatty acid transport into the mitochondrial inner membrane. Skeletal muscle CD36 mitochondrial content has been shown to be upregulated following exercise, which has been linked to its involvement in fatty-acid oxidation. Research confirmed a significant correlation between CD36 mitochondrial content and palmitate oxidation rates further supporting its important role in mitochondrial fatty-acid dependent energy production (Holloway et al., 2006).

Mitochondrial dysfunction has been hypothesised to be one of the detrimental underlying pathologies related to obesity and its comorbidities. Mitochondrial dysfunction has been linked to abnormal lipid accumulation as well as insulin resistance in insulin-sensitive tissues, including the skeletal muscle. Mitochondria play a crucial role in energy production necessary for normal muscle function, as well as ROS disposal. Mitochondrial dysfunction can therefore lead to a disturbed ROS homeostasis, further accelerating lipid accumulation due to reduced fatty-acid oxidation, further deteriorating the obese condition.

From the literature it is known that palmitate treatment has been used extensively, as a method of choice to study the effect of saturated fatty acids on mitochondrial metabolism and function. Palmitate treatment has been shown to cause mitochondrial DNA (mtDNA) damage, as well as to induce apoptosis and insulin resistance in L6 myotubes (Yuzefovych et al., 2010). Recent results suggest that mtDNA damage is linked to ROS production, which in turn resembles an important underlying mechanism of the development of the metabolic syndrome in mice (Yuzefovych et al., 2012).

6.2 Aims

The aim of this chapter was to further give mechanistic insight to the underlying metabolic process of differentiation in satellite cells derived from WT and CD36 deficient mice. The focus of this studies is the effect of CD36 deficiency on satellite cell mitochondrial function when metabolically challenged. Furthermore, this chapter addresses the impact of high fatty acid availability in regards to the mitochondrial bioenergetic profile during proliferation and differentiation in C2C12 cells. It was hypothesised that the absence of CD36 as well as the presence of palmitate would significantly alter the mitochondrial bioenergetic profile. Moreover, it was hypothesised that these alterations would be most pronounced during differentiation. To investigate this hypothesis, the following objectives were set;

- i. To investigate the impact of CD36 on mitochondrial bioenergetics in WT and CD36 KO derived satellite cells during proliferation
- ii. To investigate the impact of CD36 and high fatty acid availability on mitochondrial bioenergetics in WT and CD36 KO derived satellite cells during differentiation
- iii. To investigate the impact of CD36 inhibition and high fatty acid availability on mitochondrial bioenergetics in C2C12 cells during proliferation and differentiation

6.3 Materials and Methods

6.3.1 Seahorse XFp extracellular flux measurements

C2C12 myoblasts and isolated satellite cells were seeded at a density of 10,000 cells per well in 8-well XF plates. Cells were pre-incubated in DMEM medium supplemented with 10% horse serum, 0.5% chicken embryo extract and 1% Penicillin/Streptomycin for 24 hours. Prior to the experiment, sensor cartridges were hydrated with XF calibrate solution (pH 7.4), as recommended by the manufacturer's instructions and incubated at 37 °C in a non-CO₂ environment for 24 hours. The cell culture medium was replaced with assay medium containing 1mM sodium pyruvate and incubated for one hour in a non-CO₂ incubator. Oligomycin (1 µM final concentration), carbonyl cyanide 4-(trifluoromethoxy)phenylhydrazone (FCCP; 5 µM final concentration) and Antimycin (2.5 µM final concentration) were diluted in the assay medium and

loaded into ports A, B and C, respectively. The Seahorse XFp Analyzer was then used to measure the oxygen consumption rate (OCR) and extracellular acidification rate (ECAR) in real time. Baseline measurements of OCR and ECAR were taken before sequential injection of Oligomycin, FCCP and antimycin. After three basal assay cycles, Oligomycin was injected to inhibit the ATP synthase. Following three more cycles, FCCP was injected to measure maximal mitochondrial respiration by uncoupling ATP synthesis from electron transport. After another four more cycles, Antimycin was injected to measure the non-mitochondrial respiratory rate. Immediately after the measurement, the assay medium was aspirated and the protein concentration was measured by bicinchoninic acid assay. The seahorse data was normalised to total protein (μg) and analysed using the Wave software from Agilent Technologies.

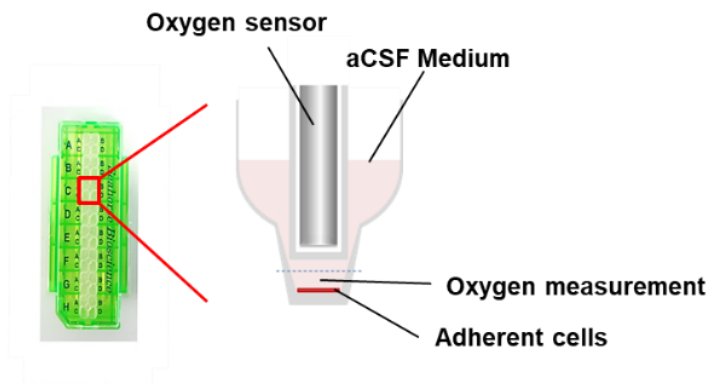
6.4 Results

6.4.1 CD36 deficient satellite cells and WT satellite cells show distinct bioenergetic profiles in the presence of high fatty acid availability

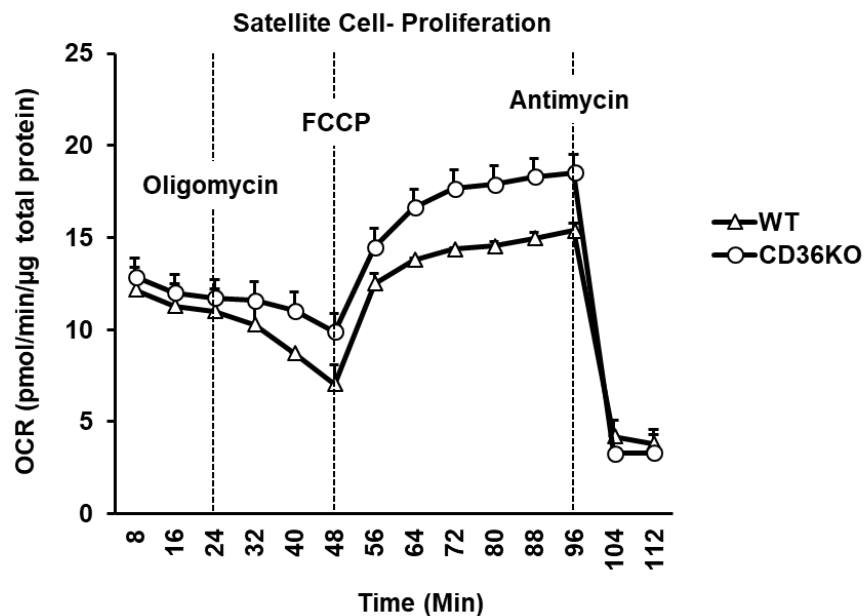
Recent findings demonstrated that mitochondrial activity is associated with specific lineage decision. Subsequent experiments aim to determine if the absence of CD36 deficiency alters mitochondrial function in primitive, undifferentiated and mature, differentiated satellite cells. Furthermore, the bioenergetic profile in the presence or absence of high free fatty acid availability was investigated in satellite cells derived from WT and CD36 KO mice. Satellite cells were isolated and cultured in GM for 24 hours (proliferation) using a Seahorse extracellular flux culture plate, to measure the oxygen consumption rate (OCR) and mitochondrial respiration in satellite cells from WT and CD36 deficient mice (**Figure 6.1A**). Undifferentiated satellite cell derived myoblasts (24 hours in GM) revealed no significant difference in the basal OCR or coupling efficiency (Basal OCR minus OCR after Oligomycin injection; Proton leak) (**Figure 6.1B,C**). Although the maximum respiratory capacity showed no difference between WT and CD36 deficient cells, the spare respiratory capacity (SRC) in satellite cells derived from CD36-deficient mice was significantly higher ($3.9 \text{ pmol/min}/\mu\text{g} \pm 1.1$) than in the WT cells ($1.5 \text{ pmol/min}/\mu\text{g} \pm 1$), indicating that

mitochondrial bioenergetics is altered and satellite cells from CD36 deficient mice are more resistant to stress. This further supports the concept that the CD36 deficient cells have an increased ability to adapt to stressful conditions. As illustrated, there was no difference in the non-mitochondrial respiration (Non-mit. Resp.) but a significant reduction in ATP production in the CD36 KO (1.4 pmol/min/ μ g \pm 0.15) derived satellite cells compared to WT (3.1 pmol/min/ μ g \pm 1.5) derived satellite cells (**Figure 6.1B,C**).

A



B



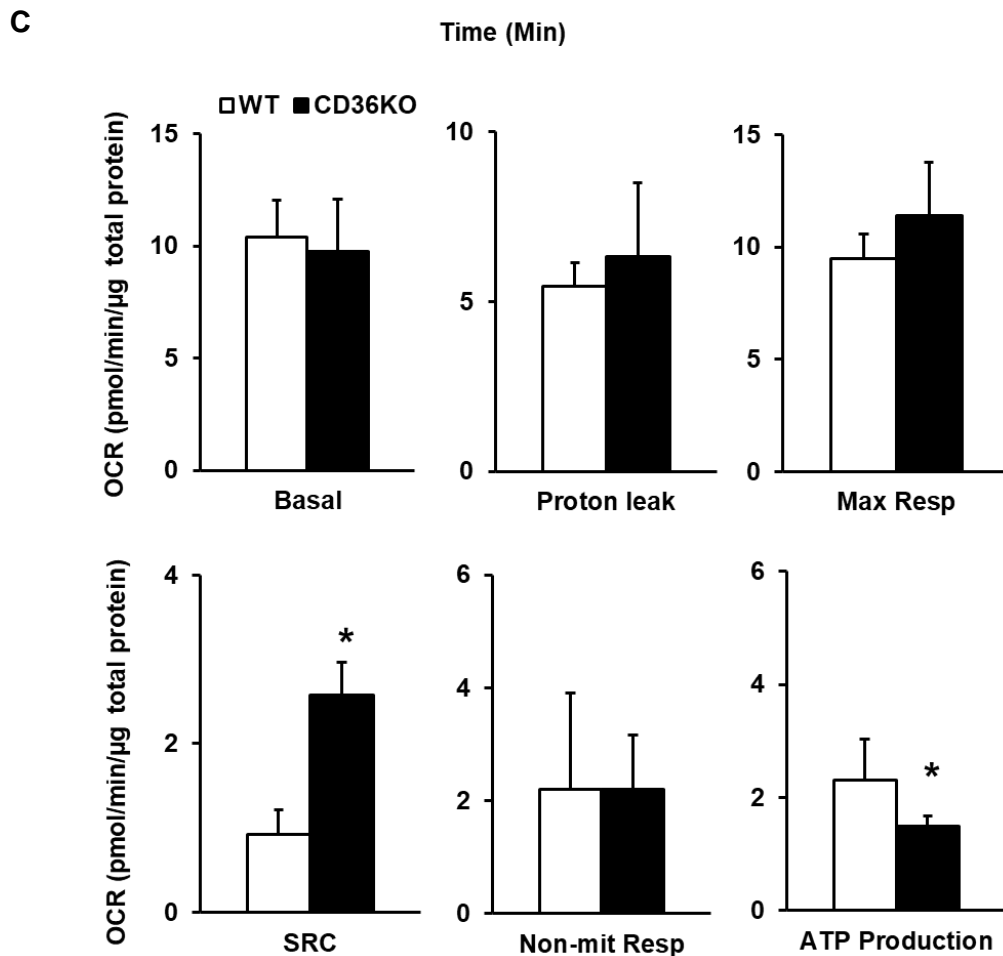
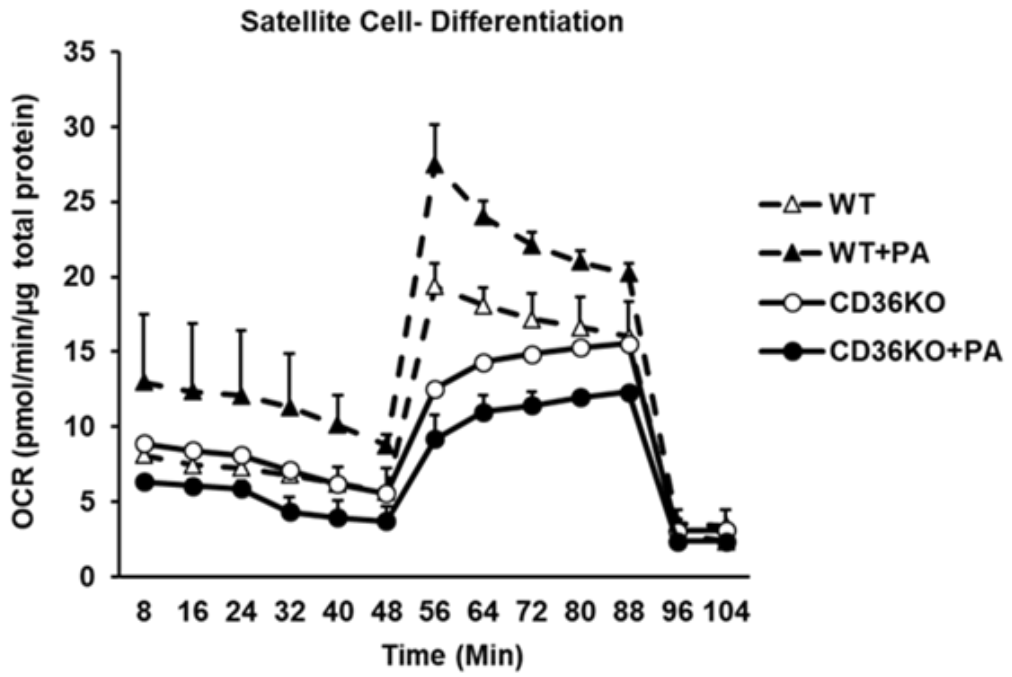


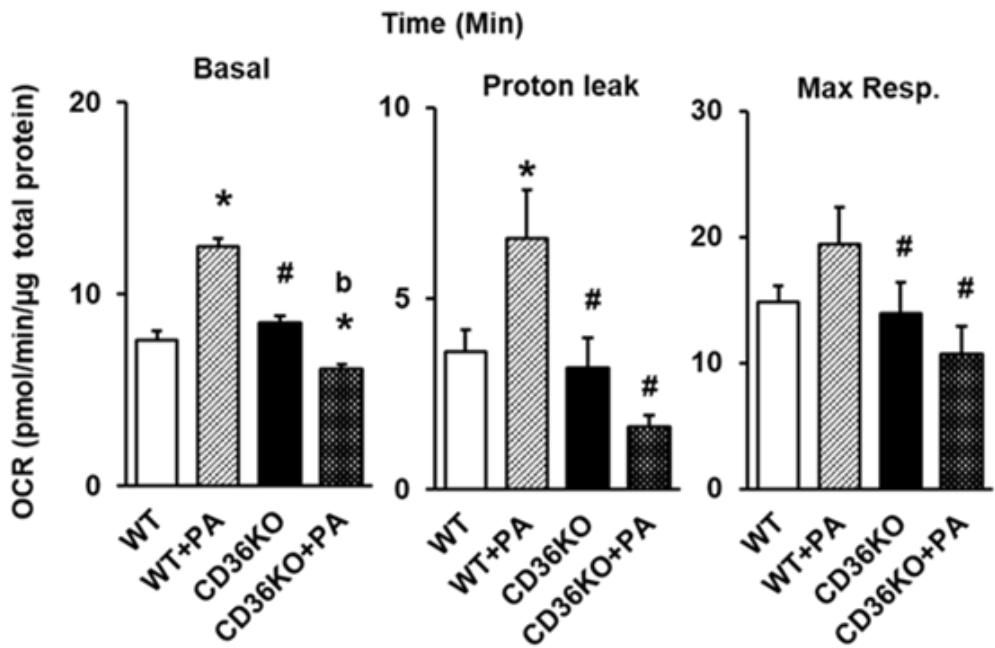
Figure 6.1. CD36 deficiency effects mitochondrial bioenergetics during proliferation. Respiration rate of isolated satellite cells was measured using the Seahorse XFp extracellular flux analyser. **(A)** Scheme of seahorse Extracellular Flux Analysis set up. **(B,C)** Proliferating (24 hours) satellite cells from WT and CD36 KO mice were cultured in a Seahorse extracellular flux cell culture plate. In total 14 OCR measurements were taken. Measurements are as follows: 3 basal respiration, 3 after the injection of Oligomycin (Inhibition of ATP synthesis), 6 after the injection of FCCP (Uncoupling of ATP synthesis) and 2 after the injection of Antimycin (Inhibition of mitochondrial respiration). The x-axis represents measurements taken over a time interval of 2 hours and OCR values are represented as a mean of 3 independent measurements, shown on the y-axis **(A)**. OCR values were normalised to total protein content and OCR changes are shown as pmol/min/μg total protein. Calculated from the original seahorse data are basal (average basal – non-mitochondrial oxygen consumption), proton leak (average after Oligomycin injection – non-mitochondrial oxygen consumption), maximal respiration (average after FCCP injection – non-mitochondrial oxygen consumption), Spare respiratory capacity (average after FCCP injection – basal), non-mitochondrial oxygen consumption (average after antimycin injection) and ATP production (basal – proton leak). Data are represented as mean±SD (N=3). Statistical analysis was performed using Students *t*-test, **p*<0.05 vs. WT ND.

Furthermore, the effect of CD36 on mitochondrial function during satellite cell differentiation was established in the presence or absence of palmitate (**Figure 6.2A**). Isolated satellite cells were cultured in GM, seeded into a seahorse extracellular flux cell culture plate until confluent and subsequently the medium was changed to differentiation medium (DM). Following differentiation (6 days DM) WT myotube mitochondria showed a significantly increased basal respiration when treated with palmitate ($12.5 \text{ pmol/min}/\mu\text{g} \pm 0.45$), whilst CD36-deficient myotubes treated with palmitate revealed a reduction in the basal OCR ($6.11 \text{ pmol/min}/\mu\text{g} \pm 0.22$) compared to WT untreated ($7.6 \text{ pmol/min}/\mu\text{g} \pm 0.5$) mitochondria. The addition of the ATP synthase inhibitor (complex V) Oligomycin led to a decrease in OCR following injection, revealing a significantly increased proton leak (Basal OCR minus OCR after Oligomycin injection), in WT derived satellite cell mitochondria when treated with palmitate ($6.57 \text{ pmol/min}/\mu\text{g} \pm 1.27$ vs. $3.6 \text{ pmol/min}/\mu\text{g} \pm 0.58$). Subsequently FCCP, an uncoupling agent, was injected to measure maximal oxygen consumption (complex IV). Addition of FCCP showed reduced maximal respiration (Max. Resp., CD36 KO $13.9 \text{ pmol/min}/\mu\text{g} \pm 2.5$ and CD36 KO +PA $10.7 \text{ pmol/min}/\mu\text{g} \pm 2.2$) as well as reduced spare respiratory capacity (SRC, CD36 KO $6.05 \text{ pmol/min}/\mu\text{g} \pm 1.19$ and CD36 KO +PA $5.07 \text{ pmol/min}/\mu\text{g} \pm 1.22$) in CD36 deficient conditions, independent of palmitate treatment (**Figure 6.2B**). Interestingly, palmitate treatment had adverse effects on WT and CD36 deficient myotubes, increasing the basal respiratory capacity and spare respiratory capacity (SRC) in WT but decreasing basal and SRC in CD36-deficient myotubes, depicted by the steep rise of OCR in the WT +PA group, peaking shortly after the FCCP injection (**Figure 6.2A**). Elevated ATP production was observed only in the WT +PA ($2.4 \text{ pmol/min}/\mu\text{g} \pm 0.22$ vs. WT $1.4 \text{ pmol/min}/\mu\text{g} \pm 0.45$) experimental condition (**Figure 6.2B**). In all, this data suggests that myotube mitochondria have an altered bioenergetic response in the presence of palmitate which seems to be, at least in part, regulated through CD36.

A



B



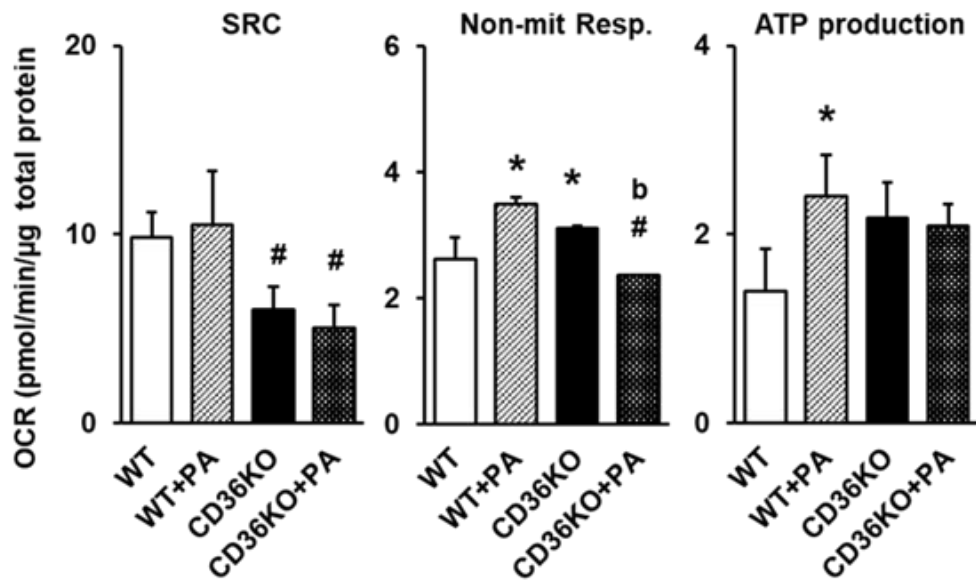
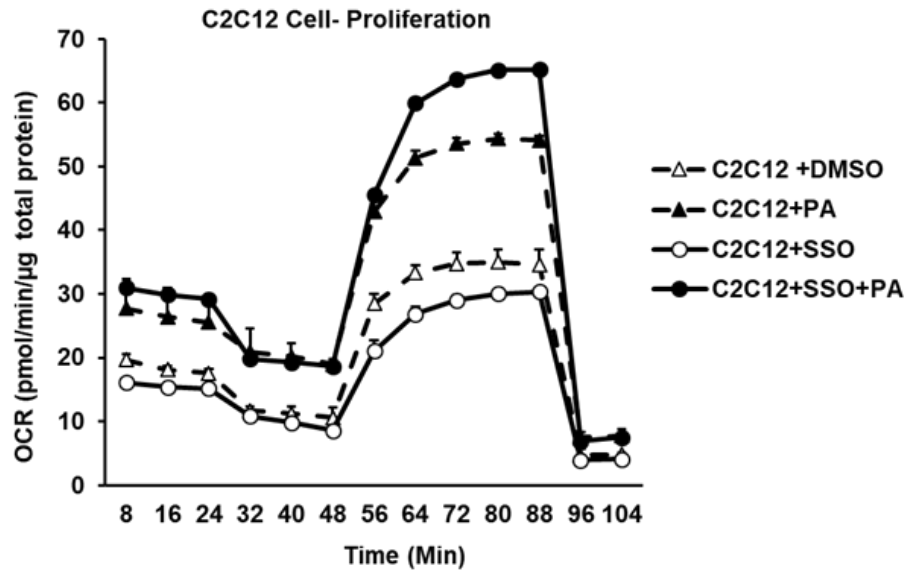


Figure 6.2. CD36 deficiency and increased fatty acid availability effect the mitochondrial bioenergetic profile during differentiation. Respiration rate of isolated satellite cells was measured using the Seahorse XFp extracellular flux analyser. **(A,B)** Proliferated and subsequently differentiated satellite cells from WT and CD36 KO mice were cultured in a seahorse extracellular flux cell culture plate and treated with SSO and/or palmitate before subsequent OCR measurements. In total 13 OCR measurements were taken. Measurements are as follows: 3 basal respiration, 3 after the injection of Oligomycin (Inhibition of ATP synthesis), 5 after the injection of FCCP (Uncoupling of ATP synthesis) and 2 after the injection of Antimycin (Inhibition of mitochondrial respiration). The x-axis represents measurements taken over a time interval of 2 hours and OCR values are represented as a mean of 3 independent measurements, shown on the y-axis **(A)**. OCR values were normalised to total protein content and OCR changes are shown as pmol/min/ μ g total protein. Calculated from the original seahorse data are basal (average basal – non-mitochondrial oxygen consumption), proton leak (average after Oligomycin injection – non-mitochondrial oxygen consumption), maximal respiration (average after FCCP injection – non-mitochondrial oxygen consumption), Spare respiratory capacity (average after FCCP injection – basal), non-mitochondrial oxygen consumption (average after antimycin injection) and ATP production (basal – proton leak). Data are represented as mean \pm SD (N=3). Statistical analysis was performed using two-way ANOVA, * p <0.05 vs. WT ND, # p <0.05 vs. WT HF, b p <0.05 vs. CD36 KO ND.

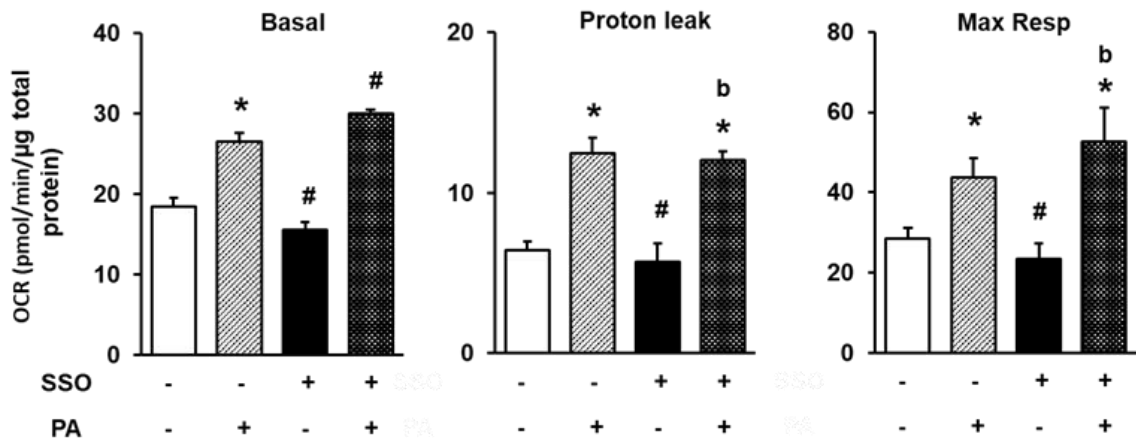
6.4.2 C2C12 cells display an altered bioenergetic profile in the presence of high fatty acid availability which is distinct from that of satellite cell derived myoblasts

To investigate fatty acid oxidation in more detail during proliferation in the presence or absence of CD36, C2C12 cells were cultured in a seahorse extracellular flux culture plate until 90% confluent. Cells were incubated with SSO to irreversibly inhibit CD36 prior to palmitate treatment. A basal rate was established, showing significantly increased OCR in C2C12 (26.57 pmol/min/ μ g \pm 1.1) and C2C12 +SSO (30.01 pmol/min/ μ g \pm 0.9) conditions when treated with palmitate compared to WT (18.5 pmol/min/ μ g \pm 1.1) conditions (**Figure 6.3A,B**). The proton leak (WT +PA 12.4 pmol/min/ μ g \pm 1 and WT +SSO +PA 12.04 vs. WT 6.41 pmol/min/ μ g \pm 0.6), which is a measure of oxygen consumption independent of ATP production and an indicator of coupling efficiency, as well as the Max.Resp (WT +PA 43.6 pmol/min/ μ g \pm 4.8 and WT +SSO +PA 52.67 pmol/min/ μ g \pm 8.3 vs. WT 28.45 pmol/min/ μ g \pm 2.7), SRC (WT +PA 24.7 pmol/min/ μ g \pm 4.8 and WT +SSO +PA 29.9 pmol/min/ μ g \pm 8.3 vs. WT 14.8 pmol/min/ μ g \pm 2.7) and non-mitochondrial respiration (WT +PA 24.7 pmol/min/ μ g \pm 4.8 and WT +SSO +PA 7.21 pmol/min/ μ g \pm 0.4 vs. WT 4.8 pmol/min/ μ g \pm 0.06) were significantly increased in palmitate treated conditions, regardless of CD36 inhibition. Additionally, C2C12 cells treated with SSO and palmitate had significantly increased ATP production (WT + SSO +PA 10.76 pmol/min/ μ g \pm 0.9 vs. WT 7.28 pmol/min/ μ g \pm 1.1) when compared to the other groups (**Figure 6.3A,B**). Previously it has been shown that premature, undifferentiated myoblasts and mature, differentiated myotubes show distinct bioenergetic profiles due to mitochondrial qualitative differences and larger mitochondrial population in differentiated myoblasts (Sin et al., 2016). Further steps aimed to investigate the impact of CD36 inhibition on the bioenergetic profile in differentiated C2C12 cells in the presence or absence of palmitate.

A



B



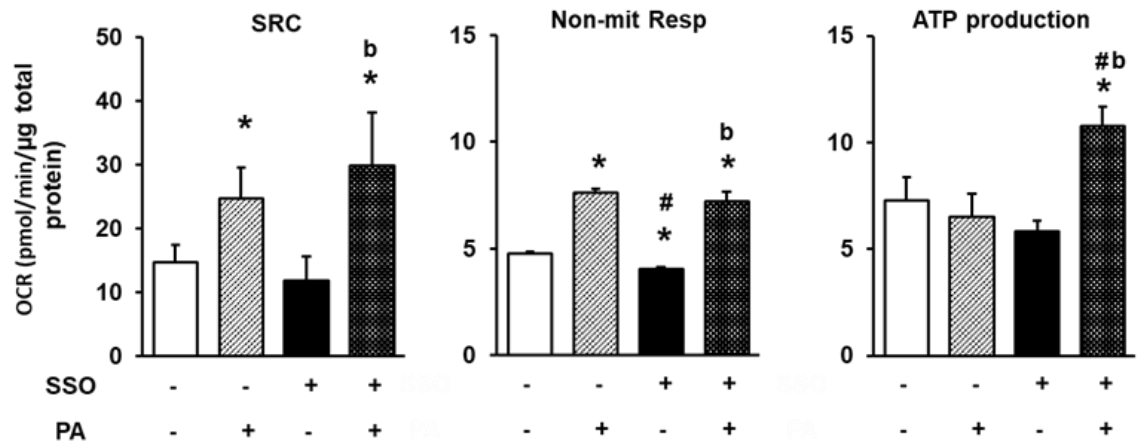
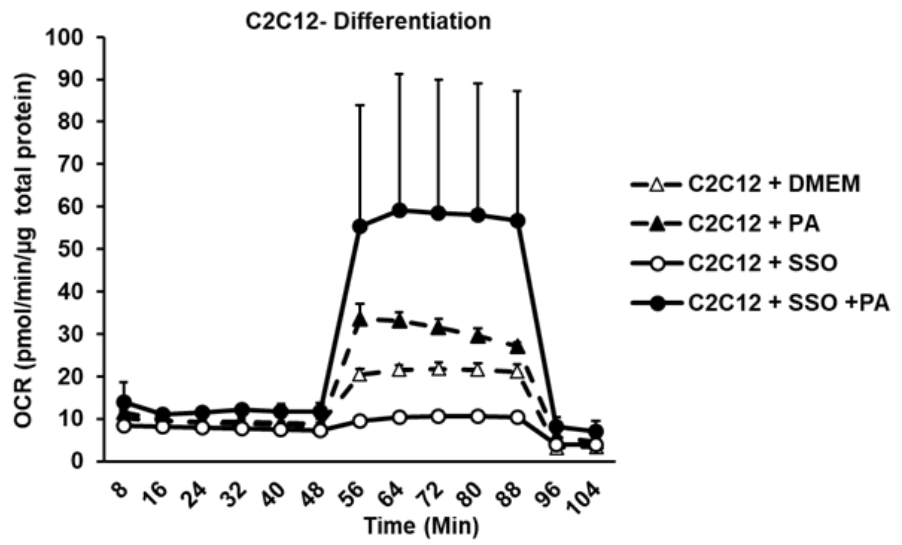


Figure 6.3. Proliferating C2C12 cells show a distinct bioenergetic profile compared to satellite cells. Respiration rate of proliferating C2C12 cells was measured using the Seahorse XFp extracellular flux analyser. **(A)** Representative measurement of C2C12 cell oxygen consumption rate (OCR). **(B)** OCR values from proliferating C2C12 cells. Calculated from the original seahorse data are basal (average basal – non-mitochondrial oxygen consumption), proton leak (average after Oligomycin injection – non-mitochondrial oxygen consumption), maximal respiration (average after FCCP injection – non-mitochondrial oxygen consumption), Spare respiratory capacity (average after FCCP injection – basal), non-mitochondrial oxygen consumption (average after antimycin injection) and ATP production (basal – proton leak). Data are represented as mean±SD (N=3). Statistical analysis was performed using two-way ANOVA, a p<0.05 vs. WT, *p<0.05 vs. WT ND, #p<0.05 vs. WT HF, b p<0.05 vs. CD36 KO ND.

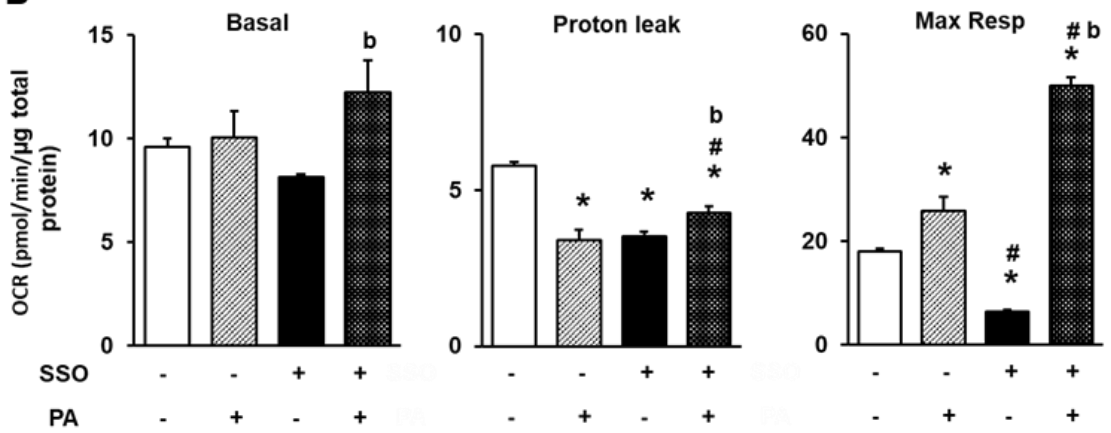
Further analysis aimed to investigate the OCR and mitochondrial function in differentiated C2C12 cells, with or without the CD36 inhibitor SSO, in the presence or absence of palmitate. To investigate this, undifferentiated C2C12 cells were cultured in a seahorse extracellular cell culture plate until 90% confluent and treated with SSO, palmitate, SSO + palmitate or palmitate alone. The seahorse extracellular flux analysis was performed after the cells differentiated and formed myotubes (6 days DM). OCR baseline levels were significantly higher in C2C12 +SSO +PA (12.2 pmol/min/μg ± 1.5 vs. WT 9.61 pmol/min/μg ± 0.83). Oligomycin addition revealed reduced mitochondrial proton leak in all experimental conditions (C2C12 +SSO +PA 4.3 pmol/min/μg ± 0.2, C2C12 +SSO 3.5 pmol/min/μg ± 0.2, C2C12 +PA 3.4 pmol/min/μg ± 0.3 vs. C2C12 5.8 pmol/min/μg ± 0.13) compared to untreated C2C12 myotubes (**Figure 6.4A,B**). Interestingly, the addition of the uncoupler FCCP in the presence of PA

enhanced the maximal respiratory capacity, resulting in increased SRC (C2C12 +PA 20.9 pmol/min/ μ g \pm 2.7, C2C12 +SSO +PA 45.3 pmol/min/ μ g \pm 1.5 vs. C2C12 11.7 pmol/min/ μ g \pm 0.5) as well as increased non-mitochondrial respiration (C2C12 +PA 5.15 pmol/min/ μ g \pm 0.9, C2C12 +SSO +PA 7.54 pmol/min/ μ g \pm 0.8 vs. C2C12 3.3 pmol/min/ μ g \pm 0.2) in both C2C12 +PA and C2C12 +SSO +PA conditions, revealing a distinct bioenergetic profile from satellite cell-derived myoblasts (**Figure 6.4B**). This indicates that maximal respiration is influenced by the cells ability to oxidise exogenous fatty acids, which determines the change in respiration in the presence of bioenergetic stress. Maximal respiration (C2C12 +SSO 6.3 pmol/min/ μ g \pm 0.5 vs.18.02 pmol/min/ μ g \pm 0.5) as well as SRC (C2C12 +SSO 2.13 pmol/min/ μ g \pm 0.5 vs. C2C12 11.7 pmol/min/ μ g \pm 0.5) were significantly reduced in C2C12 +SSO revealing an altered response to exogenous fatty acids under conditions of high energy demand by the addition of FCCP (**Figure 6.3B**). This data suggests that myotube's response to exogenous fatty acids is most pronounced under conditions of high energy demand, with distinct bioenergetic profiles in undifferentiated and differentiated C2C12 cells. Furthermore, differentiated C2C12 cells inhibited for CD36 show increased responsiveness to exogenous fatty acids in response to bioenergetic stress, whereas differentiated satellite cell showed an adverse response and reduced OCR under conditions of high energy demand, revealing detrimental differences between the two cell lines regarding their bioenergetic profile.

A



B



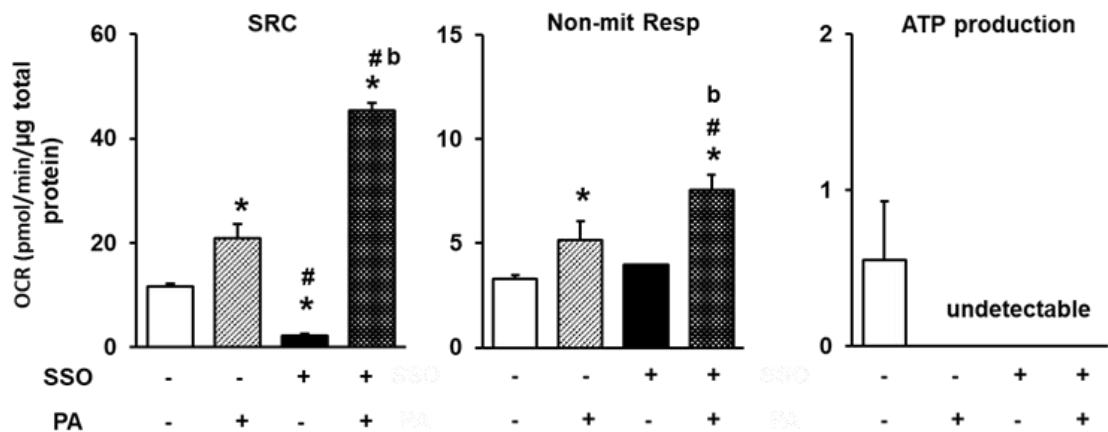


Figure 6.4. Differentiating C2C12 cells show a distinct bioenergetic profile compared to satellite cells. Respiration rate of differentiated C2C12 cells was measured using the Seahorse XFp extracellular flux analyser. **(A)** Representative measurement of C2C12 cell oxygen consumption rate (OCR). **(B)** OCR values from differentiated C2C12 cells. Calculated from the original seahorse data are basal (average basal – non-mitochondrial oxygen consumption), proton leak (average after Oligomycin injection – non-mitochondrial oxygen consumption), maximal respiration (average after FCCP injection – non-mitochondrial oxygen consumption), Spare respiratory capacity (average after FCCP injection – basal), non-mitochondrial oxygen consumption (average after antimycin injection) and ATP production (basal – proton leak). Data are represented as mean±SD (N=3). Statistical analysis was performed using two-way ANOVA, a p<0.05 vs. WT, *p<0.05 vs. WT ND, #p<0.05 vs. WT HF, b p<0.05 vs. CD36 KO ND.

6.5 Discussion

Mitochondrial dysfunction has been observed in several diseases related to the metabolic syndrome and is one of the most prominent abnormalities found in skeletal muscle of obese and diabetic individuals (Kelley et al., 2002, Mogensen et al., 2007, Sparks et al., 2005). CD36 has been shown to be involved in mitochondrial fatty acid oxidation, translocating from the cytoplasm to the mitochondrial plasma membrane during muscle contraction (Campbell et al., 2004). To assess whether loss of CD36 changes mitochondrial function in the presence of free fatty acids, the oxidative capacity and the bioenergetic profile of isolated satellite cells as well as C2C12 cells was analysed during proliferation and differentiation. In this study proliferating satellite cells from CD36 deficient mice had a significantly increased spare respiratory capacity (SRC). SRC is a critical factor implicated in cell survival and function, reflecting the ability of

mitochondria to maintain energy production in response to an increase in energy demand, like in acute or chronic stress (Pfleger et al., 2015). These findings support that proliferating satellite cells from CD36 deficient mice have an increased ability to adapt to stressful conditions such as FCCP treatment. This might be further linked to earlier findings, showing normalised satellite cell numbers in CD36 KO HF conditions during proliferation, when compared to the significantly decreased satellite cell number in WT HF conditions. Furthermore, CD36 KO-derived satellite cells show a decrease in ATP production during proliferation. This might indicate a higher degree of preserved stemness in the CD36 KO-derived satellite cells (Lonergan et al., 2007). Another possible explanation is that, in order to produce ATP, mitochondria must utilise substrates such as fatty acids. The reduced capacity of satellite cells from CD36 KO mice to use fatty acids for ATP production further explains the lower ATP level during stimulated respiration (Sin et al., 2016). Part of the myoblast differentiation process into myotubes is the extensive remodelling of the mitochondrial network. It has been proposed that, alterations in the reformation of the mitochondrial network during the transition from proliferation to differentiation can lead to the diminished ability to regenerate muscle tissue (Sin et al., 2016). Given the underlying reformation of the mitochondrial network during myogenesis, this study subsequently aimed to analyse the mitochondrial function of differentiated satellite cells in the presence or absence of palmitate (i.e. a free fatty acid). During differentiation, the oxygen consumption rate (OCR) has been shown to increase significantly as a result of the elevated energy demand (Zhang et al., 2013). In line with this are the results from this study, showing a 1.6-fold increase in WT and a 1.3-fold increase in CD36 KO derived satellite cells during the transition from proliferation to differentiation. This further supports the notion that satellite cells have an increase in maximal oxygen consumption during the process of maturation. It is noteworthy to mention, that the maximal respiratory capacity in the CD36 KO +PA satellite cells was significantly lower than the maximal respiratory capacity in WT +PA conditions, indicating their inability to use fatty acids to increase mitochondrial respiration. Furthermore, the basal OCR of WT satellite cells was significantly increased in the presence of palmitate, however CD36 KO-derived satellite cells treated with palmitate had a significantly lower OCR, suggesting that CD36 is a key regulator of β -oxidation in satellite cells

(Townsend et al., 2013). This finding provides a possible explanation for the impaired differentiation of satellite cells from CD36 KO animals reported in this study. This notion is strengthened by previous evidence showing that palmitate-induced mtDNA damage in skeletal muscle cells had deleterious effects on mitochondrial respiration (Patková et al., 2014).

Remarkably, treatment with palmitate induced opposing effects in proliferating and differentiating satellite cells isolated from CD36 KO mice, resulting in increased spare respiratory capacity during proliferation but significantly impaired spare respiratory capacity in differentiated cells. This might be an important link to previous findings in this thesis, showing impaired differentiation of CD36 KO-derived satellite cells, possibly linked to altered mitochondrial bioenergetics. Previously published data indicates an important link between ROS production and increased mitochondrial proton leak, further interfering with mitochondrial function. In this study, palmitate promotes a significantly increased mitochondrial proton leak in isolated WT satellite cells, suggesting superoxide induced electron leak (Brookes et al., 1998). Interestingly, isolated satellite cells from CD36 KO mice showed similar levels of mitochondria proton leak when compared to WT satellite cell, which is in line with our previous results suggesting decreased oxidative stress in the absence of CD36.

The C2C12 cell line is an immortal line of myoblasts, initially derived from murine satellite cells following a crush injury (Yaffe and Saxel, 1977). C2C12 cells have been used extensively in the literature to mimic satellite cell proliferation and differentiation, as well as mechanisms underlying muscle diseases such as Duchenne muscular dystrophy (Dumont et al., 2015). In this study, C2C12 cells were used to study the effect of CD36 inhibition on mitochondrial function during proliferation and differentiation.

During proliferation, basal respiration of proliferating C2C12 cells treated with free fatty acids was significantly higher than that in fatty acid free control condition. This observation was independent of CD36 inhibition by SSO. Furthermore, along with an increased basal OCR a significant increase in mitochondrial proton leak was observed, possibly indicating decreased reliance of C2C12 cells on CD36-dependent fatty acid oxidation. Proliferating and differentiating C2C12 cells

showed significantly increased maximal and spare respiratory capacity in the presence of free fatty acids. These results indicate that C2C12 rely specifically on fatty acid utilisation during bioenergetics stress, primarily oxidising exogenous fatty acids (Sin et al., 2016). Notably, the ATP production was undetectable in C2C12 cells that had been treated with SSO and/or palmitate, possibly due to a decreased sensitivity to Oligomycin, with implications for the coupling of proton transport to ATP synthesis (Antonieli et al., 2014).

6.6 Conclusion

Studies in diabetic humans demonstrated a low skeletal muscle mitochondrial content with alterations in mitochondrial dynamics, increased ROS production, ultimately leading to impaired mitochondrial function (Phielix et al., 2008, Jheng et al., 2012).

This study investigated mitochondrial function in the presence of high fatty-acid availability in WT and CD36 KO-derived satellite cells. Increased spare respiratory capacity and decreased ATP production in satellite cells isolated from CD36 deficient mice indicate an increased ability to adapt to stressful conditions as well as preserved stemness during proliferation. Interestingly, during differentiation the maximal respiratory capacity of satellite cells derived from CD36 KO mice was significantly lower than the OCR in WT satellite cells after palmitate treatment. During the process of differentiation, satellite cells switch from glycolysis to fatty-acid oxidation (Folmes et al., 2011). The inability of CD36 KO-derived satellite cells to switch to fatty acid oxidation might be an important link to the impaired differentiation seen in cell culture conditions, suggesting that CD36 is a key regulator of β -oxidation in satellite cells (Townsend et al., 2013).

Enhanced lipogenesis is an important hallmark of cancer cells, indicating an important role of fatty-acid synthesis for tumour survival. It has been shown that for example breast and liposarcoma tumours are capable of *de novo* fatty acid synthesis, further leading to the progression of the cancer cells (Zaidi et al., 2013). C2C12 myoblasts are polyploid and inactivated for *p19/Arf*, which is an important tumour suppressor (Pajcini et al., 2010). *Arf*-null mice are highly tumour-prone and show a mean survival of 19 and 32 weeks (Kamijo et al., 1999,

Ruddell et al., 2008). This might suggest that C2C12 cells, like cancer cells, have an increased potential to adapt to the lack of nutrition by alterations in their fatty acid metabolism to ensure survival. It is possible that intrinsic differences between satellite cells and C2C12 cells have significant impact on their mitochondrial stress response.

7 Chapter 7- General Discussion

7.1 Overview

The prevalence of obesity is one of today's greatest health challenges. Caused by a sedentary lifestyle, obesity is leading to the pandemic development of cardio-metabolic disorders, collectively described as the metabolic syndrome.

The more recently suggested correlation between diet-induced obesity (DIO) and impaired muscle regeneration may be brought about by changes in satellite function. In fact, ectopic lipid infiltration has been associated with metabolic deficits, further contributing to lipotoxicity and increased oxidative stress in skeletal muscle, possibly altering the satellite cell function. Satellite cells are of crucial importance for muscle maintenance and regeneration. Given the importance of lipid accumulation in the context of impaired muscle metabolism, the fatty acid translocase CD36 has recently received a great amount of attention. CD36 deficiency has been shown to protect mice from DIO. However, the underlying protective mechanism of abrogated CD36 signalling is still largely unknown. The purpose of this study was i) to investigate the impact of diet-induced obesity on the metabolic and physiological homeostasis of skeletal muscle and liver tissue, ii) to establish whether CD36-deficiency attenuates the effect of a high-fat diet on skeletal muscle homeostasis, oxidative stress and stem cell function and iii) to examine if the loss of CD36 protects from ectopic skeletal muscle lipid accumulation with a positive impact on skeletal muscle regeneration. The key findings of the thesis are:

- High-fat diet induced obesity shows a negative impact on skeletal muscle metabolic and physiological homeostasis, which was depicted by increased ectopic lipid infiltration and altered redox homeostasis.
- CD36 deficiency protects mice from weight gain on a high-fat diet and attenuates skeletal muscle lipid infiltration, possibly linked to an altered fatty acid metabolism, improved redox homeostasis and partially rescued satellite cell function.
- CD36 KO mice showed increased lipid accumulation and developed hepatic steatosis on a high-fat diet which is likely to be linked to an increase in *Fatp1* and *Fatp2*, as well as the increased expression of *Cidea*—an important regulator of lipolysis and lipid fusion.

- Lastly, CD36 was identified as a key regulator for myoblast terminal differentiation as shown by perturbed satellite cell differentiation *in vitro* as well as impaired skeletal muscle regeneration *in vivo*.

7.2 Body weight and skeletal muscle lipid metabolism

In the present study WT and CD36 KO mice were fed either a standard laboratory chow or a HF diet for 13 weeks. Interestingly, CD36 KO mice were protected from weight gain in contrast to WT animals under the same dietary conditions. During the duration of the experiment these differences in body weight became even more pronounced, demonstrating that CD36 deficient mice are protected from HF diet-induced obesity, which is in line with previous published findings in the literature (Cai et al., 2012). The observed difference in body weight was most likely attributed to the decreased WAT weight gain seen in CD36 deficient mice on an obesogenic diet. These findings are in line with other recent studies, showing that the visceral fat deposition is decreased in CD36 deficient mice (Koonen et al., 2010). This data further suggests that CD36 is a key regulator of fatty acid uptake and accumulation, with the most pronounced implications seen in WAT regarding the overall body weight gain. Moreover, these results indicate that CD36 plays a tissue specific role in fatty acid uptake and accumulation (Chapter 3). Furthermore, CD36 is a crucial fatty acid transporter in skeletal muscle (Bonen et al., 2004).

A growing body of evidence supporting the notion that increased ectopic lipid infiltration and skeletal muscle lipid accumulation is linked to obesity and insulin resistance, subsequently leading to the development of metabolic diseases such as type 2 diabetes (Goodpaster and Wolf, 2004). In the present study, CD36 deficiency had a major impact on skeletal muscle lipid infiltration in high-fat diet conditions. The CD36 KO HF mice showed no significant increase in BODIPY fluorescent signal, suggesting no increase in skeletal muscle lipid accumulation. However, WT mice on a high-fat diet displayed a significantly increased BODIPY signal following high-fat diet feeding, when compared to WT animals on a normal chow (ND). The above-mentioned findings indicate that a high-fat diet leads to a significant increase in skeletal muscle lipid deposition which is linked to CD36

mediated fatty acid uptake. These findings were further in line with the gas chromatography results showing that WT mice on a HF diet have significantly increased skeletal muscle fatty acid content which is rescued by CD36 deficiency, possibly indicating improved skeletal muscle lipid homeostasis. This data adds to the body of knowledge which suggests that CD36 is involved in the development of obesity and skeletal muscle insulin resistance due to lipid overload (Hegarty et al., 2002, Goodpaster and Wolf, 2004).

The fact that myokine gene expression such as *Fndc5* and *IL-15* are significantly upregulated in CD36 KO mice on a HF diet compared to WT mice on a HF diet further supports the notion that CD36 deficiency is linked to improved skeletal muscle lipid homeostasis for myokines. They have been shown to be highly involved in muscle lipid metabolism and overall muscle function (Lee and Jun, 2019). Additionally, increased mRNA expression of *Fndc5* and *IL-15* have been linked to exercise and improved endurance in male mice, correlated to enhanced oxidative energy metabolism (Huh et al., 2012, Dun et al., 2013, Quinn et al., 2013). Furthermore, elevated levels of Fatty acid binding protein 3 (*Fabp3*) and Carnitine palmitoyltransferase I (*Cpt1*) indicate altered fatty acid metabolism in CD36 deficient mice on a HF diet, possibly linked to the observed reduction in skeletal muscle lipid accumulation due to improved skeletal muscle lipid homeostasis.

Not only has obesity been linked to the oxidative modification of proteins, but has been shown to play a significant role in DNA damage and DNA repair inhibition, resulting from disturbed cell metabolism in oxidative stress (Zaki et al., 2018). 8-Oxoguanine glycosylase (*Ogg1*) has been described as base excision repair gene, involved in oxidative-stress induced cell death (Wang et al., 2018). Expression of *Ogg1* mRNA in skeletal muscle tissue revealed similar levels in all experimental groups. However, mRNA gene-expression of the anti-oxidant enzyme *Catalase* was significantly upregulated in WT mice on a high-fat diet and even further upregulated in CD36 KO mice independent of diet (Chapter 4). The most pronounced increase was observed for *Catalase* in CD36 KO mice on a high-fat diet, indicating a protective mechanism against oxidative stress. Furthermore, the anti-oxidant gene *Prdx1* was significantly increased in CD36 KO animals on a HF diet. *Prdx1* has been shown to preserve telomeric DNA and to

safeguard telomeres from oxygen radicals (Aeby et al., 2016), making it an important indicator for improved ROS homeostasis in CD36-deficient mice.

Improved lipid homeostasis is not only indicated by elevated expression of genes involved in muscle lipid metabolism but also by the reduction of lipid induced oxidative protein modification observed in CD36-deficient HF diet conditions. TBARS are formed as a by-product of lipid peroxidation, which is an indicator of oxidative stress. Interestingly, CD36 KO mice on a high-fat diet showed similar TBARS levels when compared to CD36 ND and WT ND control group. However, the level of TBARS were significantly increased in the WT HF diet group compared to the WT ND group, which is in line with previously published data (Furukawa et al., 2004), suggesting direct correlation between high-fat dietary conditions and increased oxidative stress. Another indicator of lipid peroxidation is the generation of reactive lipid mediators such as 4-HNE and the nitration of tyrosine residues (3NT) which occur during oxidative damage to proteins from the reaction of nitric oxide with superoxide radicals (Zhong and Yin, 2015) or through nitrite-dependent peroxidase activity (Danielson and Andersen, 2008). In support of the above-mentioned findings on TBARS levels; WT mice fed a high-fat diet showed increased levels of 4-HNE and 3NT protein adducts, which again indicates elevated protein modification and oxidative damage to proteins in HF diet conditions. Interestingly, the CD36-deficient mice on a HF diet showed similar 4-HNE and 3NT levels to CD36-deficient mice and WT mice on a ND. Moreover, elevated levels of ROS have been associated with the oxidative stress response, suggesting an essential role in the development of pathological conditions linked to oxidative protein modifications and DNA damage (Schieber and Chandel, 2014).

Taken together the above findings suggest that the absence of CD36 protects against diet-induced obesity and plays a key role in skeletal muscle lipid accumulation, possibly leading to improved lipid homeostasis and insulin sensitivity, indicated by enhanced oxidative energy metabolism and improved oxidative stress response.

7.3 Oxidative protein modification and DNA damage

Obesity and associated pathologies such as insulin resistance and diabetes have been linked to alterations in ROS homeostasis (Bailey-Downs et al., 2013). ROS are highly reactive by-products of aerobic metabolism which, under physiological conditions, function as signalling molecules involved in important biological and physiological processes (Schieber and Chandel, 2014, Zhang et al., 2016). However, evidence further reports that damage to proteins and DNA during oxidative stress is mediated by increased levels of ROS (Grimsrud et al., 2008, Cadet and Wagner, 2013). Additionally, dysregulation of ROS has been linked to pathological complications seen in diabetes (Green et al., 2004). More recent findings suggest a direct link between the production of diet-induced ROS and skeletal muscle insulin resistance leading to the development of diabetes in obesity (Marseglia et al., 2014, Bonnard et al., 2008). In the present study, CD36 KO animals on a ND revealed a significantly lower baseline DHE content when compared to WT ND animals (Chapter 4), indicating a causal role of CD36-mediated fatty acid uptake in skeletal muscle ROS production and oxidative stress which is in line with previously published data (Gharib et al., 2016, Okamura et al., 2009).

7.4 Myofibre morphology and composition

Previously published data suggests that obesity impacts skeletal muscle fibre composition, showing fewer oxidative type I and more glycolytic type IIB fibres in obese individuals. In this context, a positive correlation was established between the percentage of excess weight loss and the percentage of type I fibres in obese women (Tanner et al., 2002). Skeletal muscle is a highly plastic tissue, able to adapt to several conditions such as exercise and diet. Skeletal muscle fibre type plasticity as a response to physical and dietary parameters indicates functional adaptation of the tissue to its environment (Flück and Hoppeler, 2003). However, this study revealed that the HF-diet had no major impact on the skeletal muscle fibre type distribution independent of genotype (Chapter 3). This is paralleled by the observation that oxidative capacity -indicated by SDH staining- and relative mitochondrial activity -indicated by gene expression related to mitochondrial biogenesis (*Pgc1a*)- remained unaltered independent of diet in WT and CD36 KO

mice. This is in accordance with published data of diet-induced obesity in mice reporting minimal or no changes in fibre type composition (Turpin et al., 2009).

7.5 Impact of CD36 deficiency and HF diet conditions on satellite cell function

Sparse findings suggest that skeletal muscle ectopic lipid infiltration impairs satellite cell activation leading to a decrease of skeletal muscle regeneration potential (Xu et al., 2018, D'Souza et al., 2015). These assumptions are underlined by the data in this study showing that fibre associated satellite cell numbers were significantly decreased in WT HF diet mice as early as 24 hours after initial satellite cell activation (Chapter 5). Moreover, satellite cell numbers in WT animals on a HF diet remained low after 48- and 72-hours following activation. This data is therefore in line with the above suggested negative impact of HF diet feeding on satellite cell function, furthermore revealing a pronounced deficit in the commitment towards proliferation and differentiation. This data might explain -at least in part- the reduced muscle mass and impaired regeneration observed in obese human individuals (Hilton et al., 2008).

Interestingly, CD36 deficient mice on a HF diet showed similar satellite cell numbers at baseline as well as during activation and proliferation, when compared to WT ND conditions. The fact that satellite cell numbers remained unaffected during activation and proliferation in CD36-deficient HF diet conditions further supports the hypothesis, that obesity related impaired satellite cell function is closely linked to CD36-dependent pathways. However, a significantly lower satellite cell number was observed in CD36-deficient mice at 72 hours during differentiation which was independent of diet, leading to the assumption that CD36 plays an important role during myogenesis (Park et al., 2012) with possible implications for skeletal muscle regenerations. It is worth mentioning that neither CD36 deficiency nor diet altered the relative satellite cell transcription factor expression profiles of Pax7, MyoD and Myogenin. Further detailed analysis of CD36 KO derived satellite cells showed unaltered activation and proliferation patterns when compared to WT satellite cells, as was confirmed by the evaluated EdU/DAPI ratio in stripped satellite cell culture conditions. However, there was a

significant deficit in differentiation and myotube formation seen in stripped, isolated satellite cells from CD36-deficient mice. This data further underlines the assumption of CD36 playing a key role in satellite cell terminal differentiation.

To further consolidate these findings of impaired differentiation in the absence of CD36, gene expression of myogenic markers were quantified. *Bex1* -indicating early differentiation- and *Srf* -indicating late differentiation- were found to be significantly reduced in differentiated satellite cells from CD36-deficient mice. Interestingly, *Bex1*-deficiency has been associated with prolonged proliferation and delayed differentiation following recovery after myotrauma (Koo et al., 2007). One possible explanation for the observed decline in satellite cell capacity for differentiation in the absence of CD36 might be its interaction with AMPK. CD36 has been shown to inhibit AMPK activation and in the absence of CD36, AMPK has been shown to be constitutively active in skeletal muscle (Samovski et al., 2015). This could possibly lead to the activation and proliferation of satellite cells via non-canonical Sonic Hedgehog (Shh) signalling which induces Warburg-like glycolysis in satellite cells, required for their activation and proliferation during muscle regeneration (Fu et al., 2015). At the same time, AMPK also inhibits myoblast differentiation through PGC-1alpha-dependent pathways (Williamson et al., 2009). In this context, AMPK has been shown to inhibit mTOR signalling (Thomson, 2018), via the AMPK-Nampt-Sirt1 pathway (Fulco et al., 2008), resulting in the inhibition of differentiation (**Figure 7.5**). This could offer one plausible explanation for the observed adverse effect of CD36 on satellite cell proliferation and differentiation. This notion is supported by the observation that isolated satellite cells from WT and CD36KO mice after 5 days of culture in differentiation medium, showed no difference in absolute number (total DAPI).

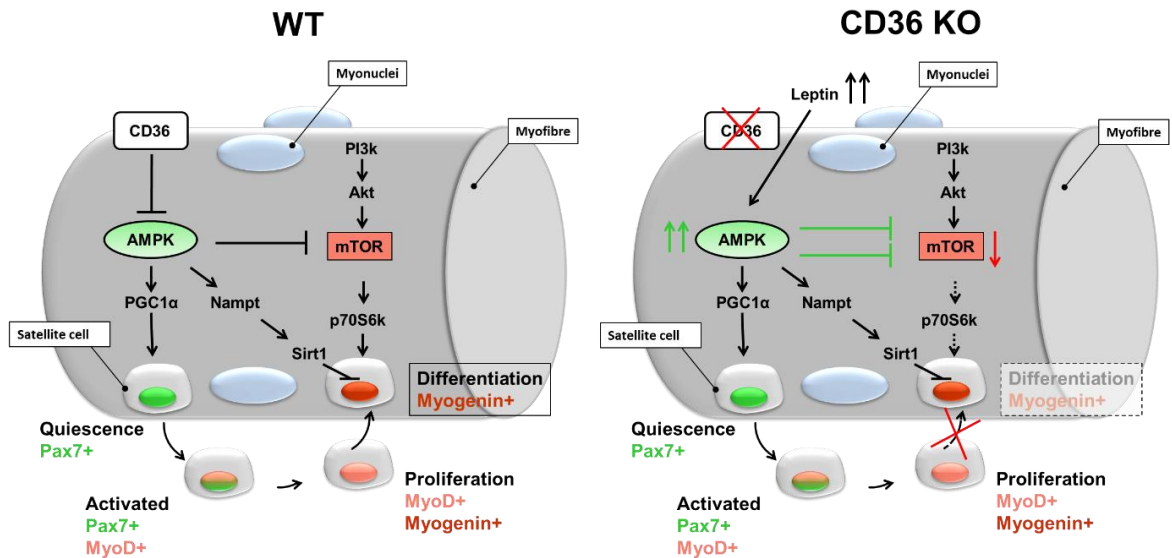


Figure 7.5: Theoretic scheme of the proposed underlying mechanism involved SC differentiation linked to CD36. CD36 has been shown to inhibit AMPK activation (left picture; WT). AMPK has been shown to be constitutively active in skeletal muscle in the absence of CD36 (right picture; CD36 KO). The right picture represents a possible mechanism for activation and proliferation of satellite cells via non-canonical Sonic Hedgehog (Shh) signalling which induces Warburg-like glycolysis in satellite cells in the absence of CD36. AMPK has been shown to inhibit mTOR signalling (right picture; CD36 KO), via the AMPK-Nampt-Sirt1 pathway, possibly resulting in the inhibition of differentiation. Collective findings by (Koo et al., 2007, Samovski et al., 2015, Fu et al., 2015, Williamson et al., 2009, Thomson, 2018, Fulco et al., 2008).

The importance of fatty acid uptake during terminal differentiation of satellite cells is further emphasised by the recently published work of Grabiec et al., showing that cell cycle exit, myogenic differentiation as well as myotube growth are promoted through a decrease in cyclin A and cyclin D1 levels mediated by the addition of palmitate (Grabiec et al., 2016). However, the same study also identified palmitate as a potent inhibitor of myoblast proliferation. This supports the findings in this thesis, showing that satellite cells derived from CD36 deficient mice display attenuated proliferation but adversely -due to the lack of sufficient fatty acid uptake-have impaired satellite cell differentiation (Chapter 5). Overall, this data further confirms the notion that CD36-mediated fatty acid uptake is detrimental for satellite cell differentiation but leads to impaired satellite cell proliferation in the presence of excess lipid availability.

In order to consolidate previous findings from isolated satellite cells, fibre-associated satellite cells from WT and CD36KO mice were treated with SSO; an irreversible inhibitor of CD36. Inhibition was performed in either the presence or absence of palmitate. During the differentiation phase at 72 hours, a significant reduction in fibre associated satellite cell number was observed in all experimental conditions when compared to the WT untreated group. This underlines previous findings, identifying CD36 as potential regulator of satellite cell differentiation (Park et al., 2012). Interestingly, palmitate treatment resulted in significantly increased DHE levels in WT satellite cells, which was attenuated in satellite cells derived from CD36 deficient mice (Chapter 4). This indicates that palmitate induces increased oxidative stress which is -at least in part- mediated via CD36- dependent pathways. Conversely, despite the frequent association of ROS with oxidative stress, it also functions as signal transduction for various biological processes, including stem cell differentiation (Holmström and Finkel, 2014, Pashkovskaia et al., 2018). Previously, it has been shown that during differentiation, the mitochondrial oxidative metabolism is activated, resulting in increased ROS production. Interestingly, this metabolic switch has been identified as a prerequisite for successful differentiation (Lee et al., 2011). In particular, mitochondrial ROS production is necessary for muscle differentiation (Lee et al., 2011), further emphasising the complex nature of ROS homeostasis and its involvement in signal transduction. These findings offer additional insight on possible underlying mechanisms related to impaired satellite cell differentiation in the absence of CD36.

7.6 Calcium signalling in oxidative stress

An increasing body of evidence further indicates that intracellular $[Ca^{2+}]$ modulates ROS generation as well as ROS clearance. This cross talk between ROS and $[Ca^{2+}]$ further impacts on the antioxidant defence system (Zhang et al., 2016). Intracellular calcium signalling plays an important role in several physiological conditions such as muscle cell contraction as well as cell signal transduction and neurotransmitter release (Tanabe et al., 1988, Clapham, 2007).

Recently published data connects CD36 to $[Ca^{2+}]_i$ signalling and the regulation of $[Ca^{2+}]$ dynamics (Xu et al., 2015). Evidence suggests that CD36-dependent signalling is involved in the cellular stress response in cardiac tissue (Pietka et al., 2012). In this study, changes in $[Ca^{2+}]_i$ by the addition of extracellular Ca^{2+} were compared between satellite cells derived from either WT or CD36 KO animals. Furthermore, WT derived satellite cells were treated with SSO; a potent and irreversible CD36 inhibitor. Palmitate treatment almost completely prevented the intracellular calcium rise which was independent of CD36 inhibition. These results lead to the belief that palmitate treatment induced alterations in Ca^{2+} flux of proliferating satellite cells, with possible implications for several physiological signalling pathways involved in the oxidative stress response (Chapter 4). In fact, it has been shown that human myoblast differentiation *in vitro* is regulated by intracellular Ca^{2+} increases (Konig et al., 2006, Liu et al., 2003), further establishing a possible link between CD36-mediated ROS signalling in the context of skeletal muscle satellite cell differentiation.

Additionally, another important phenomenon regulating skeletal muscle satellite cell differentiation is that of dramatic mitochondrial network remodelling. Mitochondrial dysfunction has been observed in several diseases related to the metabolic syndrome and is one of the most prominent abnormalities found in skeletal muscle of obese and diabetic individuals (Kelley et al., 2002, Mogensen et al., 2007, Sparks et al., 2005). CD36 has been shown to be involved in mitochondrial fatty acid oxidation, resulting in CD36 translocation from the cytoplasm to the mitochondrial plasma membrane during muscle contraction (Campbell et al., 2004). To assess whether loss of CD36 changes mitochondrial function in the presence of free fatty acids, the oxidative capacity and the bioenergetic profile of isolated satellite cells as well as C2C12 cells was analysed during proliferation and differentiation. Results show that proliferating satellite cells from CD36 deficient mice had a significantly increased spare respiratory capacity (SRC). The SRC is a critical factor implicated in cell survival and function, reflecting the ability of mitochondria to maintain energy production in response to an increase in energy demand, as it is required during acute or chronic stress (Pfleger et al., 2015). These findings support the evidence that proliferating satellite cells from CD36 deficient mice have an increased ability to

adapt to stressful conditions such as FCCP treatment (Chapter 6). This represents a possible link to earlier findings, showing normalised satellite cell numbers in CD36 KO HF conditions during proliferation, whereas WT mice on a HF diet showed significantly decreased satellite cell numbers (Chapter 5). Moreover, proliferating CD36 KO-derived satellite cells showed a decrease in ATP production. According to the literature, this might indicate a higher degree of preserved stemness in the CD36 KO-derived satellite cells (Lonergan et al., 2007). Another possible explanation is that, in order to produce ATP, mitochondria must utilise substrates such as fatty acids. The reduced capacity of satellite cells from CD36 KO mice to use fatty acids for ATP production further explains the lower ATP level during stimulated respiration (Sin et al., 2016).

As mentioned before, extensive remodelling to the mitochondrial network plays an important part in the myoblast differentiation process into myotubes. It has therefore been proposed that impaired reformation of the mitochondrial network during the transition phase from proliferation to differentiation can lead to the diminished ability to regenerate muscle tissue (Sin et al., 2016). Given the underlying importance of mitochondrial network remodelling as well as mitochondrial biogenesis during myogenesis, this study subsequently aimed to analyse the mitochondrial function of differentiated satellite cells in the presence or absence of palmitate (i.e. a free fatty acid). Differentiation of primitive myoblasts into mature myotubes requires a metabolic switch from a glycolytic state to relying predominantly on oxidative phosphorylation (OXPHOS) in myotubes to meet their high energy demand (Sin et al., 2016). During differentiation, the oxygen consumption rate (OCR) has been shown to increase significantly as a result of the elevated energy demand (Zhang et al., 2013). This complements the results from this thesis; showing a 1.6-fold increase in WT and a 1.3-fold increase in the OCR for CD36 KO-derived satellite cells during the transition from proliferation to differentiation (Chapter 6). This further supports the notion that satellite cells have an increase in maximal oxygen consumption during the process of maturation. It is noteworthy to mention, that the maximal respiratory capacity in the CD36 KO +PA satellite cells was significantly lower than the OCR in WT +PA conditions, indicating their inability to use fatty acids to increase mitochondrial respiration to adapt to their increased energy demand.

Furthermore, the basal OCR of WT satellite cells was significantly increased in the presence of palmitate, however CD36 KO-derived satellite cells treated with palmitate had a significantly lower OCR, suggesting that CD36 is a key regulator of β -oxidation in satellite cells, supporting previously published data by Townsend et al. (Townsend et al., 2013).

This finding adds to the possible explanations for the impaired differentiation of satellite cells from CD36 KO animals reported in this study. This notion is strengthened by previous evidence showing that palmitate-induced mtDNA damage in skeletal muscle cells had deleterious effects on mitochondrial respiration (Patková et al., 2014). Remarkably, treatment with palmitate induced opposing effects in proliferating and differentiating satellite cells isolated from CD36 KO mice, resulting in increased spare respiratory capacity during proliferation but significantly impaired spare respiratory capacity in differentiated cells. This might be an important link to our previous findings; showing impaired differentiation of CD36 KO-derived satellite cells (Chapter 5), possibly linked to altered mitochondrial bioenergetics.

Previously published data indicates an important link between ROS production and increased mitochondrial proton leak, further interfering with mitochondrial function. In this study, palmitate promotes a significantly increased mitochondrial proton leak in isolated WT satellite cells, suggesting superoxide induced electron leak (Brookes et al., 1998). Interestingly, isolated satellite cells from CD36 KO mice showed similar levels of mitochondria proton leak when compared to WT untreated satellite cells, which is in line with our previous results suggesting decreased oxidative stress in CD36-deficient conditions.

The C2C12 cell line is an immortalised cell line of myoblasts, initially derived from murine satellite cells following a crush injury (Yaffe and Saxel, 1977). In the literature, C2C12 cells have been used extensively to mimic satellite cell proliferation and differentiation, as well as mechanisms underlying muscular diseases such as Duchenne muscular dystrophy (Dumont et al., 2015). In this study, C2C12 cells were used to study the effect of CD36 inhibition on mitochondrial function during proliferation and differentiation.

During proliferation, basal respiration of proliferating C2C12 cells treated with palmitate was significantly higher than in control conditions without palmitate, which was independent of CD36 inhibition with SSO. Furthermore, along with an increased basal OCR, a significant increase in mitochondrial proton leak was observed, possibly indicating decreased reliance of C2C12 cells on CD36-dependent fatty acid oxidation. Proliferating and differentiating C2C12 cells showed significantly increased maximal and spare respiratory capacity in the presence of free fatty acids (Chapter 6). These results indicate that C2C12 rely specifically on fatty acid utilisation during bioenergetics stress, primarily oxidising exogenous fatty acids (Sin et al., 2016). Notably, the ATP production was undetectable in C2C12 cells that had been treated with SSO and/or palmitate, possibly due to a decreased sensitivity to Oligomycin.

7.7 Skeletal muscle injury *in vivo*

In order to confirm the *in vivo* findings indicating impaired satellite cell differentiation in the absence of CD36, skeletal muscle from WT and CD36 KO mice was assessed for its regenerative capacity following acute CTX induced injury. Haematoxylin/Eosin staining confirmed initial skeletal muscle damage and the onset of regeneration after injury, evident by centrally located nuclei. Similar CSA could be observed in regenerating fibres in WT and CD36 KO mice at day 5 post-injury, which was assessed using eMHC as an early marker for newly formed myofibres. However, the number of IgG⁺ fibres, which suggests increased numbers of dead fibres, was significantly higher in skeletal muscle cross-sections of CD36 KO mice. Moreover, CD68, which is a marker of macrophage infiltration, was significantly reduced in CD36-deficient cross-sections, indicating an altered inflammatory response post CTX injury (Chapter 5).

This thesis reveals CD36 to be an important key regulator of skeletal muscle regeneration following acute injury in the adult mouse. This was evidenced by an increased occurrence of dying and dead fibres in the injured skeletal muscle of CD36 KO mice. Additionally, results show a significant decrease in CD68 staining, indicating less macrophage infiltration in CD36 KO mice 5 days after

CTX injury. This is in line with previous data showing impaired macrophage phagocytic capacity due to CD36 inhibition (Lindsey et al., 2019). This notion is further supported by the attenuated phagocytosis seen in pharmacological inhibition of CD36 which plays an important role during tissue repair and inflammation resolution (Woo et al., 2016). Moreover, CD36 has been found to be crucial for M2 macrophage polarisation, involved in the transition from the M1 (pro-inflammatory) to the anti-inflammatory response, marked by M2 macrophages, identifying CD36-mediated uptake of triglycerol to be crucial for M2 activation (Huang et al., 2014).

In addition, the CSA was found to be significantly smaller in CD36 KO animals compared to WT animals 10 days post-injury. A decreased CSA has been associated with delayed skeletal muscle regeneration (Patsalos et al., 2017). At the same time, eMHC expression was still found to be high in CD36 KO compared to WT mice, suggesting delayed regeneration 10 days after muscle injury.

Collectively, these data show that CD36 plays a crucial role in the regenerative process after acute skeletal muscle injury. This outcome is in line with the *in vitro* data in this study, showing impaired differentiation capacity in satellite cells isolated from CD36 KO mice (Chapter 5). It can be postulated that the impaired regeneration seen *in vivo* is at least in part brought about by the reduced stem cell commitment to differentiation seen in isolated satellite cells.

7.8 Hepatic lipid accumulation

Due to an increased prevalence in obesity, non-alcoholic fatty liver disease -short NAFLD- is becoming one of the most common causes of chronic liver disease (Sarwar et al., 2018). Despite the fact that there are several pharmacological treatment agents under clinical investigation, there are no approved treatments for NAFLD at present.

Several studies have reported an association of the development of NAFLD with visceral fat accumulation and insulin resistance (Eguchi et al., 2006). This study reports a significant increase in Oil Red O positive lipid deposition in liver sections of WT mice on a HF diet, when compared to WT animals on a normal chow (Chapter 3). Interestingly, CD36 KO mice fed a HF diet showed an even stronger

phenotype with significantly increased lipid accumulation in the liver, when compared to all the other experimental groups, including WT HF diet animals. These findings are somewhat in line with recent evidence reporting an increased CD36 mRNA and protein expression in mice fed a high-fat diet (Koonen et al., 2007). Not only did the livers of CD36-deficient mice display a severe increase in lipid number, but also showed a significant increase in overall lipid size. This notion was further confirmed by the significantly increased mRNA expression of both *Fatp2* and *Fatp1* found in livers of CD36 KO HF diet animals when compared to control WT mice. Previously published data demonstrated that *Fatp2* knock-down in a mouse model of obesity showed reduced fatty acid uptake and ameliorated signs of hepatic steatosis (Falcon et al., 2010). In line with this; *Fatp1* has been identified as an insulin-sensitive fatty acid transporter involved in diet induced obesity. Similar to CD36, FATP1 has been shown to be able to translocate from intracellular compartments of the cell to the plasma membrane in response to insulin signalling (Wu et al., 2006). *Fatp1*-null mice are protected against diet-induced obesity and decreased insulin sensitivity. Under normal circumstances, *Fatp1* is not detectable or only expressed at low levels in the human liver (Martin et al., 2000). It has, however, been suggested that FATP1 plays a crucial role in the redistribution of fatty acids from adipose and skeletal muscle tissue to the liver (Wu et al., 2006). This is in line with the findings from this thesis revealing increased expression of *Fatp2* and *Fatp1* in CD36 KO mice on a HF diet, suggesting the development of hepatic steatosis in the absence of CD36. Furthermore, the expression of *Cidea*, an important regulator of lipolysis and lipid fusion (Puri et al., 2008, Viswakarma et al., 2007), was 25-fold increased in CD36 KO HF diet mice when compared to WT control animals. This data indicates a key role of CD36 in the development of lipid accumulation and hepatic steatosis. Collectively, these findings suggest opposing effects of CD36 deficiency with a protective role in the skeletal muscle due to reduced lipid accumulation, but at the same time leading to an overload of lipid deposition in the liver tissue, possibly as a compensatory mechanism.

7.9 Limitations

Mouse models are used extensively to model human disease, however, mice frequently respond to experimental interventions very differently to humans. One important aspect to consider is that murine and human biology renders them to different dietary requirements. Although both mice and humans are omnivores, mice preferentially consume a diet of unprocessed grains and cereals which is further related to the different microbiomes that can be found in mice and humans. Additionally, the relative length of the gastrointestinal tract differs between the two species. These underlying anatomical and biological discrepancies between humans and mice result in different outcomes of dietary intervention accounting for metabolic variations in the context of diet-induced obesity. For example, relative transcript expression of CD36 in mice subcutaneous fat is around 140 reads per kilo base per million mapped reads (RPKM), whereas in humans CD36 expression was found to be above 500 RPKM (Yue et al., 2014, Fagerberg et al., 2014). Irrespective of the difference in relative expression level, CD36 expression was found to be high in fat and heart tissue, whereas only low expression was found in the liver in both humans and mice (NCBI gene). Nevertheless, genetic differences between mice and humans have to be taken into account when extrapolating data from murine models to human diseases.

It is further worth mentioning, that measuring of reactive oxygen species (ROS) with fluorescence holds challenges and limitations due to the nature of ROS. ROS are highly reactive with a range of different stabilities and lifetimes in a biological system. The short-life of ROS limits its direct detection (Dickinson and Chang, 2011). DHE, a ROS-sensitive fluorescence probe, has -although widely used- several limitations, including unspecific oxidation of DHE. Furthermore, DHE staining was performed in frozen tissue sections, which could have influenced the signal due to the ephemeral nature and rapid reactivity of reactive oxygens.

7.10 Future Work

For this study a whole-body CD36-deficient mouse model has been characterised with focus on the satellite cell function in the context of obesity. Although this

takes into account the complexity of fatty acid metabolism, including insulin-sensitive tissues such as adipose tissue and the liver, it would be advantageous to define other further aspects of muscle biology in a skeletal muscle-specific CD36 KO model. Additionally, the use of a western-type diet instead of a high-fat diet may be a more relevant model to study the metabolic syndrome, especially in the context of insulin sensitivity.

7.11 Concluding remarks

Satellite cells; the myogenic precursor stem cell population of the skeletal muscle, are of pivotal importance for skeletal muscle homeostasis and regeneration. Sparse evidence suggests that skeletal muscle regeneration is severely impaired in obese individuals possibly due to increased lipid deposition and perturbed satellite cell function. The fatty acid transporter, CD36, plays an important role in skeletal muscle fatty acid transport and utilisation. This thesis shows that CD36-deficient mice are protected from HF diet-induced weight gain. This notion is supported by previous findings. Most importantly, CD36 was also identified as a key regulator of satellite cell function and myogenic differentiation, with severe implications for muscle regeneration after acute injury.

This thesis shows that CD36 KO mice have attenuated skeletal muscle lipid infiltration in diet-induced obesity, possibly linked to altered fatty acid metabolism as well as improved redox homeostasis. Enhanced lipid storage and accumulation of lipids in skeletal muscle is an important hallmark obesity and the development of insulin resistance. CD36 deficient mice showed attenuated lipid deposition, emphasising the role of CD36-facilitated skeletal muscle fatty acid uptake with possible implications for skeletal muscle insulin sensitivity. These findings highlight the importance of CD36 for skeletal muscle energy homeostasis. Interestingly, although upregulated in CD36 KO HF fed mice, alternative fatty acid transporters such as *Fabp3*, did not appear sufficient to compensate for the defect in fatty acid uptake due to the loss of CD36. Moreover, skeletal muscle metabolism seemed to be altered, revealing increased myokine mRNA levels such as *Fndc5* and *IL-15*, which have been shown to be increased

in skeletal muscle in response to exercise and downregulated in diabetic conditions (Lee and Jun, 2019, Dun et al., 2013).

Limited data hints towards impaired satellite cell function in the presence of increased skeletal muscle ectopic lipid infiltration, suggesting an underlying cause for the observed decrease of skeletal muscle regeneration in obese individuals. This is paralleled by the findings in this thesis, showing a significant reduction in satellite cell numbers in WT mice on a HF diet. The fact that satellite cell numbers were unaffected in CD36 deficient mice strongly suggests that obesity impairs satellite cell function via CD36-dependent pathways. One main finding of this thesis was therefore that HF diet induced impaired satellite cell function is partly rescued by CD36-deficiency. However, significantly lower satellite cell numbers were observed in satellite cells derived from CD36 deficient mice during differentiation *in vitro*. Since this finding was independent of diet, it further indicates the importance of CD36 during skeletal myogenesis. This was confirmed by the significant deficit in skeletal muscle regeneration seen in CD36 KO mice after acute CTX induced injury, 5 and 10 days *in vivo*.

One possible explanation for the involvement of CD36 in skeletal myogenesis is its interaction with AMPK. CD36 has been shown to inhibit AMPK activation and in the absence of CD36, AMPK has been shown to be constitutively active in muscle. This could possibly lead to the activation and proliferation of satellite cells via non-canonical Sonic Hedgehog signalling which induces Warburg-like glycolysis in satellite cells; required for their activation and proliferation during muscle regeneration. AMPK also inhibits myoblast differentiation through PGC-1alpha-dependent pathways. Moreover, AMPK has been shown to inhibit mTOR signalling, via the AMPK-Nampt-Sirt1 pathway, resulting in the inhibition of differentiation. This line of thought offers a plausible explanation for the adverse effect of CD36 deficiency on satellite cell proliferation and differentiation. Furthermore, CD36 has been suggested to play a crucial role in macrophage tissue infiltration important for the post-inflammatory resolution phase and debris removal. This hints towards a second focal point necessary for the regenerative process after acute skeletal muscle injury.

Additionally, mitochondrial dysfunction, which has been observed in several diseases related to the metabolic syndrome, is one of the most prominent abnormalities found in skeletal muscle of obese and diabetic individuals. CD36 has been previously identified to be involved in mitochondrial fatty acid oxidation. Mitochondrial spare respiratory capacity is a critical factor implicated in cell survival and function, reflecting the ability of mitochondria to adapt to acute or chronic stress. However, the extensive remodelling of the mitochondrial network is another very important part of the myoblast differentiation process. This thesis shows that during differentiation, the mitochondrial oxygen consumption rate was increased significantly as a result of the elevated energy demand. However, CD36 KO derived satellite cells were unable to increase their OCR during the process of differentiation. This finding provides further evidence suggesting impaired satellite cell differentiation in CD36 KO animals.

This thesis demonstrates that the impaired regeneration seen *in vivo* is at least in part brought about by the reduced stem cell commitment to differentiation seen in isolated satellite cells.

CD36 deficiency is known to result in hyperlipidaemia under both standard or a high fat diet. The CD36 KO mice maintained on a HF diet had decreased levels of fatty acid accumulation in the skeletal muscle, however, adverse effects were seen in the liver tissue, evidenced by large lipid-droplets associated with hepatic steatosis. These findings parallel previously published results by Goudriaan et al., showing that CD36 deficiency in mice increases skeletal muscle insulin sensitivity in skeletal muscle, but induces insulin resistance in the liver (Goudriaan et al., 2003, Goudriaan et al., 2005). A significant observation in the present study is that liver *Fatp1* mRNA contents are almost 4-fold higher in CD36 KO HF versus WT HF and WT ND mice. This indicates that in CD36 deficient mice, upregulation of *Fatp1* plays a key role in the development of hepatic steatosis in the presence of elevated free fatty acid availability. These results mirror the observation made in human CD36 deficiency, showing impaired fatty acid uptake by the heart but no restriction in the liver. FATP1 might therefore represent a potential therapeutic target to prevent lipid overload to the liver in CD36 deficiency.

These observations were further underlined by the more than 20-fold increase in the expression level of *Cidea* in liver from CD36 KO mice on a high-fat diet compared to WT HF fed animals. *Cidea* positively correlates with lipid droplet enlargement, fusion and the development of fatty liver disease, which further confirms the important link between CD36-deficiency and the development of NAFLD.

This thesis further elucidates the complexity of the underlying alterations in mitochondrial fatty acid oxidation and bioenergetics related to obesity, supporting evidence of the contribution of CD36 to the development of the metabolic syndrome. Most importantly, CD36-deficient mice exhibited impaired satellite cell differentiation and skeletal muscle regeneration, which identifies CD36 as a key regulator of these processes. Further research will be necessary to clarify the underlying mechanism of impaired skeletal muscle regeneration in the absence of CD36 to provide a basis to better understand the link between CD36-mediated skeletal muscle lipid metabolism in the context of muscle regeneration in obesity.

8 References

- ADACHI, T., KIKUCHI, N., YASUDA, K., ANAHARA, R., GU, N., MATSUNAGA, T., YAMAMURA, T., MORI, C., TSUJIMOTO, G., TSUDA, K. & ISHIHARA, A. 2007. Fibre type distribution and gene expression levels of both succinate dehydrogenase and peroxisome proliferator-activated receptor-gamma coactivator-1alpha of fibres in the soleus muscle of Zucker diabetic fatty rats. *Exp Physiol*, 92, 449-55.
- AEBY, E., AHMED, W., REDON, S., SIMANIS, V. & LINGNER, J. 2016. Peroxiredoxin 1 Protects Telomeres from Oxidative Damage and Preserves Telomeric DNA for Extension by Telomerase. *Cell Rep*, 17, 3107-3114.
- AGRAWAL, A., SURYAKUMAR, G. & RATHOR, R. 2018. Role of defective Ca. *J Cell Commun Signal*, 12, 645-659.
- AGUER, C., MERCIER, J., MAN, C. Y., METZ, L., BORDENAVE, S., LAMBERT, K., JEAN, E., LANTIER, L., BOUNOUA, L., BRUN, J. F., RAYNAUD DE MAUVERGER, E., ANDREELLI, F., FORETZ, M. & KITZMANN, M. 2010. Intramyocellular lipid accumulation is associated with permanent relocation ex vivo and in vitro of fatty acid translocase (FAT)/CD36 in obese patients. *Diabetologia*, 53, 1151-63.
- AKHMEDOV, D. & BERDEAUX, R. 2013. The effects of obesity on skeletal muscle regeneration. *Front Physiol*, 4, 371.
- ALFARADHI, M. Z., FERNANDEZ-TWINN, D. S., MARTIN-GRONERT, M. S., MUSIAL, B., FOWDEN, A. & OZANNE, S. E. 2014. Oxidative stress and altered lipid homeostasis in the programming of offspring fatty liver by maternal obesity. *Am J Physiol Regul Integr Comp Physiol*, 307, R26-34.
- ALMROTH, B. C., STURVE, J., BERGLUND, A. & FÖRLIN, L. 2005. Oxidative damage in eelpout (*Zoarces viviparus*), measured as protein carbonyls and TBARS, as biomarkers. *Aquat Toxicol*, 73, 171-80.
- ALONSO-MARTIN, S., ROCHAT, A., MADEMTZOGLU, D., MORAIS, J., DE REYNIÈS, A., AURADÉ, F., CHANG, T. H., ZAMMIT, P. S. & RELAIX, F. 2016. Gene Expression Profiling of Muscle Stem Cells Identifies Novel Regulators of Postnatal Myogenesis. *Front Cell Dev Biol*, 4, 58.
- ALVES-BEZERRA, M. & COHEN, D. E. 2017. Triglyceride Metabolism in the Liver. *Compr Physiol*, 8, 1-8.
- ALWAY, S. E., MYERS, M. J. & MOHAMED, J. S. 2014. Regulation of satellite cell function in sarcopenia. *Front Aging Neurosci*, 6, 246.
- ANDERSON, C. M. & STAHL, A. 2013. SLC27 fatty acid transport proteins. *Mol Aspects Med*, 34, 516-28.
- ANDERSON, J. E. 2000. A role for nitric oxide in muscle repair: nitric oxide-mediated activation of muscle satellite cells. *Mol Biol Cell*, 11, 1859-74.
- ANG, Z., XIONG, D., WU, M. & DING, J. L. 2018. FFAR2-FFAR3 receptor heteromerization modulates short-chain fatty acid sensing. *FASEB J*, 32, 289-303.
- ANGULO, P. 2002. Nonalcoholic fatty liver disease. *N Engl J Med*, 346, 1221-31.
- ANTONIEL, M., GIORGIO, V., FOGOLARI, F., GLICK, G. D., BERNARDI, P. & LIPPE, G. 2014. The oligomycin-sensitivity conferring protein of mitochondrial ATP synthase: emerging new roles in mitochondrial pathophysiology. *Int J Mol Sci*, 15, 7513-36.
- ARNOLD, L., HENRY, A., PORON, F., BABA-AMER, Y., VAN ROOIJEN, N., PLONQUET, A., GHERARDI, R. K. & CHAZAUD, B. 2007. Inflammatory monocytes recruited after skeletal muscle injury switch into antiinflammatory macrophages to support myogenesis. *J Exp Med*, 204, 1057-69.
- ATHYROS, V. G., TZIOMALOS, K., GOSSIOS, T. D., GRIVA, T., ANAGNOSTIS, P., KARGIOTIS, K., PAGOURELIAS, E. D., THEOCHARIDOU, E., KARAGIANNIS, A., MIKHAILIDIS, D. P. & GROUP, G. S. C. 2010. Safety and efficacy of long-term statin treatment for cardiovascular events in patients with coronary heart disease and abnormal liver tests

- in the Greek Atorvastatin and Coronary Heart Disease Evaluation (GREACE) Study: a post-hoc analysis. *Lancet*, 376, 1916-22.
- BAILEY-DOWNS, L. C., TUCSEK, Z., TOTH, P., SOSNOWSKA, D., GAUTAM, T., SONNTAG, W. E., CSISZAR, A. & UNGVARI, Z. 2013. Aging exacerbates obesity-induced oxidative stress and inflammation in perivascular adipose tissue in mice: a paracrine mechanism contributing to vascular redox dysregulation and inflammation. *J Gerontol A Biol Sci Med Sci*, 68, 780-92.
- BAJAJ, P., REDDY, B., MILLET, L., WEI, C., ZORLUTUNA, P., BAO, G. & BASHIR, R. 2011. Patterning the differentiation of C2C12 skeletal myoblasts. *Integr Biol (Camb)*, 3, 897-909.
- BARBIERI, E. & SESTILI, P. 2012. Reactive oxygen species in skeletal muscle signaling. *J Signal Transduct*, 2012, 982794.
- BECCAFICO, S., PUGLIELLI, C., PIETRANGELO, T., BELLOMO, R., FANÒ, G. & FULLE, S. 2007. Age-dependent effects on functional aspects in human satellite cells. *Ann N Y Acad Sci*, 1100, 345-52.
- BERGER, M., RASLAN, Z., ABURIMA, A., MAGWENZI, S., WRAITH, K. S., SPURGEON, B. E. J., HINDLE, M. S., LAW, R., FEBBRAIO, M. & NASEEM, K. M. 2019. Atherogenic lipid stress induces platelet hyperactivity through CD36-mediated hyposensitivity to prostacyclin; the role of phosphodiesterase 3A. *Haematologica*.
- BERRIDGE, M. J. 2003. Cardiac calcium signalling. *Biochem Soc Trans*, 31, 930-3.
- BEZAIRE, V., BRUCE, C. R., HEIGENHAUSER, G. J., TANDON, N. N., GLATZ, J. F., LUIKEN, J. J., BONEN, A. & SPRIET, L. L. 2006. Identification of fatty acid translocase on human skeletal muscle mitochondrial membranes: essential role in fatty acid oxidation. *Am J Physiol Endocrinol Metab*, 290, E509-15.
- BLAAUW, B. & REGGIANI, C. 2014. The role of satellite cells in muscle hypertrophy. *J Muscle Res Cell Motil*, 35, 3-10.
- BLAIR, H. C., SCHLESINGER, P. H., HUANG, C. L. & ZAIDI, M. 2007. Calcium signalling and calcium transport in bone disease. *Subcell Biochem*, 45, 539-62.
- BLOEMBERG, D. & QUADRILATERO, J. 2012. Rapid determination of myosin heavy chain expression in rat, mouse, and human skeletal muscle using multicolor immunofluorescence analysis. *PLoS One*, 7, e35273.
- BONEN, A., DYCK, D. J., IBRAHIMI, A. & ABUMRAD, N. A. 1999. Muscle contractile activity increases fatty acid metabolism and transport and FAT/CD36. *Am J Physiol*, 276, E642-9.
- BONEN, A., DYCK, D. J. & LUIKEN, J. J. 1998. Skeletal muscle fatty acid transport and transporters. *Adv Exp Med Biol*, 441, 193-205.
- BONEN, A., HAN, X. X., HABETS, D. D., FEBBRAIO, M., GLATZ, J. F. & LUIKEN, J. J. 2007. A null mutation in skeletal muscle FAT/CD36 reveals its essential role in insulin- and AICAR-stimulated fatty acid metabolism. *Am J Physiol Endocrinol Metab*, 292, E1740-9.
- BONEN, A., PAROLIN, M. L., STEINBERG, G. R., CALLES-ESCANDON, J., TANDON, N. N., GLATZ, J. F., LUIKEN, J. J., HEIGENHAUSER, G. J. & DYCK, D. J. 2004. Triacylglycerol accumulation in human obesity and type 2 diabetes is associated with increased rates of skeletal muscle fatty acid transport and increased sarcolemmal FAT/CD36. *FASEB J*, 18, 1144-6.
- BONNARD, C., DURAND, A., PEYROL, S., CHANSEAUME, E., CHAUVIN, M. A., MORIO, B., VIDAL, H. & RIEUSSET, J. 2008. Mitochondrial dysfunction results from oxidative stress in the skeletal muscle of diet-induced insulin-resistant mice. *J Clin Invest*, 118, 789-800.
- BROOKES, P. S., LAND, J. M., CLARK, J. B. & HEALES, S. J. 1998. Peroxynitrite and brain mitochondria: evidence for increased proton leak. *J Neurochem*, 70, 2195-202.
- BROWN, L. A., LEE, D. E., PATTON, J. F., PERRY, R. A., BROWN, J. L., BAUM, J. I., SMITH-BLAIR, N., GREENE, N. P. & WASHINGTON, T. A. 2015. Diet-induced obesity alters anabolic signalling in mice at the onset of skeletal muscle regeneration. *Acta Physiol (Oxf)*, 215, 46-57.

- BRUCE, C. R., ANDERSON, M. J., CAREY, A. L., NEWMAN, D. G., BONEN, A., KRIKETOS, A. D., COONEY, G. J. & HAWLEY, J. A. 2003. Muscle oxidative capacity is a better predictor of insulin sensitivity than lipid status. *J Clin Endocrinol Metab*, 88, 5444-51.
- BRUNDERT, M., HEEREN, J., MERKEL, M., CARAMBIA, A., HERKEL, J., GROITL, P., DOBNER, T., RAMAKRISHNAN, R., MOORE, K. J. & RINNINGER, F. 2011. Scavenger receptor CD36 mediates uptake of high density lipoproteins in mice and by cultured cells. *J Lipid Res*, 52, 745-58.
- CADET, J. & WAGNER, J. R. 2013. DNA base damage by reactive oxygen species, oxidizing agents, and UV radiation. *Cold Spring Harb Perspect Biol*, 5.
- CAI, L., WANG, Z., JI, A., MEYER, J. M. & VAN DER WESTHUYZEN, D. R. 2012. Scavenger receptor CD36 expression contributes to adipose tissue inflammation and cell death in diet-induced obesity. *PLoS One*, 7, e36785.
- CAMERON-SMITH, D., BURKE, L. M., ANGUS, D. J., TUNSTALL, R. J., COX, G. R., BONEN, A., HAWLEY, J. A. & HARGREAVES, M. 2003. A short-term, high-fat diet up-regulates lipid metabolism and gene expression in human skeletal muscle. *Am J Clin Nutr*, 77, 313-8.
- CAMPBELL, S. E., TANDON, N. N., WOLDEGIORGIS, G., LUIKEN, J. J., GLATZ, J. F. & BONEN, A. 2004. A novel function for fatty acid translocase (FAT)/CD36: involvement in long chain fatty acid transfer into the mitochondria. *J Biol Chem*, 279, 36235-41.
- CARROLL, A. M., PALMER, A. A. & LIONIKAS, A. 2011. QTL Analysis of Type I and Type IIA Fibers in Soleus Muscle in a Cross between LG/J and SM/J Mouse Strains. *Front Genet*, 2, 99.
- CHABOWSKI, A., GÓRSKI, J., GLATZ, J. F., P LUIKEN, J. J. & BONEN, A. 2008. Protein-mediated Fatty Acid Uptake in the Heart. *Curr Cardiol Rev*, 4, 12-21.
- CHANDRAN, R., KUMAR, M., KESAVAN, L., JACOB, R. S., GUNASEKARAN, S., LAKSHMI, S., SADASIVAN, C. & OMKUMAR, R. V. 2019. Cellular calcium signaling in the aging brain. *J Chem Neuroanat*, 95, 95-114.
- CHEN, G. Q., MOU, C. Y., YANG, Y. Q., WANG, S. & ZHAO, Z. W. 2011. Exercise training has beneficial anti-atrophy effects by inhibiting oxidative stress-induced MuRF1 upregulation in rats with diabetes. *Life Sci*, 89, 44-9.
- CHENG, C. S., EL-ABD, Y., BUI, K., HYUN, Y. E., HUGHES, R. H., KRAUS, W. E. & TRUSKEY, G. A. 2014. Conditions that promote primary human skeletal myoblast culture and muscle differentiation in vitro. *Am J Physiol Cell Physiol*, 306, C385-95.
- CLAPHAM, D. E. 2007. Calcium signaling. *Cell*, 131, 1047-58.
- CLUGSTON, R. D., JIANG, H., LEE, M. X., PIANTEDOSI, R., YUEN, J. J., RAMAKRISHNAN, R., LEWIS, M. J., GOTTESMAN, M. E., HUANG, L. S., GOLDBERG, I. J., BERK, P. D. & BLANER, W. S. 2011. Altered hepatic lipid metabolism in C57BL/6 mice fed alcohol: a targeted lipidomic and gene expression study. *J Lipid Res*, 52, 2021-31.
- COBURN, C. T., KNAPP, F. F., FEBBRAIO, M., BEETS, A. L., SILVERSTEIN, R. L. & ABUMRAD, N. A. 2000. Defective uptake and utilization of long chain fatty acids in muscle and adipose tissues of CD36 knockout mice. *J Biol Chem*, 275, 32523-9.
- CONSITT, L. A., BELL, J. A. & HOUMARD, J. A. 2009. Intramuscular lipid metabolism, insulin action, and obesity. *IUBMB Life*, 61, 47-55.
- D'SOUZA, D. M., TRAJCEVSKI, K. E., AL-SAJEE, D., WANG, D. C., THOMAS, M., ANDERSON, J. E. & HAWKE, T. J. 2015. Diet-induced obesity impairs muscle satellite cell activation and muscle repair through alterations in hepatocyte growth factor signaling. *Physiol Rep*, 3.
- DANDONA, P., ALJADA, A. & BANDYOPADHYAY, A. 2004. Inflammation: the link between insulin resistance, obesity and diabetes. *Trends Immunol*, 25, 4-7.
- DANIELSON, S. R. & ANDERSEN, J. K. 2008. Oxidative and nitrative protein modifications in Parkinson's disease. *Free Radic Biol Med*, 44, 1787-94.
- DAWN-LINSLEY, M., EKINCI, F. J., ORTIZ, D., ROGERS, E. & SHEA, T. B. 2005. Monitoring thiobarbituric acid-reactive substances (TBARs) as an assay for oxidative damage in neuronal cultures and central nervous system. *J Neurosci Methods*, 141, 219-22.

- DE GUIA, R. M., AGERHOLM, M., NIELSEN, T. S., CONSITT, L. A., SØGAARD, D., HELGE, J. W., LARSEN, S., BRANDAUER, J., HOUMARD, J. A. & TREEBAK, J. T. 2019. Aerobic and resistance exercise training reverses age-dependent decline in NAD. *Physiol Rep*, 7, e14139.
- DE MELLO, A. H., COSTA, A. B., ENGEL, J. D. G. & REZIN, G. T. 2018. Mitochondrial dysfunction in obesity. *Life Sci*, 192, 26-32.
- DENIES, M. S., JOHNSON, J., MALIPHOL, A. B., BRUNO, M., KIM, A., RIZVI, A., RUSTICI, K. & MEDLER, S. 2014. Diet-induced obesity alters skeletal muscle fiber types of male but not female mice. *Physiol Rep*, 2, e00204.
- DI FILIPPO, E. S., MANCINELLI, R., PIETRANGELO, T., LA ROVERE, R. M., QUATTROCELLI, M., SAMPAOLESI, M. & FULLE, S. 2016. Myomir dysregulation and reactive oxygen species in aged human satellite cells. *Biochem Biophys Res Commun*, 473, 462-70.
- DI MEO, S., IOSSA, S. & VENDITTI, P. 2017. Skeletal muscle insulin resistance: role of mitochondria and other ROS sources. *J Endocrinol*, 233, R15-R42.
- DICKINSON, B. C. & CHANG, C. J. 2011. Chemistry and biology of reactive oxygen species in signaling or stress responses. *Nat Chem Biol*, 7, 504-11.
- DIKALOV, S. I. & HARRISON, D. G. 2014. Methods for detection of mitochondrial and cellular reactive oxygen species. *Antioxid Redox Signal*, 20, 372-82.
- DOEGE, H., BAILLIE, R. A., ORTEGON, A. M., TSANG, B., WU, Q., PUNREDDY, S., HIRSCH, D., WATSON, N., GIMENO, R. E. & STAHL, A. 2006. Targeted deletion of FATP5 reveals multiple functions in liver metabolism: alterations in hepatic lipid homeostasis. *Gastroenterology*, 130, 1245-58.
- DOEGE, H., GRIMM, D., FALCON, A., TSANG, B., STORM, T. A., XU, H., ORTEGON, A. M., KAZANTZIS, M., KAY, M. A. & STAHL, A. 2008. Silencing of hepatic fatty acid transporter protein 5 in vivo reverses diet-induced non-alcoholic fatty liver disease and improves hyperglycemia. *J Biol Chem*, 283, 22186-92.
- DONALDSON, J. G. 2001. Immunofluorescence staining. *Curr Protoc Cell Biol*, Chapter 4, Unit 4.3.
- DROVER, V. A., AJMAL, M., NASSIR, F., DAVIDSON, N. O., NAULI, A. M., SAHOO, D., TSO, P. & ABUMRAD, N. A. 2005. CD36 deficiency impairs intestinal lipid secretion and clearance of chylomicrons from the blood. *J Clin Invest*, 115, 1290-7.
- DUMONT, N. A., WANG, Y. X., VON MALTZAHN, J., PASUT, A., BENTZINGER, C. F., BRUN, C. E. & RUDNICKI, M. A. 2015. Dystrophin expression in muscle stem cells regulates their polarity and asymmetric division. *Nat Med*, 21, 1455-63.
- DUN, S. L., LYU, R. M., CHEN, Y. H., CHANG, J. K., LUO, J. J. & DUN, N. J. 2013. Irisin-immunoreactivity in neural and non-neural cells of the rodent. *Neuroscience*, 240, 155-62.
- DURAIYAN, J., GOVINDARAJAN, R., KALIYAPPAN, K. & PALANISAMY, M. 2012. Applications of immunohistochemistry. *J Pharm Bioallied Sci*, 4, S307-9.
- EGUCHI, Y., EGUCHI, T., MIZUTA, T., IDE, Y., YASUTAKE, T., IWAKIRI, R., HISATOMI, A., OZAKI, I., YAMAMOTO, K., KITAJIMA, Y., KAWAGUCHI, Y., KUROKI, S. & ONO, N. 2006. Visceral fat accumulation and insulin resistance are important factors in nonalcoholic fatty liver disease. *J Gastroenterol*, 41, 462-9.
- ELASHRY, M. I., ELDAEY, A., GLENSKE, K., MATSAKAS, A., WENISCH, S., ARNHOLD, S. and PATEL, K. 2019. The effect of high-fat diet on the morphological properties of the forelimb musculature in hypertrophic myostatin null mice, *J Anat*, 235(4), pp. 825-835.
- FAGERBERG, L., HALLSTRÖM, B. M., OKSVOLD, P., KAMPF, C., DJUREINOVIC, D., ODEBERG, J., HABUKA, M., TAHMASEBPOOR, S., DANIELSSON, A., EDLUND, K., ASPLUND, A., SJÖSTEDT, E., LUNDBERG, E., SZIGYARTO, C. A., SKOGS, M., TAKANEN, J. O., BERLING, H., TEGEL, H., MULDER, J., NILSSON, P., SCHWENK, J. M., LINDSKOG, C., DANIELSSON, F., MARDINOGLU, A., SIVERTSSON, A., VON FEILITZEN, K., FORSBERG, M., ZWAHLEN, M., OLSSON, I., NAVANI, S., HUSS, M., NIELSEN, J., PONTEN, F. & UHLÉN, M. 2014.

- Analysis of the human tissue-specific expression by genome-wide integration of transcriptomics and antibody-based proteomics. *Mol Cell Proteomics*, 13, 397-406.
- FALCON, A., DOEGE, H., FLUITT, A., TSANG, B., WATSON, N., KAY, M. A. & STAHL, A. 2010. FATP2 is a hepatic fatty acid transporter and peroxisomal very long-chain acyl-CoA synthetase. *Am J Physiol Endocrinol Metab*, 299, E384-93.
- FEBBRAIO, M., ABUMRAD, N. A., HAJJAR, D. P., SHARMA, K., CHENG, W., PEARCE, S. F. & SILVERSTEIN, R. L. 1999. A null mutation in murine CD36 reveals an important role in fatty acid and lipoprotein metabolism. *J Biol Chem*, 274, 19055-62.
- FEBBRAIO, M., HAJJAR, D. P. & SILVERSTEIN, R. L. 2001. CD36: a class B scavenger receptor involved in angiogenesis, atherosclerosis, inflammation, and lipid metabolism. *J Clin Invest*, 108, 785-91.
- FERNÁNDEZ, F., GUTIÉRREZ, J., SORLÓZANO, A., ROMERO, J. M., SOTO, M. J. & RUIZ-CABELLO, F. 2006. Comparison of the SYBR Green and the hybridization probe format for real-time PCR detection of HHV-6. *Microbiol Res*, 161, 158-63.
- FERNÁNDEZ-SÁNCHEZ, A., MADRIGAL-SANTILLÁN, E., BAUTISTA, M., ESQUIVEL-SOTO, J., MORALES-GONZÁLEZ, A., ESQUIVEL-CHIRINO, C., DURANTE-MONTIEL, I., SÁNCHEZ-RIVERA, G., VALADEZ-VEGA, C. & MORALES-GONZÁLEZ, J. A. 2011. Inflammation, oxidative stress, and obesity. *Int J Mol Sci*, 12, 3117-32.
- FERRARI, M. B., ROHRBOUGH, J. & SPITZER, N. C. 1996. Spontaneous calcium transients regulate myofibrillogenesis in embryonic *Xenopus* myocytes. *Dev Biol*, 178, 484-97.
- FLÜCK, M. & HOPPELER, H. 2003. Molecular basis of skeletal muscle plasticity--from gene to form and function. *Rev Physiol Biochem Pharmacol*, 146, 159-216.
- FOLMES, C. D., NELSON, T. J., MARTINEZ-FERNANDEZ, A., ARRELL, D. K., LINDOR, J. Z., DZEJA, P. P., IKEDA, Y., PEREZ-TERZIC, C. & TERZIC, A. 2011. Somatic oxidative bioenergetics transitions into pluripotency-dependent glycolysis to facilitate nuclear reprogramming. *Cell Metab*, 14, 264-71.
- FORTIN, M., VIDEMAN, T., GIBBONS, L. E. & BATTIÉ, M. C. 2014. Paraspinal muscle morphology and composition: a 15-yr longitudinal magnetic resonance imaging study. *Med Sci Sports Exerc*, 46, 893-901.
- FRAYN, K. N., ARNER, P. and YKI-JÄRVINEN, H. 2006. Fatty acid metabolism in adipose tissue, muscle and liver in health and disease, *Essays Biochem*, 42, pp. 89-103.
- FRONTERA, W. R. & OCHALA, J. 2015. Skeletal muscle: a brief review of structure and function. *Calcif Tissue Int*, 96, 183-95.
- FU, X., ZHU, M., ZHANG, S., FORETZ, M., VIOLLET, B. & DU, M. 2016. Obesity Impairs Skeletal Muscle Regeneration Through Inhibition of AMPK. *Diabetes*, 65, 188-200.
- FU, X., ZHU, M. J., DODSON, M. V. & DU, M. 2015. AMP-activated protein kinase stimulates Warburg-like glycolysis and activation of satellite cells during muscle regeneration. *J Biol Chem*, 290, 26445-56.
- FULCO, M., CEN, Y., ZHAO, P., HOFFMAN, E. P., MCBURNEY, M. W., SAUVE, A. A. & SARTORELLI, V. 2008. Glucose restriction inhibits skeletal myoblast differentiation by activating SIRT1 through AMPK-mediated regulation of Nampt. *Dev Cell*, 14, 661-73.
- FURUHASHI, M., URA, N., NAKATA, T., TANAKA, T. & SHIMAMOTO, K. 2004. Genotype in human CD36 deficiency and diabetes mellitus. *Diabet Med*, 21, 952-3.
- FURUKAWA, S., FUJITA, T., SHIMABUKURO, M., IWAKI, M., YAMADA, Y., NAKAJIMA, Y., NAKAYAMA, O., MAKISHIMA, M., MATSUDA, M. & SHIMOMURA, I. 2004. Increased oxidative stress in obesity and its impact on metabolic syndrome. *J Clin Invest*, 114, 1752-61.
- GEOLEN, A., HELIN, L., GEERAERT, B., MALAUD, E., HOLVOET, P. & MARGUERIE, G. 2012. CD36 inhibitors reduce postprandial hypertriglyceridemia and protect against diabetic dyslipidemia and atherosclerosis. *PLoS One*, 7, e37633.

- GHARIB, M., TAO, H., FUNGWE, T. V. & HAJRI, T. 2016. Cluster Differentiating 36 (CD36) Deficiency Attenuates Obesity-Associated Oxidative Stress in the Heart. *PLoS One*, 11, e0155611.
- GIMENO, R. E. 2007. Fatty acid transport proteins. *Curr Opin Lipidol*, 18, 271-6.
- GLATZ, J. F., ANGIN, Y., STEINBUSCH, L. K., SCHWENK, R. W. & LUIKEN, J. J. 2013. CD36 as a target to prevent cardiac lipotoxicity and insulin resistance. *Prostaglandins Leukot Essent Fatty Acids*, 88, 71-7.
- GOLDBERG, I. J., ECKEL, R. H. & ABUMRAD, N. A. 2009. Regulation of fatty acid uptake into tissues: lipoprotein lipase- and CD36-mediated pathways. *J Lipid Res*, 50 Suppl, S86-90.
- GOODPASTER, B. H., THAETE, F. L. & KELLEY, D. E. 2000. Thigh adipose tissue distribution is associated with insulin resistance in obesity and in type 2 diabetes mellitus. *Am J Clin Nutr*, 71, 885-92.
- GOODPASTER, B. H. & WOLF, D. 2004. Skeletal muscle lipid accumulation in obesity, insulin resistance, and type 2 diabetes. *Pediatr Diabetes*, 5, 219-26.
- GOUDRIAAN, J. R., DAHLMANS, V. E., TEUSINK, B., OUWENS, D. M., FEBBRAIO, M., MAASSEN, J. A., ROMIJN, J. A., HAVEKES, L. M. & VOSHOL, P. J. 2003. CD36 deficiency increases insulin sensitivity in muscle, but induces insulin resistance in the liver in mice. *J Lipid Res*, 44, 2270-7.
- GOUDRIAAN, J. R., DEN BOER, M. A., RENSEN, P. C., FEBBRAIO, M., KUIPERS, F., ROMIJN, J. A., HAVEKES, L. M. & VOSHOL, P. J. 2005. CD36 deficiency in mice impairs lipoprotein lipase-mediated triglyceride clearance. *J Lipid Res*, 46, 2175-81.
- GRABIEC, K., MAJEWSKA, A., WICIK, Z., MILEWSKA, M., BŁASZCZYK, M. & GRZELKOWSKA-KOWALCZYK, K. 2016. The effect of palmitate supplementation on gene expression profile in proliferating myoblasts. *Cell Biol Toxicol*, 32, 185-98.
- GRABIEC, K., MILEWSKA, M., BŁASZCZYK, M., GAJEWSKA, M. & GRZELKOWSKA-KOWALCZYK, K. 2015. Palmitate exerts opposite effects on proliferation and differentiation of skeletal myoblasts. *Cell Biol Int*, 39, 1044-52.
- GREEN, K., BRAND, M. D. & MURPHY, M. P. 2004. Prevention of mitochondrial oxidative damage as a therapeutic strategy in diabetes. *Diabetes*, 53 Suppl 1, S110-8.
- GREISING, S. M., GRANSEE, H. M., MANTILLA, C. B. & SIECK, G. C. 2012. Systems biology of skeletal muscle: fiber type as an organizing principle. *Wiley Interdiscip Rev Syst Biol Med*, 4, 457-73.
- GRIMSRUD, P. A., XIE, H., GRIFFIN, T. J. & BERNLOHR, D. A. 2008. Oxidative stress and covalent modification of protein with bioactive aldehydes. *J Biol Chem*, 283, 21837-41.
- HAJRI, T., HAN, X. X., BONEN, A. & ABUMRAD, N. A. 2002. Defective fatty acid uptake modulates insulin responsiveness and metabolic responses to diet in CD36-null mice. *J Clin Invest*, 109, 1381-9.
- HAMES, K. C., VELLA, A., KEMP, B. J. & JENSEN, M. D. 2014. Free fatty acid uptake in humans with CD36 deficiency. *Diabetes*, 63, 3606-14.
- HAN, X. X., CHABOWSKI, A., TANDON, N. N., CALLES-ESCANDON, J., GLATZ, J. F., LUIKEN, J. J. & BONEN, A. 2007. Metabolic challenges reveal impaired fatty acid metabolism and translocation of FAT/CD36 but not FABPpm in obese Zucker rat muscle. *Am J Physiol Endocrinol Metab*, 293, E566-75.
- HANSON, J. & HUXLEY, H. E. 1953. Structural basis of the cross-striations in muscle. *Nature*, 172, 530-2.
- HARDY, D., BESNARD, A., LATIL, M., JOUVION, G., BRIAND, D., THÉPENIER, C., PASCAL, Q., GUGUIN, A., GAYRAUD-MOREL, B., CAVAILLON, J. M., TAJBAKHS, S., ROCHETEAU, P. & CHRÉTIEN, F. 2016. Comparative Study of Injury Models for Studying Muscle Regeneration in Mice. *PLoS One*, 11, e0147198.
- HEGARTY, B. D., COONEY, G. J., KRAEGEN, E. W. & FURLER, S. M. 2002. Increased efficiency of fatty acid uptake contributes to lipid accumulation in skeletal muscle of high fat-fed insulin-resistant rats. *Diabetes*, 51, 1477-84.

- HERZOG, W. 2018. Correction to: skeletal muscle mechanics: questions, problems and possible solutions. *J Neuroeng Rehabil*, 15, 16.
- HILTON, T. N., TUTTLE, L. J., BOHNERT, K. L., MUELLER, M. J. & SINACORE, D. R. 2008. Excessive adipose tissue infiltration in skeletal muscle in individuals with obesity, diabetes mellitus, and peripheral neuropathy: association with performance and function. *Phys Ther*, 88, 1336-44.
- HIRANO, K., KUWASAKO, T., NAKAGAWA-TOYAMA, Y., JANABI, M., YAMASHITA, S. & MATSUZAWA, Y. 2003. Pathophysiology of human genetic CD36 deficiency. *Trends Cardiovasc Med*, 13, 136-41.
- HIRSCH, D., STAHL, A. & LODISH, H. F. 1998. A family of fatty acid transporters conserved from mycobacterium to man. *Proc Natl Acad Sci U S A*, 95, 8625-9.
- HOLLOWAY, G. P., BEZAIRE, V., HEIGENHAUSER, G. J., TANDON, N. N., GLATZ, J. F., LUIKEN, J. J., BONEN, A. & SPRIET, L. L. 2006. Mitochondrial long chain fatty acid oxidation, fatty acid translocase/CD36 content and carnitine palmitoyltransferase I activity in human skeletal muscle during aerobic exercise. *J Physiol*, 571, 201-10.
- HOLMSTRÖM, K. M. & FINKEL, T. 2014. Cellular mechanisms and physiological consequences of redox-dependent signalling. *Nat Rev Mol Cell Biol*, 15, 411-21.
- HU, Z., WANG, H., LEE, I. H., MODI, S., WANG, X., DU, J. & MITCH, W. E. 2010. PTEN inhibition improves muscle regeneration in mice fed a high-fat diet. *Diabetes*, 59, 1312-20.
- HUANG, S. C., EVERTS, B., IVANOVA, Y., O'SULLIVAN, D., NASCIMENTO, M., SMITH, A. M., BEATTY, W., LOVE-GREGORY, L., LAM, W. Y., O'NEILL, C. M., YAN, C., DU, H., ABUMRAD, N. A., URBAN, J. F., ARTYOMOV, M. N., PEARCE, E. L. & PEARCE, E. J. 2014. Cell-intrinsic lysosomal lipolysis is essential for alternative activation of macrophages. *Nat Immunol*, 15, 846-55.
- HUH, J. Y., PANAGIOTOU, G., MOUGIOS, V., BRINKOETTER, M., VAMVINI, M. T., SCHNEIDER, B. E. & MANTZOROS, C. S. 2012. FNDC5 and irisin in humans: I. Predictors of circulating concentrations in serum and plasma and II. mRNA expression and circulating concentrations in response to weight loss and exercise. *Metabolism*, 61, 1725-38.
- HUNTER, G. R., SINGH, H., CARTER, S. J., BRYAN, D. R. & FISHER, G. 2019. Sarcopenia and Its Implications for Metabolic Health. *J Obes*, 2019, 8031705.
- HUXLEY, A. F. & NIEDERGERKE, R. 1954. Structural changes in muscle during contraction; interference microscopy of living muscle fibres. *Nature*, 173, 971-3.
- ICHIMURA, A., HASEGAWA, S., KASUBUCHI, M. & KIMURA, I. 2014. Free fatty acid receptors as therapeutic targets for the treatment of diabetes. *Front Pharmacol*, 5, 236.
- IMAI, M., TANAKA, T., KINTAKA, T., IKEMOTO, T., SHIMIZU, A. & KITAURA, Y. 2002. Genomic heterogeneity of type II CD36 deficiency. *Clin Chim Acta*, 321, 97-106.
- INGRAM, K. H., HILL, H., MOELLERING, D. R., HILL, B. G., LARA-CASTRO, C., NEWCOMER, B., BRANDON, L. J., INGALLS, C. P., PENUMETCHA, M., RUPP, J. C. & GARVEY, W. T. 2012. Skeletal muscle lipid peroxidation and insulin resistance in humans. *J Clin Endocrinol Metab*, 97, E1182-6.
- JACKSON, M. J. & MCARDLE, A. 2011. Age-related changes in skeletal muscle reactive oxygen species generation and adaptive responses to reactive oxygen species. *J Physiol*, 589, 2139-45.
- JAIN, S. S., LUIKEN, J. J., SNOOK, L. A., HAN, X. X., HOLLOWAY, G. P., GLATZ, J. F. & BONEN, A. 2015. Fatty acid transport and transporters in muscle are critically regulated by Akt2. *FEBS Lett*, 589, 2769-75.
- JANSSEN, W. J. & HENSON, P. M. 2012. Cellular regulation of the inflammatory response. *Toxicol Pathol*, 40, 166-73.
- JENSEN, J., RUSTAD, P. I., KOLNES, A. J. & LAI, Y. C. 2011. The role of skeletal muscle glycogen breakdown for regulation of insulin sensitivity by exercise. *Front Physiol*, 2, 112.

- JHENG, H. F., TSAI, P. J., GUO, S. M., KUO, L. H., CHANG, C. S., SU, I. J., CHANG, C. R. & TSAI, Y. S. 2012. Mitochondrial fission contributes to mitochondrial dysfunction and insulin resistance in skeletal muscle. *Mol Cell Biol*, 32, 309-19.
- KAHN, B. B. & FLIER, J. S. 2000. Obesity and insulin resistance. *J Clin Invest*, 106, 473-81.
- KAMIJO, T., BODNER, S., VAN DE KAMP, E., RANDLE, D. H. & SHERR, C. J. 1999. Tumor spectrum in ARF-deficient mice. *Cancer Res*, 59, 2217-22.
- KAMIYA, M., NAKAGOMI, A., TOKITA, Y., YASUTAKE, V. M., KUSAMA, Y., TAKAYAMA, M. & TAKANO, T. 2006. Type I CD36 Deficiency Associated with Metabolic Syndrome and Vasospastic Angina: A Case Report. *J Cardiol*, 48, 41-44.
- KAWANO, Y. & COHEN, D. E. 2013. Mechanisms of hepatic triglyceride accumulation in non-alcoholic fatty liver disease. *J Gastroenterol*, 48, 434-41.
- KAZANTZIS, M. & STAHL, A. 2012. Fatty acid transport proteins, implications in physiology and disease. *Biochim Biophys Acta*, 1821, 852-7.
- KELLEY, D. E., HE, J., MENSHIKOVA, E. V. & RITOV, V. B. 2002. Dysfunction of mitochondria in human skeletal muscle in type 2 diabetes. *Diabetes*, 51, 2944-50.
- KENNEDY, D. J. & KASHYAP, S. R. 2011. Pathogenic role of scavenger receptor CD36 in the metabolic syndrome and diabetes. *Metab Syndr Relat Disord*, 9, 239-45.
- KENNEDY, D. J., KUCHIBHOTLA, S., WESTFALL, K. M., SILVERSTEIN, R. L., MORTON, R. E. & FEBBRAIO, M. 2011. A CD36-dependent pathway enhances macrophage and adipose tissue inflammation and impairs insulin signalling. *Cardiovasc Res*, 89, 604-13.
- KIM, J. & SO, W. Y. 2018. High Body Mass Index Is Associated with the Extent of Muscle Damage after Eccentric Exercise. *Int J Environ Res Public Health*, 15.
- KNOBLAUCH, M. A., O'CONNOR, D. P. & CLARKE, M. S. 2013. Obese mice incur greater myofiber membrane disruption in response to mechanical load compared with lean mice. *Obesity (Silver Spring)*, 21, 135-43.
- KOENIG, M., HOFFMAN, E. P., BERTELSON, C. J., MONACO, A. P., FEENER, C. & KUNKEL, L. M. 1987. Complete cloning of the Duchenne muscular dystrophy (DMD) cDNA and preliminary genomic organization of the DMD gene in normal and affected individuals. *Cell*, 50, 509-17.
- KONIG, S., BÉGUET, A., BADER, C. R. & BERNHEIM, L. 2006. The calcineurin pathway links hyperpolarization (Kir2.1)-induced Ca²⁺ signals to human myoblast differentiation and fusion. *Development*, 133, 3107-14.
- KOO, J. H., SMILEY, M. A., LOVERING, R. M. & MARGOLIS, F. L. 2007. Bex1 knock out mice show altered skeletal muscle regeneration. *Biochem Biophys Res Commun*, 363, 405-10.
- KOONEN, D. P., JACOBS, R. L., FEBBRAIO, M., YOUNG, M. E., SOLTYS, C. L., ONG, H., VANCE, D. E. & DYCK, J. R. 2007. Increased hepatic CD36 expression contributes to dyslipidemia associated with diet-induced obesity. *Diabetes*, 56, 2863-71.
- KOONEN, D. P., SUNG, M. M., KAO, C. K., DOLINSKY, V. W., KOVES, T. R., ILKAYEVA, O., JACOBS, R. L., VANCE, D. E., LIGHT, P. E., MUOIO, D. M., FEBBRAIO, M. & DYCK, J. R. 2010. Alterations in skeletal muscle fatty acid handling predisposes middle-aged mice to diet-induced insulin resistance. *Diabetes*, 59, 1366-75.
- KOTTLORS, M. & KIRSCHNER, J. 2010. Elevated satellite cell number in Duchenne muscular dystrophy. *Cell Tissue Res*, 340, 541-8.
- KOVES, T. R., USSHER, J. R., NOLAND, R. C., SLENTZ, D., MOSEDALE, M., ILKAYEVA, O., BAIN, J., STEVENS, R., DYCK, J. R., NEWGARD, C. B., LOPASCHUK, G. D. & MUOIO, D. M. 2008. Mitochondrial overload and incomplete fatty acid oxidation contribute to skeletal muscle insulin resistance. *Cell Metab*, 7, 45-56.
- KRAEMER, W. & FLECK, S. J. 2014. *Exercise Physiology: Integrating Theory and Application*.
- KRAUSE, M. P., MORADI, J., NISSAR, A. A., RIDDELL, M. C. & HAWKE, T. J. 2011. Inhibition of plasminogen activator inhibitor-1 restores skeletal muscle regeneration in untreated type 1 diabetic mice. *Diabetes*, 60, 1964-72.

- KUDA, O., JENKINS, C. M., SKINNER, J. R., MOON, S. H., SU, X., GROSS, R. W. & ABUMRAD, N. A. 2011. CD36 protein is involved in store-operated calcium flux, phospholipase A2 activation, and production of prostaglandin E2. *J Biol Chem*, 286, 17785-95.
- KUDA, O., PIETKA, T. A., DEMIANOVA, Z., KUDOVA, E., CVACKA, J., KOPECKY, J. & ABUMRAD, N. A. 2013. Sulfo-N-succinimidyl oleate (SSO) inhibits fatty acid uptake and signaling for intracellular calcium via binding CD36 lysine 164: SSO also inhibits oxidized low density lipoprotein uptake by macrophages. *J Biol Chem*, 288, 15547-55.
- LAMON, S., WALLACE, M. A. & RUSSELL, A. P. 2014. The STARS signaling pathway: a key regulator of skeletal muscle function. *Pflugers Arch*, 466, 1659-71.
- LE FOLL, C., DUNN-MEYNELL, A. A. & LEVIN, B. E. 2015. Role of FAT/CD36 in fatty acid sensing, energy, and glucose homeostasis regulation in DIO and DR rats. *Am J Physiol Regul Integr Comp Physiol*, 308, R188-98.
- LEE, J. H. & JUN, H. S. 2019. Role of Myokines in Regulating Skeletal Muscle Mass and Function. *Front Physiol*, 10, 42.
- LEE, S., TAK, E., LEE, J., RASHID, M. A., MURPHY, M. P., HA, J. & KIM, S. S. 2011. Mitochondrial H₂O₂ generated from electron transport chain complex I stimulates muscle differentiation. *Cell Res*, 21, 817-34.
- LEON, B., JENKINS, S., PEPIN, K., CHAUDHRY, H., SMITH, K., ZALOS, G., MILLER, B. V., CHEN, K. Y., REMALEY, A. T., WACLAWIW, M. A., SUMNER, A. E. & CANNON, R. O. 2013. Insulin and extremity muscle mass in overweight and obese women. *Int J Obes (Lond)*, 37, 1560-4.
- LEPPER, C. & FAN, C. M. 2012. Generating tamoxifen-inducible Cre alleles to investigate myogenesis in mice. *Methods Mol Biol*, 798, 297-308.
- LI, Y., LIU, L., WANG, B., WANG, J. & CHEN, D. 2013. Metformin in non-alcoholic fatty liver disease: A systematic review and meta-analysis. *Biomed Rep*, 1, 57-64.
- LINDSEY, M. L., JUNG, M., YABLUCHANSKIY, A., CANNON, P. L., IYER, R. P., FLYNN, E. R., DELEON-PENNELL, K. Y., VALERIO, F. M., HARRISON, C. L., RIPPLINGER, C. M., HALL, M. E. & MA, Y. 2019. Exogenous CXCL4 infusion inhibits macrophage phagocytosis by limiting CD36 signalling to enhance post-myocardial infarction cardiac dilation and mortality. *Cardiovasc Res*, 115, 395-408.
- LIU, J. H., KÖNIG, S., MICHEL, M., ARNAUDEAU, S., FISCHER-LOUGHEED, J., BADER, C. R. & BERNHEIM, L. 2003. Acceleration of human myoblast fusion by depolarization: graded Ca²⁺ signals involved. *Development*, 130, 3437-46.
- LIVAK, K. J. & SCHMITTGEN, T. D. 2001. Analysis of relative gene expression data using real-time quantitative PCR and the 2⁻(Delta Delta C(T)) Method. *Methods*, 25, 402-8.
- LONERGAN, T., BAVISTER, B. & BRENNER, C. 2007. Mitochondria in stem cells. *Mitochondrion*, 7, 289-96.
- LONGYEAR, T., WALCOTT, S. & DEBOLD, E. P. 2017. The molecular basis of thin filament activation: from single molecule to muscle. *Sci Rep*, 7, 1822.
- LOVE-GREGORY, L. & ABUMRAD, N. A. 2011. CD36 genetics and the metabolic complications of obesity. *Curr Opin Clin Nutr Metab Care*, 14, 527-34.
- LOVE-GREGORY, L., SHERVA, R., SCHAPPE, T., QI, J. S., MCCREA, J., KLEIN, S., CONNELLY, M. A. & ABUMRAD, N. A. 2011. Common CD36 SNPs reduce protein expression and may contribute to a protective atherogenic profile. *Hum Mol Genet*, 20, 193-201.
- LOWE, M. E. 2002. The triglyceride lipases of the pancreas. *J Lipid Res*, 43, 2007-16.
- LUIKEN, J. J., GLATZ, J. F. & BONEN, A. 2000. Fatty acid transport proteins facilitate fatty acid uptake in skeletal muscle. *Can J Appl Physiol*, 25, 333-52.
- LUTZ, T. A. & WOODS, S. C. 2012. Overview of animal models of obesity. *Curr Protoc Pharmacol*, Chapter 5, Unit5.61.
- LY, L. D., XU, S., CHOI, S. K., HA, C. M., THOUDAM, T., CHA, S. K., WIEDERKEHR, A., WOLLHEIM, C. B., LEE, I. K. & PARK, K. S. 2017. Oxidative stress and calcium dysregulation by palmitate in type 2 diabetes. *Exp Mol Med*, 49, e291.

- MANSOR, L. S., SOUSA FIALHO, M. D. L., YEA, G., COUMANS, W. A., WEST, J. A., KERR, M., CARR, C. A., LUIKEN, J. J. F. P., GLATZ, J. F. C., EVANS, R. D., GRIFFIN, J. L., TYLER, D. J., CLARKE, K. & HEATHER, L. C. 2017. Inhibition of sarcolemmal FAT/CD36 by sulfo-N-succinimidyl oleate rapidly corrects metabolism and restores function in the diabetic heart following hypoxia/reoxygenation. *Cardiovasc Res*, 113, 737-748.
- MARCHESINI, G., MOSCATIELLO, S., DI DOMIZIO, S. & FORLANI, G. 2008. Obesity-associated liver disease. *J Clin Endocrinol Metab*, 93, S74-80.
- MARSEGLIA, L., MANTI, S., D'ANGELO, G., NICOTERA, A., PARISI, E., DI ROSA, G., GITTO, E. & ARRIGO, T. 2014. Oxidative stress in obesity: a critical component in human diseases. *Int J Mol Sci*, 16, 378-400.
- MARTIN, G., NEMOTO, M., GELMAN, L., GEFFROY, S., NAJIB, J., FRUCHART, J. C., ROEVENS, P., DE MARTINVILLE, B., DEEB, S. & AUWERX, J. 2000. The human fatty acid transport protein-1 (SLC27A1; FATP-1) cDNA and gene: organization, chromosomal localization, and expression. *Genomics*, 66, 296-304.
- MASUDA, D., HIRANO, K., OKU, H., SANDOVAL, J. C., KAWASE, R., YUASA-KAWASE, M., YAMASHITA, Y., TAKADA, M., TSUBAKIO-YAMAMOTO, K., TOCHINO, Y., KOSEKI, M., MATSUURA, F., NISHIDA, M., KAWAMOTO, T., ISHIGAMI, M., HORI, M., SHIMOMURA, I. & YAMASHITA, S. 2009. Chylomicron remnants are increased in the postprandial state in CD36 deficiency. *J Lipid Res*, 50, 999-1011.
- MATSAKAS, A., MOUISEL, E., AMTHOR, H. and PATEL, K. 2010. Myostatin knockout mice increase oxidative muscle phenotype as an adaptive response to exercise', *J Muscle Res Cell Motil*, 31(2), pp. 111-25.
- MATSAKAS, A. & PATEL, K. 2009. Skeletal muscle fibre plasticity in response to selected environmental and physiological stimuli. *Histol Histopathol*, 24, 611-29.
- MATSAKAS, A., PROSDOCIMO, D. A., MITCHELL, R., COLLINS-HOOPER, H., GIALLOUROU, N., SWANN, J. R., POTTER, P., EPTING, T., JAIN, M. K. & PATEL, K. 2015. Investigating mechanisms underpinning the detrimental impact of a high-fat diet in the developing and adult hypermuscular myostatin null mouse. *Skelet Muscle*, 5, 38.
- MATSAKAS, A., YADAV, V., LORCA, S. and NARKAR, V. 2013. Muscle ERR α mitigates Duchenne muscular dystrophy via metabolic and angiogenic reprogramming, *FASEB J*, 27(10), pp. 4004-16.
- MAURO, A. 1961. Satellite cell of skeletal muscle fibers. *J Biophys Biochem Cytol*, 9, 493-5.
- MCARDLE, A., PATTWELL, D., VASILAKI, A., GRIFFITHS, R. D. & JACKSON, M. J. 2001. Contractile activity-induced oxidative stress: cellular origin and adaptive responses. *Am J Physiol Cell Physiol*, 280, C621-7.
- MCFARLAN, J. T., YOSHIDA, Y., JAIN, S. S., HAN, X. X., SNOOK, L. A., LALLY, J., SMITH, B. K., GLATZ, J. F., LUIKEN, J. J., SAYER, R. A., TUPLING, A. R., CHABOWSKI, A., HOLLOWAY, G. P. & BONEN, A. 2012. In vivo, fatty acid translocase (CD36) critically regulates skeletal muscle fuel selection, exercise performance, and training-induced adaptation of fatty acid oxidation. *J Biol Chem*, 287, 23502-16.
- MEBAREK, S., KOMATI, H., NARO, F., ZEILLER, C., ALVISI, M., LAGARDE, M., PRIGENT, A. F. & NÉMOZ, G. 2007. Inhibition of de novo ceramide synthesis upregulates phospholipase D and enhances myogenic differentiation. *J Cell Sci*, 120, 407-16.
- MEEH, R. C. R., BLAAK, E. E. & VAN LOON, L. J. C. 2019. Lipotoxicity plays a key role in the development of both insulin resistance and muscle atrophy in patients with type 2 diabetes. *Obes Rev*, 20, 1205-1217.
- MELOV, S., TARNOPOLSKY, M. A., BECKMAN, K., FELKEY, K. & HUBBARD, A. 2007. Resistance exercise reverses aging in human skeletal muscle. *PLoS One*, 2, e465.
- MENG, S. J. & YU, L. J. 2010. Oxidative stress, molecular inflammation and sarcopenia. *Int J Mol Sci*, 11, 1509-26.

- MENSHIKOVA, E. V., RITOV, V. B., FAIRFULL, L., FERRELL, R. E., KELLEY, D. E. & GOODPASTER, B. H. 2006. Effects of exercise on mitochondrial content and function in aging human skeletal muscle. *J Gerontol A Biol Sci Med Sci*, 61, 534-40.
- MISHRA, P., VARUZHANYAN, G., PHAM, A. H. & CHAN, D. C. 2015. Mitochondrial Dynamics is a Distinguishing Feature of Skeletal Muscle Fiber Types and Regulates Organellar Compartmentalization. *Cell Metab*, 22, 1033-44.
- MOGENSEN, M., SAHLIN, K., FERNSTRÖM, M., GLINTBORG, D., VIND, B. F., BECK-NIELSEN, H. & HØJLUND, K. 2007. Mitochondrial respiration is decreased in skeletal muscle of patients with type 2 diabetes. *Diabetes*, 56, 1592-9.
- MONTARRAS, D., MORGAN, J., COLLINS, C., RELAIX, F., ZAFFRAN, S., CUMANO, A., PARTRIDGE, T. & BUCKINGHAM, M. 2005. Direct isolation of satellite cells for skeletal muscle regeneration. *Science*, 309, 2064-7.
- MOOTHA, V. K., LINDGREN, C. M., ERIKSSON, K. F., SUBRAMANIAN, A., SIHAG, S., LEHAR, J., PUIGSERVER, P., CARLSSON, E., RIDDERSTRÅLE, M., LAURILA, E., HOUSTIS, N., DALY, M. J., PATTERSON, N., MESIROV, J. P., GOLUB, T. R., TAMAYO, P., SPIEGELMAN, B., LANDER, E. S., HIRSCHHORN, J. N., ALTSHULER, D. & GROOP, L. C. 2003. PGC-1alpha-responsive genes involved in oxidative phosphorylation are coordinately downregulated in human diabetes. *Nat Genet*, 34, 267-73.
- MORAES, L. H., BOLLINELI, R. C., MIZOBUTI, D. S., SILVEIRA, L. O. R., MARQUES, M. J. & MINATEL, E. 2015. Effect of N-acetylcysteine plus deferoxamine on oxidative stress and inflammation in dystrophic muscle cells. *Redox Rep*, 20, 109-15.
- MOTOHASHI, N., ASAKURA, Y. & ASAKURA, A. 2014. Isolation, culture, and transplantation of muscle satellite cells. *J Vis Exp*.
- MOULLÉ, V. S., CANSELL, C., LUQUET, S. & CRUCIANI-GUGLIELMACCI, C. 2012. The multiple roles of fatty acid handling proteins in brain. *Front Physiol*, 3, 385.
- MURACH, K. A., ENGLUND, D. A., DUPONT-VERSTEEGDEN, E. E., MCCARTHY, J. J. & PETERSON, C. A. 2018. Myonuclear Domain Flexibility Challenges Rigid Assumptions on Satellite Cell Contribution to Skeletal Muscle Fiber Hypertrophy. *Front Physiol*, 9, 635.
- NABESHIMA, Y., HANAOKA, K., HAYASAKA, M., ESUMI, E., LI, S. & NONAKA, I. 1993. Myogenin gene disruption results in perinatal lethality because of severe muscle defect. *Nature*, 364, 532-5.
- NADER, G. A., VON WALDEN, F., LIU, C., LINDVALL, J., GUTMANN, L., PISTILLI, E. E. & GORDON, P. M. 2014. Resistance exercise training modulates acute gene expression during human skeletal muscle hypertrophy. *J Appl Physiol (1985)*, 116, 693-702.
- NAGATA, Y., KOBAYASHI, H., UMEDA, M., OHTA, N., KAWASHIMA, S., ZAMMIT, P. S. & MATSUDA, R. 2006. Sphingomyelin levels in the plasma membrane correlate with the activation state of muscle satellite cells. *J Histochem Cytochem*, 54, 375-84.
- NEAL, A., BOLDRIN, L. & MORGAN, J. E. 2012. The satellite cell in male and female, developing and adult mouse muscle: distinct stem cells for growth and regeneration. *PLoS One*, 7, e37950.
- NGUYEN, M. H., CHENG, M. & KOH, T. J. 2011. Impaired muscle regeneration in ob/ob and db/db mice. *ScientificWorldJournal*, 11, 1525-35.
- NGUYEN, P., LERAY, V., DIEZ, M., SERISIER, S., LE BLOC'H, J., SILIART, B. & DUMON, H. 2008. Liver lipid metabolism. *J Anim Physiol Anim Nutr (Berl)*, 92, 272-83.
- NILWIK, R., SNIJDERS, T., LEENDERS, M., GROEN, B. B., VAN KRANENBURG, J., VERDIJK, L. B. & VAN LOON, L. J. 2013. The decline in skeletal muscle mass with aging is mainly attributed to a reduction in type II muscle fiber size. *Exp Gerontol*, 48, 492-8.
- OBERBACH, A., BOSSENZ, Y., LEHMANN, S., NIEBAUER, J., ADAMS, V., PASCHKE, R., SCHÖN, M. R., BLÜHER, M. & PUNKT, K. 2006. Altered fiber distribution and fiber-specific glycolytic and oxidative enzyme activity in skeletal muscle of patients with type 2 diabetes. *Diabetes Care*, 29, 895-900.

- OKAMURA, D. M., PENNATHUR, S., PASICHNYK, K., LÓPEZ-GUISA, J. M., COLLINS, S., FEBBRAIO, M., HEINECKE, J. & EDDY, A. A. 2009. CD36 regulates oxidative stress and inflammation in hypercholesterolemic CKD. *J Am Soc Nephrol*, 20, 495-505.
- PAJCINI, K. V., CORBEL, S. Y., SAGE, J., POMERANTZ, J. H. & BLAU, H. M. 2010. Transient inactivation of Rb and ARF yields regenerative cells from postmitotic mammalian muscle. *Cell Stem Cell*, 7, 198-213.
- PAOLINI, A., OMAIRI, S., MITCHELL, R., VAUGHAN, D., MATSAKAS, A., VAIYAPURI, S., RICKETTS, T., RUBINSZTEIN, D. C. and PATEL, K. 2018. Attenuation of autophagy impacts on muscle fibre development, starvation induced stress and fibre regeneration following acute injury. *Sci Rep*, 8(1), pp. 9062.
- PARK, J. W., LEE, J. H., KIM, S. W., HAN, J. S., KANG, K. S., KIM, S. J. & PARK, T. S. 2018. Muscle differentiation induced up-regulation of calcium-related gene expression in quail myoblasts. *Asian-Australas J Anim Sci*, 31, 1507-1515.
- PARK, S. W., GOODPASTER, B. H., STROTMEYER, E. S., DE REKENEIRE, N., HARRIS, T. B., SCHWARTZ, A. V., TYLAVSKY, F. A. & NEWMAN, A. B. 2006. Decreased muscle strength and quality in older adults with type 2 diabetes: the health, aging, and body composition study. *Diabetes*, 55, 1813-8.
- PARK, S. Y., YUN, Y. & KIM, I. S. 2012. CD36 is required for myoblast fusion during myogenic differentiation. *Biochem Biophys Res Commun*, 427, 705-10.
- PASHKOVSKAIA, N., GEY, U. & RÖDEL, G. 2018. Mitochondrial ROS direct the differentiation of murine pluripotent P19 cells. *Stem Cell Res*, 30, 180-191.
- PATEL, M. S., OWEN, O. E., GOLDMAN, L. I. & HANSON, R. W. 1975. Fatty acid synthesis by human adipose tissue. *Metabolism*, 24, 161-73.
- PATKOVÁ, J., ANDĚL, M. & TRNKA, J. 2014. Palmitate-induced cell death and mitochondrial respiratory dysfunction in myoblasts are not prevented by mitochondria-targeted antioxidants. *Cell Physiol Biochem*, 33, 1439-51.
- PATSALOS, A., PAP, A., VARGA, T., TRENCSENYI, G., CONTRERAS, G. A., GARAI, I., PAPP, Z., DEZSO, B., PINTYE, E. & NAGY, L. 2017. In situ macrophage phenotypic transition is affected by altered cellular composition prior to acute sterile muscle injury. *J Physiol*, 595, 5815-5842.
- PEPINO, M. Y., KUDA, O., SAMOVSKI, D. & ABUMRAD, N. A. 2014. Structure-function of CD36 and importance of fatty acid signal transduction in fat metabolism. *Annu Rev Nutr*, 34, 281-303.
- PERUTKA, Z. & ŠEBELA, M. 2018. Pseudotrypsin: A Little-Known Trypsin Proteoform. *Molecules*, 23.
- PETERSEN, K. F., BEFROY, D., DUFOUR, S., DZIURA, J., ARIYAN, C., ROTHMAN, D. L., DIPIETRO, L., CLINE, G. W. & SHULMAN, G. I. 2003. Mitochondrial dysfunction in the elderly: possible role in insulin resistance. *Science*, 300, 1140-2.
- PETERSON, J. M., BRYNER, R. W. & ALWAY, S. E. 2008. Satellite cell proliferation is reduced in muscles of obese Zucker rats but restored with loading. *Am J Physiol Cell Physiol*, 295, C521-8.
- PFLEGER, J., HE, M. & ABDELLATIF, M. 2015. Mitochondrial complex II is a source of the reserve respiratory capacity that is regulated by metabolic sensors and promotes cell survival. *Cell Death Dis*, 6, e1835.
- PHIELIX, E., SCHRAUWEN-HINDERLING, V. B., MENSINK, M., LENAERS, E., MEEEX, R., HOEKS, J., KOOI, M. E., MOONEN-KORNIPS, E., SELS, J. P., HESSELINK, M. K. & SCHRAUWEN, P. 2008. Lower intrinsic ADP-stimulated mitochondrial respiration underlies in vivo mitochondrial dysfunction in muscle of male type 2 diabetic patients. *Diabetes*, 57, 2943-9.
- PHILLIPS, S. M. 2014. A brief review of critical processes in exercise-induced muscular hypertrophy. *Sports Med*, 44 Suppl 1, S71-7.

- PIETKA, T. A., SULKIN, M. S., KUDA, O., WANG, W., ZHOU, D., YAMADA, K. A., YANG, K., SU, X., GROSS, R. W., NERBONNE, J. M., EFIMOV, I. R. & ABUMRAD, N. A. 2012. CD36 protein influences myocardial Ca²⁺ homeostasis and phospholipid metabolism: conduction anomalies in CD36-deficient mice during fasting. *J Biol Chem*, 287, 38901-12.
- PILLON, N. J., CROZE, M. L., VELLA, R. E., SOULÈRE, L., LAGARDE, M. & SOULAGE, C. O. 2012. The lipid peroxidation by-product 4-hydroxy-2-nonenal (4-HNE) induces insulin resistance in skeletal muscle through both carbonyl and oxidative stress. *Endocrinology*, 153, 2099-111.
- POHL, J., RING, A., KORKMAZ, U., EHEHALT, R. & STREMMEL, W. 2005. FAT/CD36-mediated long-chain fatty acid uptake in adipocytes requires plasma membrane rafts. *Mol Biol Cell*, 16, 24-31.
- PONCHEL, F., TOOMES, C., BRANSFIELD, K., LEONG, F. T., DOUGLAS, S. H., FIELD, S. L., BELL, S. M., COMBARET, V., PUISIEUX, A., MIGHELL, A. J., ROBINSON, P. A., INGLEHEARN, C. F., ISAACS, J. D. & MARKHAM, A. F. 2003. Real-time PCR based on SYBR-Green I fluorescence: an alternative to the TaqMan assay for a relative quantification of gene rearrangements, gene amplifications and micro gene deletions. *BMC Biotechnol*, 3, 18.
- POWERS, S. K., JI, L. L., KAVAZIS, A. N. & JACKSON, M. J. 2011. Reactive oxygen species: impact on skeletal muscle. *Compr Physiol*, 1, 941-69.
- PULLEN, D. L., LIESMAN, J. S. & EMERY, R. S. 1990. A species comparison of liver slice synthesis and secretion of triacylglycerol from nonesterified fatty acids in media. *J Anim Sci*, 68, 1395-9.
- PURI, V., RANJIT, S., KONDA, S., NICOLORO, S. M., STRAUBHAAR, J., CHAWLA, A., CHOUINARD, M., LIN, C., BURKART, A., CORVERA, S., PERUGINI, R. A. & CZECH, M. P. 2008. Cidea is associated with lipid droplets and insulin sensitivity in humans. *Proc Natl Acad Sci U S A*, 105, 7833-8.
- QUINN, L. S., ANDERSON, B. G., CONNER, J. D. & WOLDEN-HANSON, T. 2013. IL-15 overexpression promotes endurance, oxidative energy metabolism, and muscle PPAR δ , SIRT1, PGC-1 α , and PGC-1 β expression in male mice. *Endocrinology*, 154, 232-45.
- RAC, M. E., SAFRANOW, K. & PONCYLJUSZ, W. 2007. Molecular basis of human CD36 gene mutations. *Mol Med*, 13, 288-96.
- RELAIX, F. & ZAMMIT, P. S. 2012. Satellite cells are essential for skeletal muscle regeneration: the cell on the edge returns centre stage. *Development*, 139, 2845-56.
- RIO, D. C., ARES, M., HANNON, G. J. & NILSEN, T. W. 2010. Purification of RNA using TRIzol (TRI reagent). *Cold Spring Harb Protoc*, 2010, pdb.prot5439.
- ROZO, M., LI, L. & FAN, C. M. 2016. Targeting β 1-integrin signaling enhances regeneration in aged and dystrophic muscle in mice. *Nat Med*, 22, 889-96.
- RUDELL, A., KELLY-SPRATT, K. S., FURUYA, M., PARGHI, S. S. & KEMP, C. J. 2008. p19/Arf and p53 suppress sentinel lymph node lymphangiogenesis and carcinoma metastasis. *Oncogene*, 27, 3145-55.
- SALTIEL, A. R. & OLEFSKY, J. M. 2017. Inflammatory mechanisms linking obesity and metabolic disease. *J Clin Invest*, 127, 1-4.
- SAMOVSKI, D., SUN, J., PIETKA, T., GROSS, R. W., ECKEL, R. H., SU, X., STAHL, P. D. & ABUMRAD, N. A. 2015. Regulation of AMPK activation by CD36 links fatty acid uptake to β -oxidation. *Diabetes*, 64, 353-9.
- SAPOZNIK, E., NIU, G., ZHOU, Y., PRIM, P. M., CRISWELL, T. L. & SOKER, S. 2018. A real-time monitoring platform of myogenesis regulators using double fluorescent labeling. *PLoS One*, 13, e0192654.
- SARWAR, R., PIERCE, N. & KOPPE, S. 2018. Obesity and nonalcoholic fatty liver disease: current perspectives. *Diabetes Metab Syndr Obes*, 11, 533-542.
- SCHIAFFINO, S. & REGGIANI, C. 2011. Fiber types in mammalian skeletal muscles. *Physiol Rev*, 91, 1447-531.

- SCHIEBER, M. & CHANDEL, N. S. 2014. ROS function in redox signaling and oxidative stress. *Curr Biol*, 24, R453-62.
- SCHMIDT, M., SCHÜLER, S. C., HÜTTNER, S. S., VON EYSS, B. & VON MALTZAHN, J. 2019. Adult stem cells at work: regenerating skeletal muscle. *Cell Mol Life Sci*, 76, 2559-2570.
- SCHULTZ, E., GIBSON, M. C. & CHAMPION, T. 1978. Satellite cells are mitotically quiescent in mature mouse muscle: an EM and radioautographic study. *J Exp Zool*, 206, 451-6.
- SCHÄFER, M. & WERNER, S. 2008. Oxidative stress in normal and impaired wound repair. *Pharmacol Res*, 58, 165-71.
- SCULLY, D., SFYRI, P., VERPOORTEN, S., PAPADOPOULOS, P., MUÑOZ-TURRILLAS, M. C., MITCHELL, R., ABURIMA, A., PATEL, K., GUTIÉRREZ, L., NASEEM, K. M. & MATSAKAS, A. 2019. Platelet releasate promotes skeletal myogenesis by increasing muscle stem cell commitment to differentiation and accelerates muscle regeneration following acute injury. *Acta Physiol (Oxf)*, 225, e13207.
- SEBASTIÁN, D., GUITART, M., GARCIA-MARTINEZ, C., MAUVEZIN, C., ORELLANA-GAVALDARELLANA, J. M., SERRA, D., GOMEZ-FOIX, A. M., HEGARDT, F. G. and ASINS, G. 2009. Novel role of FATP1 in mitochondrial fatty acid oxidation in skeletal muscle cells, *J Lipid Res*, 50(9), pp. 1789-99.
- SEALE, P., SABOURIN, L. A., GIRGIS-GABARDO, A., MANSOURI, A., GRUSS, P. & RUDNICKI, M. A. 2000. Pax7 is required for the specification of myogenic satellite cells. *Cell*, 102, 777-86.
- SEENE, T., KAASIK, P. & ALEV, K. 2011. Muscle protein turnover in endurance training: a review. *Int J Sports Med*, 32, 905-11.
- SEIMON, T. A., NADOLSKI, M. J., LIAO, X., MAGALLON, J., NGUYEN, M., FERIC, N. T., KOSCHINSKY, M. L., HARKEWICZ, R., WITZTUM, J. L., TSIMIKAS, S., GOLENBOCK, D., MOORE, K. J. & TABAS, I. 2010. Atherogenic lipids and lipoproteins trigger CD36-TLR2-dependent apoptosis in macrophages undergoing endoplasmic reticulum stress. *Cell Metab*, 12, 467-82.
- Sfyri, P. P., YULDASHEVA, N. Y., TZIMOU, A., GIALLOUROU, N., CRISPI, V., ABURIMA, A., BELTRAN-ALVAREZ, P., PATEL, K., MOUGIOS, V., SWANN, J. R., KEARNEY, M. T. and MATSAKAS, A. 2018. Attenuation of oxidative stress-induced lesions in skeletal muscle in a mouse model of obesity-independent hyperlipidaemia and atherosclerosis through the inhibition of Nox2 activity, *Free Radic Biol Med*, 129, pp. 504-519.
- SHANNON, E. K., STEVENS, A., EDRINGTON, W., ZHAO, Y., JAYASINGHE, A. K., PAGE-MCCAW, A. & HUTSON, M. S. 2017. Multiple Mechanisms Drive Calcium Signal Dynamics around Laser-Induced Epithelial Wounds. *Biophys J*, 113, 1623-1635.
- SHEA, K. L., XIANG, W., LAPORTA, V. S., LICHT, J. D., KELLER, C., BASSON, M. A. & BRACK, A. S. 2010. Sprouty1 regulates reversible quiescence of a self-renewing adult muscle stem cell pool during regeneration. *Cell Stem Cell*, 6, 117-29.
- SHINZAWA, K. & TSUJIMOTO, Y. 2003. PLA2 activity is required for nuclear shrinkage in caspase-independent cell death. *J Cell Biol*, 163, 1219-30.
- SHORTREED, K. E., KRAUSE, M. P., HUANG, J. H., DHANANI, D., MORADI, J., CEDDIA, R. B. & HAWKE, T. J. 2009. Muscle-specific adaptations, impaired oxidative capacity and maintenance of contractile function characterize diet-induced obese mouse skeletal muscle. *PLoS One*, 4, e7293.
- SIMONEAU, J. A. & BOUCHARD, C. 1995. Genetic determinism of fiber type proportion in human skeletal muscle. *FASEB J*, 9, 1091-5.
- SIN, J., ANDRES, A. M., TAYLOR, D. J., WESTON, T., HIRAUMI, Y., STOTLAND, A., KIM, B. J., HUANG, C., DORAN, K. S. & GOTTLIEB, R. A. 2016. Mitophagy is required for mitochondrial biogenesis and myogenic differentiation of C2C12 myoblasts. *Autophagy*, 12, 369-80.
- SINHA, R., DUFOUR, S., PETERSEN, K. F., LEBON, V., ENOKSSON, S., MA, Y. Z., SAVOYE, M., ROTHMAN, D. L., SHULMAN, G. I. & CAPRIO, S. 2002. Assessment of skeletal muscle

- triglyceride content by ¹H nuclear magnetic resonance spectroscopy in lean and obese adolescents: relationships to insulin sensitivity, total body fat, and central adiposity. *Diabetes*, 51, 1022-7.
- SIPARSKY, P. N., KIRKENDALL, D. T. & GARRETT, W. E. 2014. Muscle changes in aging: understanding sarcopenia. *Sports Health*, 6, 36-40.
- SMITH, A. C., MULLEN, K. L., JUNKIN, K. A., NICKERSON, J., CHABOWSKI, A., BONEN, A. & DYCK, D. J. 2007. Metformin and exercise reduce muscle FAT/CD36 and lipid accumulation and blunt the progression of high-fat diet-induced hyperglycemia. *Am J Physiol Endocrinol Metab*, 293, E172-81.
- SOFI, F., MACCHI, C., ABBATE, R., GENSINI, G. F. & CASINI, A. 2013. Mediterranean diet and health. *Biofactors*, 39, 335-42.
- SOUKUP, T., ZACHAROVÁ, G. & SMERDU, V. 2002. Fibre type composition of soleus and extensor digitorum longus muscles in normal female inbred Lewis rats. *Acta Histochem*, 104, 399-405.
- SOULAGE, C. O., SARDÓN PUIG, L., SOULÈRE, L., ZARROUKI, B., GUICHARDANT, M., LAGARDE, M. & PILLON, N. J. 2018. Skeletal muscle insulin resistance is induced by 4-hydroxy-2-hexenal, a by-product of n-3 fatty acid peroxidation. *Diabetologia*, 61, 688-699.
- SPARKS, L. M., XIE, H., KOZA, R. A., MYNATT, R., HULVER, M. W., BRAY, G. A. & SMITH, S. R. 2005. A high-fat diet coordinately downregulates genes required for mitochondrial oxidative phosphorylation in skeletal muscle. *Diabetes*, 54, 1926-33.
- SQUIRE, J. M. 2016. Muscle contraction: Sliding filament history, sarcomere dynamics and the two Huxleys. *Glob Cardiol Sci Pract*, 2016, e201611.
- STORCH, J. & MCDERMOTT, L. 2009. Structural and functional analysis of fatty acid-binding proteins. *J Lipid Res*, 50 Suppl, S126-31.
- STORCH, J. & THUMSER, A. E. 2010. Tissue-specific functions in the fatty acid-binding protein family. *J Biol Chem*, 285, 32679-83.
- STRASSER, B., VOLAKLIS, K., FUCHS, D. & BURTSCHER, M. 2018. Role of Dietary Protein and Muscular Fitness on Longevity and Aging. *Aging Dis*, 9, 119-132.
- SUNDARESAN, S., SHAHID, R., RIEHL, T. E., CHANDRA, R., NASSIR, F., STENSON, W. F., LIDDLE, R. A. & ABUMRAD, N. A. 2013. CD36-dependent signaling mediates fatty acid-induced gut release of secretin and cholecystokinin. *FASEB J*, 27, 1191-202.
- SWOMLEY, A. M., FÖRSTER, S., KEENEY, J. T., TRIPLETT, J., ZHANG, Z., SULTANA, R. & BUTTERFIELD, D. A. 2014. Abeta, oxidative stress in Alzheimer disease: evidence based on proteomics studies. *Biochim Biophys Acta*, 1842, 1248-57.
- SYVERUD, B. C., LEE, J. D., VANDUSEN, K. W. and LARKIN, L. M. 2014. Isolation and Purification of Satellite Cells for Skeletal Muscle Tissue Engineering, *J Regen Med*, 3(2).
- TAMILARASAN, K. P., TEMMEL, H., DAS, S. K., AL ZOUGHBI, W., SCHAUER, S., VESELY, P. W. & HOEFLER, G. 2012. Skeletal muscle damage and impaired regeneration due to LPL-mediated lipotoxicity. *Cell Death Dis*, 3, e354.
- TANABE, T., BEAM, K. G., POWELL, J. A. & NUMA, S. 1988. Restoration of excitation-contraction coupling and slow calcium current in dysgenic muscle by dihydropyridine receptor complementary DNA. *Nature*, 336, 134-9.
- TANNER, C. J., BARAKAT, H. A., DOHM, G. L., PORIES, W. J., MACDONALD, K. G., CUNNINGHAM, P. R., SWANSON, M. S. & HOUMARD, J. A. 2002. Muscle fiber type is associated with obesity and weight loss. *Am J Physiol Endocrinol Metab*, 282, E1191-6.
- TELLIS, C. M., ROSEN, C., THEKDI, A. & SCIOTE, J. J. 2004. Anatomy and fiber type composition of human interarytenoid muscle. *Ann Otol Rhinol Laryngol*, 113, 97-107.
- THOMSON, D. M. 2018. The Role of AMPK in the Regulation of Skeletal Muscle Size, Hypertrophy, and Regeneration. *Int J Mol Sci*, 19.
- TIELAND, M., TROUWBORST, I. & CLARK, B. C. 2018. Skeletal muscle performance and ageing. *J Cachexia Sarcopenia Muscle*, 9, 3-19.

- TOMIYAMA, Y., TAKE, H., IKEDA, H., MITANI, T., FURUBAYASHI, T., MIZUTANI, H., YAMAMOTO, N., TANDON, N. N., SEKIGUCHI, S. & JAMIESON, G. A. 1990. Identification of the platelet-specific alloantigen, Naka, on platelet membrane glycoprotein IV. *Blood*, 75, 684-7.
- TONTONOZ, P., NAGY, L., ALVAREZ, J. G., THOMAZY, V. A. & EVANS, R. M. 1998. PPARgamma promotes monocyte/macrophage differentiation and uptake of oxidized LDL. *Cell*, 93, 241-52.
- TOWNSEND, K. L., AN, D., LYNES, M. D., HUANG, T. L., ZHANG, H., GOODYEAR, L. J. & TSENG, Y. H. 2013. Increased mitochondrial activity in BMP7-treated brown adipocytes, due to increased CPT1- and CD36-mediated fatty acid uptake. *Antioxid Redox Signal*, 19, 243-57.
- TSAI, F. C., KUO, G. H., CHANG, S. W. & TSAI, P. J. 2015. Ca²⁺ signaling in cytoskeletal reorganization, cell migration, and cancer metastasis. *Biomed Res Int*, 2015, 409245.
- TU, M. K., LEVIN, J. B., HAMILTON, A. M. & BORODINSKY, L. N. 2016. Calcium signaling in skeletal muscle development, maintenance and regeneration. *Cell Calcium*, 59, 91-7.
- TUCSEK, Z., TOTH, P., SOSNOWSKA, D., GAUTAM, T., MITSCHELEN, M., KOLLER, A., SZALAI, G., SONNTAG, W. E., UNGVARI, Z. & CSISZAR, A. 2014. Obesity in aging exacerbates blood-brain barrier disruption, neuroinflammation, and oxidative stress in the mouse hippocampus: effects on expression of genes involved in beta-amyloid generation and Alzheimer's disease. *J Gerontol A Biol Sci Med Sci*, 69, 1212-26.
- TURPIN, S. M., LANCASTER, G. I., DARBY, I., FEBBRAIO, M. A. & WATT, M. J. 2006. Apoptosis in skeletal muscle myotubes is induced by ceramides and is positively related to insulin resistance. *Am J Physiol Endocrinol Metab*, 291, E1341-50.
- TURPIN, S. M., RYALL, J. G., SOUTHGATE, R., DARBY, I., HEVENER, A. L., FEBBRAIO, M. A., KEMP, B. E., LYNCH, G. S. & WATT, M. J. 2009. Examination of 'lipotoxicity' in skeletal muscle of high-fat fed and ob/ob mice. *J Physiol*, 587, 1593-605.
- VALDEZ, G., TAPIA, J. C., LICHTMAN, J. W., FOX, M. A. & SANES, J. R. 2012. Shared resistance to aging and ALS in neuromuscular junctions of specific muscles. *PLoS One*, 7, e34640.
- VILAR-GOMEZ, E., MARTINEZ-PEREZ, Y., CALZADILLA-BERTOT, L., TORRES-GONZALEZ, A., GRA-ORAMAS, B., GONZALEZ-FABIAN, L., FRIEDMAN, S. L., DIAGO, M. & ROMERO-GOMEZ, M. 2015. Weight Loss Through Lifestyle Modification Significantly Reduces Features of Nonalcoholic Steatohepatitis. *Gastroenterology*, 149, 367-78.e5; quiz e14-5.
- VINCENT, H. K., MORGAN, J. W. & VINCENT, K. R. 2004. Obesity exacerbates oxidative stress levels after acute exercise. *Med Sci Sports Exerc*, 36, 772-9.
- VISWAKARMA, N., YU, S., NAIK, S., KASHIREDDY, P., MATSUMOTO, K., SARKAR, J., SURAPUREDDI, S., JIA, Y., RAO, M. S. & REDDY, J. K. 2007. Transcriptional regulation of Cidea, mitochondrial cell death-inducing DNA fragmentation factor alpha-like effector A, in mouse liver by peroxisome proliferator-activated receptor alpha and gamma. *J Biol Chem*, 282, 18613-24.
- WALTHER, T. C. & FARESE, R. V. 2012. Lipid droplets and cellular lipid metabolism. *Annu Rev Biochem*, 81, 687-714.
- WANG, C., LIU, W., NIE, Y., QAHER, M., HORTON, H. E., YUE, F., ASAKURA, A. & KUANG, S. 2017. Loss of MyoD Promotes Fate Transdifferentiation of Myoblasts Into Brown Adipocytes. *EBioMedicine*, 16, 212-223.
- WANG, Q. & ZOU, M. H. 2018. Measurement of Reactive Oxygen Species (ROS) and Mitochondrial ROS in AMPK Knockout Mice Blood Vessels. *Methods Mol Biol*, 1732, 507-517.
- WANG, R., LI, C., QIAO, P., XUE, Y., ZHENG, X., CHEN, H., ZENG, X., LIU, W., BOLDOGH, I. & BA, X. 2018. OGG1-initiated base excision repair exacerbates oxidative stress-induced parthanatos. *Cell Death Dis*, 9, 628.
- WANG, Y. X. 2010. PPARs: diverse regulators in energy metabolism and metabolic diseases. *Cell Res*, 20, 124-37.

- WANG, Y. X., ZHANG, C. L., YU, R. T., CHO, H. K., NELSON, M. C., BAYUGA-OCAMPO, C. R., HAM, J., KANG, H. & EVANS, R. M. 2004. Regulation of muscle fiber type and running endurance by PPARdelta. *PLoS Biol*, 2, e294.
- WAKABAYASHI, T. 2015. Mechanism of the calcium-regulation of muscle contraction--in pursuit of its structural basis, *Proc Jpn Acad Ser B Phys Biol Sci*, 91(7), pp. 321-50.
- WEISLEDER, N., BROTTTO, M., KOMAZAKI, S., PAN, Z., ZHAO, X., NOSEK, T., PARNES, J., TAKESHIMA, H. & MA, J. 2006. Muscle aging is associated with compromised Ca²⁺ spark signaling and segregated intracellular Ca²⁺ release. *J Cell Biol*, 174, 639-45.
- WHO EURO, W. H. O. 2019. *Health topics- noncommunicable-diseases/obesity* [Online]. <http://www.euro.who.int/en/health-topics/noncommunicable-diseases/obesity/obesity>. [Accessed 13.10.2019 2019].
- WHO, W. H. O. 2019. *Health topics- Obesity* [Online]. <https://www.who.int/topics/obesity/en/>. [Accessed 13.10.2019 2019].
- WILLIAMSON, D. L., BUTLER, D. C. & ALWAY, S. E. 2009. AMPK inhibits myoblast differentiation through a PGC-1alpha-dependent mechanism. *Am J Physiol Endocrinol Metab*, 297, E304-14.
- WILSON, C. G., TRAN, J. L., ERION, D. M., VERA, N. B., FEBBRAIO, M. & WEISS, E. J. 2016. Hepatocyte-Specific Disruption of CD36 Attenuates Fatty Liver and Improves Insulin Sensitivity in HFD-Fed Mice. *Endocrinology*, 157, 570-85.
- WOLFE, R. R. 2006. The underappreciated role of muscle in health and disease. *Am J Clin Nutr*, 84, 475-82.
- WOO, M. S., YANG, J., BELTRAN, C. & CHO, S. 2016. Cell Surface CD36 Protein in Monocyte/Macrophage Contributes to Phagocytosis during the Resolution Phase of Ischemic Stroke in Mice. *J Biol Chem*, 291, 23654-23661.
- WU, L., ZHOU, L., CHEN, C., GONG, J., XU, L., YE, J., LI, D. & LI, P. 2014. Cidea controls lipid droplet fusion and lipid storage in brown and white adipose tissue. *Sci China Life Sci*, 57, 107-16.
- WU, Q., ORTEGON, A. M., TSANG, B., DOEGE, H., FEINGOLD, K. R. & STAHL, A. 2006. FATP1 is an insulin-sensitive fatty acid transporter involved in diet-induced obesity. *Mol Cell Biol*, 26, 3455-67.
- XU, P., WERNER, J. U., MILERSKI, S., HAMP, C. M., KUZENKO, T., JÄHNERT, M., GOTTMANN, P., DE ROY, L., WARNECKE, D., ABAEI, A., PALMER, A., HUBER-LANG, M., DÜRSELEN, L., RASCHE, V., SCHÜRMAN, A., WABITSCH, M. & KNIPPSCHILD, U. 2018. Diet-Induced Obesity Affects Muscle Regeneration After Murine Blunt Muscle Trauma-A Broad Spectrum Analysis. *Front Physiol*, 9, 674.
- XU, S., JAY, A., BRUNALDI, K., HUANG, N. & HAMILTON, J. A. 2013. CD36 enhances fatty acid uptake by increasing the rate of intracellular esterification but not transport across the plasma membrane. *Biochemistry*, 52, 7254-61.
- XU, S., NAM, S. M., KIM, J. H., DAS, R., CHOI, S. K., NGUYEN, T. T., QUAN, X., CHOI, S. J., CHUNG, C. H., LEE, E. Y., LEE, I. K., WIEDERKEHR, A., WOLLHEIM, C. B., CHA, S. K. & PARK, K. S. 2015. Palmitate induces ER calcium depletion and apoptosis in mouse podocytes subsequent to mitochondrial oxidative stress. *Cell Death Dis*, 6, e1976.
- YAFFE, D. & SAXEL, O. 1977. Serial passaging and differentiation of myogenic cells isolated from dystrophic mouse muscle. *Nature*, 270, 725-7.
- YAN, Z., LIRA, V. A. & GREENE, N. P. 2012. Exercise training-induced regulation of mitochondrial quality. *Exerc Sport Sci Rev*, 40, 159-64.
- YAN, Z., OKUTSU, M., AKHTAR, Y. N. & LIRA, V. A. 2011. Regulation of exercise-induced fiber type transformation, mitochondrial biogenesis, and angiogenesis in skeletal muscle. *J Appl Physiol (1985)*, 110, 264-74.
- YANG, J., PARK, K. W. & CHO, S. 2018. Inhibition of the CD36 receptor reduces visceral fat accumulation and improves insulin resistance in obese mice carrying the BDNF-. *J Biol Chem*, 293, 13338-13348.

- YE, J., COULOURIS, G., ZARETSKAYA, I., CUTCUTACHE, I., ROZEN, S. & MADDEN, T. L. 2012. Primer-BLAST: a tool to design target-specific primers for polymerase chain reaction. *BMC Bioinformatics*, 13, 134.
- YUE, F., CHENG, Y., BRESCHI, A., VIERSTRA, J., WU, W., RYBA, T., SANDSTROM, R., MA, Z., DAVIS, C., POPE, B. D., SHEN, Y., PERVOUCHINE, D. D., DJEBALI, S., THURMAN, R. E., KAUL, R., RYNES, E., KIRILUSHA, A., MARINOV, G. K., WILLIAMS, B. A., TROUT, D., AMRHEIN, H., FISHER-AYLOR, K., ANTOSHECHKIN, I., DESALVO, G., SEE, L. H., FASTUCA, M., DRENKOW, J., ZALESKI, C., DOBIN, A., PRIETO, P., LAGARDE, J., BUSSOTTI, G., TANZER, A., DENAS, O., LI, K., BENDER, M. A., ZHANG, M., BYRON, R., GROUDINE, M. T., MCCLEARY, D., PHAM, L., YE, Z., KUAN, S., EDSALL, L., WU, Y. C., RASMUSSEN, M. D., BANSAL, M. S., KELLIS, M., KELLER, C. A., MORRISSEY, C. S., MISHRA, T., JAIN, D., DOGAN, N., HARRIS, R. S., CAYTING, P., KAWLI, T., BOYLE, A. P., EUSKIRCHEN, G., KUNDAJE, A., LIN, S., LIN, Y., JANSEN, C., MALLADI, V. S., CLINE, M. S., ERICKSON, D. T., KIRKUP, V. M., LEARNED, K., SLOAN, C. A., ROSENBLOOM, K. R., LACERDA DE SOUSA, B., BEAL, K., PIGNATELLI, M., FLICEK, P., LIAN, J., KAHVECI, T., LEE, D., KENT, W. J., RAMALHO SANTOS, M., HERRERO, J., NOTREDAME, C., JOHNSON, A., VONG, S., LEE, K., BATES, D., NERI, F., DIEGEL, M., CANFIELD, T., SABO, P. J., WILKEN, M. S., REH, T. A., GISTE, E., SHAFER, A., KUTYAVIN, T., HAUGEN, E., DUNN, D., REYNOLDS, A. P., NEPH, S., HUMBERT, R., HANSEN, R. S., DE BRUIJN, M., et al. 2014. A comparative encyclopedia of DNA elements in the mouse genome. *Nature*, 515, 355-64.
- YUZEFOVYCH, L., WILSON, G. & RACHEK, L. 2010. Different effects of oleate vs. palmitate on mitochondrial function, apoptosis, and insulin signaling in L6 skeletal muscle cells: role of oxidative stress. *Am J Physiol Endocrinol Metab*, 299, E1096-105.
- YUZEFOVYCH, L. V., SOLODUSHKO, V. A., WILSON, G. L. & RACHEK, L. I. 2012. Protection from palmitate-induced mitochondrial DNA damage prevents from mitochondrial oxidative stress, mitochondrial dysfunction, apoptosis, and impaired insulin signaling in rat L6 skeletal muscle cells. *Endocrinology*, 153, 92-100.
- ZAIDI, N., LUPIEN, L., KUEMMERLE, N. B., KINLAW, W. B., SWINNEN, J. V. & SMANS, K. 2013. Lipogenesis and lipolysis: the pathways exploited by the cancer cells to acquire fatty acids. *Prog Lipid Res*, 52, 585-9.
- ZAKI, M., BASHA, W., EL-BASSYOUNI, H. T., EL-TOUKHY, S. & HUSSEIN, T. 2018. Evaluation of DNA damage profile in obese women and its association to risk of metabolic syndrome, polycystic ovary syndrome and recurrent preeclampsia. *Genes Dis*, 5, 367-373.
- ZAMMIT, P. S., GOLDING, J. P., NAGATA, Y., HUDON, V., PARTRIDGE, T. A. & BEAUCHAMP, J. R. 2004. Muscle satellite cells adopt divergent fates: a mechanism for self-renewal? *J Cell Biol*, 166, 347-57.
- ZAMMIT, P. S., HESLOP, L., HUDON, V., ROSENBLATT, J. D., TAJBAKHS, S., BUCKINGHAM, M. E., BEAUCHAMP, J. R. & PARTRIDGE, T. A. 2002. Kinetics of myoblast proliferation show that resident satellite cells are competent to fully regenerate skeletal muscle fibers. *Exp Cell Res*, 281, 39-49.
- ZAMMIT, P. S., RELAIX, F., NAGATA, Y., RUIZ, A. P., COLLINS, C. A., PARTRIDGE, T. A. & BEAUCHAMP, J. R. 2006. Pax7 and myogenic progression in skeletal muscle satellite cells. *J Cell Sci*, 119, 1824-32.
- ZHANG, J., WANG, X., VIKASH, V., YE, Q., WU, D., LIU, Y. & DONG, W. 2016. ROS and ROS-Mediated Cellular Signaling. *Oxid Med Cell Longev*, 2016, 4350965.
- ZHANG, Y., MARSBOOM, G., TOTH, P. T. & REHMAN, J. 2013. Mitochondrial respiration regulates adipogenic differentiation of human mesenchymal stem cells. *PLoS One*, 8, e77077.
- ZHONG, H. & YIN, H. 2015. Role of lipid peroxidation derived 4-hydroxynonenal (4-HNE) in cancer: focusing on mitochondria. *Redox Biol*, 4, 193-9.

- ZIPPER, H., BRUNNER, H., BERNHAGEN, J. & VITZTHUM, F. 2004. Investigations on DNA intercalation and surface binding by SYBR Green I, its structure determination and methodological implications. *Nucleic Acids Res*, 32, e103.
- ZOGBY, A. M., DAYANIDHI, S., CHAMBERS, H. G., SCHENK, S. & LIEBER, R. L. 2017. Skeletal muscle fiber-type specific succinate dehydrogenase activity in cerebral palsy. *Muscle Nerve*, 55, 122-124.

9 Appendix

9.1 List of materials

Materials	Supplier	Cat. Number
Acrylamide/Bis Solution 30%, 29:1	BioRad	1610156
Bodipy 493/503	Fisher Scientific	D3922
Bovine Serum Albumin	PAA Cell Culture Company	K41-002
Carestream® Kodak® autoradiography GBX developer/replenisher	Sigma-Aldrich	P7042
Carestream® Kodak® autoradiography GBX fixer/replenisher	Sigma-Aldrich	P7167
Chicken embryo extract	APS, UK	MD-004D-UK
Click-iT® EdU Cell Proliferation Assay	BaseClick, Germany	BCK-EdU488
Collagenase	Sigma Aldrich, UK	C2674
DAPI	Sigma Aldrich	D9542
Dihydroethidium (DHE)	Thermo Scientific, UK	D-1168
Dimethyl sulfoxide (DMSO)	Fisher Scientific	10103483
DMEM, high glucose, GlutaMAX™ Supplement, pyruvate	Thermo Scientific, UK	10569010
DNase I, Rnase-free	ThermoFisher Scientific	EN0521
DPX Mounting Medium	Fisher Scientific	10050080
Eosin	Sigma, UK	E.4382
E.Z.N.A Total RNA kit I	Omega Bio-Tek, USA	R6834-01
FCCP	Sigma Aldrich	
Fetal Bovine Serum, Heat inactivated (FBS)	Sigma Aldrich	F0804
Filter Paper Pierce Western Blotting	Fisher Scientific	11814131
Fluorescent Mounting Medium	Dako	S3023
Hematoxylin Solution Harris Modified	Sigma Aldrich, UK	HHS32
Horse Serum-Gibco	Fisher Scientific, UK	16050122
HyClone Dulbecco's High Glucose Modified Eagles Medium (DMEM)	Fisher Scientific, UK	SH30022.01
Hydrophobic PAP pen	Sigma Aldrich, UK	Z377821
Hydromount	National Diagnostics	HS-106
IRDye 800CW goat anti- Mouse IgG	LI-COR Biosciences	925-32210
Isopentane/ 2- Methylbutane	Acros Organics	397221000

Isopropyl alcohol	Fisher Scientific	10366430
Matrigel	Corning, UK	354234
Microscopy glass slides	Thermo Scientific, UK	J2800AMNT
Naja pallida cardiotoxin	Latoxan, Valence France	56574-47-1
Nitrotetrazolium Blue Chloride, NBT	Sigma Aldrich	N5514
Optimal cutting temperature compound (OCT)	VWR, UK	00411243
Oil Red O	Sigma Aldrich	O0625
Oxidised Protein Western Blot Detection Kit	Abcam	ab178020
OxiSelect™ TBARS Assay Kit	Cell Biolabs	STA-330
Oxoid Phosphate Buffer Saline Tablets	ThermoFisher Scientific	BR0014G
PageRuler™ Plus Prestained 10-250kda Protein Ladder		11852124
Paraformaldehyde	Sigma Aldrich	P6148-500G
Penicillin/streptomycin	Thermo Scientific, UK	15140122
Pierce BCA Protein Assay Kit	ThermoFisher Scientific	23225
RiboZol RNA Extraction Reagent	VWR Life Science AMRESCO, UK	N580-30ML
RevertAid H Minus First Strand cDNA Synthesis Kit	Thermo Scientific, UK	K1632
Sodium Dodecyl Sulphate, SDS	Fisher Scientific	10356463
SSO	Cayman Chemical	11211
SYBR Green	Thermo Scientific, UK	4364344
Triton X-100	Sigma Aldrich	T8787
Trypan Blue	Thermo Scientific, UK	15250061
Trypsin-EDTA	Sigma Aldrich	T4174
Tween 20	Sigma Aldrich	P9416

9.2 List of antibodies

Antigen	Species	Dilution	Supplier, Cat Number
Primary			
MYH3	Mouse	1:200	Santa Cruz, sc-53091
Mhcl	Mouse	1:1	DSHB, A4.84
MhclIA	Mouse	1:2	DSHB, A4.74
MhclIB	Mouse	1:1	DSHB, BF.F3
Pax7	Mouse	1:200	Santa Cruz, sc-81648
MyoD	Rabbit	1:200	Santa Cruz, sc-760
Myogenin	Rabbit	1:200	Santa Cruz, sc-570
Cyclin D1	Mouse	1:200	Santa Cruz, sc-450
Scrib	Mouse	1:200	Santa Cruz, sc-374139
PDGF-B	Mouse	1:200	Santa Cruz, sc-365805
VEGF	Mouse	1:200	Santa Cruz, sc-7269
IGF-1R α	Rabbit	1:200	Santa Cruz, sc-271606
Ki-67	Rat	1:200	ThermoFisher, 14-5698-80
CD31	Rat	1:40	AbD serotec MCA2388
CD68	Mouse	1:200	Santa Cruz, sc-20060
IL-10	Mouse	1:200	Santa Cruz, sc-8438
VEGF-C	Mouse	1:200	Santa Cruz, sc-374628
PCNA	Mouse	1:200	Santa Cruz, sc-56
TLR4	Mouse	1:200	Santa Cruz, sc-293072
ICAM-1	Mouse	1:200	Santa Cruz, sc-8439
3NT	Mouse	1:500	Santa Cruz 32757
4HNE	Mouse	1:1,000	R&D Systems MAB3249
β tubulin	Mouse	1:1,000	EMD Millipore 05-661
Secondary			
Alexa fluor 488 anti-rat	Goat	1:200	Life Technologies A11006

Alexa fluor 488 anti-mouse	Goat	1:200	Life Technologies A11029
Alexa fluor 488 anti-rabbit	Goat	1:200	Life Technologies A11034
Alexa fluor 594 anti-rabbit	Goat	1:200	Life Technologies A11037
Alexa fluor 633 anti-mouse	Goat	1:200	Life Technologies A20146
HRP conjugated anti-mouse	Goat	1:10,000	Sigma

9.3 PCR primer sequences

<i>Acta1</i>	Forward	CCCAAAGCTAACCGGGAGAAG
	Reverse	GACAGCACCGCCTGGATAG
<i>Bex1</i>	Forward	ATGGAGTCCAAAGATCAAGGCG
	Reverse	CTGGCTCCCTTCTGATGGTA
<i>Cat</i>	Forward	GGATTATGGCCTCCGAGATCTT
	Reverse	TAAAACGTCCAGGACGGGTAA
<i>Cidea</i>	Forward	CATGGTTTGAAACTCGAAAAGGG
	Reverse	TGACATTCATGGGATTGCAGAC
<i>Cpt1</i>	Forward	CACCAACGGGCTCATCTTCTA
	Reverse	CAAAATGACCTAGCCTTCTATCGAA
<i>Fabp3</i>	Forward	ACCTGGAAGCTAGTGGACAG
	Reverse	TGATGGTAGTAGGCTTGGTCAT
<i>Fatp1</i>	Forward	AGGTCAATGAGGACAACGATGGAG
	Reverse	CTGGTACATTGAGTTAGGGTCCAA
<i>Fatp2</i>	Forward	GATGCCGTGTCCGTCTTTTAC
	Reverse	GACTTCAGACCTCCACGACTC
<i>Fatp3</i>	Forward	ACAGTGCCAGGGATTCTACCA
	Reverse	GAACTTGGGTTTCAGCACCAC
<i>Fatp5</i>	Forward	TCTATGGCCTAAAGTTCAGGCG
	Reverse	CTTGCCGCTCTAAAGCATCC
<i>Fndc5</i>	Forward	TTGCCATCTCTCAGCAGAAGA
	Reverse	GGCCTGCACATGGACGATA
<i>IL-15</i>	Forward	CATCCATCTCGTGCTACTTGTG
	Reverse	GCCTCTGTTTTAGGGAGACCT
<i>Mgst1</i>	Forward	CCTCCTATGCAACGATCATTCTT
	Reverse	ACCTTGTTGGTTATCCCTCTGG
<i>Mhc1</i>	Forward	AGTCCCAGGTCAACAAGCTG
	Reverse	TTCCACCTAAAGGGCTGTTG
<i>Myogenin</i>	Forward	GAGACATCCCCCTATTTCTACCA
	Reverse	GCTCAGTCCGCTCATAGCC
<i>Nox2</i>	Forward	TGAATGCCAGAGTCGGGATT
	Reverse	CGAGTCACGGCCACATACA

<i>Ogg1</i>	Forward	CAACAACATTGCTCGCATTACTG
	Reverse	TCAAGCTGAATGAGTCGAGGT
<i>Prdx1</i>	Forward	CTGGCATGGATTAACACACCC
	Reverse	GGTGCGCTTGGGATCTGAT
<i>Sod1</i>	Forward	TATGGGGACAATACACAAGGC
	Reverse	CGGGCCACCATGTTTCTTAGA
<i>Srf</i>	Forward	CTGCCTCAACTCGCCAGAC
	Reverse	TCAGATTCCGACACCTGGTAG
<i>Tmem8c</i>	Forward	GTGATGGGCCTGGTTTGTCT
	Reverse	GCATTGTGAAGGTCGATCTCTG